



Barbara Konrad, MSc

**Biochemical and Physiological Characterization of
the Berberine Bridge Enzyme-like family in
*Arabidopsis thaliana***

DISSERTATION

Zur Erlangung des akademischen Grades
einer Doktorin der technischen Wissenschaften (Dr. *techn.*)

Erreicht an der
Technischen Universität Graz

Betreuer: Univ.-Prof. Mag. *rer. nat.* Dr. *rer. nat.* Peter Macheroux

Institut für Biochemie
Technische Universität Graz

Graz, 2018

Acknowledgments

First of all, I would like to thank all people who accompanied, supported and motivated me during my PhD project the last four years. I am grateful for the nice working atmosphere, the lively and interesting discussions, for the nice people who I met during my time at this institute and especially for the friendships that came out.

I want to express my gratitude to my supervisor Prof. Peter Macheroux for giving me the opportunity to work in his research group on such an interesting project. He gave me the freedom to realize my own ideas and he supported and encouraged me to do a part of my PhD thesis abroad. I am grateful that he gave me the possibility to steer my project in a very interesting direction which allowed me, as a Biologist, to immerse into the plant world.

I want to thank the University of Technology of Graz and the Doctoral program “Molecular Enzymology” for giving me the opportunity to visit interesting international conferences and other laboratories abroad whereby it was possible to discuss my project with other interesting talented colleagues. Due to the inspiring environment, many new ideas emerged and I did not only received scientific education but I also learned for my life through such experiences.

I acknowledge my thesis committee members Prof. Karl Gruber and Prof. Wolfgang Kroutil for giving me interesting inputs at our meetings. Furthermore, I heartily would like to thank Prof. Maria Müller for her support and help on my thesis. She gave me the opportunity to perform most of my work at the Institute of Biology, Section Plant Sciences, Karl-Franzens University of Graz.

I also want to thank all my colleagues who contributed to my work and without their help this project would not have been realized. Therefore, many thanks go to Dr. Silvia Wallner, who sparked my interest for the BBE project already during my master thesis. Thanks Silvia for your great helpfulness and your endless patience to explain me everything about biochemistry. It is nice that we got to know each other through this project and became friends. Further, I would like to thank Dr. Bastian Daniel, with whom I continued my work with BBE-like enzymes in *Arabidopsis*. Thanks Bastian for your scientific support, for the fruitful discussions and your positive motivation to focus my project especially at sophisticated moments.

I want to thank all people who joined the BBE team during my PhD thesis, Dr. Domen Zafred and especially Dr. Alexandra Jammer. Thank you Alexandra for supporting the BBE-like team and for introducing me to diverse aspects of plant work and guiding me during difficulties in

my project. Many thanks for your great help, for your time and for your coordinating talent and special thanks for the great time together at the Plant Science Section of the Institute of Biology.

During the last four years, I also had the pleasure to co-supervise and guide young and talented students during their bachelor thesis. Thanks to Peter Eibensteiner, Lukas Petrowitsch, Merima Ramic, Inés Sumann and Kordula Schnabl for contributing to my project and joining the BBE-like team. Moreover, special thanks to Kordula for fighting with me to clone *AtBBE*-like overexpression lines. It was a pleasure for me working together with such a talented and motivated young scientist.

I am also grateful to all collaboration partners abroad realizing my project and making my work more diverse. Therefore, I am very grateful to Prof. Thomas Roitsch for hosting me at the University of Copenhagen at the Department of Plant and Environmental Sciences. Thanks to Dr. Eric van der Graaff for his supervision and previous work on *AtBBE*-like transgenic plants. He gave me a comprehensive introduction in handling and cultivation of plants and I got the opportunity to study phenotyping of *Arabidopsis thaliana*. I want to thank Dr. Jozef Mravec for helping me with the phloroglucinol staining at the Section for Plant Glycobiology. Further, I would like to thank Prof. Catherine Lapierre (Institute Jean-Pierre Bourgin, France) for a detailed lignin analysis by thioacidolysis.

During my PhD thesis, I spend most of my time at the Institute of Biochemistry. I want to thank the whole working group, especially my lab colleague, Dr. Peter Augustin, for helping and creating an amazing working atmosphere. Further, many thanks go to Dr. Karlheinz Grillitsch for his help, motivation and above all for his friendship. He really influenced my everyday work positively.

Last but not least, I want to express my gratitude to my family. I want to thank my parents for their love and constant support and I am deeply grateful to my husband, Günter, for being on my side during the last years, for his love and his endless patience. Thank you for your understanding and your help, without it would not have been possible to finish my thesis. I am infinitely grateful for my daughter Emma and for the wonderful days since she has been with me.

Abstract

Biological oxidations play an essential role in life and are involved in a variety of different metabolic pathways. The plant kingdom harbors a large number of proteins catalyzing oxidative reactions and among them is a very interesting family, the berberine bridge enzyme-like (BBE-like) superfamily (Pfam 08031). The BBE-like superfamily belongs to the FAD-linked oxidases (SCOPE d.58.32), which exhibit a characteristic feature, the typical fold of vanillyl-alcohol oxidase (VAO-fold) possessing a FAD and a substrate binding domain. A well-known representative among the BBE-like enzymes in plants is the berberine bridge enzyme from California poppy (*Eschscholzia californica*), which is a branch-point enzyme in the benzyloquinoline alkaloid biosynthesis and possesses a bicovalently attached FAD cofactor with the characteristic 6-S-cysteinyl-, 8 α -N1-histidyl-FAD linkage.

In the first section of my work, *EcBBE* variants G164A, V169I and G164AV169I were successfully generated and produced in *Komagataella phaffii* to analyze the oxygen reactivity. A specific oxygen binding pocket was identified on the *re*-side of the FAD cofactor opposite to the substrate binding pocket and the gatekeeper amino acid residue isoleucine controls oxygen access and reactivity. The oxidase *EcBBE* was compared with a further BBE-like enzyme member, the grass pollen allergen Phl p 4, which possesses glucose dehydrogenase activity. An inverse exchange of a valine in the oxidase *EcBBE* to the gatekeeper residue isoleucine resulted in a decrease of O₂ reactivity by a factor of 500 and led to the conversion into a dehydrogenase. The substitution of a glycine at the gatekeeper position of *EcBBE* with an alanine had a slightly stronger effect on oxygen reactivity. The analysis of the double variant revealed no significantly stronger influence.

The biochemical function of many BBE-like enzymes in the plant kingdom is still unexplored. Therefore, we chose the BBE-like protein family of *Arabidopsis thaliana* to broaden our understanding of BBE-like enzymes in plants. The genome of *A. thaliana* contains 27 genes encoding for BBE-like proteins, and the main objective of the presented thesis was the biochemical characterization of *AtBBE*-like protein 13 and the investigation of the *in planta* function mainly of *AtBBE*-like protein 13, 15 and 26. *AtBBE*-like protein 15 was previously identified as a monolignol oxidoreductase, and the same function was shown for *AtBBE*-like protein 13. Both enzymes catalyze the oxidation of monolignols, the building blocks of lignin, to the corresponding aldehydes, suggesting a role in monolignol metabolism and lignin formation. Analysis of the active site composition by multiple sequence alignments revealed four different active site types, which appeared frequently in *A. thaliana* but also in the whole Brassicaceae family. Thirteen BBE-like proteins in *A. thaliana* show active site type I, which

has been described for monolignol oxidoreductases. A detailed sequence analysis of specific amino acid residues at the substrate binding pocket led to the discovery of another monolignol oxidoreductase, *AtBBE*-like protein 26.

Due to the fact that the physiological function of *AtBBE*-like enzymes is largely unknown, we decided to study the phenotype of T-DNA insertional mutant lines, mainly for monolignol oxidoreductases. Seedlings from putative loss-of function mutants for *AtBBE*-like protein 13 and 15 showed developmental defects *in vitro* under salt stress compared to wild type. The increased salt sensitivity of *Atbbe*-like protein 13 mutants could be confirmed in experiments with soil-grown plants. Moreover, we were able to engineer a putative double mutant for *AtBBE*-like protein 13 and 15, and first salt stress experiments on soil indicated at least the same phenotype as for *Atbbe*-like protein 13. Another important part of this project was a detailed lignin analysis of the putative *Atbbe*-like protein 13 and 15 mutant plants. Thioacidolysis showed a lower aldehyde content and a reduction of the total lignin amount, suggesting a role of monolignol oxidoreductases in providing extracellular aldehydes for the subsequent polymerization of lignin.

A further objective was the physiological investigation of *AtBBE*-like protein 28. The oxidase *AtBBE*-like protein 28 features a novel active site composition with a mono-covalent instead of a bi-covalent FAD tethering. Multiple sequence alignments showed that *AtBBE*-like protein 28 exhibits an active site type II, which only occurs in Brassicaceae. First phenotyping experiments of a putative *AtBBE*-like protein 28 loss-of-function mutant showed a 10% reduction of biomass under standard growth conditions on soil, and *in vitro* salt stress experiments showed a reproducible phenotype with a significantly lower number of healthy green seedlings compared to wild type. The phenotype observed in putative *Atbbe*-like protein 13, 15 and 28 mutants indicates a role of these proteins in salt stress response.

Kurzfassung

Biologische Oxidationen spielen eine wichtige Rolle in unserem Leben und sind an den verschiedensten Stoffwechselwegen beteiligt. Das Pflanzenreich umfasst eine Vielzahl an Proteinen, die solche oxidativen Reaktionen katalysieren und unter denen es eine große interessante Familie, die *berberine bridge enzyme-like* (BBE-like) Superfamilie (Pfam 08031), gibt. Die BBE-like Superfamilie gehört zu den FAD-verknüpften Oxidasen (SCOPE d.58.32), die ein charakteristisches Merkmal aufweisen, die typische Vanillyl-Alkohol Oxidase Faltung (VAO-Faltung) mit einer FAD- und Substrat-Bindedomäne. Ein bekannter Vertreter innerhalb der BBE-like Enzyme in Pflanzen ist das *berberine bridge enzyme* aus dem kalifornischen Mohn (*Eschscholzia californica*), welches an der Benzylochinolinalkaloid-Biosynthese beteiligt ist und einen bikoalent verknüpften FAD Kofaktor mit der charakteristischen 6-S-Cysteinylierung und 8 α -N1-Histinylierung aufweist.

Im ersten Abschnitt meiner Arbeit wurden die *EcBBE* Varianten G164A, V169I und G164AV169I erfolgreich generiert und in *Komagataella phaffii* hergestellt, um die Sauerstoffreaktivität zu analysieren. Eine spezifische Sauerstoffbindetasche wurde an der *re*-Seite des FAD Kofaktors, gegenüber der Substratbindetasche, identifiziert. Die Aminosäure Isoleucin weist hier eine Schrankenfunktion auf, indem sie den Zugang sowie die Reaktivität mit Sauerstoff kontrolliert. Die Oxidase *EcBBE* wurde mit einem weiteren Mitglied der BBE-like Enzyme verglichen, dem Pollen Allergen Phl p 4 aus Gräsern, welches Glucose Dehydrogenase Aktivität aufweist. Der Austausch eines Valins mit der Schrankenaminoäure Isoleucin in der Oxidase *EcBBE* verursachte eine Abnahme der O₂ Reaktivität um einen Faktor von 500 und führte zu einer Dehydrogenase. Der Austausch eines Glycins mit einem Alanin an der Schrankenposition in *EcBBE* hatte einen etwas stärkeren Einfluss auf die Sauerstoffreaktivität. Die Doppelmutante hingegen zeigte keinen signifikant stärkeren Einfluss.

Viele biochemische Funktionen der BBE-like Enzyme im Pflanzenreich sind immer noch unerforscht. Daher haben wir beschlossen unser Verständnis anhand der BBE-like Proteinfamilie in der Acker-Schmalwand (*Arabidopsis thaliana*) zu erweitern. Das Genom der Acker-Schmalwand umfasst 27 Gene, die für BBE-like Proteine codieren. Das Hauptziel dieser Doktorarbeit war die biochemische Charakterisierung von *AtBBE-like* Protein 13 sowie die Erforschung der pflanzlichen Funktionen hauptsächlich von *AtBBE-like* Protein 13, 15 und 26. *AtBBE-like* Protein 15 wurde bereits zuvor als Monolignoloxidoreduktase identifiziert und dieselbe Funktion konnte für *AtBBE-like* Protein 13 gezeigt werden. Beide Enzyme oxidieren Monolignole, die Bausteine des Lignins, zu den korrespondierenden Aldehyden was auf eine Rolle im Monolignolmetabolismus und in der Bildung von Lignin hinweist. Sequenzvergleiche

des aktiven Zentrums ergaben vier unterschiedlich häufig auftretende Typen des aktiven Zentrums, einerseits in der Acker-Schmalwand aber auch in der gesamten Familie Brassicaceae. In dreizehn BBE-like Proteine der Acker-Schmalwand zeigte sich der Typ I des aktiven Zentrums, welcher für Monolignoloxidoreduktasen beschrieben wurde. Eine detaillierte Sequenzanalyse der spezifischen Aminosäuren an der Substratbindetasche ergab eine weitere Monolignoloxidoreduktase, *AtBBE*-like Protein 26.

Aufgrund der Tatsache, dass die physiologischen Funktionen der *AtBBE*-like Enzyme weitgehend unbekannt sind, entschlossen wir uns zur Phänotypisierung von T-DNA Insertions-Linien, hauptsächlich von Monolignoloxidoreduktasen. Keimlinge von mutmaßlichen Funktionsverlustmutanten von *AtBBE*-like Protein 13 und 15 zeigten *in vitro* stärkere Entwicklungsstörungen bei Salzstress verglichen mit dem Wild Typ. Eine höhere Salzsensitivität der *Atbbe*-like Protein 13 Mutante konnte auf Erde bestätigt werden. Außerdem konnten wir eine mutmaßliche Doppelmutante von *AtBBE*-like protein 13 und 15 generieren und erste Salzstressexperimente auf Erde zeigten immerhin denselben Phänotyp wie *Atbbe*-like Protein 13 Pflanzen. Ein weiterer wichtiger Teil dieser Arbeit bildet die detaillierte Ligninanalyse der mutmaßlichen Mutanten *Atbbe*-like Protein 13 und 15. Thioacidolyse ergab einen geringeren Aldehyd Gehalt sowie eine Reduktion des gesamten Lignins, was auf eine Rolle der Monolignoloxidoreduktasen in der Bereitstellung extrazellulärer Aldehyde schließen lässt, welche für die anschließende Polymerisation von Lignin benötigt werden.

Ein weiteres Ziel war die physiologische Untersuchung von *AtBBE*-like Protein 28. Die Oxidase *AtBBE*-like Protein 28 besitzt eine neuartige Zusammensetzung des aktiven Zentrums und hat eine mono-kovalente anstatt einer bi-kovalenten FAD Verknüpfung. Multiple Sequenzvergleiche zeigten, dass *AtBBE*-like Protein 28 den aktiven Zentrum Typ II aufweist, welcher nur in Brassicaceae zu finden ist. Eine erste Phänotypisierung der *Atbbe*-like Protein 28 Mutante ergab eine 10% Reduktion der Biomasse bei normalen Wachstumsbedingungen auf Erde. Salzstress Experimente *in vitro* zeigten einen reproduzierbaren Phänotyp mit einer signifikant geringeren Anzahl an grünen Keimlingen verglichen mit dem Wild Typ. Der beobachtete Phänotyp der *Atbbe*-like Protein 13, 15 und 28 Mutanten weist auf eine Rolle dieser Proteine in der Salzstressantwort hin.

EIDESSTATTLICHE ERKLÄRUNG

Ich erkläre an Eides statt, dass ich die vorliegende Arbeit selbständig verfasst, andere als die angegebenen Quellen/Hilfsmittel nicht benutzt, und die den benutzten Quellen wörtlich und inhaltlich entnommene Stellen als solche kenntlich gemacht habe.

STATUTORY DECLARATION

I declare that I have authored this thesis independently, that I have not used other than the declared sources/resources, and that I have explicitly marked all material which has been quoted either literally or by content from the used sources.

Graz,

.....

Table of Contents

ACKNOWLEDGMENTS	III
ABSTRACT	V
KURZFASSUNG	VII
STATUTORY DECLARATION	IX
TABLE OF CONTENTS	XI
CHAPTER 1	1
1. RATIONALLY ENGINEERED FLAVIN-DEPENDENT OXIDASE REVEALS STERIC CONTROL OF DIOXYGEN REDUCTION	2
1.1. Abstract.....	3
1.2. Introduction	4
1.3. Results	8
1.3.1. Biochemical characterization of the BBE and Phl p 4 variants.....	8
1.3.2. Structural features of the variants and crystallographic experiments with surrogates ..	10
1.3.3. Dioxygen reaction mechanism and putative transition states	13
1.4. Discussion.....	15
1.4.1. Towards a unifying concept of dioxygen reactivity in flavoenzymes	17
1.4.2. Possible mechanisms of dioxygen reactivity.....	20
1.5. Conclusion	21
1.6. Experimental Procedures	22
1.6.1. Reagents	22
1.6.2. Cloning, expression and purification.....	22
1.6.3. Transient Kinetics.....	22
1.6.4. Reductive half-reaction	23
1.6.5. Oxidative half-reaction	23
1.6.6. Redox potential determination	23
1.6.7. Crystallization, data collection and structural characterization	23
1.7. References	25
CHAPTER 2	29
2. OXIDATION OF MONOLIGNOLS BY MEMBERS OF THE BERBERINE BRIDGE ENZYME FAMILY SUGGESTS A ROLE IN PLANT CELL WALL METABOLISM	30
2.1. Abstract.....	31
2.2. Introduction	32

2.3. Experimental Procedures	35
2.3.1. Chemicals	35
2.3.2. Molecular cloning.....	35
2.3.3. Protein expression and purification.....	35
2.3.4. Site-directed mutagenesis: Generation of the L182V variant.....	36
2.3.5. Crystallization	36
2.3.6. Data collection and processing	37
2.3.7. Thermofluor experiments	37
2.3.8. Rapid reaction kinetics using stopped flow spectrophotometry	38
2.3.9. Product identification	38
2.3.10. Synthesis of monolignol glycosides	39
2.3.11. Phylogenetic tree construction	39
2.3.12. Docking	39
2.4. Results	40
2.4.1. Enzymatic properties and identification of substrates of <i>AtBBE</i> -like 13 and <i>AtBBE</i> -like 15.....	40
2.4.2. Crystal structure of <i>AtBBE</i> -like 15.....	42
2.4.3. Docking of substrates to the active site	45
2.4.4. Functional and structural characterization of the BBE-like family in <i>A. thaliana</i>	46
2.5. Discussion.....	51
2.5.1. Catalytic mechanism of monolignol oxidation.....	51
2.5.2. Structural comparison with other members of the VAO family.....	51
2.5.3. Proposed role of <i>AtBBE</i> -like15/monolignol oxidoreductases in plants	54
2.6. References	56
2.7. Supplementary Information	60
CHAPTER 3	67
3. STRUCTURE OF A BERBERINE BRIDGE ENZYME-LIKE ENZYME WITH AN ACTIVE SITE SPECIFIC TO THE PLANT FAMILY BRASSICACEAE.....	68
3.1. Abstract.....	69
3.2. Introduction	70
3.3. Results	72
3.3.1. Structural characterization of <i>AtBBE</i> -like 28.....	72
3.3.2. Biochemical characterization	75
3.3.3. Sequence comparison and phylogenetic inference.....	78
3.3.4. Active site type distribution of BBE-like enzymes	82
3.4. Discussion.....	84

3.4.1.	The active site type II	84
3.4.2.	Oxygen reactivity of <i>At</i> BBE-like 28	85
3.4.3.	Comparison of <i>At</i> BBE-like to another BBE-like protein: Phl p 4.....	86
3.4.4.	Analysis of the phenotype of the <i>At</i> BBE-like 28 loss-of-function mutant	87
3.5.	Experimental Procedures	88
3.5.1.	Cloning and transformation	88
3.5.2.	Expression and purification	88
3.5.3.	Crystallization and crystal structure determination	89
3.5.4.	Redox potential determination	92
3.5.5.	Photoreduction.....	92
3.5.6.	Determination of the oxidative rate	92
3.5.7.	Plant growth experiments	92
3.5.8.	Phylogenetic analysis	93
3.6.	References	94
3.7.	Supplementary Information	98
CHAPTER 4	105
4.	THE FAMILY OF BERBERINE BRIDGE ENZYME-LIKE ENZYMES: A TREASURE-TROVE OF OXIDATIVE REACTIONS	106
4.1.	Abstract.....	107
4.2.	Introduction	108
4.3.	Structural characteristics of BBE-like proteins	109
4.3.1.	Differentiation from other families of FAD-linked oxidases	109
4.3.2.	Bi-covalent attachment of the flavin cofactor via His and Cys residues	112
4.3.3.	The reactivity of BBE-like enzymes with oxygen.....	113
4.3.4.	Protein-substrate interactions in BBE-like proteins	114
4.3.5.	Occurrence and development of the BBE-like protein family	116
4.3.6.	BBE-like proteins in bacteria	118
4.3.7.	BBE-like proteins in fungi.....	118
4.3.8.	BBE-like proteins in plants	118
4.4.	Reactions catalyzed by BBE-like enzymes	120
4.4.1.	Reactions catalyzed by BBE-like enzymes from plants: alkaloid and cannabinoid biosynthesis	120
4.4.2.	Reactions catalyzed by BBE-like enzymes from plants: alcohol oxidation	124
4.4.3.	Reactions of BBE-like proteins from bacteria.....	127
4.4.4.	BBE-like enzymes from fungi.....	132
4.5.	Outlook	135

4.6. References	137
4.7. Supplementary Information	144
CHAPTER 5	151
5. BERBERINE BRIDGE ENZYME-LIKE PROTEINS IN <i>ARABIDOPSIS THALIANA</i> PARTICIPATE IN MONOLIGNOL METABOLISM AND STRESS RESPONSE	152
5.1. Abstract.....	152
5.2. Introduction	153
5.2.1. Occurrence and function of BBE-like proteins in the plant kingdom	154
5.2.2. Catalytic and physiological function of BBE-like enzymes in plants	155
5.3. Experimental Procedures	159
5.3.1. Plant materials and growth conditions.....	159
5.3.2. Construction of GUS reporter transgenic plants.....	160
5.3.3. Construction of <i>AtBBE</i> -like overexpression transgenic plants	162
5.3.4. Salt stress experiments on plates and soil.....	162
5.3.5. Drought stress experiments on PEG-infused plates	164
5.3.6. Root length and shoot weight experiments on plates under salt stress.....	165
5.3.7. Preliminary test of quantitative RT-PCR (qRT-PCR) analysis under salt stress.....	165
5.3.8. Histochemical staining to visualize lignin.....	166
5.3.9. Lignin quantification with acetyl bromide method	166
5.3.10. Root growth phenotyping of transgenic <i>Atbbe</i> -like protein 28 seedlings.....	167
5.3.11. Lignin analysis by thioacidolysis and gas chromatography-mass spectrometry (GC-MS).....	168
5.3.12. Statistical analysis	170
5.4. Results	171
5.4.1. Tolerance of putative <i>Atbbe</i> -like protein mutants to salt and drought stress.....	171
5.4.2. Root length and shoot weight of putative <i>Atbbe</i> -like protein mutants under salt stress....	202
5.4.3. Lignin content of <i>Atbbe</i> -like protein 13 and 15 mutant cell walls determined by the acetyl bromide method	206
5.4.4. Lignin composition analysis of <i>Atbbe</i> -like protein 13 and 15 mutant cell walls by thioacidolysis and Gas Chromatography-Mass Spectrometry (GC-MS)	207
5.4.5. <i>Atbbe</i> -like protein 15 gene expression under salt stress analyzed by qRT-PCR.....	209
5.4.6. Root apical meristem and root diameter of putative <i>Atbbe</i> -like protein 28 mutant seedlings	209
5.4.7. Status of GUS-reporter and 35S transgenic <i>AtBBE</i> -like lines.....	211
5.4.8. Wiesner staining to detect lignin in stem sections of transgenic <i>Atbbe</i> -like protein 13 and 15 lines.....	211

5.5. Discussion.....	216
5.5.1. Phenotype analysis of putative <i>AtBBE</i> -like loss-of-function mutants under osmotic stress	216
5.5.1.1. Phenotype of a putative <i>Atbbe</i> -like protein 13 mutant	218
5.5.1.2. Phenotype of a putative <i>Atbbe</i> -like protein 15 mutant	218
5.5.1.3. Phenotype of a putative <i>Atbbe</i> -like protein 13*15 double mutant.....	219
5.5.1.4. Phenotype of a putative <i>Atbbe</i> -like protein 26 mutant	219
5.5.1.5. Drought stress response of the putative <i>Atbbe</i> -like protein 13, 15, 13*15 and 26 mutants.....	220
5.5.1.6. Phenotyping of a putative <i>Atbbe</i> -like protein 28 mutant	221
5.5.2. Role of <i>AtBBE</i> -like proteins in monolignol metabolism of <i>Arabidopsis thaliana</i>	222
5.6. Conclusion and Outlook	225
5.7. New Insights	226
5.8. References	231
5.9. Supplementary Information	237
LIST OF ABBREVIATIONS.....	253
CURRICULUM VITAE	257

CHAPTER 1

Rationally engineered flavin-dependent oxidase reveals steric control of dioxygen reduction

Author contributions

Information and results regarding the *EcBBE* variants G164A, V169I and G164A V169I are summarized in the following chapter 1. Dr. Domen Zafred initiated the project and he started with the investigation of a BBE-like gene in Timothy grass (*Phleum pratense*), termed Phl p 4. He designed and expressed Phl p 4 variants, Phl p 4 N158H, Phl p 4 I153V, Phl p 4 I153V N158H, successfully in *Komagataella phaffii* and he characterized these variants biochemically. I performed the studies on the *EcBBE* variants G164A, V169I and G164A V169I, which I expressed in *Komagataella phaffii*, purified and enzymatically characterized together with my colleague Dr. Silvia Wallner. I determined kinetic parameters, oxidative and reductive rates, redox potential and the catalytic turnover numbers, of *EcBBE* variants using a stopped-flow device and HPLC. Crystal structures were elucidated and described by Dr. Domen Zafred.

Chapter 1

1. Rationally engineered flavin-dependent oxidase reveals steric control of dioxygen reduction

Domen Zafred,^{1,2} Barbara Steiner,¹ Andrea R. Teufelberger,^{2‡} Altijana Hromic,² P. Andrew Karplus,³ Christopher J. Schofield,⁴ Silvia Wallner¹ and Peter Macheroux¹

¹ Institute of Biochemistry, Graz University of Technology, A-8010 Graz, Austria.

² Institute of Molecular Biosciences, University of Graz, A-8010 Graz, Austria.

³ Department of Biochemistry and Biophysics, Oregon State University, Oregon 97331, U.S.A.

⁴ Chemistry Research Laboratory, Department of Chemistry, University of Oxford, Oxford, OX1 3TA, United Kingdom.

[‡] Present address: University Hospital Ghent, Ghent University, De Pintelaan 185, 9000 Ghent, Belgium.

To whom correspondence should be addressed: Domen Zafred, Institute of Biochemistry, Graz University of Technology, Petersgasse 12/II, A-8010 Graz, Austria, Tel.: +43-699-1007 8283, Fax.: +43-316-873 6952; Email: zafred.domen@gmail.com

This chapter was published in the FEBS Journal:

Zafred, D. *et al.* (2015) Rationally engineered flavin-dependent oxidase reveals steric control of dioxygen reduction. *FEBS J* 282, 3060–3074.

Author contributions

S.W., B.S., A.H. expressed, purified and enzymatically characterized BBE variants. D.Z., S.W., A.R.T. expressed, purified and enzymatically characterized Phl p 4 variants. D.Z. designed research, crystallized and structurally characterized proteins, prepared figures. Manuscript was written by D.Z., P.M., S.W., P.A.K., C.J.S

1.1. Abstract

The ability of flavoenzymes to reduce dioxygen varies greatly, and is controlled by the protein environment, which may cause either a rapid reaction (oxidases) or a sluggish reaction (dehydrogenases). Previously, a “gatekeeper” amino acid residue was identified that controls the reactivity to dioxygen in proteins from the vanillyl alcohol oxidase superfamily of flavoenzymes. We have identified an alternative gatekeeper residue that similarly controls dioxygen reactivity in the grass pollen allergen Phl p 4, a member of this superfamily that has glucose dehydrogenase activity and the highest redox potential measured in a flavoenzyme. A substitution at the alternative gatekeeper site (I153V) transformed the enzyme into an efficient oxidase by increasing dioxygen reactivity by a factor of 60 000. An inverse exchange (V169I) in the structurally related berberine bridge enzyme (BBE) decreased its dioxygen reactivity by a factor of 500. Structural and biochemical characterization of these and additional variants showed that our model enzymes possess a cavity that binds an anion and resembles the “oxyanion hole” in the proximity of the flavin ring. We showed also that steric control of access to this site is the most important parameter affecting dioxygen reactivity in BBE-like enzymes. Analysis of flavin-dependent oxidases from other superfamilies revealed similar structural features, suggesting that dioxygen reactivity may be governed by a common mechanistic principle.

1.2. Introduction

Flavin-dependent enzymes catalyze redox reactions ranging from oxidations of alcohols, aldehydes and amines, to mono-oxygenation, halogenation, complex bond formation and cyclization reactions [1–3]. Flavoenzymes that use dioxygen as an electron acceptor may function as oxidases, reducing oxygen to hydrogen peroxide, or as mono-oxygenases, splitting the molecule such that one oxygen atom is incorporated into a hydroxylated product and the other into water. Kinetically, transfer of the first electron to dioxygen appears to be the rate-limiting step in the process (Fig. 1), and while free reduced flavin in solution reacts relatively slowly with dioxygen, flavin-bound proteins may decelerate or accelerate this reaction substantially, spreading its rate over six orders of magnitude [4,5].

A flavin-(4a)-hydroperoxide adduct has been characterized in FAD-dependent mono-oxygenases [6], and recent studies of dioxygen activation have shed light on the mechanism of dioxygen utilization in these enzymes [7,8]. Based on the occurrence of the flavin-(4a)-adduct, the reactive carbon atom has been accepted as the site of electron transfer in reaction with dioxygen in flavoenzymes, however, the resulting hydroperoxide intermediate has never been observed in flavin-dependent oxidases (Fig. 1) [5,9]. While recent characterizations of single-atom adducts suggested that the flavin-(4a)-hydroperoxy adduct is a likely intermediate in some flavin dependent oxidases [10,11], there is evidence that the reaction might also proceed without formation of this adduct [12,13].

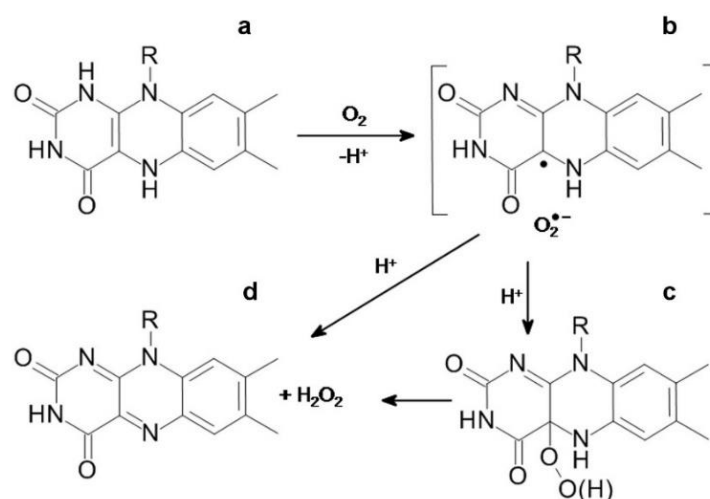


Fig. 1. Oxidative half-reaction of flavoenzyme oxidases. First electron transfer in the reaction of a reduced FAD (a) with an oxygen molecule is the rate-limiting step that yields a radical pair (b) [4]. The pair may form a covalent bond to produce hydroperoxy adduct (c), the intermediate found in monooxygenases that has an sp³ hybridized C(4a) atom, and subsequent elimination of the hydrogen peroxide yields oxidized FAD (d). Alternatively, the second electron transfer may take place without a bond formation [4].

In recent years, several studies have provided insights into the specific roles of certain residues in flavoenzymes. Model proteins have been used to identify putative oxygen channels, influences of substrate and inhibitor binding, and altered flavin redox potentials [5,9,14]. Active-site residues, such as histidine H516 in the proximity of FAD in glucose oxidase (PDB ID 1GPE) [15] or the conserved lysine in the proximity of N(5) in fructosamine oxidase (PDB ID 3DJE) and monomeric sarcosine oxidase (PDB ID 1L9E), have suggested an important role of a positively charged amino acid residue in regulating the dioxygen reactivity of reduced flavins [16–18]. Despite this progress, it is still questionable whether there is a common catalytic principle that governs the reactivity of the reduced flavin toward dioxygen.

The vanillyl alcohol oxidase (VAO) structural superfamily, which is also referred to as the *p*-cresol methylhydroxylase (PCMH) structural superfamily, includes FAD-dependent hydroxylases, oxidases and dehydrogenases, most of which employ a mono- or bicovalently bound cofactor [19,20]. These enzymes have a two-domain structure, with the cofactor buried in the FAD-binding domain and the redox-active isoalloxazine ring oriented with its *si*-face towards the active site cavity, where substrate binding is organized by the substrate-binding domain [21,22]. The *re*-face of the FAD is surrounded by a conserved 18-residue segment of chain that we refer to as the “oxygen reactivity motif”, which creates the environment of the isoalloxazine ring above the C(4a) reactive carbon atom. This motif contains what was described by Leferink *et al.* [23] as the “gatekeeper” residue, at a position suitable for the control of dioxygen reactivity in the VAO superfamily. In their model enzyme L-galactono- γ -lactone dehydrogenase (GALDH), replacement of a gatekeeper alanine with glycine (A113G) increased oxygen reactivity 400-fold. The correlation in the VAO superfamily was not perfect, as seven of the 30 oxidases listed in their study (see their supplementary Table 1) had an alanine or a proline at the gatekeeper position, suggesting that there are additional complexities that define oxidase activity in the superfamily.

In the present study, we have further investigated the control of oxygen reactivity in the VAO superfamily by using the berberine bridge enzyme (BBE, EC 1.21.3.3) and the BBE-like protein pollen allergen Phl p 4 as models. BBE-like enzymes are a sub-group of the VAO/PCMH superfamily, classified as pfam08031 (superfamily cl06869) in the Conserved Domain Database [24]. BBE from the California poppy (*Eschscholzia californica*) catalyzes the oxidative cyclization of (*S*)-reticuline to (*S*)-scoulerine by formation of a carbon-carbon bond, the berberine bridge [25]. Phl p 4 from Timothy grass (*Phleum pratense*) shows extensive similarity to BBE (34% sequence identity), and has a similar overall topology (the RMSD of aligned C α atoms is 1.53 Å) and a conserved bicovalent linkage of the FAD [22]. Despite these

structural similarities, Phl p 4 does not catalyze carbon-carbon bond formation, but instead oxidizes D-glucose. In contrast to BBE and other previously characterized BBE-like enzymes, reduced Phl p 4 reacts sluggishly with dioxygen, suggesting that the FAD cofactor is reoxidized by an alternative electron acceptor *in vivo*. In other words, Phl p 4 behaves like a dehydrogenase rather than an oxidase, despite having glycine at the gatekeeper position. As this is a feature common to all known BBE-like enzymes [26], the gatekeeper identified by Leferink *et al.* does not explain suppressed oxygen reactivity of Phl p 4 and we sought to find a novel structural feature.

Closer inspection of the active sites of BBE and Phl p 4 revealed that, while the position of FAD and the topology of the protein backbone are highly conserved, this is not the case for several amino acid side chains near the isoalloxazine ring, such as H459/Y439 on the *si*-face or H174/N158 and V169/I153 on the *re*-face of BBE and Phl p 4, respectively (Fig. 2A). The backbone nitrogen of cysteine C166/C150 (the residue covalently attached at the flavin C6 position) is in a loop above the *re*-face of the flavin in BBE-like enzymes, and is too far away to interact with the isoalloxazine ring or any protein residue (e.g. by formation of a hydrogen bond, Fig. 2). In contrast, the backbone nitrogen of the preceding W165/V149 is within hydrogen bond distance of the C(4)=O carbonyl group. These two residues are oriented towards the *re*-face of the flavin, and placed adjacent to a small cavity that is positioned above the C(4a) carbon atom and lined by the side chains of V169, H174 and L145 in BBE (Fig. 2). This small cavity, with nearby partial positively charged backbone nitrogens available for hydrogen bonding, is reminiscent of the “oxyanion hole” observed in certain hydrolases [27], and is potentially able to bind oxygen in BBE-like oxidases. Here we refer to it as an “oxygen pocket”, a term that was introduced by Lindqvist *et al.* for a similar structural feature described in glycolate oxidase [28]. Interestingly, the oxygen pocket does not exist in Phl p 4 because the C δ methyl group of I153 projects towards the C(4a) and fills the cavity (Fig. 2B).

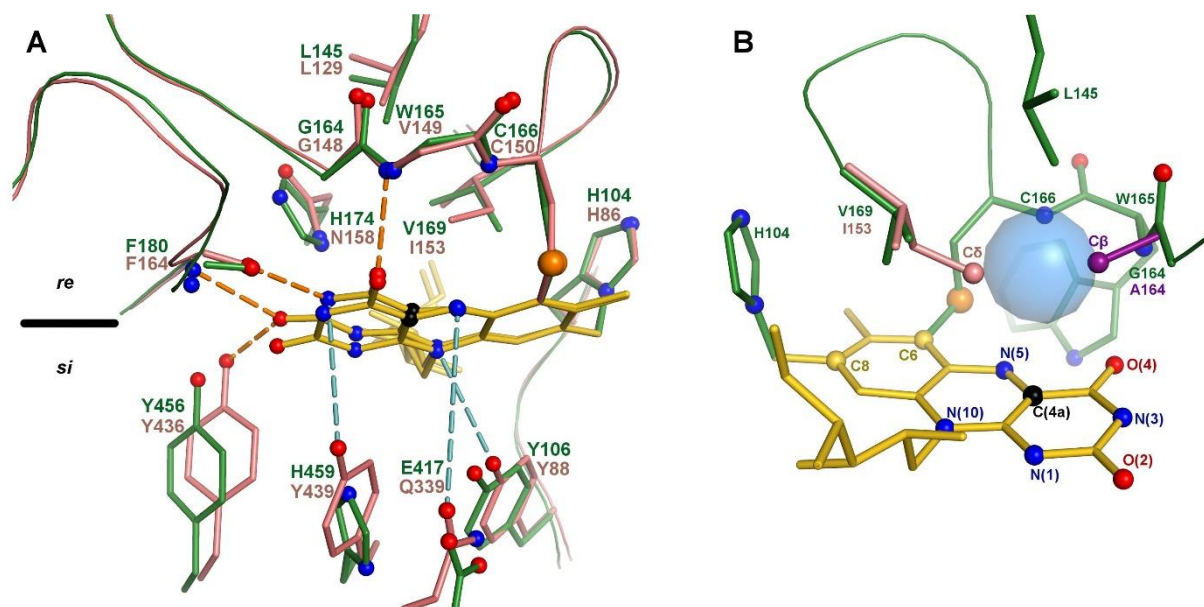


Fig. 2. BBE and Phl p 4 active sites. (A) Aligned structures of wild-type BBE (PDB ID 3D2H, green) and Phl p 4 (PDB ID 4PVE, pink) in the proximity of FAD (yellow). Three atoms from the isoalloxazine ring are used for 3D alignment of proteins throughout this paper: C(6), C(8) and N(10). Hydrogen bonds between flavin and the protein matrix are in orange; larger distances that correspond to weak interactions are shown in blue. The active sites are well conserved, with important exceptions: V169/I153 and H174/N158 on the *re*-face of the isoalloxazine ring and H459/Y439 and E417/Q339 on the substrate-binding *si*-face. (B) View of the *re*-face of the FAD in wild-type BBE in which a cavity (blue sphere) forms the oxygen pocket together with the backbone nitrogen atoms of C166 and W165, the proposed proton donors. The BBE G164A variant (PDB ID 4PZF, purple) and Phl p 4 (pink) are aligned to show how side chains of the alternative gatekeeper I169/I153 and the gatekeeper A164 eliminate the cavity by pointing towards the reactive C(4a) carbon atom (black).

Based on these considerations, we created a set of BBE (G164A, V169I and G164A V169I) and Phl p 4 variants (I153V, N158H and I153V N158H) to investigate the role of the side chains involved in shaping of the oxygen pocket formed by the oxygen reactivity motif on the *re*-face of the isoalloxazine ring. The Phl p 4 I153V variant had a remarkable 60 000-fold higher dioxygen reactivity compared to the wild-type enzyme, leading us to identify this position as an alternate gatekeeper residue that is crucial for the control of oxygen reactivity in BBE-like enzymes. These results not only make it possible to predict the oxygen reactivity of members of the BBE-like enzyme family, but, as we discuss, also have implications for other flavoenzyme families that appear to have an analogous oxygen pocket in the proximity of the reactive C(4a).

1.3. Results

1.3.1. Biochemical characterization of the BBE and Phl p 4 variants

All BBE and Phl p 4 variants were successfully expressed in *Komagataella pastoris* (formerly *Pichia pastoris*), and purified to homogeneity as described in Experimental Procedures. While BBE variants, wildtype Phl p 4 and Phl p 4 N158H were stable over longer periods of time, changes in the UV/Vis absorption spectrum of the Phl p 4 I153V single and I153V N158H double variant indicated slow formation of spirohydantoin during purification and storage [29].

Kinetic parameters were determined for the BBE and Phl p 4 variants, and the oxidative and reductive rates are summarized in Table 1. In the case of BBE, the single variants showed a similar rate constant (G164A) and a fivefold lower rate constant (V169I) for the reduction by its substrate (*S*)-reticuline. In contrast, the rate of re-oxidation of the reduced variants by dioxygen decreased by 500-1000-fold, from $\sim 50\,000$ to $\sim 50\text{ M}^{-1}\text{ s}^{-1}$, and did not decrease further in the double variant (Table 1).

Table 1. Kinetic data and redox potentials.

	$k_{\text{red}} [\text{s}^{-1}]$	$k_{\text{ox}} [\text{M}^{-1}\text{ s}^{-1}]$	$E_0 [\text{mV}]$	Oxygen reactivity motif
BBE wild-type ^a	103 ± 4	$(5 \pm 1) \cdot 10^4$	132 ± 4	163 AGWCPTVGTGGHISGGGF 180
BBE G164A	106 ± 13	60 ± 8	109 ± 3	163 AAWCPTVGTGGHISGGGF 180
BBE V169I	18.5 ± 1.4	98 ± 9	109 ± 2	163 AGWCPTIGTGGHISGGGF 180
BBE G164A V169I	0.04 ± 0.002	50 ± 3	110 ± 3	163 AAWCPTIGTGGHISGGGF 180
Phl p 4 wild-type	55 ± 1^b	1.3 ± 0.1	211 ± 2	147 AGVCPTVGVGGNFAGGGF 164
Phl p 4 N158H	108 ± 1^b	2.1 ± 0.4	208 ± 1	147 AGVCPTVGVGGHFAGGGF 164
Phl p 4 I153V	53 ± 3^b	$(7.1 \pm 0.2) \cdot 10^4$	205 ± 4	147 AGVCPTIGVGGNFAGGGF 164
Phl p 4 I153V N158H	85 ± 1^b	$(3.9 \pm 0.6) \cdot 10^4$	203 ± 1	147 AGVCPTIGVGGHFAGGGF 164
Free FADH ₂ /FAD	/	250^c	-209^d	
O ₂ /H ₂ O ₂	/	/	270^d	

^a Kinetic data taken from Winkler *et al.* [25].

^b k_{obs} at 1 mM glucose concentration.

^c Data taken from Massey [4].

^d Data taken from Mayhew [52].

Wild-type Phl p 4 and its three variants showed similar reactivity with glucose (Table 1), and no saturation was observed even at 10 mM glucose. In contrast to BBE, reduced wild-type Phl p 4 reacts with dioxygen at a rate of $1.2\text{ M}^{-1}\text{ s}^{-1}$, more than two orders of magnitude below that of free FAD ($250\text{ M}^{-1}\text{ s}^{-1}$). The N158H variant showed a similar rate of re-oxidation; however, both the single I153V and the I153V N158H double variant exhibited much higher rates of re-oxidation, with values of 7.1 and $3.9 \times 10^4\text{ M}^{-1}\text{ s}^{-1}$, respectively. Thus it is evident

that residue I153 plays a major role in controlling dioxygen reactivity in Phl p 4, and the I153V residue exchange very effectively converted this dehydrogenase into an oxidase by increasing its dioxygen reactivity more than four orders of magnitude (Table 1).

Bivalent modification of the isoalloxazine ring contributes to the positive redox potential found in BBE and other flavoproteins of the VAO superfamily [25,30], and, because this may play a role in reactivity, we measured the redox potentials of the various enzyme forms. The three BBE variants exhibited redox potentials of $\sim +110$ mV, which is comparable to that of the wild-type enzyme ($E_0 = 132$ mV, Table 1). Wild-type Phl p 4 and its variants had redox potentials in the range of $+200$ mV, approaching the O_2/H_2O_2 redox couple (270 mV), and roughly 400 mV more positive than the redox potential of free FAD (Fig. 3 and Table 1).

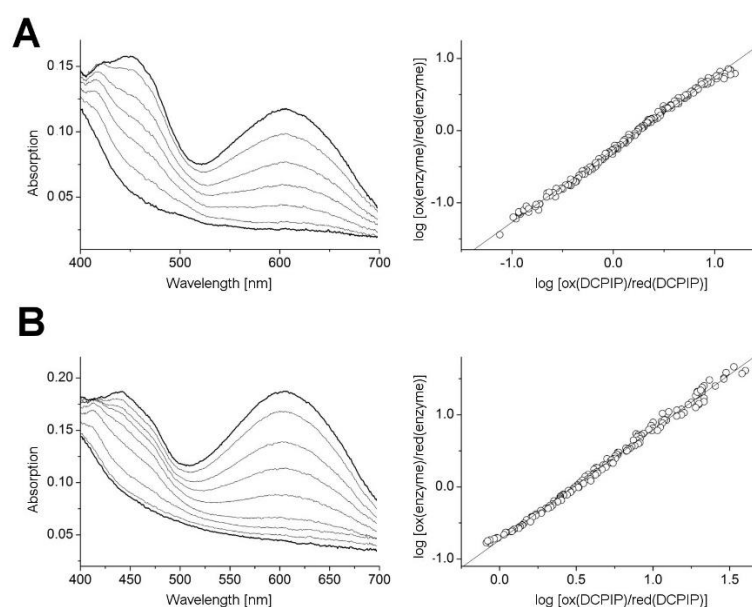


Fig. 3. Redox potential determination. Plots of selected spectra of the course of reduction are shown for wild-type Phl p 4 (A) and the double mutant Phl p 4 I153V N158H (B). The double logarithmic plots were used in the evaluation of data as described by Minnaert [47].

1.3.2. Structural features of the variants and crystallographic experiments with surrogates

Intrigued by the strong effects of the V169I and G164A exchanges in BBE and the I153V substitution in Phl p 4, we solved a set of crystal structures at 1.3-2.3 Å resolution (Table 2) to obtain insight into the structural changes that affect the properties of the variants. Overall, the structures determined for Phl p 4 variants were virtually superimposable with the respective wild-type structure, and no structural perturbations were observed. The I153V exchange in Phl p 4 creates space at the *re*-face of the isoalloxazine ring, resulting in formation of a pocket similar to that in wild-type BBE. In the latter, the oxygen pocket is removed by replacement of the glycine in the gatekeeper position with an alanine, i.e. G164A, in which the C β of the alanine side chain protrudes towards the FAD and pushes the isoalloxazine ring slightly in the direction of the *si*-face (Fig. 2B). While the structure of the BBE V169I mutant was not determined, it is reasonable to expect that the extra methyl group fills the cavity, analogously to the wild-type Phl p 4. Thus it appears that the key structural difference between wild-type BBE and Phl p 4 involved in control of oxygen reactivity concerns the existence of an oxygen pocket in the proximity of the reactive C(4a) carbon atom (Fig. 2).

Xenon pressurization experiments using crystals of Phl p 4 I153V yielded a structure with two xenon atoms located in hydrophobic pockets of the FAD-binding domain, but not in the proximity of the isoalloxazine ring (Fig. 4A and Table 2). It has been shown for other flavoproteins oxidases that halide ions may be used as a surrogate for locating putative oxygen-binding sites [31], and when halide ions were used in our crystal soaking experiments, an ion at low occupancy was observed in the engineered oxygen pocket of Phl p 4 variants I153V and I153V N158H, with the best results being obtained for sodium bromide and the Phl p 4 I153V N158H (Fig. 4 and Table 2). The presence of the halide ion at this site was confirmed by an anomalous difference map, and the ion was fitted into the F_o-F_c difference electron density peak. This anion bound in the oxygen pocket is positioned ~ 2.5 Å above the C(4a) atom on the *re*-face, and ~ 3.6 Å away from the C γ -methyl of V153 (Fig. 4B). The ion is stabilized by the backbone amide nitrogens of C150 and V149 at a distance of ~ 3.4 Å. Superposition of this structure with the structure of wild-type Phl p 4 shows that ion binding is not feasible in the wild-type enzyme due to a clash with C δ atom of I153 (Fig. 4B).

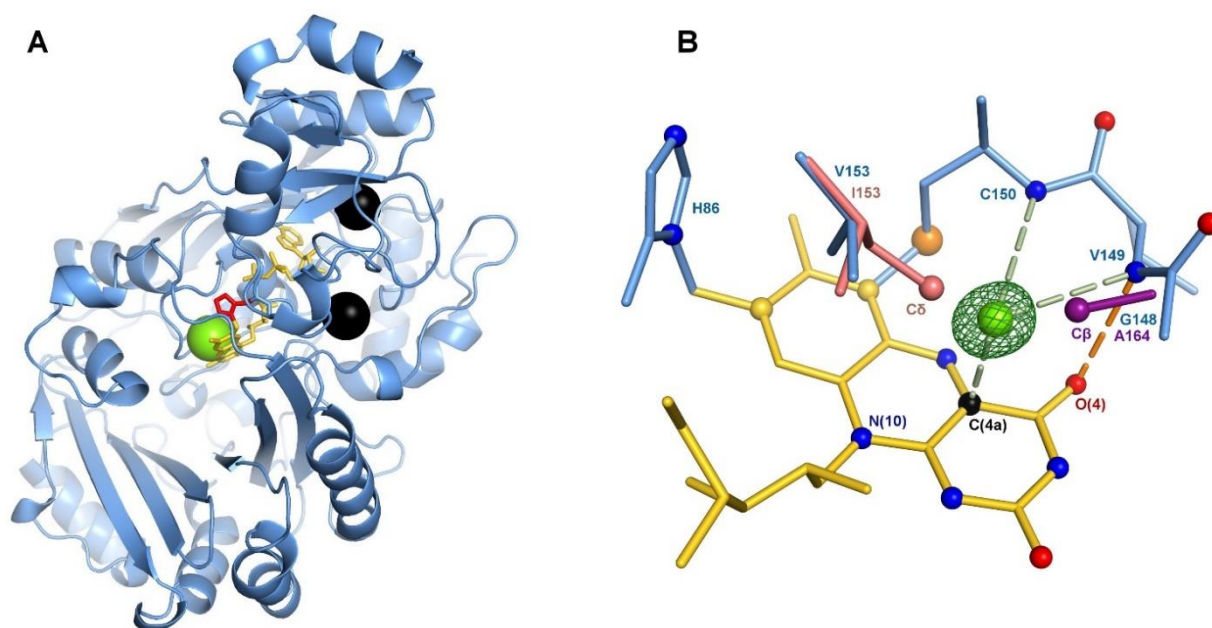


Fig. 4. Structures with oxygen surrogates. (A) Cartoon representation of Phl p 4 I153V variant (PDB ID 4PWB) with FAD (yellow) in stick representation and the H86 in red for easier orientation. The substrate-binding site is formed by a large cavity below the flavin ring (*si*-face). Xenon atoms are shown as black spheres, and a bromide ion, shown in green at the *re*-face of the FAD, is aligned from the bromide soak structure (Table 2). (B) The Phl p 4 I153V N158H variant (PDB ID 4PWC, blue) accommodates a bromide in the oxygen pocket. The oxygen surrogate placed into the difference omit map (green mesh) is positioned 2.5 Å above the reactive C(4a) (black atom in yellow FAD) and 3.4 Å from backbone nitrogen atoms of C150 and V149, the latter of which is within hydrogen bond distance of the carbonyl O(4) (orange). In our structures, the bromide ion is only 1.5 Å and 1.7 Å from the side chains of I153 and A164 in aligned wild-type Phl p 4 (PDB ID 4PVE, pink) and BBE G164A (PDB ID 4PZF, purple), respectively.

Table 2. Data collection and refinement statistics.

PDB ID	4PVE	4PVH	4PVJ	4PVK	4PWB	4PWC	4PZF
Protein variant	Phl p 4 wildtype	Phl p 4 N158H	Phl p 4 I153V	Phl p 4 I153V N158H	Phl p 4 I153V Xenon pressurized	Phl p 4 I153V N158H 3.5 M NaBr	BBE G164A
Space group	P 6 ₁ 2 2	P 6 ₁ 2 2	P 6 ₁ 2 2	P 6 ₁ 2 2	P 6 ₁ 2 2	P 6 ₁ 2 2	P 2 2 2 ₁
a/b/c (Å)	117.2/117.2/201.5	118.0/118.0/201.1	117.7/117.7/201.7	117.4/117.4/201.0	117.6/117.6/203.0	117.2/117.2/201.5	80.8/175.4/195.8
Number of molecules in asymmetric unit	1	1	1	1	1	1	4
Data collection (outer shell)							
Wavelength (Å)	1.033	0.980	0.92	0.915	0.92	0.915	0.972
Resolution (Å)	49.2-1.5 (1.554-1.5)	40.7-1.4 (1.450-1.4)	49.4-1.8 (1.864-1.8)	49.3-1.3 (1.346-1.3)	49.4-1.9 (1.968-1.9)	29.3-2.3 (2.382-2.3)	47.4-2.2 (2.279-2.2)
Unique reflections	130268 (12827)	159566 (15565)	76838 (7555)	197673 (18761)	65841 (6459)	37013 (3605)	140140 (13780)
Completeness (%)	100 (100)	98.7 (97.7)	100 (99.9)	99.4 (95.7)	100 (100)	100 (99.9)	98.9 (98.2)
Redundancy	19.6 (19.7)	4.3 (4.2)	19.6 (18.9)	17.4 (7.6)	78.6 (77.2)	39.4 (41.2)	8.3 (8.2)
R _{SYM} (%)	0.12 (1.8)	0.085 (1.5)	0.28 (2.9)	0.090 (2.2)	0.38 (5.4)	0.35 (3.1)	0.12 (1.1)
CC _{1/2} ^a	1.0 (0.76)	1.0 (0.42)	1.0 (0.54)	1.0 (0.27)	1.0 (0.69)	1.0 (0.79)	1.0 (0.79)
Mean I/σ(I)	16.8 (1.7)	11.8 (1.1)	13.0 (1.0)	18.58 (0.71)	26.6 (1.6)	24.9 (2.0)	11.8 (1.52)
Refinement							
R _{work} /R _{free}	0.133/0.154	0.146/0.167	0.152/0.186	0.141/0.160	0.160/0.187	0.186/0.225	0.220/0.242
Protein atoms	3852	3854	3851	3853	3851	3853	15713
Water atoms	620	700	508	601	377	150	308
Bond length dev. (Å)	0.009	0.009	0.011	0.008	1.34	0.008	0.004
Bond angles dev. (°)	1.32	1.35	1.33	1.32	0.012	1.19	0.84
Clash score	1.78	2.01	1.78	1.39	1.91	5.11	3.38
Mean B factor (Å ²)							
Protein	20.4	17.8	23.9	19.5	24.4	48.5	54.1
Water	34.1	33.4	35.0	32.5	35.1	46.3	44.2
φ,ψ favoured (%) ^b	96	96	96	96	96	96	95
φ,ψ outliers (%) ^b	0	0	0	0	0	0	0.5

^a CC_{1/2} is the correlation between two halves of a dataset, as defined by Karplus and Diederichs [53].

^b Calculated using Phenix [50].

1.3.3. Dioxygen reaction mechanism and putative transition states

FAD in all our Phl p 4 structures adopted a butterfly bent shape [22], resembling reduced FAD that is bent due to sp^3 hybridization of the N(5) and N(10) atoms in the central pyrazine ring. The putative intermediate in the reaction of reduced FAD with dioxygen is expected to be further twisted due to sp^3 hybridization of the carbon in the C(4a) position, but the shape of the bent isoalloxazine ring derivative may vary significantly. To gain a sense for what structures can be modeled in the active sites of our Phl p 4 and BBE variants, we have compared four flavin derivatives (5). The distal oxygen atom of the peroxy adduct in our models was positioned analogously to the position of C(18) in 4a,5-epoxyethano-3-methyl-4a,5-dihydrolumiflavin (Emmdh-flavin).

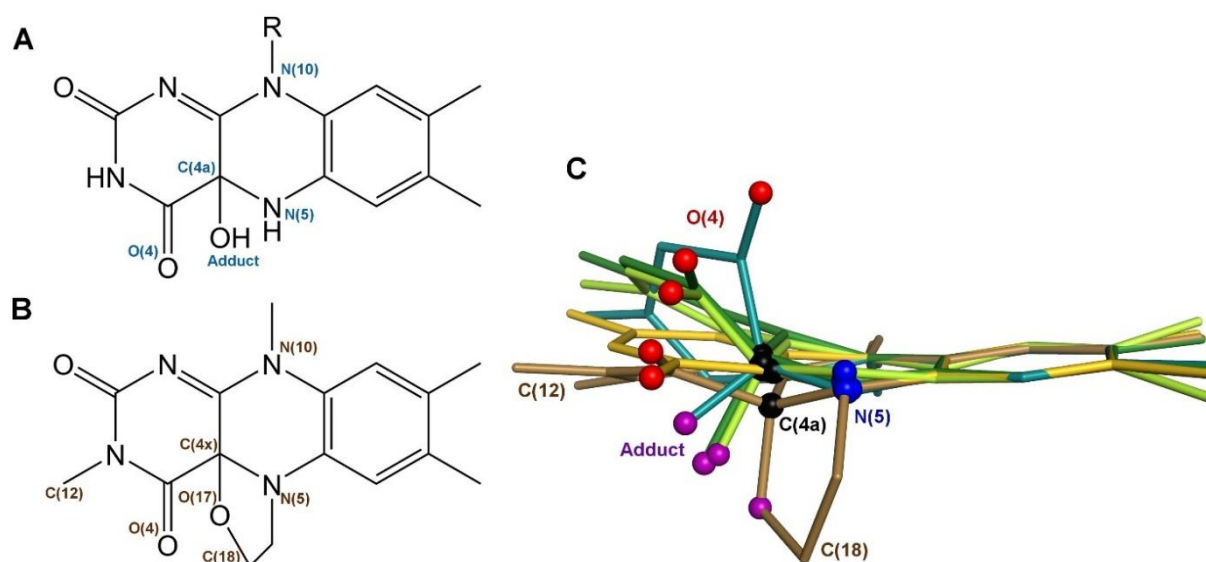


Fig. 5. Four flavin derivatives used for models of putative C(4a) adduct intermediate states. (A) Flavin derivative from crystal structure of choline oxidase (PDB ID 2JBV) with the oxygen adduct placed at the position at which authors of the structure assigned an “unknown atom” [10]. (B) 4a,5-epoxyethano-3-methyl-4a,5-dihydrolumiflavin (Emmdh-flavin) [38]. The position of C(18) was used in our models of hydroperoxy flavins for placing the distal oxygen atom in a proposed orientation relative to N(5). (C) 3D alignment of a set of enantiomers of flavin derivatives showing that orientation of the adduct and movement of the carbonyl C(4)=O out of the plane may vary significantly. FAD from a Phl p 4 structure (PDB ID 4PVK) is shown in yellow, Emmdh-flavin is shown in brown, and three derivatives from protein X-ray structures are also shown: pyranose dehydrogenase (PDB ID 4H7U, light green) [11], human monoamine oxidase B (PDB ID 2XCG, dark green) [54] and choline oxidase (PDB ID 2JBV, cyan) [10].

When models of flavin-4a-hydroperoxides with the peroxy group protruding on the *re*-face are aligned with the structure of Phl p 4 I153V N158H, the adduct fits into the oxygen pocket but C(4)=O clashes with the side chain of Y439 in all models except when Emmdh-flavin is used (Fig. 6B). No clashes were observed when derivatives were modeled in the

structure of wild-type BBE (data not shown). When alignments with the peroxy adduct at the *si*-face are performed, the C(4)=O atom fitted into the oxygen pocket (Fig. 6A).

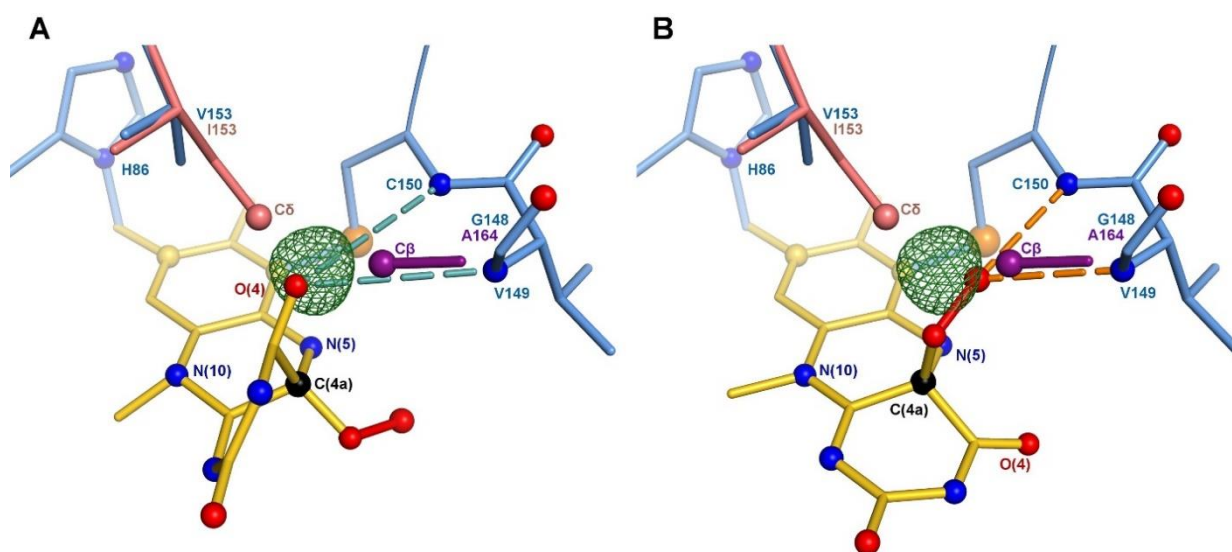


Fig. 6. Models of putative intermediates placed in Phl p 4. Models of flavin derivative are placed in the structure of bromide-soaked Phl p 4 I153V N158H bromide soak (PDB ID 4PWC, blue), and the position of the bromide ion is shown with its F_o-F_c difference density (green mesh). The structures of wild-type Phl p 4 (pink) and BBE G164A (purple) are aligned and represented by the gatekeeper residues. (A) Model based on the derivative structure from choline oxidase (PDB ID 2JBV), with the C(4a) hydroperoxy adduct on its *si*-face shows that C(4)=O oxygen atom may freely move into the oxygen pocket in the wild-type BBE and the Phl p 4 I153V variants. The blue dashed lines represent distances larger than 3.5 Å. (B) Model based on the structure of Emmdh-flavin, with the C(4a) hydroperoxy adduct on its *re*-face, showing that the adduct fits into the oxygen pocket where it forms hydrogen bonds (orange dashed lines) with the backbone nitrogens of C150 and possibly also V149. This intermediate cannot form in BBE G164A variant due to a clash with the gatekeeper residue, nor does it form in wild-type Phl p 4 or BBE V169I variant due to a clash with C δ of the alternative gatekeeper residue I169/I153.

1.4. Discussion

BBE has been studied extensively, and, while several variants comprising amino acid exchange in the active site have been created to identify the residues involved in substrate binding and catalysis, none of these replacements had a significant effect on the oxidative half-reaction with dioxygen (Table 3) [25,29,32,33]. The substitutions previously studied in BBE include residues implicated as important by corresponding studies with other flavoenzymes [9,17]. Although the (at least partial) positive charge in close proximity of the FAD was eliminated in the H459A, H174A and H104A BBE variants, the dioxygen reactivity was hardly affected. Moreover, removing hydrogen bond donors in the proximity of N(10) on the *si*-face of the isoalloxazine ring in Y106F and H459A BBE variants did not have a substantial effect on the rate of flavin re-oxidation (Table 3). In the present study, a new set of BBE and Phl p 4 variants was generated and characterized, with the aim of identifying amino acids responsible for the control of dioxygen reactivity in the VAO superfamily.

Table 3. Summary of kinetic parameters of BBE variants.

BBE variant	k_{red} [s^{-1}]	k_{ox} [$\text{M}^{-1}\cdot\text{s}^{-1}$]	k_{cat} [s^{-1}]	E_0 [mV]
Wild-type ^a	103 ± 4	$(5 \pm 1) \cdot 10^4$	8.0 ± 0.2	132 ± 4
C166A ^a	0.28 ± 0.02	$(10 \pm 1) \cdot 10^4$	0.48 ± 0.05	53 ± 2
H104A ^b	3.4 ± 0.3	$(8 \pm 1) \cdot 10^4$	0.54 ± 0.02	28 ± 4
H174N ^c	3.0 ± 0.5	$(4.1 \pm 1.7) \cdot 10^4$	1.2 ± 0.1	75 ± 3
H174A ^c	0.08 ± 0.01	$(7.0 \pm 0.3) \cdot 10^3$	0.07 ± 0.01	44 ± 3
H459A ^d	88 ± 4	$(2.9 \pm 0.3) \cdot 10^4$	3.1 ± 0.7	<i>n.d.</i>
Y106F ^d	6.7 ± 0.6	$(3.2 \pm 0.3) \cdot 10^4$	0.7 ± 0.1	<i>n.d.</i>
E417Q ^d	0.067 ± 0.007	$(5.3 \pm 0.2) \cdot 10^4$	0.054 ± 0.006	<i>n.d.</i>
G164A ^e	106 ± 13	60 ± 8	0.02 ± 0.002	109 ± 2
V169I ^e	18.5 ± 1.4	98 ± 9	0.02 ± 0.005	109 ± 3
G164A V169I ^e	0.04 ± 0.002	50 ± 3	0.007 ± 0.001	110 ± 3

^a Kinetic data taken from Winkler *et al.* [25].

^b Kinetic data taken from Winkler *et al.* [32].

^c Kinetic data taken from Wallner *et al.* [33].

^d Kinetic data taken from Winkler *et al.* [29].

^e New data published in this paper.

Reciprocal single amino acid substitutions at the *re*-face of the FAD were created to study the effect on the oxidative half-reaction of the reduced enzyme with dioxygen by incorporating BBE-derived amino acid residues in Phl p 4 and vice versa (Figs 2 and 4, and Table 1). In the

case of Phl p 4, substitution of the “alternative gatekeeper” residue isoleucine I153 by valine prompted in a 60 000-fold increase in the rate of oxidation, while the inverse amino acid exchange in BBE (V169I) resulted in a less pronounced but still substantial 500-fold decrease in oxygen reactivity (Table 1). Introduction of an alanine at the “gatekeeper” position of BBE (G164A) had a slightly stronger effect on dioxygen reactivity, and introduction of both mutations did not further suppress the reaction (Table 1). Even though the decrease in oxygen reactivity of the BBE variants was smaller, the level of reactivity observed is considerably lower than the reactivity of free reduced FAD (Table 1). The redox potentials of the enzyme-bound FAD were not substantially affected by the amino acid substitutions in any of the variants (Table 1), showing that redox potential has no effect on oxygen reactivity even in Phl p 4, a protein that exhibits the highest redox potential ever measured in a flavin-dependent enzyme.

X-ray crystal structure analysis enabled us to demonstrate that the only considerable difference between the oxygen-reactive and non-reactive variants is the existence of the “oxygen pocket” formed by the “oxygen reactivity motif”, containing two backbone amide nitrogens pointing towards the *re*-face of the FAD above the reactive C(4a) (Fig. 4). This cavity may be removed by introduction of a single methyl group on either side: frontal above the C(4)=O where the gatekeeper resides at a conserved position, or on the opposite side of the cavity where the Phl p 4-derived alternative gatekeeper is located in some VAO subfamilies, including the BBE-like enzymes. In the case of BBE, valine in this position allows access to the oxygen pocket, whereas the additional methyl group of isoleucine causes steric hindrance in Phl p 4 (Figs 2 and 4). We conclude that the observed effects on the oxidative rates were caused exclusively by changes in the accessibility of the backbone amide nitrogens of W165/V149 and C166/C150 and accessibility of the *re*-face of the FAD. The existence of a partial positive charge in the cavity was supported by our halide soaking experiments, which showed that, even though tightly packed, a halide ion can be bound in the oxygen pocket but a xenon atom cannot (Fig. 4). As shown previously, xenon readily binds in hydrophobic pockets and thus putative dioxygen binding sites, but not at dioxygen reaction sites [31,34]. A similar halide-binding site was previously observed in the VAO crystal structure (Fig. 7), and was suggested to present the dioxygen binding site [5,35].

Interestingly, the complete environment at the *re*-face of FAD is defined by the oxygen reactivity motif in VAO superfamily enzymes. While the gatekeeper residue and the position of the neighboring amide nitrogen are conserved among all VAO superfamily enzymes, the rest of the motif varies significantly (Fig. 7). For instance, in VAO, there is no alternative gatekeeper residue that could be aligned with the I153 of Phl p 4 (Fig. 7). Another example is

alditol oxidase (PDB ID 2VFR), which is an oxidase even though it has alanine A105 at the gatekeeper position and isoleucine I110 at the alternative gatekeeper position. It is a backbone shift of the oxygen reactivity motif that moves the gatekeepers away from the reactive C(4a) in this enzyme (Fig. 7 and Table 4) [36].

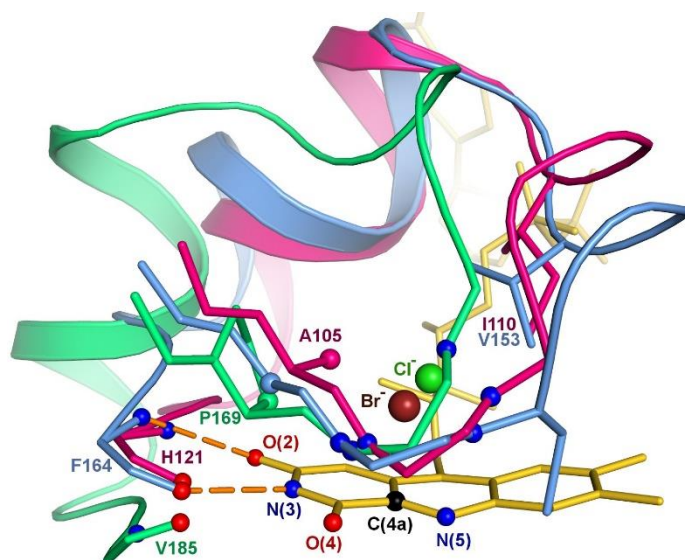


Fig. 7. The oxygen reactivity motif. The motif determining dioxygen reactivity in VAO enzymes is shown in aligned structures of bromide-soaked Phl p 4 I153V N158H (PDB ID 4PWC, blue), VAO (PDB ID 1VAO, green) and alditol oxidase (PDB ID 2VFR, purple). The position of the gatekeeper residues G148/P169/A105 and the position of the first proton donor backbone nitrogen (blue spheres above O(4)) are highly conserved. The rest of the backbone is less well-aligned, which influences the spatial position and size of the oxygen pocket, represented here by the bromide (brown) and chloride (green) anions that are present in the cavities of Phl p 4 and VAO, respectively. The motif ends in residues F164/V185/H121, which form two strong and conserved hydrogen bonds (shown for Phl p 4 in orange dashed lines) with N(3) and O(2) through their backbone oxygen and nitrogen atoms.

While universal predictions do not extend to all members of the VAO superfamily, reliable predictions are possible within sub-families that have members with solved representative structures. For example, BBE-like enzymes, which are abundant in the plant kingdom (the model plant *Arabidopsis thaliana* contains 28 genes encoding BBE-like enzymes [26]), have an invariant glycine at the gatekeeper position, while the residue at the Phl p 4 derived alternate gatekeeper position is either a valine, leucine or isoleucine, suggesting that oxidases and dehydrogenases are present.

1.4.1. Towards a unifying concept of dioxygen reactivity in flavoenzymes

As our study revealed that access to the oxygen pocket in flavoenzymes of the VAO superfamily is essential for dioxygen reactivity, we explored whether equivalent structural parameters exist in other flavoenzyme superfamilies. Interestingly, the existence and role of an analogous structural feature in dioxygen reactivity had already been discussed for *p*-

hydroxybenzoate hydroxylase (PHBH, PDB ID 1PHH) more than two decades ago by Schreuder *et al.* [37]. These authors realized that the structure of Emmdh-flavin [38] fits perfectly into the active site of PHBH with the C(4)=O gaining two strong hydrogen bonds upon moving into a hole formed by two backbone nitrogens, which they termed the “carbonyl oxygen binding pocket”. They stressed that the binding pocket strongly resembles the oxyanion hole, which was already known as a key feature of various proteases. PHBH is a member of the glucose/methanol/choline oxidoreductase (GMC) family, which includes other well-studied flavoenzymes such as choline oxidase, glucose oxidase and D-amino acid oxidase [10,39,40]. In contrast to the VAO superfamily, the organic substrate binds on the *re*-face of the flavin and the oxygen pocket is on the *si*-face, making these functional similarities an interesting case of convergent evolution (Fig. 8).

A few years later, a cavity termed the “oxygen pocket” was described by Lindqvist *et al.* [28], who studied structural features of FMN dependent glycolate oxidase (PDB IDs 1GOX and 1AL7). The protein was compared to flavocytochrome *b*₂, a dehydrogenase in which the proton donor is absent due to a backbone shift (PDB ID 1FCB) [28]. This pocket is located at the *re*-face of the FMN, and is filled with a water molecule in the native structure of glycolate oxidase (Fig. 8). Unlike in VAO and GMC oxidoreductases, where two amide groups serve as the proton donors, the oxygen pocket of glycolate oxidase is formed by a serine S106 side chain, positioned at hydrogen bond distance from the backbone oxygen of T78, and a side chain of glutamine Q127 (Fig. 8).

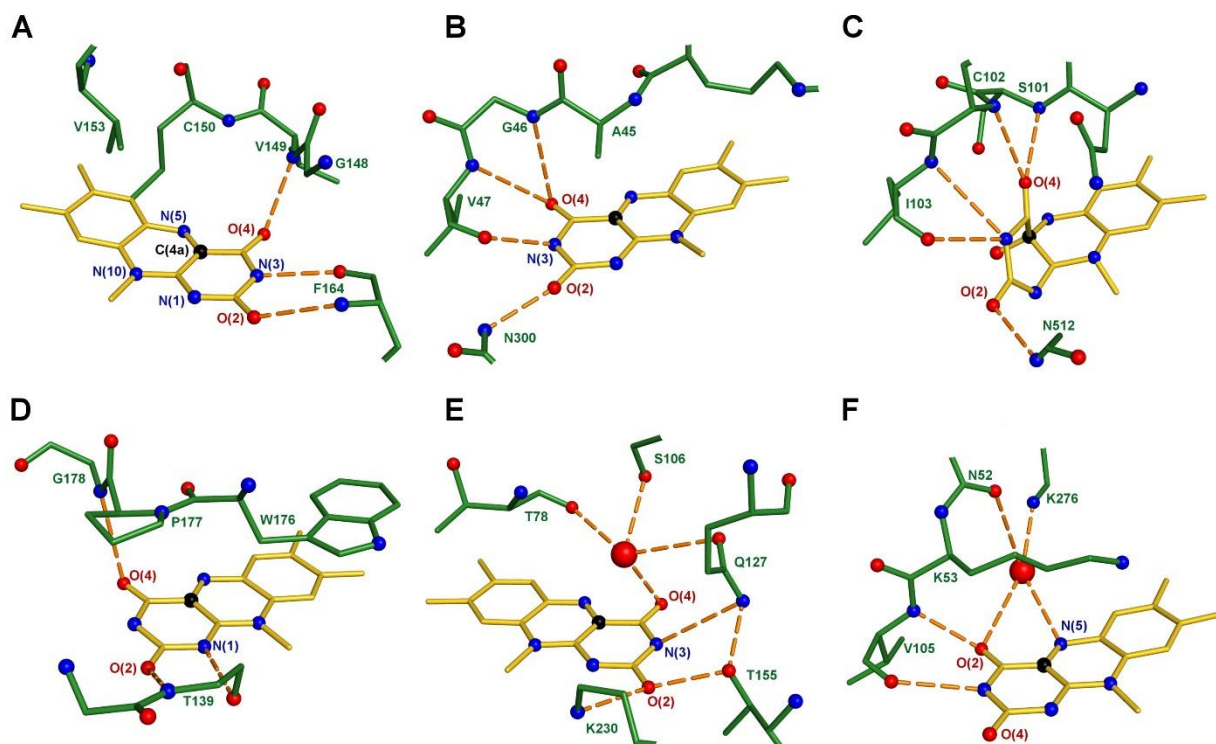


Fig. 8. Flavoenzyme oxidases from various structural superfamilies. At the first glance, environments of FAD in Phl p 4 (PDB ID 4PVE) (A) and PHBH (PDB ID 1PHH) (B) appear to be mirror images. The putative oxygen pocket accommodates the C(4)=O carbonyl atom of FAD in the structure of choline oxidase (PDB ID 2JBV) (C), which, like PHBH, belongs to the GMC structural superfamily. Peroxysomal acyl-CoA oxidase (PDB ID 1IS2) (D) belongs to the acyl-CoA dehydrogenase superfamily, and has a putative oxygen pocket at the *si*-face of the FAD where backbone nitrogens of P177 and G178 are located. The proposed oxygen pocket in glycolate oxidase (PDB ID 1GOX) (E), which belongs to the superfamily of FMN-linked oxidoreductases, is formed by the side chains of S106 and Q127 and is filled with a water molecule in the native crystal [28]. A strongly bound water molecule is also found in fructosamine oxidase (PDB ID 3DJE) (F), in which the proton donors of the oxygen pocket may be the water molecule and the backbone nitrogen of V105.

We find similar structural patterns also in flavin dependent oxidases from other structural superfamilies, where structural features analogous to the oxygen pocket have not been previously discussed. Enzymes of the acyl-CoA oxidase family exhibit two backbone nitrogen atoms at the *si*-face of the FAD, at a distance that allows strong hydrogen bonding upon movement of the C(4)=O, analogous to that proposed for PHBH (Fig. 8) [41]. In the case of fructosamine oxidase and monomeric sarcosine oxidase, replacement of a conserved lysine in the active site removes a strongly bound water molecule in the proximity of the N(5) atom [17,18,42]. In the light of the assumed importance of the oxygen pocket, we suggest that this water molecule, together with the adjacent backbone nitrogen of V105, may be involved in formation of the oxygen pocket (Fig. 8).

These examples illustrate that the concept of an “oxygen pocket” may be generally applicable to flavoenzyme oxidases, albeit with a great deal of variation in the structural organization, which depends on how the isoalloxazine ring is embedded into the protein matrix.

1.4.2. Possible mechanisms of dioxygen reactivity

Dioxygen reaction with free reduced flavin does not distinguish between the sides of the isoalloxazine ring, however, in enzymes this is not the case as the protein matrix renders the *re*- and *si*-faces asymmetric. We assume that the oxygen reaction occurs at the C(4a) carbon in our model enzymes [4,9], but our experiments do not allow us to distinguish a radical reaction from the reaction with a hydroperoxy intermediate (Fig. 1). Nonetheless, we believe that the conformation, orientation and spatial arrangement of radicals in case of the radical reaction would be similar to the covalent derivatives. As C(4a) peroxy flavin derivatives have been observed in flavin-dependent mono-oxygenases, and are probably intermediates in certain oxidases [9], we have built models with FAD derivatives, the putative reaction intermediates occurring during the proposed re-oxidation reaction (Fig. 1). Our models were based on four structures of flavin derivatives, three of which were found in proteins (Fig. 5). A large variation of movements of carbonyl C(4)=O out of the plane upon C(4a) sp³ hybridization may be observed in these derivatives, apparently due to the protein environment. We were able to align these models in the active sites of our proteins with confidence, because the flavin ring is firmly anchored within the protein matrix and is severely restricted in its movement in BBE-like proteins due to the covalent bonds to the cysteine and histidine side chains in combination with a strongly bound ribityl moiety.

According to our modeling, major movements of the C(4)=O carbonyl group out of the plane and into the oxygen pocket, occurring upon oxygen adduct formation at the *si*-face, are only possible in oxidase variants (Fig. 6). In the non-reactive variants, the presence of alanine at the gatekeeper position as well as isoleucine in the position of the alternative gatekeeper prevents movements of the carbonyl oxygen towards the proton donors. Similarly, adduct formation is sterically possible on either side of the ring in our oxidase variants, but only on the *si*-face in the non-reactive variants. Therefore, two scenarios are sterically possible, whereby an accessible oxygen pocket plays a major role in dioxygen reactivity in our model proteins: either the pocket stabilizes the peroxy adduct directly on the *re*-face of FAD, or, if dioxygen attack occurs from the *si*-face, it stabilizes the C(4)=O carbonyl oxygen in its twisted conformation (Fig. 6).

It is worth pointing out that the two reaction options in BBE-like enzymes may not be mutually exclusive, and theoretically both may occur in certain members of the superfamily,

while in some cases, such as enzymes of the acyl-CoA dehydrogenase or GMC superfamily, only one reaction mode is sterically feasible. Also, it is important to stress that both discussed reaction paths provide a rationale for how the sp^3 hybridized transition state is stabilized during re-oxidation of the reduced flavin, and thus rationalize a fundamental principle of enzyme catalysis.

1.5. Conclusion

In this study, we have achieved substantial changes in the oxygen reactivity of flavin-dependent enzymes based on a rational mutagenesis of active-site residues. Our combined biochemical analysis and structural results reveal that hydrophobic residues in proximity to the isoalloxazine ring govern the dioxygen reaction by controlling the access to the oxygen pocket, a feature that strongly resembles the oxyanion hole. In addition, we have demonstrated that these structural features enable the prediction and manipulation of dioxygen reactivity in BBE-like enzymes. The conservation of the oxygen pocket in the VAO/PCMH superfamily suggests that amino acid replacements with equivalent structural impact will have similar effects on the oxygen reactivity of other members; however, reliable predictions of dioxygen reactivity that are based solely on sequence alignment are only possible within sub-groups of structurally highly related proteins. Furthermore, exploration of the structures of flavin-dependent oxidases from other superfamilies indicates that dioxygen reactivity may be governed by similar principles, i.e. the occurrence of and access to an oxygen pocket in the proximity of the reactive C(4a) carbon atom.

1.6. Experimental Procedures

1.6.1. Reagents

Chemicals were purchased from Sigma-Aldrich (St. Louis, MO, USA), and oligonucleotide primers were obtained from VBC-Biotech (Vienna, Austria). (*S*)-reticuline was obtained from the natural product collection of the Donald Danforth Plant Science Center (St. Louis, MO, USA), and *rac*-reticuline was synthesized as described previously [43].

1.6.2. Cloning, expression and purification

Mutagenesis was performed to create the [pPICZ α - BBE V169I], [pPICZ α - BBE G164A], and [pPICZ α - BBE G164A V169I] expression plasmids using a QuikChange® XL site-directed mutagenesis Kit (Stratagene, La Jolla, CA, USA). As a template for PCR, the expression vector [pPICZ α -BBE-ER] was used as described previously [44]. Non-glycosylated Phl p 4.0202 was used in this study (UniProt Protein Database ID B2ZWE9). Genes of all Phl p 4 variants were ordered from GenScript (Piscataway, NJ, USA) and cloned into pPICZ α vector (Life Technologies, Carlsbad, CA, USA).

Expression plasmids were transformed using electroporation into *Komagataella pastoris* expression strain KM71H co-expressing the *Saccharomyces cerevisiae* protein disulfide isomerase. Integration of the expression cassettes into the *Komagataella* genome was verified using colony PCR. Protein production was performed in a BBI CT5-2 fermenter (Sartorius, Göttingen, Germany) as described previously [43], and stopped after 100-150 h of methanol induction. Purification of BBE variants was performed as described previously [43], and purification of Phl p 4 was performed according to a protocol adopted from that described by Nandy *et al.* [43].

1.6.3. Transient Kinetics

Reductive and oxidative half-reactions were analyzed using a stopped-flow device (SF-61DX2, TgK Scientific, Bradford-on-Avon, UK) at 25 °C in an anaerobic atmosphere provided within a glove box (Belle Technology, Dorset, UK). All samples were rendered oxygen-free by flushing with nitrogen and subsequent incubation in the glove box. Spectral changes of the flavin cofactor were followed using a KinetaScanT diode array detector (model MG-6560, TgK Scientific).

1.6.4. Reductive half-reaction

In BBE variants, rate constants were determined in 100 mM Tris/HCl, pH 9.0, at substrate concentrations from 30 to 500 μM (*S*)-reticuline. Apparent rate constants were plotted against the respective substrate concentrations, and fitting of the resulting data with a non-linear hyperbolic curve allowed determination of the reductive rate constant k_{red} . Measurements of Phl p 4 variants were performed in 80 mM KH_2PO_4 , pH 6.7, with 100 mM NaCl, using 5 μM to 100 mM final D-glucose concentrations. Fitting of obtained transients at 450 nm was performed with Kinetic Studio Software (TgK Scientific).

1.6.5. Oxidative half-reaction

Rates were determined by mixing air-saturated buffers with an oxygen-free substrate-reduced enzyme solution. Reduction of the FAD cofactor was performed using sub-stoichiometric amounts of *rac*-reticuline or glucose in order to prevent lag phases in the re-oxidation process.

1.6.6. Redox potential determination

Redox potentials were determined at 25 °C using a method adapted from that described by Stankovich *et al.* [46]. Experiments with BBE variants were performed in 50 mM potassium phosphate buffer, pH 7.0, while Phl p 4 variants were measured in 50 mM HEPES, pH 7.0. All experiments were performed in a glove box as described above. Toluylene blue ($E_0=115$ mV) was used as redox dye for redox potential determination of BBE, and dichlorophenolindophenol (DCPIP, $E_0=217$ mV) was used for Phl p 4. The standard protein potentials were calculated from a plotted Nernst equation as described by Minnaert [47].

1.6.7. Crystallization, data collection and structural characterization

BBE G164A was crystallized in batch, mixing protein (35 $\text{mg}\cdot\text{mL}^{-1}$ in 20 mM Tris, pH 7.0) in 1:1 ratio with crystallization buffer (100 mM HEPES, pH 7.5, 2.0 M ammonium sulfate). Phl p 4 variants were crystallized using the sitting-drop method that was used before [22], mixing the protein (7 $\text{mg}\cdot\text{mL}^{-1}$ in 20 mM Tris pH 7.0) in 3:2 ratio with crystallization buffer (70% Tacsimate, pH 7.0; Hampton Research, Aliso Viejo, CA, USA); 43% PEG 2000 was used as the reservoir solution. All crystals were soaked in a solution comprising crystallization buffer with 20% glycerol, and frozen in liquid nitrogen. To obtain the crystal structure with bromide, crystals were soaked in crystallization solution with 20% glycerol and 3.5 M sodium bromide prior to freezing [31,34]. To obtain the structure with xenon, crystals were soaked in crystallization solution with 20% glycerol, and pressurized at 40 bar (4 MPa) xenon in a home-

built device. The crystal was frozen instantly after pressure was released. Datasets were collected at beamlines FIP-BM30A, ID29 and ID23-1 (European Synchrotron Radiation Facility, Grenoble, France), I04-1 (Diamond Light Source, Didcot, UK) and P11 (Petra III, Deutsches Elektronen Synchrotron, Hamburg, Germany). Data were processed using XDS [48], molecular replacement was performed with Phaser [49], and structures were refined using PHENIX [50] and Coot [51]. Structures of wild-type Phl p 4 and variants have a positive electron density in the active site at the *si*-face of the FAD that varies in size and shape. It is probably derived from ingredients of crystallization buffer, glycerol and protein impurities (such as the sulfite adduct), and therefore we left it empty in deposited structures. Proteins were superimposed in PyMol (Schrödinger, Cambridge, MA, USA) by aligning three FAD atoms: C(6), C(8) and N(10). Models of peroxy adducts are based on the structure of 4a,5-epoxyethano-3-methyl-4a,5-dihydrolumiflavin [38]. Models and figures were prepared using PyMol and finished using Gimp (the open source GNU Image Manipulation Program, www.gimp.org).

1.7. References

- 1 Fagan RL & Palfey BA (2010) Flavin-dependent enzymes. In *Comprehensive Natural Products II* (Begley TP, ed), 7th ed., pp. 37–114. Elsevier, Amsterdam.
- 2 Teufel R, Miyanaga A, Michaudel Q, Stull F, Louie G, Noel JP, Baran PS, Palfey B & Moore BS (2013) Flavin-mediated dual oxidation controls an enzymatic Favorskii-type rearrangement. *Nature* **503**, 552–556.
- 3 Liu Y-C, Li Y-S, Lyu S-Y, Hsu L-J, Chen Y-H, Huang Y-T, Chan H-C, Huang C-J, Chen G-H, Chou C-C, Tsai M-D & Li T-L (2011) Interception of teicoplanin oxidation intermediates yields new antimicrobial scaffolds. *Nat. Chem. Biol.* **7**, 304–309.
- 4 Massey V (1994) Activation of molecular oxygen by flavins and flavoprotein. *J. Biol. Chem.* **269**, 22459–22462.
- 5 Mattevi A (2006) To be or not to be an oxidase: challenging the oxygen reactivity of flavoenzymes. *Trends Biochem. Sci.* **31**, 276–283.
- 6 Vervoort J, Muller F, Lee J, van den Berg WAM & Moonen CTW (1986) Identifications of the true carbon-13 nuclear magnetic resonance spectrum of the stable intermediate II in bacterial luciferase. *Biochemistry* **25**, 8062–8067.
- 7 Orru R, Dudek HM, Martinoli C, Torres Pazmiño DE, Royant A, Weik M, Fraaije MW & Mattevi A (2011) Snapshots of enzymatic Baeyer-Villiger catalysis: oxygen activation and intermediate stabilization. *J. Biol. Chem.* **286**, 29284–29291.
- 8 Thotsaporn K, Chenprakhon P, Sucharitakul J, Mattevi A & Chaiyen P (2011) Stabilization of C4a-hydroperoxyflavin in a two-component flavin-dependent monooxygenase is achieved through interactions at flavin N5 and C4a atoms. *J. Biol. Chem.* **286**, 28170–28180.
- 9 Chaiyen P, Fraaije MW & Mattevi A (2012) The enigmatic reaction of flavins with oxygen. *Trends Biochem. Sci.* **37**, 373–380.
- 10 Orville AM, Lountos GT, Finnegan S, Gadda G & Prabhakar R (2009) Crystallographic, spectroscopic, and computational analysis of a flavin C4a-oxygen adduct in choline oxidase. *Biochemistry* **48**, 720–728.
- 11 Tan TC, Spadiut O, Wongnate T, Sucharitakul J, Krondorfer I, Sygmund C, Haltrich D, Chaiyen P, Peterbauer CK & Divne C (2013) The 1.6 Å crystal structure of pyranose dehydrogenase from *Agaricus meleagris* rationalizes substrate specificity and reveals a flavin intermediate. *PLoS One* **8**, e53567.
- 12 Pennati A & Gadda G (2011) Stabilization of an intermediate in the oxidative half-reaction of human liver glycolate oxidase. *Biochemistry* **50**, 1–3.
- 13 Gannavaram S & Gadda G (2013) Relative timing of hydrogen and proton transfers in the reaction of flavin oxidation catalyzed by choline oxidase. *Biochemistry* **52**, 1221–1226.
- 14 Baron R, Riley C, Chenprakhon P, Thotsaporn K, Winter RT, Alfieri A, Forneris F, van Berkel WJH, Chaiyen P, Fraaije MW *et al.* (2009) Multiple pathways guide oxygen diffusion into flavoenzyme active sites. *Proc Natl Acad Sci USA* **106**, 10603–10608.
- 15 Klinman JP (2007) How do enzymes activate oxygen without inactivating themselves? *Acc. Chem. Res.* **40**, 325–333.

- 16 Gadda G (2012) Oxygen activation in flavoprotein oxidases: the importance of being positive. *Biochemistry* **51**, 2662–9.
- 17 McDonald CA, Fagan RL, Collard F, Monnier VM & Palfey BA (2011) Oxygen reactivity in flavoenzymes: context matters. *J. Am. Chem. Soc.* **133**, 16809–16811.
- 18 Zhao G, Bruckner RC & Jorns MS (2008) Identification of the oxygen activation site in monomeric sarcosine oxidase: role of Lys265 in catalysis. *Biochemistry* **47**, 9124–9135.
- 19 Leferink NGH, Heuts DPHM, Fraaije MW & van Berkel WJH (2008) The growing VAO flavoprotein family. *Arch. Biochem. Biophys.* **474**, 292–301.
- 20 Macheroux P, Kappes B & Ealick SE (2011) Flavogenomics - a genomic and structural view of flavin-dependent proteins. *FEBS J.* **278**, 2625–2634.
- 21 Fraaije MW, van Berkel WJH, Benen JAE, Visser J & Mattevi A (1998) A novel oxidoreductase family sharing a conserved FAD-binding domain. *Trends Biochem. Sci.* **23**, 206–207.
- 22 Zafred D, Nandy A, Pump L, Kahlert H & Keller W (2013) Crystal structure and immunologic characterization of the major grass pollen allergen Phl p 4. *J. Allergy Clin. Immunol.* **132**, 696–703.
- 23 Leferink NGH, Fraaije MW, Joosten H-J, Schaap PJ, Mattevi A & van Berkel WJH (2009) Identification of a gatekeeper residue that prevents dehydrogenases from acting as oxidases. *J. Biol. Chem.* **284**, 4392–4397.
- 24 Marchler-Bauer A, Zheng C, Chitsaz F, Derbyshire MK, Geer LY, Geer RC, Gonzales NR, Gwadz M, Hurwitz DI, Lanczycki CJ *et al.* (2013) CDD: conserved domains and protein three-dimensional structure. *Nucleic Acids Res* **41**, D348-D352.
- 25 Winkler A, Kutchan TM & Macheroux P (2007) 6-S-cysteinylation of bi-covalently attached FAD in berberine bridge enzyme tunes the redox potential for optimal activity. *J. Biol. Chem.* **282**, 24437–24443.
- 26 Wallner S, Dully C, Daniel B & Macheroux P (2012) Berberine bridge enzyme and the family of bicovalent flavoenzymes. In *Flavoproteins: 1* (Hille R, Miller SM, & Palfey B, eds), pp. 1–30. De Gruyter, Berlin.
- 27 Hedstrom L (2002) Serine protease mechanism and specificity. *Chem. Rev.* **102**, 4501–4524.
- 28 Lindqvist Y, Brändén CI, Mathews FS & Lederer F (1991) Spinach glycolate oxidase and yeast flavocytochrome b2 are structurally homologous and evolutionarily related enzymes with distinctly different function and flavin mononucleotide binding. *J. Biol. Chem.* **266**, 3198–3207.
- 29 Winkler A, Lyskowski A, Riedl S, Puhl M, Kutchan TM, Macheroux P & Gruber K (2008) A concerted mechanism for berberine bridge enzyme. *Nat. Chem. Biol.* **4**, 739–741.
- 30 Heuts DPHM, Scrutton NS, McIntire WS & Fraaije MW (2009) What's in a covalent bond? On the role and formation of covalently bound flavin cofactors. *FEBS J.* **276**, 3405–3427.
- 31 Kommoju P, Chen Z, Bruckner RC, Mathews FS & Jorns MS (2011) Probing oxygen activation sites in two flavoprotein oxidases. *Biochemistry* **50**, 5521–5534.
- 32 Winkler A, Motz K, Riedl S, Puhl M, Macheroux P & Gruber K (2009) Structural and mechanistic studies reveal the functional role of bicovalent flavinylation in berberine bridge enzyme. *J. Biol. Chem.* **284**, 19993–20001.

- 33 Wallner S, Winkler A, Riedl S, Dully C, Horvath S, Gruber K & Macheroux P (2012) Catalytic and structural role of a conserved active site histidine in berberine bridge enzyme. *Biochemistry* **51**, 6139–6147.
- 34 Colloc'h N, Gabison L, Monard G, Altarsha M, Chiadmi M, Marassio G, Sopkova-de Oliveira Santos J, El Hajji M, Castro B, Abraini JH & Prangé T (2008) Oxygen pressurized X-ray crystallography: probing the dioxygen binding site in cofactorless urate oxidase and implications for its catalytic mechanism. *Biophys. J.* **95**, 2415–2422.
- 35 Mattevi A, Fraaije MW, Mozzarelli A, Olivi L, Coda A & van Berkel WJ (1997) Crystal structures and inhibitor binding in the octameric flavoenzyme vanillyl-alcohol oxidase: the shape of the active-site cavity controls substrate specificity. *Structure* **5**, 907–920.
- 36 Heuts DPHM, van Hellemond EW, Janssen DB & Fraaije MW (2007) Discovery, characterization, and kinetic analysis of an alditol oxidase from *Streptomyces coelicolor*. *J. Biol. Chem.* **282**, 20283–20291.
- 37 Schreuder HA, Hol WGJ & Drenth J (1988) Molecular modeling reveals the possible importance of a carbonyl oxygen binding pocket for the catalytic mechanism of p-hydroxybenzoate hydroxylase. *J. Biol. Chem.* **263**, 3131–3136.
- 38 Bolognesi M, Ghisla S & Incoccia L (1978) The crystal and molecular structure of two models of catalytic flavo(co)enzyme intermediates. *Acta Crystallogr. Sect. B Struct. Crystallogr. Cryst. Chem.* **34**, 821–828.
- 39 Rosini E, Molla G, Ghisla S & Pollegioni L (2011) On the reaction of D-amino acid oxidase with dioxygen: O₂ diffusion pathways and enhancement of reactivity. *FEBS J.* **278**, 482–492.
- 40 Mizutani H, Miyahara I, Hirotsu K, Nishina Y, Shiga K, Setoyama C & Miura R (2000) Three-dimensional structure of the purple intermediate of porcine kidney D-amino acid oxidase. Optimization of the oxidative half-reaction through alignment of the product with reduced flavin. *J. Biochem.* **128**, 73–81.
- 41 Nakajima Y, Miyahara I, Hirotsu K, Nishina Y, Shiga K, Setoyama C, Tamaoki H & Miura R (2002) Three-dimensional structure of the flavoenzyme acyl-CoA oxidase-II from rat liver, the peroxisomal counterpart of mitochondrial acyl-CoA dehydrogenase. *J. Biochem.* **131**, 365–374.
- 42 Jorns MS, Chen ZW & Mathews FS (2010) Structural characterization of mutations at the oxygen activation site in monomeric sarcosine oxidase. *Biochemistry* **49**, 3631–3639.
- 43 Schrittwieser JH, Resch V, Wallner S, Lienhart WD, Sattler JH, Resch J, Macheroux P & Kroutil W (2011) Biocatalytic organic synthesis of optically pure (*S*)-scoulerine and berbine and benzyloquinoline alkaloids. *J. Org. Chem.* **76**, 6703–6714.
- 44 Winkler A, Hartner F, Kutchan TM, Glieder A & Macheroux P (2006) Biochemical evidence that berberine bridge enzyme belongs to a novel family of flavoproteins containing a bi-covalently attached FAD cofactor. *J. Biol. Chem.* **281**, 21276–21285.
- 45 Nandy A, Petersen A, Wald M, Suck R, Kahlert H, Weber B, Becker WM, Cromwell O & Fiebig H (2005) Primary structure, recombinant expression, and molecular characterization of Phl p 4, a major allergen of timothy grass (*Phleum pratense*). *Biochem. Biophys. Res. Commun.* **337**, 563–570.
- 46 Stankovich MT, Schopfer LM & Massey V (1978) Determination of glucose oxidase oxidation-reduction potentials and the oxygen reactivity of fully reduced and semiquinoid forms. *J. Biol. Chem.* **253**, 4971–4979.

- 47 Minnaert K (1965) Measurement of the equilibrium constant of the reaction between cytochrome c and cytochrome a. *Biochim. Biophys. Acta* **110**, 42–56.
- 48 Kabsch W (2010) XDS. *Acta Crystallogr. D. Biol. Crystallogr.* **66**, 125–132.
- 49 McCoy AJ, Grosse-Kunstleve RW, Adams PD, Winn MD, Storoni LC & Read RJ (2007) Phaser crystallographic software. *J. Appl. Crystallogr.* **40**, 658–674.
- 50 Adams PD, Afonine P V, Bunkóczi G, Chen VB, Davis IW, Echols N, Headd JJ, Hung L-W, Kapral GJ, Grosse-Kunstleve RW, McCoy AJ, Moriarty NW, Oeffner R, Read RJ, Richardson DC, Richardson JS, Terwilliger TC & Zwart PH (2010) PHENIX: a comprehensive Python-based system for macromolecular structure solution. *Acta Crystallogr. D. Biol. Crystallogr.* **66**, 213–221.
- 51 Emsley P, Lohkamp B, Scott WG & Cowtan K (2010) Features and development of Coot. *Acta Crystallogr. D. Biol. Crystallogr.* **66**, 486–501.
- 52 Mayhew SG (1999) The effects of pH and semiquinone formation on the oxidation-reduction potentials of flavin mononucleotide. A reappraisal. *Eur. J. Biochem.* **265**, 698–702.
- 53 Karplus PA & Diederichs K (2012) Linking crystallographic model and data quality. *Science* **336**, 1030–1033.
- 54 Bonivento D, Milczek EM, McDonald GR, Binda C, Holt A, Edmondson DE & Mattevi A (2010) Potentiation of ligand binding through cooperative effects in monoamine oxidase B. *J. Biol. Chem.* **285**, 36849–36856.

CHAPTER 2

Oxidation of monolignols by members of the berberine bridge enzyme family suggests a role in plant cell wall metabolism

Author contributions

Two BBE-like enzymes of *A. thaliana*, termed *AtBBE*-like protein 13 and 15, are identified as monolignol oxidoreductases. Dr. Bastian Daniel initiated the project and structurally and biochemically characterized *AtBBE*-like protein 15. *AtBBE*-like protein 15 catalyzes the oxidation of monolignols to the corresponding aldehydes and *AtBBE*-like protein 13 was shown to have the same catalytic function. I contributed to this project by characterizing *AtBBE*-like protein 13 biochemically. I expressed the protein in *Komagataella phaffii* and I performed large-scale protein expression using a bioreactor. The protein was purified and the reductive and oxidative half-reactions were determined using a stopped-flow device.

Chapter 2

2. Oxidation of monolignols by members of the berberine bridge enzyme family suggests a role in plant cell wall metabolism

Bastian Daniel,¹ Tea Pavkov-Keller,^{2,3} Barbara Steiner,¹ Anđela Dordic,^{2,3} Alexander Gutmann,⁴ Bernd Nidetzky,⁴ Christoph W. Sensen,⁵ Eric van der Graaff,⁶ Silvia Wallner,¹ Karl Gruber² and Peter Macheroux^{1*†}

¹From Graz University of Technology, Institute of Biochemistry, Graz, Austria

²University of Graz, Institute of Molecular Biosciences, Graz, Austria

³ACIB GmbH, Graz, Austria

⁴Graz University of Technology, Institute of Biotechnology and Biochemical Engineering, Graz, Austria

⁵Graz University of Technology, Institute of Molecular Biotechnology, Graz, Austria

⁶Copenhagen University, Copenhagen, Denmark

To whom correspondence should be addressed: Peter Macheroux, Graz University of Technology, Institute of Biochemistry, Petersgasse 12/II, A-8010 Graz, Austria, Tel.: +43-316-873 6450, Fax: +43-316-873 6952; Email: peter.macheroux@tugraz.at

This chapter was published in the Journal of Biological Chemistry:

Daniel, B. *et al.* (2015) Oxidation of Monolignols by Members of the Berberine Bridge Enzyme Family Suggests a Role in Plant Cell Wall Metabolism. *J Biol Chem* 290, 18770-18781.

Author contributions

B.D., K.G. and P.M. initiated and designed the research; B.D., B.S. and S.W. carried out biochemical research; A.G. and B.N. synthesized glycosylated monolignol derivatives; A.D., T.P.-K., B.D. and K.G. crystallised proteins and solved the X-ray crystal structure; B.D., C.S. and E.v.d.G performed phylogenetic analysis and evaluated the data; B.D. E.v.d.G., K.G. and P.M. wrote the manuscript.

2.1. Abstract

Plant genomes contain a large number of genes encoding for berberine bridge enzyme (BBE)-like enzymes. Despite the widespread occurrence and abundance of this protein family in the plant kingdom, the biochemical function remains largely unexplored. In this study, we have expressed two members of the BBE-like enzyme family from *Arabidopsis thaliana* in the host organism *Komagataella pastoris*. The two proteins, termed *AtBBE*-like 13 and *AtBBE*-like 15, were purified, and their catalytic properties were determined. In addition, *AtBBE*-like 15 was crystallized and structurally characterized by x-ray crystallography. Here, we show that the enzymes catalyze the oxidation of aromatic allylic alcohols, such as coumaryl, sinapyl, and coniferyl alcohol, to the corresponding aldehydes and that *AtBBE*-like 15 adopts the same fold as vanillyl alcohol oxidase as reported previously for berberine bridge enzyme and other FAD-dependent oxidoreductases. Further analysis of the substrate range identified coniferin, the glycosylated storage form of coniferyl alcohol, as a substrate of the enzymes, whereas other glycosylated monolignols were rather poor substrates. A detailed analysis of the motifs present in the active sites of the BBE-like enzymes in *A. thaliana*, suggested that 14 out of 28 members of the family might catalyze similar reactions. Based on these findings, we propose a novel role of BBE-like enzymes in monolignol metabolism that was previously not recognized for this enzyme family

2.2. Introduction

Flavoproteins are a large and diverse protein family employing the FAD cofactor for catalysis. Among them the berberine bridge enzyme (BBE)-like proteins (pfam 08031) can be set apart due to their unusual bicovalent attachment of the FAD cofactor. The namesake of this protein family is berberine bridge enzyme (BBE) from *Eschscholzia californica* (California poppy) that catalyzes the formation of the so-called “berberine bridge” by oxidation of the *N*-methyl group of (*S*)-reticuline yielding (*S*)-scoulerine (1). This step constitutes a branch point in the biosynthesis of numerous isoquinoline alkaloids (2,3). In recent years, a large number of genes encoding BBE-like enzymes have been identified in plants and bacteria in the course of genome sequencing efforts. The number of BBE-like genes in individual plant species varies considerably from a single gene in the moss *Physcomitrella patens* to 64 in the western poplar (*Populus trichocarpa*) (4). In the model plant *Arabidopsis thaliana*, 28 BBE-like genes were identified (termed *AtBBE*-like 1-28, (4)). However, the role of these BBE homologs in *A. thaliana* and most of the other plants is unknown, as most do not synthesize alkaloids of the benzyloisoquinoline family. Examination of microarray data (5) revealed the expression of *AtBBE*-like genes during certain developmental stages, such as root elongation and maturation, proliferation as well as embryonal development (Table 1). Similarly, osmotic stress and pathogen attack were shown to cause up-regulation of *AtBBE*-likes by up to 400-fold. This up-regulation was also seen in other plants, such as citrus fruit and poplar (6,7). The role in pathogen defense appears to be related to a carbohydrate oxidase activity that was reported previously for tobacco (nectarin V), sunflower and lettuce (8,9). Similar oxidation reactions occur in the biosynthesis of antibiotics generated in various bacterial species, such as *Streptomyces* (10-12). However, the role of BBE-homologs in plant development remains enigmatic.

Table 1. Expression of *AtBBE*-homologs in *planta*. Data were retrieved from the Arabidopsis eFP-browser.

Subgroup	Name	Most significant expression value / up-regulation	Second significant expression value / up-regulation	Localization: MS/MS	Locus
1	<i>AtBBE</i> -like 18	822 seed linear cotyledon		unknown	AT4G20820.1
1	<i>AtBBE</i> -like 27	1117 root		unknown	AT5G44410.1
1	<i>AtBBE</i> -like 28	6000 shift dark to light	927 quiescent center root	extracellular	AT5G44440.1
2	<i>AtBBE</i> -like 3	2457 / 438 fold osmotic stress seedling	2318 / 457 fold infection <i>P. infestans</i>	Endoplasmic reticulum	AT1G26380.1
2	<i>AtBBE</i> -like 4	2070 / 78 fold infection <i>P. syringae</i>	391 root regeneration	unknown	AT1G26390.1
2	<i>AtBBE</i> -like 5	665 cotyledon	475 cotyledon greens	unknown	AT1G26400.1
2	<i>AtBBE</i> -like 6	604 / 42 fold osmotic stress	278 / 36 fold infection <i>P. syringae</i>	unknown	AT1G26410.1
2	<i>AtBBE</i> -like 7	1562 / 412 fold osmotic stress	800 / 163 fold mock infection	unknown	AT1G26420.1
2	<i>AtBBE</i> -like 17	7772 mycophylar endosperm		unknown	AT4G20800.1
3	<i>AtBBE</i> -like 10	4899 lateral root cap	912 / 57 fold mock infection	unknown	AT1G30720.1
3	<i>AtBBE</i> -like 11	4988 root epidermis	762 / 10 fold infection <i>P. syringae</i>	extracellular	AT1G30730.1
4	<i>AtBBE</i> -like 9	7582 mature pollen		unknown	AT1G30710.1
4	<i>AtBBE</i> -like 14	50 seed		unknown	AT1G34575.1
4	<i>AtBBE</i> -like 16	3682 root maturation zone	1537 stigma and ovaries	unknown	AT2G34810.1
5	<i>AtBBE</i> -like 1	11626 pollen	5509 mature pollen	plasma membrane, Golgi	AT1G01980.1
5	<i>AtBBE</i> -like 2	5088 pollen	2000 pollen tubes	unknown	AT1G11770.1
5	<i>AtBBE</i> -like 8	2557 root maturation zone	1157 / 246 fold infection <i>P. syringae</i>	unknown	AT1G30700.1
5	<i>AtBBE</i> -like 12	642 endosperm		unknown	AT1G30740.1
5	<i>AtBBE</i> -like 20	4000 root elongation zone	1394 / 10 fold infection <i>P. syringae</i>	extracellular, plasma membrane	AT4G20830.2
5	<i>AtBBE</i> -like 21	973 root elongation zone		plasma membrane	AT4G20840.1
6	<i>AtBBE</i> -like 13	2144 lateral root initiation	1594 xylem root maturation zone	unknown	AT1G30760.1
6	<i>AtBBE</i> -like 15	4927 xylem root	439 seed stage 8 curled	extracellular, plasma membrane	AT2G34790.1
6	<i>AtBBE</i> -like 24	32075 lateral root cap	1412 cotyledon	extracellular	AT5G44380.1
6	<i>AtBBE</i> -like 25	491 procambium root	164 / 5 fold infection <i>P. syringae</i>	extracellular	AT5G44390.1
6	<i>AtBBE</i> -like 26	604 / 5 fold osmotic stress root	250 / 3 fold infection <i>P. syringae</i>	extracellular	AT5G44400.1
7	<i>AtBBE</i> -like 22	1641 lateral root initiation	1427 / 13 fold infection <i>P. syringae</i>	plasma membrane, cytosol	AT4G20860.1
7	<i>AtBBE</i> -like 23	824 root	649 seed cotyledon heart stage	unknown	AT5G44360.1

For this study, we have chosen *AtBBE*-like 15 (At2g34790) for further studies into the role of the BBE-like enzyme family in plants because gene disruption resulted in defects in female gametophyte development (*i.e.* unfused polar nuclei and endosperm development arrest) (13). Furthermore, mass spectrometric analysis has shown that *AtBBE*-like 15 is located in the cell wall and thus might participate in as yet undefined reactions relevant for the formation of the cell wall (14). In addition, we have selected *AtBBE*-like 13 (At1g30760) for further analysis due to its close sequence relationship of 81% identity to *AtBBE*-like 15.

Structural analysis of recombinant *AtBBE*-like 15 by x-ray crystallography confirmed a topology similar to that of berberine bridge enzyme from *E. californica* (*EcBBE*) and Δ 1-tetrahydrocannabinolic acid synthase (THCA-synthase) from *Cannabis sativa* (15,16). However, composition and architecture of the active site of *AtBBE*-like 15 indicated distinct catalytic properties. To identify potential substrates, we screened a small compound library with regard to its effect on the protein's thermal stability. This approach produced several hits and allowed the identification of cinnamyl alcohol as a lead structure. Further analysis showed that the *p*-hydroxylated derivatives of cinnamyl alcohol, *i.e.* the monolignols *p*-coumaryl-, coniferyl- and sinapyl alcohol are rapidly oxidized to their corresponding aldehydes. Furthermore, the β -*O*-glycosylated form of coniferyl alcohol (coniferin) is also accepted as a substrate. Because monolignols and their β -glycosylated derivatives (coniferin, syringin and *p*-coumaryl- β -glycoside) are important building blocks and monolignol storage forms, respectively, the catalytic reactions performed by *AtBBE*-like 13 and *AtBBE*-like 15 constitute a novel link between the phenylpropanoid pathway and the formation of plant polymerization products, such as lignin and suberin. The characteristic active site found in *AtBBE*-like 13 and *AtBBE*-like 15 is conserved in the majority of BBE-like enzymes in *A. thaliana* (14 of 28) suggesting that they either exhibit different substrate preferences or have distinct spatial (*e.g.* different plant tissues) or temporal (*e.g.* in response to pathogens or herbivores) functions *in planta*.

2.3. Experimental Procedures

2.3.1. Chemicals

All chemicals were from Sigma Aldrich (St. Louis, MO, USA) and were of the highest grade commercially available. Restriction enzymes were obtained from Fermentas (Waltham, MA, USA). Nickel-Sepharose 6 Fast Flow column material was from GE Healthcare (Little Chalfont, UK.). Synthetic genes coding for *AtBBE*-like 15 and *AtBBE*-like 13 were obtained from Life Technologies (Carlsbad, CA, USA) with codon usage optimized for *Komagataella pastoris*.

2.3.2. Molecular cloning

The proteins were expressed using *Komagataella pastoris* as expression host, according to the EasySelect™ *Pichia* expression kit provided by Invitrogen (Waltham, MA, USA). The genes were adapted to the *K. pastoris* codon usage, and a C-terminal His-tag was added. SignalP was used to identify the native signal sequence of 30 and 27 amino acids for *AtBBE*-like 13 and *AtBBE*-like 15, respectively (17). The genes lacking the signal sequence were cloned into pPICZ α vector® (Invitrogen) using standard techniques. *K. pastoris* strain KM71H was transformed with the pPICK-PDI vector harboring the gene for the protein-disulfide isomerase from *Saccharomyces cerevisiae*. The modified KM71H strain was transformed with the linearized [pPICZ α -*AtBBE*-like 13] or [pPICZ α -*AtBBE*-like 15] construct using electroporation. Optimal expression strains were identified using the method proposed by Weis *et al.* (18).

2.3.3. Protein expression and purification

Expression was carried out using a BBI CT5-2 fermenter (Sartorius, Göttingen, Germany) using a basal salt minimal medium as described by Schrittwieser *et al.* (19). After 96 h of methanol induction, the pH was set to 8.0 with sodium hydroxide, and imidazole was added to a final concentration of 10 mM. The cells were removed by centrifugation at 4000 rpm at 4 °C for 30 min. The supernatant was incubated with 50 mL of nickel-Sepharose 6 Fast Flow material at 4 °C for 45 min. Then the affinity material was packed into a column and washed with 5 column volumes of 50 mM phosphate buffer, pH 8.0, containing 150 mM NaCl and 20 mM imidazole. The protein was eluted using 50 mM phosphate buffer, pH 8.0, containing 150 mM NaCl and 150 mM imidazole. Fractions containing *AtBBE*-like 15 were concentrated using Amicon Ultra centrifugal filter units and subsequently loaded on a Superdex 200 gel filtration column using an Äkta system and separated using 50 mM Tris buffer, pH 8.0, containing 150

mM sodium chloride. The purity of purified protein was monitored by SDS-PAGE. The final yield from 3.5 liters of fermentation supernatant was 520 mg of purified protein. The large-scale expression of *AtBBE*-like 13 was conducted as described for *AtBBE*-like15. In contrast to *AtBBE*-like 15, *AtBBE*-like 13 was not secreted, and hence the protein was isolated from cells and not the cultivation medium. Briefly, the cell pellet was harvested and redissolved (1:3 w/v) in cell lysis buffer (50 mM NaH₂PO₄, 300 mM NaCl, 20 mM imidazole, pH 8.0), disrupted by zirconia/silica beads using a Merckenschlager homogenizer. The lysate was separated from the cell debris by centrifugation (18000 rpm, 30 min, 4 °C), filtered, and incubated with nickel-sepharose 6 Fast Flow material (GE Healthcare, Little Chalfont, U.K.). The column was packed with the Sepharose material, and after extensive washing (50 mM NaH₂PO₄, 300 mM NaCl, 50 mM imidazole, pH 8.0), the protein was eluted with elution buffer containing 500 mM imidazole. Subsequent purification was performed as described for *AtBBE*-like 15.

2.3.4. Site-directed mutagenesis: Generation of the L182V variant

Site-directed mutagenesis was performed according to the instructions of the QuickChange XL kit (Stratagene, La Jolla, CA, USA) for site-directed mutagenesis. The pPICZ α -*AtBBE*-like 15 vector was used as template for the polymerase chain reaction. The introduction of the desired codon causing a change of leucine in position 182 to valine was verified by sequencing. Transformation of the gene was performed as described before. Expression of the mutated gene and purification of the *AtBBE*-like 15 L182V variant was performed as described for wild-type *AtBBE*-like 15.

2.3.5. Crystallization

Initial crystal screening of *AtBBE*-like 15(27-532) was performed with an Oryx8 robot (Douglas Instruments, Berkshire, UK) using commercially available Index (Hampton Research, Aliso Viejo, CA, USA) and JCSG+ (Molecular Dimensions, Suffolk, UK) screens. Screening was performed in Swissci triple well plates (Molecular Dimensions) using the sitting drop method with a reservoir volume of 33 μ L. Drops of 1 μ L were pipetted in 1:1 ratio of protein and reservoir solution with two different protein stock solutions, 22 and 50 mg/mL in 50 mM Tris buffer, pH 8.0, containing 150 mM sodium chloride, respectively. Plates were sealed with the thermal seal A sealing films (Sigma-Aldrich, St. Louis, MA, USA) and were incubated at 289 K. First crystals appeared after 1 week in JCSG+ screen condition 1-14 (0.2 M sodium thiocyanate and 20% w/v PEG 3350) with the higher protein concentration. Crystals from this drop were pipetted out and crushed in 100 μ L of the original 1-14 solution and used as a seeding stock. Cross-seeding setups (20) were performed in the same manner as initial screening with

drops consisting of 0.5 μL of protein stock solution (37 mg/mL), 0.2 μL of the seeding stock, and 0.5 μL of the JCSG+ screen solutions from the reservoir. The best diffracting crystals appeared after 4 and a half weeks in a serial dilution setup done manually in Crystal Clear duo plates for sitting drop (Douglas Instruments). The 1.2 μL drops consisted of 0.5 μL of protein stock solution (36 mg/mL), 0.2 μL of the seeding stock, and 0.5 μL of the JCSG+ screen condition 2-33 (0.1 M potassium thiocyanate and 30% w/v PEG 2000 MME) from the reservoir.

2.3.6. Data collection and processing

X-ray diffraction data were collected at 100 K at Elettra (Trieste) without additional cryoprotectant. Data processing was performed with the XDS program package (21). Unit cell parameters and assigned space groups as well as data statistics are shown in Table 3. The solvent content was estimated based on the calculated Matthews coefficient (22). Molecular replacement was performed with Phaser (23) using the structure of *EcBBE* as the search template. Structure refinement was done with Phenix (24) followed by manual inspection and model rebuilding in Coot (25). The program Readysset! (included in Phenix) was used to generate restraints for metal coordination and the PEG fragment included in the refinement. In total, three sodium and one potassium ion were found to bind to the protein surface without structural impact. The TLSMD server was used to generate partitioning groups (three for chain A and four for chain B) to improve refinement (26). Several refinement cycles were done until all visible residues were assigned, and no significant changes in *R* and *R*_{free} were observed. Structure validation was performed using MolProbity (27).

Chain A of the model consists of residues Ser-27 to Gly-532. Chain B starts with residue Gln-30 and extends to Gly-532. Some residues at the N-terminal part could not be modeled into the electron density most likely due to their high flexibility (Val-43 and Ser-44 in chain A as well Gln-40, Ser-41, and Asp-42 in chain B). In addition, no clear electron density was visible for a loop region (residues 301-305) in both chains.

2.3.7. Thermofluor experiments

Thermofluor experiments were performed using a CFX Connect real time PCR system (BioRad, Hercules, CA, USA). The experiments were performed using Sypro[®] Orange as fluorescent dye in 50 mM MES buffer pH 7.0. Stock solutions of all substrates were prepared in water with a concentration of 10 mg/mL. For substrates with a lower solubility, a saturated solution was used. The total volume in each well was 25 μL with a protein concentration of 0.4 mg/mL and 2 mg/mL substrate. The starting temperature of 20 °C was kept for 5 min and then

the temperature was increased at a rate of 0.5 °C/min to 95 °C. Melting temperatures were determined using the program Bio-Rad CFX Manager 3.0.

2.3.8. Rapid reaction kinetics using stopped flow spectrophotometry

Reductive and oxidative half-reactions were determined with a stopped-flow device (SF-61DX2, TgK Scientific, UK) at 25 °C under anoxic conditions in a glove box (Belle Technology, Weymouth, UK). Oxygen was removed from the sample by flushing with nitrogen and subsequent incubation of the samples in the glove box for 1 h. Spectral changes of the flavin cofactor were followed at a wavelength of 450 nm using a KinetaScanT diode array detector (MG-6560, Hi-Tech) employing the Kinetic Studio software (TgK Scientific, UK). Reductive half-reactions were assayed by mixing 60 µM *AtBBE*-like 15 or 13 in 50 mM potassium phosphate buffer, pH 7.0, with various substrate concentrations. The observed rate constants at different substrate concentrations (k_{obs}) were determined using the Kinetic Studio software by fitting the data to an exponential function. If suitable, the dissociation constant was determined performing a sigmoidal fit of the observed rate constants employing Origin 7 (OriginLab Corporation, Northampton, USA). The oxidative half-reaction was determined by mixing oxygen free photo-reduced 60 µM *AtBBE*-like 15 or 13 with air-saturated buffer. Photoreduction was carried out according to Massey and Hemmerich (28).

2.3.9. Product identification

Products resulting from the conversion of monolignols and their glycosides were separated and identified using HPLC. Reactions were performed in 1.5 mL reaction vials in 50 mM potassium phosphate buffer, pH 7.0, at 30 °C and 700 rpm. Substrates were used at a concentration of 2.5 mM and 30 µg/mL of *AtBBE*-like 15. After 24 h, the reaction was quenched by mixing 500 µL sample with 500 µL methanol. Samples were spun for 10 min at 9400 x *g* in a bench-top centrifuge before the clear supernatant was applied to the HPLC. The products were identified by retention time and by comparing their UV absorption spectra with authentic standards. HPLC analyses were done using a Dionex UltiMate 3000 HPLC (Thermo Fisher Scientific, Waltham, MA, USA) equipped with an Atlantis[®] dC18 5µM (4.6 x 250 mm) column. Separation of all compounds was achieved using a linear gradient with water with 0.1% TFA as solvent A and acetonitrile with 0.1 TFA as solvent B and a flow rate of 0.5 mL/min. Separations were started with a mobile phase of 80% solvent A and 20% solvent B. The concentration of solvent B was increased to 50% within 20 min followed by a steep ramp to 100% solvent B in 10 min. At the end of the protocol, the concentration of solvent B was again decreased to 20% over 5 min. Retention times of authentic standard compounds were

determined using the described protocol. Under these experimental conditions, the following retention times were observed: coniferyl alcohol, 16.06 min; coniferyl aldehyde, 21.39 min; ferulic acid, 18.27 min; coumaryl alcohol, 15.52 min; coumaryl aldehyde, 21.07 min; *p*-coumaric acid, 17.67 min; sinapyl alcohol, 15.40 min; sinapyl aldehyde, 21.01 min and sinapic acid, 17.76 min.

2.3.10. Synthesis of monolignol glycosides

A glucosyltransferase from apple (UGT71A15, *Malus x domestica*) was used for the synthesis of 4-*O*- β -D-glucopyranosides of the monolignols (29). Heterologous expression in *Escherichia coli* and purification of the glucosyltransferase will be published elsewhere. Briefly, glucosylation of the aglyca (5 mM) from 7.5 mM uridine UDP-glucose was performed in 50 mM Tris/Cl buffer, pH 7.5, containing 50 mM MgCl₂, 0.13% BSA, and 10% DMSO in the presence of 6 μ M UGT71A15.

2.3.11. Phylogenetic tree construction

M-Coffee was used to create a multiple sequence alignment, including all 28 *AtBBE*-like family members (30). The alignment was edited by hand using Jalview (31). The PHYLIP package (PHYLIP 3.69) was used to create a bootstrapped phylogenetic tree using the programs SEQBOOT, PROTDIST, FITCH, and CONSENSE (32). We created 1000 Jackknife sub-alignments with SEQBOOT, which were subsequently subjected to a bootstrapped protein-distance analysis. We chose *EcBBE* as the outgroup sequence. The tree shown in supplementary Figure S1 was visualized using Figtree (Tree Figure Drawing Tool, version 1.4.0 by Andrew Rambaut). The accession codes for the sequences used for the analysis are given in the legend of supplementary Figure S1.

2.3.12. Docking

Docking of coniferyl alcohol was performed using AutoDock Vina using the default docking parameters (33, 34). Point charges were assigned according to the AMBER03 force field (35). The setup of the receptor was done with the YASARA molecular modeling program (36). Twenty five Vina docking runs were performed, and after clustering all runs, four distinct complex conformations with a binding energy of -6.4, -6.1, -5.0, and -4.6 kJ mol⁻¹ were found. The complex with a binding energy of -6.4 kJ mol⁻¹ and a conformation that is in agreement with the catalytic activity found for *AtBBE*-like 15 is shown in Figure 3. 8% of the docks cluster in this top pose.

2.4. Results

2.4.1. Enzymatic properties and identification of substrates of *AtBBE-like 13* and *AtBBE-like 15*

AtBBE-like 13 and *AtBBE-like 15* were expressed in *K. pastoris* and purified from the culture medium by nickel-Sepharose affinity chromatography and subsequent gel filtration yielding ~10 and 150 mg of protein from 1 liter of fermentation culture, respectively. To identify potential substrates, we inspected the chemical nature of substrates recently identified for vanillyl alcohol oxidase (VAO) superfamily members. This revealed that oxidation of primary and secondary alcohol groups is a prevailing feature in all of these reactions (4). In view of this recurring motif, we have assembled a library comprising predominantly compounds with one or more hydroxyl groups (see supplementary Table S1). Because strong protein-ligand interactions are known to increase the thermal stability of proteins, we first screened our library with regard to an increase in the melting temperature of *AtBBE-like 15* using the ThermoFluor method (37). This approach produced a number of promising hits, yielding a substantial increase of the melting temperature (up to 17 °C, for a complete list see supplementary Table S1). The compounds with the strongest effect on the thermal stability were tested as substrates revealing that cinnamyl alcohol was oxidized to cinnamyl aldehyde by *AtBBE-like 15*. Using cinnamyl alcohol as a lead structure, we tested several other naturally occurring aromatic alcohols as putative substrates and found that *AtBBE-like 15* oxidizes the monolignols *p*-coumaryl-, coniferyl-, and sinapyl alcohol to their corresponding aldehydes. To gain more detailed information on substrate specificity and kinetic parameters, reductive half-reactions were studied using stopped-flow spectrophotometry (a summary of kinetic parameters is given in Table 2). Reduction of *AtBBE-like 15* and 13, using either coniferyl or sinapyl alcohol, was very fast and essentially complete within the dead time of the instrument (~5 ms) indicating that the rate of reduction exceeds 500 s⁻¹. In the case of *p*-coumaryl alcohol, the rate of reduction could be analyzed as a function of substrate concentration, yielding a dissociation constant of 700 μM and a limiting rate of 332 s⁻¹. Because monosaccharides, such as D-glucose, had such a profound effect on the protein's thermal stability, we also analyzed the β-*O*-glycosylated derivatives of the monolignols and found that coniferin was accepted as a substrate exhibiting a dissociation constant of 660 μM and a limiting rate of reduction of 171 s⁻¹. However, the β-*O*-glycosylated derivatives of *p*-coumaryl- and sinapyl alcohol (syringin) were relatively poor substrates of the enzyme. An equivalent set of experiments was conducted with *AtBBE-like 13* demonstrating similar catalytic properties (summarized in Table 2). The observed rate constants for selected substrates determined for *AtBBE-like 15* and 13 are shown in Figure 1, A and B.

Thus, we propose that *AtBBE*-like 13 and *AtBBE*-like 15 are in fact monoglignol oxidoreductases.

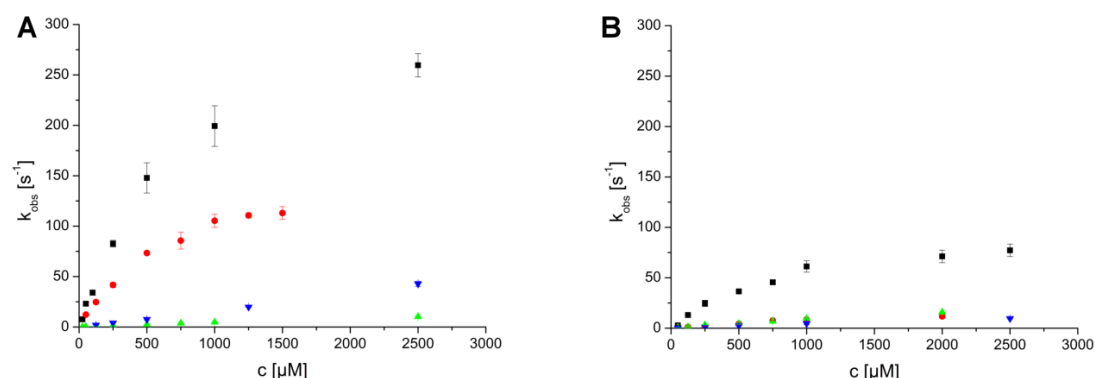


Figure 1: Rate constants observed for the reductive half-reaction of *AtBBE*-like 15 (A) and *AtBBE*-like 13 (B). A stopped-flow device was used to determine the rate constants of the reductive half-reaction of *AtBBE*-like 15 and 13 with *p*-coumaryl alcohol (■), cinnamyl alcohol (▲), conferyl alcohol β-glycoside (●), and sinapyl alcohol β-glycoside (▼). The course of the reaction was determined by following the absorption of the oxidized flavin at 450 nm. As the reactions follow pseudo-first order kinetics, rates were calculated from a mono exponential fit.

Table 2: Chemical structures of substrates and their kinetic parameters for *AtBBE*-like 13 and *AtBBE*-like 15. Dissociation constants and observed rates of reduction of *AtBBE*-like 13 and *AtBBE*-like 15 with different monoglignols and their glycosylated derivatives are shown.

Substrate		<i>AtBBE</i> -like 15 K_d [μM]	<i>AtBBE</i> -like 13 K_d [μM]	<i>AtBBE</i> -like 15 k_{obs} at 500 μM [s ⁻¹]	<i>AtBBE</i> -like 13 k_{obs} at 500 μM [s ⁻¹]
cinnamyl alcohol		n.a.*	n.a.*	2.6 ± 0.1	4.4 ± 0.4
<i>p</i> -coumaryl alcohol		700 ± 120	867 ± 123	156 ± 8	36.5 ± 1
conferyl alcohol		n.a.**	n.a.**	> 500**	> 500**
sinapyl alcohol		n.a.**	n.a.**	> 500**	> 500**
<i>p</i> -coumaryl alcohol β-glycoside		n.a.*	n.a.*	0.01 ± 0.001	0.01 ± 0.001
conferyl alcohol β-glycoside		660 ± 100	1856 ± 624	73 ± 1	4.4 ± 1.1
sinapyl alcohol β-glycoside		n.a.*	n.a.*	7.5 ± 0.7	2.4 ± 0.2

* Data were not determined due to solubility limitation.

** Reaction was too fast to be measured.

Reoxidation of photo-reduced *AtBBE*-like 13 and *AtBBE*-like 15 by molecular dioxygen was very slow yielding an oxidative rate constant of $3.3 \pm 0.6 \text{ M}^{-1} \text{ s}^{-1}$ and $27.5 \pm 1.4 \text{ M}^{-1} \text{ s}^{-1}$, respectively, thus indicating that the enzymes suppress the reduction of oxygen by the reduced FAD cofactor. Recently, we have reported that oxygen reactivity in the BBE family is controlled by the side chain of a gatekeeper residue in the “oxygen reactivity loop” on the *re*-side of the isoalloxazine ring. In the case of *AtBBE*-like 15, the gatekeeper residue is a leucine (Leu-182), and thus oxygen reactivity is suppressed because the side chain blocks access to the oxygen pocket (38). Replacement of Leu-182 to valine in *AtBBE*-like 15 increased the rate of reoxidation ~ 400 -fold to $1 * 10^4 \text{ M}^{-1} \text{ s}^{-1}$, *i.e.* very similar to the rate found with *EcBBE* ($k_{\text{ox}} = 5 * 10^4 \text{ M}^{-1} \text{ s}^{-1}$) (39), which also possesses a valine residue in the gatekeeper position. Because the reaction of the reduced FAD with dioxygen is very slow, we assume that an alternative electron acceptor is required for reoxidation of the reduced FAD cofactor of *AtBBE*-like 13 and *AtBBE*-like 15 *in planta*.

2.4.2. Crystal structure of *AtBBE*-like 15

To better understand the enzymatic reaction mechanism and substrate binding to the active site, we have elucidated the three-dimensional structure of *AtBBE*-like 15 by means of x-ray crystallography (Protein Data Bank code 4ud8). Protein crystals were obtained using sitting drop conditions yielding diffraction data to 2.1 Å. The structure was solved by molecular replacement using *EcBBE* (Protein Data Bank 3D2H) with two molecules in the asymmetric unit (data collection and statistics are given in Table 3). *AtBBE*-like 15 adopts the same fold as other BBE-like enzymes, *i.e.* the VAO-fold that is characterized by a FAD-binding and a substrate-binding domain (Figure 2C, shown in green and orange, respectively). The substrate-binding domain consists of a seven-stranded antiparallel β -sheet, which is covered by α -helices. The substrate-binding pocket and the active site are formed by two short loops (termed loop $\beta 2$ - $\beta 3$ and loop αL - αM), the “oxygen reactivity motif” consisting of loop αD - αE , helix αE and loop αE - $\beta 6$. Additionally, the three strands $\beta 14$, $\beta 15$, and $\beta 16$ contribute to the active site (Figure 2B, nomenclature of secondary structure elements according to (15)). The FAD cofactor is bicovalently linked to the peptide chain via a covalent bond of His-115 to the 8α -methyl group and of Cys-179 to the C6-position of the isoalloxazine ring.

Table 3: Data acquisition and refinement parameters for x-ray crystallography.

(JCSG+ #2-33)	
Beamline	Elettra XRD1
Wavelength (Å)	0.971670
Unit cell parameters (Å,°)	63.6, 94.7, 188.3, 90, 90, 90
Space group	P2 ₁ 2 ₁ 2 ₁
Resolution limits (Å)	50-2.09 (2.21-2.09)
R _{meas}	0.209 (0.865)
R _{merge}	0.191 (0.794)
Total number of observations	415743 (58987)
Total number unique	67102 (9501)
<I/σ(I)>	7.73 (2.23)
Completeness (%)	97.8 (87.0)
Redundancy	6.2
Wilson B factor (Å ²)	32.02
Matthews coefficient (Å ³ Da ⁻¹)	2.36
Molecules per ASU	2
Solvent content (%)	48
<i>Refinement</i>	
Resolution (Å)	47.37 – 2.09
R (%)	18.35
R _{free} (%)	22.09
<i>R.m.s.d. stereochemistry</i>	
Bond lengths (Å)	0.008
Bond angles (°)	0.825
No. of protein atoms	7946
No. of non-protein atoms	247
No. of water molecules	615
Average B factor (Å ²)	25.54
<i>Ramachandran analysis</i>	
Favoured (%)	95.96
Allowed (%)	3.94
Disallowed (%)	0.1
<i>PDB code</i>	4ud8

As hydride transfer from the substrate to the N5-locus of the flavin cofactor is a generally accepted mode of reduction, a sphere with a radius of 10 Å around this locus was examined for putative catalytic residues. As shown in Figure 2A, Tyr-117 and Gln-438 are engaged in a hydrogen bond on the *si*-side of the isoalloxazine ring (2.6 Å). These residues are positioned between the active site and the binding pocket and thus must interact with the substrate when it enters the active site. Therefore, these residues were defined as substrate coordination motif. The hydroxyl groups of Tyr-117, Tyr-479, and Tyr-193 point towards the active site with distances to the N5-locus of 4.8 Å, 4.6 Å, and 5.0 Å, respectively. The two phenolic hydroxyl groups of Tyr-479 and Tyr-193 are within hydrogen bond distance (2.4 Å, Figure 2A). The ε-amino group of Lys-436 is located 3.1 Å above the plane of the aromatic ring of Tyr-193 and engages in a cation-π interaction. This arrangement of Tyr-479, Tyr-193, and Lys-436 presumably favors deprotonation of the phenolic hydroxyl group of Tyr-193 and activates this residue as a putative active site base, and thus these residues were defined as catalytic base motif.

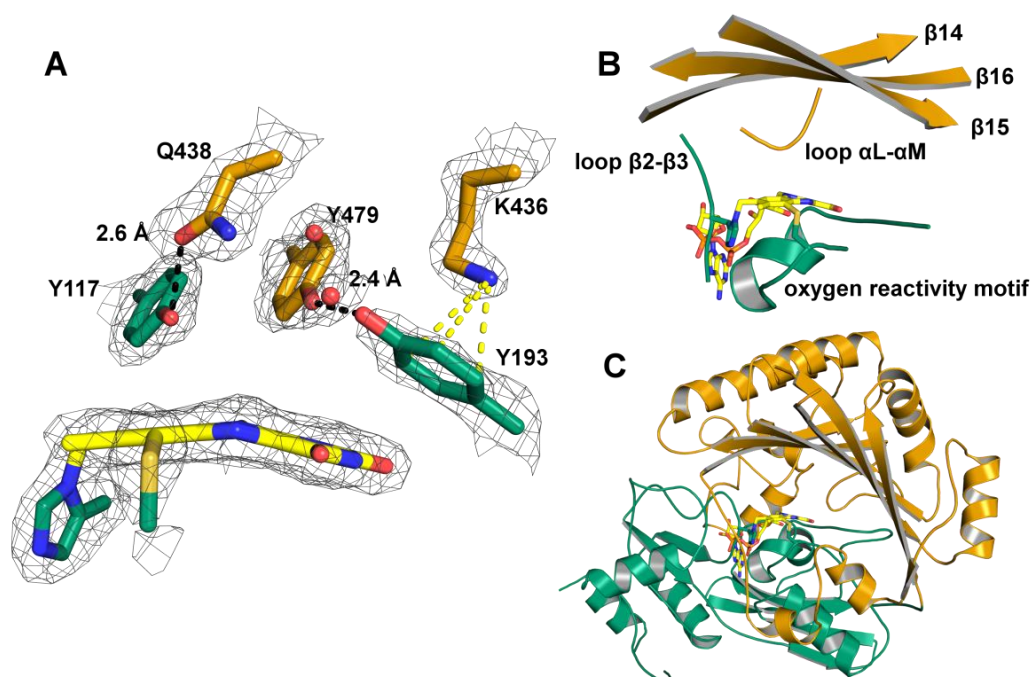


Figure 2: (A) Close-up view of the amino acids with a proposed role in substrate binding and catalysis. Tyr-117 and Gln-438 form a hydrogen bond. Lys-436 and Tyr-193 are involved in a cation- π interaction, and Tyr-193 forms a hydrogen bond to Tyr-479. Two well defined water molecules are found in the active site (red spheres). The electron density was cut off at a sigma value of 1.5 Å. (B) Close-up view of the active site: Loop $\beta 2$ - $\beta 3$ and the oxygen reactivity motif originate from the FAD-binding domain and harbor His-115 and Cys-179, which form the two covalent linkages to the isoalloxazine ring of the FAD. Strands $\beta 14$, $\beta 15$, and $\beta 16$ and loop αL - αM originate from the substrate-binding domain. They harbor amino acids defining the *si*-face near the N5-locus (<10 Å) that are putatively involved in the catalytic mechanism. (C) Overall topology of *AtBBE*-like 15: *AtBBE*-like 15 adopts the VAO topology consisting of a FAD-binding domain (green) and a substrate-binding domain (orange). Furthermore, it features a bicovalently attached FAD typical for BBE-like proteins. The FAD cofactor is shown in stick representation in yellow.

2.4.3. Docking of substrates to the active site

Because co-crystallization with the identified substrates was unsuccessful, we conducted docking experiments using coniferyl alcohol as a model substrate in order to gain further insights into the interaction of substrates with amino acid residues in the active site. At the *si*-side of the isoalloxazine ring a hydrophobic pocket is formed by residues Phe-373, Phe-377, Leu-407, and Leu-440 and the dimethylbenzene moiety of the isoalloxazine ring. As shown in Figure 3, the substrate fits into this hydrophobic pocket (binding energy of -6.4 kJ mol^{-1}). The docking result suggests that the orientation of the allylic alcohol towards the proposed catalytic base Tyr-193 is possible, although the aromatic ring is located in the hydrophobic pocket, and thus this orientation is consistent with the productive catalysis found for *AtBBE*-like 15 with this ligand.

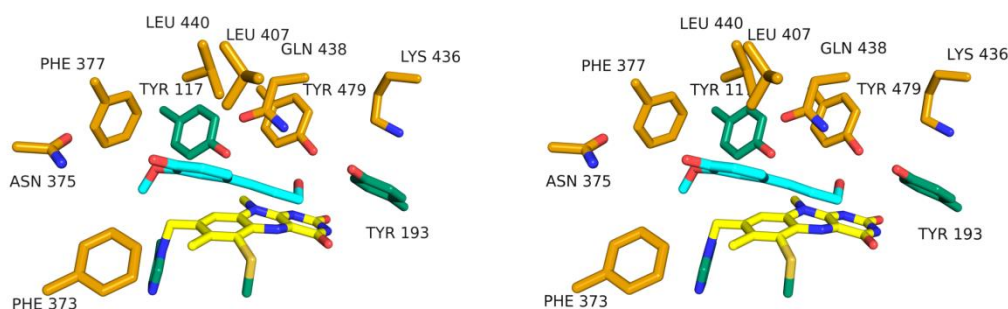


Figure 3: Substrate binding to *AtBBE*-like 15. The substrate-binding cavity and active site of *AtBBE*-like 15 are shown in stereo view. The isoalloxazine ring is shown in yellow and conferyl alcohol in light blue as a stick model. Conferyl alcohol was docked into the cavity using YASARA. The aromatic moiety is located in the hydrophobic binding pocket formed by Phe-377, Phe-373, Leu-407, Leu-440, and Tyr-117, and the isoalloxazine ring, whereas the allyl alcohol is facing the active site. All residues shown in this figure are conserved in *AtBBE*-like 13.

2.4.4. Functional and structural characterization of the BBE-like family in *A. thaliana*

The identification of critical active site residues with a role in substrate binding and catalysis in *AtBBE*-like 15 raised the question whether these are conserved in all *AtBBE*-like family members. To investigate this issue, we have constructed a protein distance tree (Figure 4, left). Seven distinct groups can be identified in the phylogenetic tree within the family of BBE-like enzymes in *A. thaliana*, in good agreement with previously published work (9). Based on these distinct groups, we have created sequence logos for each of the elements forming the active site, *i.e.* the three strands at the ceiling of the active site cavity and the three loops in the vicinity of the isoalloxazine ring (Figure 4, right). The histidine residue (His-115) in loop β 2- β 3 that forms the covalent bond to the 8α -methyl group of the flavin isoalloxazine ring is conserved in all *AtBBE*-like enzymes, and thus it can be assumed that the covalent linkage is present in all family members. In contrast, the cysteine residue (Cys-179) located in the “oxygen reactivity motif” is only conserved in phylogenetic groups 2, 4, 5, and 7, whereas the remaining groups feature other amino acids, such as histidine (group 1), serine (group 3) or tyrosine (group 1 and 6). We assume that these four *AtBBE*-like enzymes possess a single covalent linkage whereas the remaining 24 feature a bicovalent linkage of the FAD cofactor as already shown for *EcBBE* (40), *Dbv29* (41), glucooligosaccharide oxidase (*GOOX*) (42), and *THCA* synthase (15).

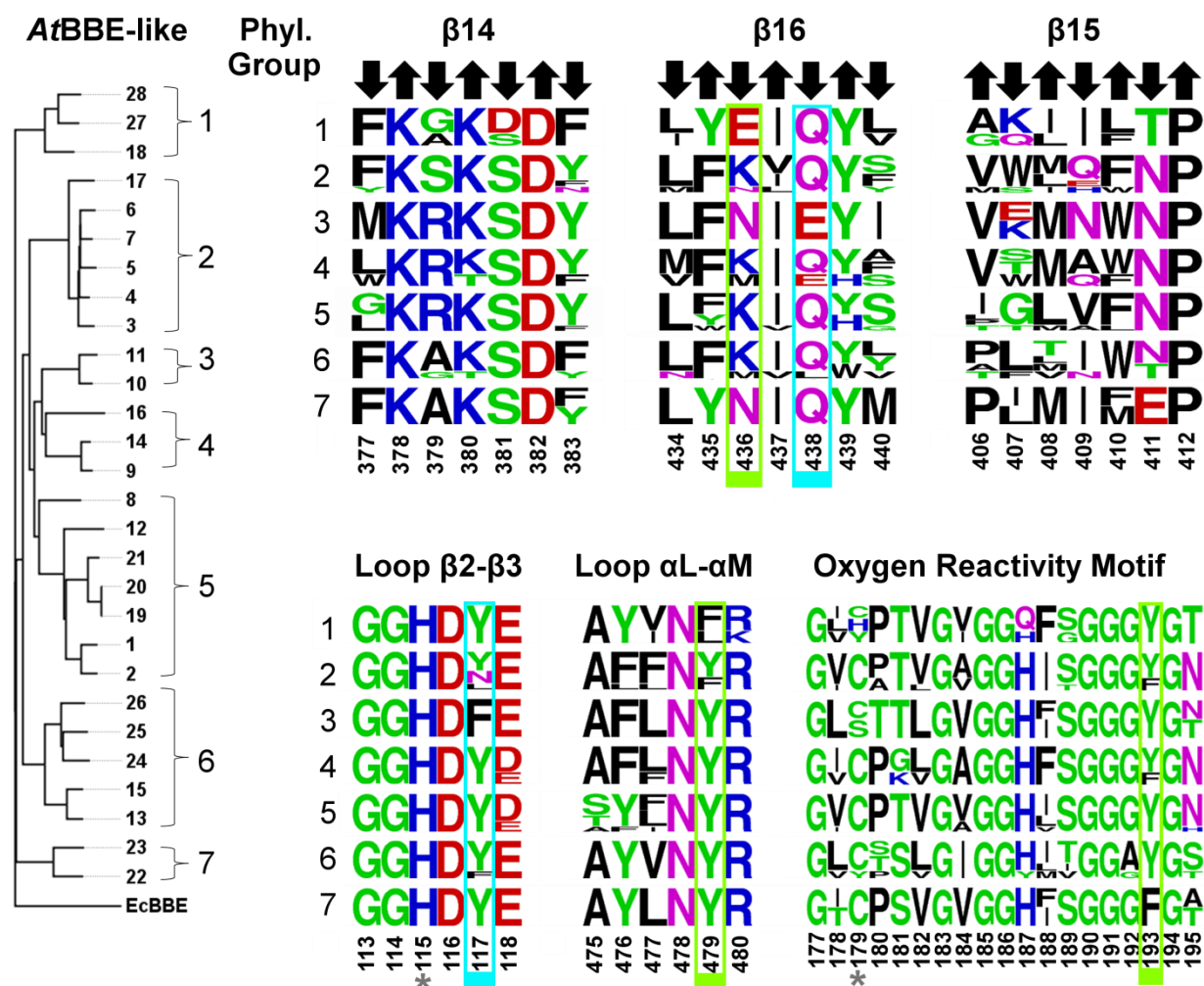


Figure 4: Chemical nature of the active sites present in different phylogenetic groups is represented by sequence logos of the active site forming secondary structure elements. Left: Protein distance tree of all BBE-like enzymes from *A. thaliana* with EcBBE as outgroup. Right: Sequence logos representing the structural elements forming the active site of the seven phylogenetic groups reveal highly conserved motifs. Arrows indicate the orientation of the residues in the β -strands. An upward arrow indicates that the residue points away from the active site. These residues were found to be structurally relevant. A downward arrow indicates the residue points towards the active site and thereby contributes to the decoration. Residues highlighted in a green and cyan box define the substrate coordination and catalytic motifs, respectively. Both motifs are putatively involved in the catalytic mechanism (see also Figure 5 and 6). Positions labeled with an asterisk highlight the two potential sites of covalent linkage.

Further analysis of the sequence logos generated for the three strands of the β -sheet provided important insights into the functions of amino acid side chains. Generally, amino acids oriented towards the α -helices (Figure 4, upward pointing arrows) are conserved because they are important for the structural integrity of the protein. For example, Lys-380 and Asp-382 in strand $\beta 14$ form salt bridges to Asp-481 (2.7 Å) and Arg-473 (3.3 Å), respectively. Thus, these amino acids are invariant in the whole family, because all of them adopt the same overall topology. In contrast, amino acid residues pointing towards the active site (Figure 4, downward

pointing arrows) are only conserved within certain phylogenetic groups, indicating that the composition of the active site differs markedly. In the case of *AtBBE*-like 15 (group 6 in Figure 4), the active site residues Tyr-117, Tyr-193, Lys-436, Gln-438, and Tyr-479 are important for substrate binding and catalysis (boxed residues in Figure 4 and shown as stick models in Figure 5A). While residues Tyr-193, Tyr-479, and Lys-436 concertededly act as an active site base (Figure 5A, “catalytic motif”, shown in green), Tyr-117 and Gln-438 appear to be involved in determining the substrate preference (“substrate coordination motif”, shown in cyan). Both motifs are strictly conserved in 14 members of the BBE-like enzymes in *A. thaliana* (see Table 4), indicating that their catalytic mechanism and substrate preference will be similar, *i.e.* oxidation of alcohols to their corresponding aldehyde products. This analysis was extended to other plants revealing that the active site signature found in *AtBBE*-like 13 and *AtBBE*-like 15 is conserved in soybean (*Glycine max*; 21 homologs out of 43 BBE-like enzymes), eucalyptus (*Eucalyptus grandis*; 18 out of 27), poplar (*Populus trichocarpa*; 17 out of 64) and potato (*Solanum tuberosum*; 6 out of 18). Interestingly, monocotyledonous species such as maize (*Zea mays*; 16 BBE-like enzymes) and rice (*Oriza sativa*, 11 BBE-like enzymes) appear to lack monolignol oxidoreductase activity, because the catalytic and substrate coordination motifs are not found in any of the BBE-like enzymes.

In contrast, major variations in the catalytic and/or substrate coordination motif are seen in groups one, three and seven. In group one, Lys-436 in the catalytic motif is replaced by glutamic acid (Figure 4, strand β 16, and Figure 5B) and Tyr-479 by phenylalanine or leucine, respectively (Figure 4, α L- α M), although the substrate coordination motif is conserved. In group three, the substrate coordination motif (Tyr-117 and Gln-438 are replaced by phenylalanine and glutamic acid, respectively) as well as the catalytic motif residues (Lys-438 replaced by asparagine) are modified (Figure 5C). Group seven features a conserved substrate coordination motif, but in the catalytic motif residues Lys-436 and Tyr-193 are replaced by asparagine and phenylalanine, respectively (Figure 5D). It is worthwhile noting that in all cases where the catalytic motif appears to be disrupted, an alternative catalytic base is present, for example glutamic acid instead of Lys-436 or Asp-411 in groups one and seven, respectively. Similarly, Gln-438 in group three is replaced by glutamic acid. Overall, we conclude that the BBE-like enzymes of these groups have distinct catalytic properties and act on different yet unidentified substrates. Interestingly, the presence of a catalytic active base appears to be an important feature in BBE-like enzymes, as it was also observed in *EcBBE* (16), *Dbv29* (41), *GilR* (43), *GOOX* (42) and *THCA*-synthase (15).

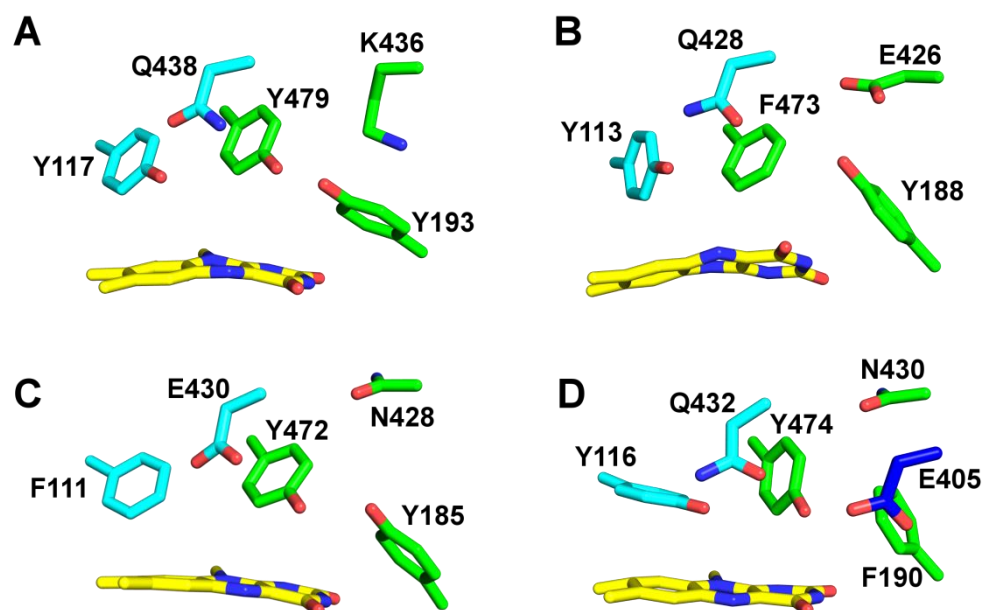


Figure 5: Active site composition predominantly present in different phylogenetic groups. The active site compositions shown in B, C and D were visualized using homology models created with YASARA. A: Active site composition of *AtBBE*-like 15 that is representative for groups 2 and 4-6. B: This active site composition is found in group 1 (numbering according to *AtBBE*28). The catalytic base as found in *AtBBE*-like 15 has been disrupted. Lys-436 has been replaced by a glutamic acid that putatively can recover the catalytic base function. C: This active site composition is found in group 3 (numbering according to *AtBBE*11). The catalytic base motif is inconsistent, Gln-438 has been replaced by a glutamic acid what putatively recovers the catalytic base function. D: Active site composition as found in group 7 (numbering according to *AtBBE*22). In the catalytic base motif, Lys-436 has been replaced by an asparagine and Tyr-193 by a phenylalanine. In β 15, a glutamic acid can be found that putatively recovers the catalytic base function in this active site.

Table 4: Composition of the substrate coordination (Tyr-117 and Gln-438) and catalytic motif (Tyr-193, Lys-436, and Tyr-479).

	Phyl group	Y117	Q438	Y193	K436	Y479
<i>AtBBE18</i>	1	Y	Q	Y	E	L
<i>AtBBE27</i>	1	Y	Q	Y	E	F
<i>AtBBE28</i>	1	Y	Q	Y	E	F
<i>AtBBE3</i>	2	N	Q	Y	K	Y
<i>AtBBE4</i>	2	Y	Q	Y	K	Y
<i>AtBBE5</i>	2	Y	Q	F	N	F
<i>AtBBE6</i>	2	N	Q	F	K	F
<i>AtBBE7</i>	2	L	Q	Y	K	Y
<i>AtBBE17</i>	2	Y	Q	Y	K	Y
<i>AtBBE10</i>	3	F	E	Y	N	Y
<i>AtBBE11</i>	3	F	E	Y	N	Y
<i>AtBBE9</i>	4	Y	Q	Y	K	Y
<i>AtBBE14</i>	4	Y	Q	Y	K	Y
<i>AtBBE16</i>	4	Y	E	F	M	Y
<i>AtBBE1</i>	5	Y	Q	Y	K	Y
<i>AtBBE2</i>	5	Y	Q	Y	K	Y
<i>AtBBE8</i>	5	Y	Q	Y	K	Y
<i>AtBBE12</i>	5	Y	Q	Y	K	Y
<i>AtBBE19</i>	5	Y	Q	Y	K	Y
<i>AtBBE20</i>	5	Y	Q	Y	K	Y
<i>AtBBE21</i>	5	Y	Q	Y	K	Y
<i>AtBBE13</i>	6	Y	Q	Y	K	Y
<i>AtBBE15</i>	6	Y	Q	Y	K	Y
<i>AtBBE24</i>	6	F	L	Y	K	Y
<i>AtBBE25</i>	6	Y	Q	Y	M	Y
<i>AtBBE26</i>	6	Y	Q	Y	K	Y
<i>AtBBE22</i>	7	Y	Q	F	N	Y
<i>AtBBE23</i>	7	Y	Q	F	N	Y

2.5. Discussion

2.5.1. Catalytic mechanism of monolignol oxidation

Based on the crystallographic structure of *At*BBE-like 15 and the results obtained by substrate docking, we propose the following catalytic mechanism: Tyr-193 is positioned such that the phenolic hydroxyl group points toward the substrate's alcohol group. Lys-436 forms a cation- π interaction with the aromatic ring of Tyr-193 thereby lowering the pK_a and thus stabilizing the deprotonated state. We also assume that Tyr-479 stabilizes the deprotonated state of Tyr-193 by hydrogen bonding (Figures 2 and 3). Thus, these three amino acids make up the core catalytic machinery for deprotonation of the substrate's hydroxyl group that results in the concomitant transfer of a hydride from the C γ position to the N5 locus of the isoalloxazine ring of the flavin. A schematic reaction mechanism for the oxidation of monolignols by *At*BBE-like 15 is shown in Figure 6. To test this hypothesis, we have initiated a site-directed mutagenesis study of the pertinent active site residues.

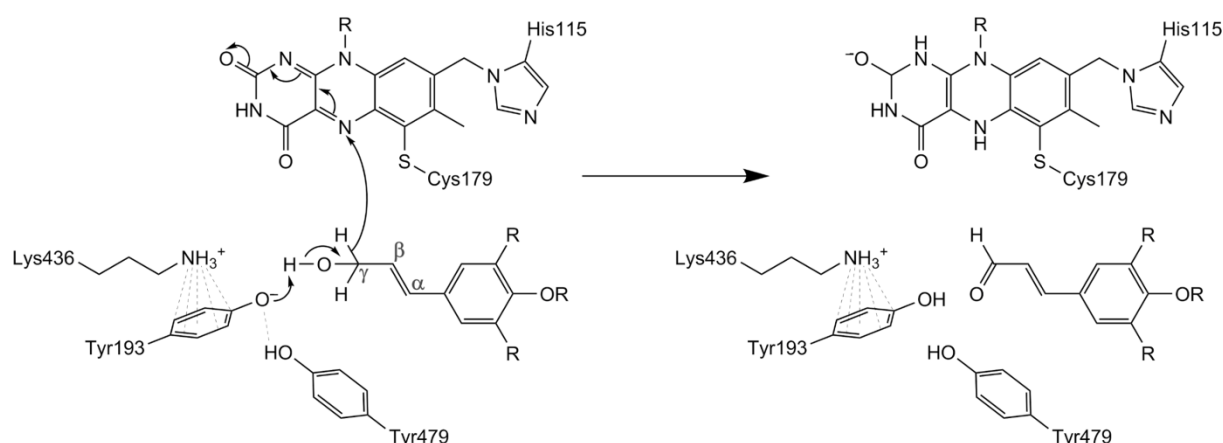


Figure 6: Proposed reaction mechanism for substrate oxidation. Tyr-193, Tyr-479, and Lys-436 concertedly act as an active site base abstracting a proton from the alcohol with subsequent hydride transfer to the N5 of the isoalloxazine ring.

2.5.2. Structural comparison with other members of the VAO family

In recent years, the structures of several other members of the VAO family were determined that share a high degree of structural similarity despite low similarity on the sequence level. Structural superposition of *At*BBE-like 15 with Dbv29, GOOX, AknOx and *Ec*BBE gives a root mean square deviation of 1.45 Å (for 1652 backbone atoms), 1.36 Å (for 1556 backbone atoms), 1.47 Å (for 1526 backbone atoms) and 0.95 Å (for 2068 backbone atoms) respectively, whereas sequence identities of 22, 22, 23, and 41%, respectively, are found. The bacterial

oxidases Dbv29 and AknOx catalyze similar oxidations of alcohol groups and thus possess a very similar catalytic motif consisting of both tyrosine residues and the lysine residue also present in *AtBBE*-like 15, whereas the substrate recognition motif is clearly different as depicted in Figure 7 (C and D, respectively). In any case, these enzymes act on alcohol substrates that show no similarity to the substrates identified for *AtBBE*-like 15 and 13 and, moreover, are not related to lignin metabolism. Importantly, for Dbv29 and AknOx it was found that both tyrosine residues are crucial for catalysis thus supporting the proposed role of Tyr-193 and Tyr-479 in the mechanism shown in Figure 6 for *AtBBE*-like 15 (and *AtBBE*-like 13) (10,41). Although Dbv29 and AknOx resemble *AtBBE*-like 15 and 13 concerning the composition of the active site on the *si*-side of the isoalloxazine ring, the residue that determines the reactivity towards dioxygen, *i.e.* Leu-182 in the case of *AtBBE*-like 15, is a valine in both enzymes, defining them as oxidases (38). The active site of GOOX has the same substrate recognition motif but a distinct catalytic motif featuring a glutamate residue (shown in blue in Figure 7E) instead of the tyrosine and lysine seen in *AtBBE*-like 15 (compare B and E in Figure 7). In fact, this active site composition is similar to group one of the *AtBBE*-like family, and thus it is conceivable that these BBE-homologs are also involved in the oxidation of carbohydrates as already reported for some plant BBE-like enzymes (8,9). Not surprisingly, the biggest difference in active site composition is seen with *EcBBE* as this enzyme catalyzes an unusual oxidative ring closure reaction in alkaloid biosynthesis; although the overall topology shows high similarity (Figure 7A), except for the tyrosine in the substrate recognition motif (Tyr-106), all other residues vary (compare B and F in Figure 7). Moreover, Glu-417 replacing the glutamine of the substrate recognition motif assumes a crucial role in the reaction mechanism of *EcBBE* and thus becomes part of the catalytic machinery of the enzyme (16). This comparison illustrates that this enzyme family can be tuned for new reactivities by strategic single or multiple exchanges of amino acids in the active site. In fact, even within a given active site different (oxidation), reactions are supported depending on the available substrates further demonstrating the plasticity of the active site (44).

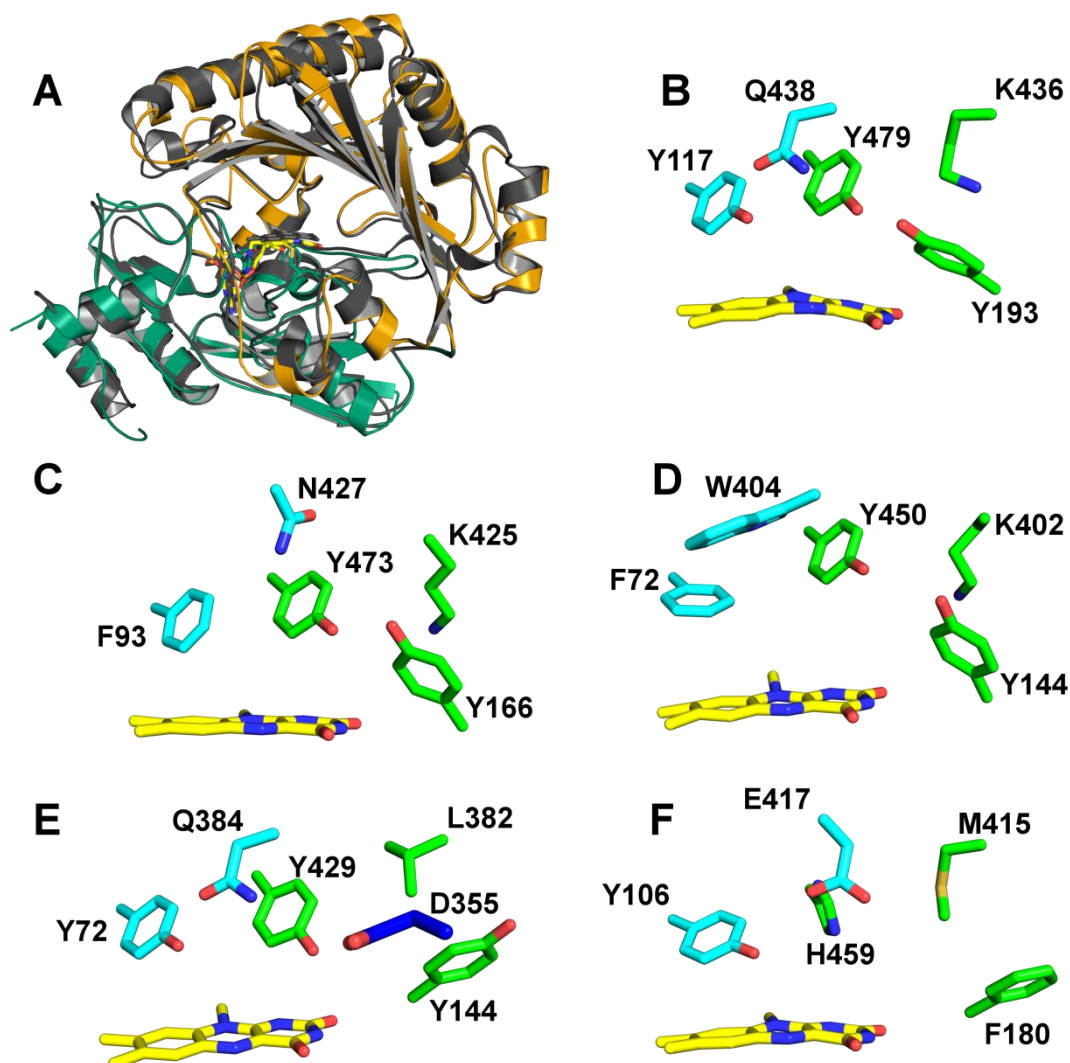


Figure 7: Comparison of overall topology and active site composition of various BBE-like enzymes and VAO superfamily members. Panel A: Overall topology of *AtBBE*-like 15 and superposition with *EcBBE*. B-F show the substrate coordination and catalytic motif in green and cyan, respectively, for the following BBE-like proteins. B, *AtBBE*-like 15, the substrate coordination motif consists of Tyr-117 and Gln-438, and the catalytic motif is formed by Tyr-479, Tyr-193, and Lys-436. C, *Dbv29*, the catalytic motif is invariant, whereas the substrate coordination motif is different. D, *AknOx*, the catalytic motif is invariant, whereas the substrate coordination motif differs. E, *GOOX*, the catalytic motif is disrupted, and it appears to be restored by the presence of another catalytic base, *i.e.* Asp-355. F, *EcBBE*, both motifs are disrupted with Glu-417 serving as a catalytic base.

2.5.3. Proposed role of *AtBBE-like15/monolignol oxidoreductases in plants*

Monolignols are secreted into the apoplast and polymerized to various cell wall components. Although monolignols are thought to be secreted in their alcohol forms, not all monolignol-derived cell wall components are coupling products of monolignols but the aldehydes are also incorporated into the cell wall (45). It has been shown by mass spectrometry that *AtBBE-like 15* is located in the apoplastic fluid of *A. thaliana*, and thus our findings that *AtBBE-like 15* (and *AtBBE-like 13*) oxidizes monolignols to their corresponding aldehydes indicates that they are likely physiological substrates (46). In addition, the glycosylated form of coniferyl alcohol (coniferin) is also accepted as substrate. Additionally, oxidation of coniferin to its corresponding aldehydes has been postulated by Tsuji *et al.* (47) for the plant *Ginkgo biloba*. According to their hypothesis, oxidation of the β -glycosylated monolignols precedes hydrolysis to the free monolignols and thus plays an important role for the mobilization of monolignols from their glycosidic storage forms. Hence, the demonstrated activity of *AtBBE-like 13* and *AtBBE-like 15 in vitro* suggests that the enzymes may participate in the mobilization and oxidation of monolignols required for polymerization processes in the plant cell wall (*e.g.* lignification). Interestingly, more than 20 different glycoside hydrolases were also identified during this proteome analysis, suggesting that *AtBBE-like 15* and potentially also other members of the family work in concert with these hydrolases to mobilize building blocks from their storage forms. This concept receives further support by co-expression data retrieved from the ATTET II server (CoExSearch Version 4.1). Among the enzymes co-expressed with *AtBBE-like 15* are phenylalanine ammonia-lyase 4 (PAL4), an important rate-determining entry point of the phenylpropanoid pathway, and β -glucosidase 41 clustering with the monolignol glucoside hydrolases At1g61810 (BGLU45) and At1g61820 (BGLU46) (see supplementary Table S2) (48,49). Thus, we suggest that *AtBBE-like 13* and *AtBBE-like 15* participate in the adaptation of the extracellular monolignol pool prior to polymerization and are thus involved in cell wall formation required during certain growth phases and in response to stressors. Because the active site motifs found in *AtBBE-like 13* and *AtBBE-like 15* are conserved in 12 other members of the BBE-like enzyme family in *A. thaliana*, we predict that they play similar roles in the plant potentially with diverging substrate specificities or, alternatively, with different spatial (*i.e.* different tissues) or temporal (*i.e.* induced by different biotic or abiotic stressors) features. The presence of homologs of *AtBBE-like 13* and *AtBBE-like 15* in many other plants (see above) indicates a general role of this enzyme family in the plant kingdom. In contrast, enzymes such as *EcBBE* and THCA-synthase serve in “secondary” pathways restricted to certain plant families or genera, and hence these have evolved, *e.g.* by gene duplication and subsequent

diversification by mutation, from the primordial monolignol oxidoreductases, a phenomenon well documented for the evolution of new plant defense compounds (50).

From the analysis of the active site signatures, it is also evident that *AtBBE*-like enzymes in phylogenetic groups one, three, and seven possess distinct catalytic machineries and probably act on as yet unidentified substrates. These BBE homologs are currently the target of further studies to reveal their biochemical properties and physiological function. In addition, we have initiated the generation, identification, and characterization of gene knock-out plants with the aim to investigate the role of *AtBBE*-likes in cell wall metabolism during plant development and stress response.

2.6. References

1. Winkler, A., Hartner, F., Kutchan, T. M., Glieder, A., and Macheroux, P. (2006) Biochemical evidence that berberine bridge enzyme belongs to a novel family of flavoproteins containing a bi-covalently attached FAD cofactor *J. Biol. Chem.* **281**, 21276-21285
2. Facchini, P. J., Penzes, C., Johnson, A. G., and Bull, D. (1996) Molecular characterisation of berberine bridge enzyme genes from opium poppy *Plant Physiol.* **112**, 1669-1677
3. Kutchan, T. M., and Dittrich, H. (1995) Characterization and mechanism of the berberine bridge enzyme, a covalently flavinylated oxidase of benzophenanthridine alkaloid biosynthesis in plants *J. Biol. Chem.* **270**, 24475-24481
4. Wallner, S., Dully, C., Daniel, B., and Macheroux, P. (2012) Berberine bridge enzyme and the family of bicovalent flavoenzymes. in *Handbook of flavoproteins*, de Gruyter. pp 1-24
5. Winter, D., Vinegar, B., Nahal, H., Ammar, R., Wilson, G. V., and Provart, N. J. (2007) An "Electronic Fluorescent Pictograph" browser for exploring and analyzing large-scale biological data sets *PLoS One* **2**, e718
6. Gonzalez-Candelas, L., Alamar, S., Sanchez-Torres, P., Zacarias, L., and Marcos, J. F. (2010) A transcriptomic approach highlights induction of secondary metabolism in citrus fruit in response to *Penicillium digitatum* infection *BMC Plant Biol.* **10**, 194
7. Attila, C., Ueda, A., Cirillo, S. L., Cirillo, J. D., Chen, W., and Wood, T. K. (2008) *Pseudomonas aeruginosa* PAO1 virulence factors and poplar tree response in the rhizosphere *Microb. Biotechnol.* **1**, 17-29
8. Carter, C. J., and Thornburg, R. W. (2004) Tobacco nectarin V is a flavin-containing berberine bridge enzyme-like protein with glucose oxidase activity *Plant Physiol.* **134**, 460-469
9. Custers, J. H., Harrison, S. J., Sela-Buurlage, M. B., van Deventer, E., Lageweg, W., Howe, P. W., van der Meijs, P. J., Ponstein, A. S., Simons, B. H., Melchers, L. S., and Stuiver, M. H. (2004) Isolation and characterisation of a class of carbohydrate oxidases from higher plants, with a role in active defence *Plant J.* **39**, 147-160
10. Alexeev, I., Sultana, A., Mäntsälä, P., Niemi, J., and Schneider, G. (2007) Aclacinomycin oxidoreductase (AknOx) from the biosynthetic pathway of the antibiotic aclacinomycin is an unusual flavoenzyme with a dual active site *Proc. Natl. Acad. Sci. USA* **104**, 6170-6175
11. Carlson, J. C., Li, S., Gunatilleke, S. S., Anzai, Y., Burr, D. A., Podust, L. M., and Sherman, D. H. (2011) Tirandamycin biosynthesis is mediated by co-dependent oxidative enzymes *Nature Chem.* **3**, 628-633
12. Mo, X., Huang, H., Ma, J., Wang, Z., Wang, B., Zhang, S., Zhang, C., and Ju, J. (2011) Characterization of TrdL as a 10-hydroxy dehydrogenase and generation of new analogues from a tirandamycin biosynthetic pathway *Org. Lett.* **13**, 2212-2215
13. Pagnussat, G. C., Yu, H. J., Ngo, Q. A., Rajani, S., Mayalagu, S., Johnson, C. S., Capron, A., Xie, L. F., Ye, D., and Sundaresan, V. (2005) Genetic and molecular identification of genes required for female gametophyte development and function in *Arabidopsis* *Development* **132**, 603-614
14. Hooper, C. M., Tanz, S. K., Castleden, I. R., Vacher, M. A., Small, I. D., and Millar, A. H. (2014) SUBAcon: a consensus algorithm for unifying the subcellular localization data of the *Arabidopsis* proteome *Bioinformatics* **30**, 3356-3364

15. Shoyama, Y., Tamada, T., Kurihara, K., Takeuchi, A., Taura, F., Arai, S., Blaber, M., Morimoto, S., and Kuroki, R. (2012) Structure and function of 1-tetrahydrocannabinolic acid (THCA) synthase, the enzyme controlling the psychoactivity of *Cannabis sativa* *J. Mol. Biol.* **423**, 96-105
16. Winkler, A., Lyskowski, A., Riedl, S., Puhl, M., Kutchan, T. M., Macheroux, P., and Gruber, K. (2008) A concerted mechanism for berberine bridge enzyme *Nature Chem. Biol.* **4**, 739-741
17. Petersen, T. N., Brunak, S., von Heijne, G., and Nielsen, H. (2011) SignalP 4.0: discriminating signal peptides from transmembrane regions *Nature Meth.* **8**, 785-786
18. Weis, R., Luiten, R., Skranc, W., Schwab, H., Wubbolts, M., and Glieder, A. (2004) Reliable high-throughput screening with *Pichia pastoris* by limiting yeast cell death phenomena *FEMS Yeast Res.* **5**, 179-189
19. Schrittwieser, J. H., Resch, V., Wallner, S., Lienhart, W. D., Sattler, J. H., Resch, J., Macheroux, P., and Kroutil, W. (2011) Biocatalytic organic synthesis of optically pure (S)-scoulerine and berbine and benzyloquinoline alkaloids *J. Org. Chem.* **76**, 6703-6714
20. D'Arcy, A., Villard, F., and Marsh, M. (2007) An automated microseed matrix-screening method for protein crystallization *Acta Crystallogr.* **D63**, 550-554
21. Kabsch, W. (2010) Integration, scaling, space-group assignment and post-refinement *Acta Crystallogr.* **D66**, 125-132
22. Kantardjiev, K. A., and Rupp, B. (2003) Matthews coefficient probabilities: Improved estimates for unit cell contents of proteins, DNA, and protein-nucleic acid complex crystals *Protein Sci.* **12**, 1865-1871
23. McCoy, A. J., Grosse-Kunstleve, R. W., Adams, P. D., Winn, M. D., Storoni, L. C., and Read, R. J. (2007) Phaser crystallographic software *J. Appl. Crystallogr.* **40**, 658-674
24. Adams, P. D., Afonine, P. V., Bunkoczi, G., Chen, V. B., Davis, I. W., Echols, N., Headd, J. J., Hung, L.-W., Kapral, G. J., Grosse-Kunstleve, R. W., McCoy, A. J., Moriarty, N. W., Oeffner, R., Read, R. J., Richardson, D. C., Richardson, J. S., Terwilliger, T. C., and Zwart, P. H. (2010) PHENIX: a comprehensive Python-based system for macromolecular structure solution *Acta Crystallogr.* **D66**, 213-221
25. Emsley, P., and Cowtan, K. (2004) Coot: Model-building tools for molecular graphics *Acta Crystallogr.* **D60**, 2126-2132
26. Painter, J., and Merritt, E. A. (2006) Optimal description of a protein structure in terms of multiple groups undergoing TLS motion *Acta Crystallogr.* **D62**, 439-450
27. Chen, V. B., Arendall, W. B., 3rd, Headd, J. J., Keedy, D. A., Immormino, R. M., Kapral, G. J., Murray, L. W., Richardson, J. S., and Richardson, D. C. (2010) MolProbity: all-atom structure validation for macromolecular crystallography *Acta Crystallogr.* **D66**, 12-21
28. Massey, V., and Hemmerich, P. (1978) Photoreduction of flavoproteins and other biological compounds catalyzed by deazaflavins *Biochemistry* **17**, 9-17
29. Gosch, C., Halbwirth, H., Schneider, B., Hölscher, D., and Stich, K. (2010) Cloning and heterologous expression of glycosyltransferases from *Malus x domestica* and *Pyrus communis*, which convert phloretin to phloretin 2'-O-glucoside (phloridzin) *Plant Sci.* **178**, 299-306
30. Wallace, I. M., O'Sullivan, O., Higgins, D.G., and Notredame, C. (2006) M-Coffee: combining multiple sequence alignment methods with T-Coffee *Nucleic Acids Res.* **34**, 1692-1699

31. Waterhouse, A. M., Procter, J. B., Martin, D. M., Clamp, M., and Barton, G. J. (2009) Jalview Version 2--a multiple sequence alignment editor and analysis workbench *Bioinformatics* **25**, 1189-1191
32. Felsenstein, J. (2005) PHYLIP - Phylogeny Inference Package v 3.6. *Department of Genome Sciences, University of Washington, Seattle*
33. Morris, G. M., Goodsell, D. S., Huey, R., and Olson, A. J. (1996) Distributed automated docking of flexible ligands to proteins: parallel applications of AutoDock 2.4 *J. Comput. Aided Mol. Des.* **10**, 293-304
34. Goodsell, D. S., Morris, G. M., and Olson, A. J. (1996) Automated docking of flexible ligands: applications of AutoDock *J. Mol. Recognit.* **9**, 1-5
35. Duan, Y., Wu, C., Chowdhury, S., Lee, M. C., Xiong, G., Zhang, W., Yang, R., Cieplak, P., Luo, R., Lee, T., Caldwell, J., Wang, J., and Kollman, P. (2003) A point-charge force field for molecular mechanics simulations of proteins based on condensed-phase quantum mechanical calculations *J. Comput. Chem.* **24**, 1999-2012
36. Krieger, E., Koraimann, G., and Vriend, G. (2002) Increasing the precision of comparative models with YASARA NOVA--a self-parameterizing force field *Proteins* **47**, 393-402.
37. Cummings, M. D., Farnum, M. A., and Nelen, M. I. (2006) Universal screening methods and applications of ThermoFluor *J. Biomol. Screen.* **11**, 854-863
38. Zafred, D., Steiner, B., Teufelberger, A. R., Hromic, A., Karplus, P. A., Schofield, C. J., Wallner, S., and Macheroux, P. (2015) Rationally engineered flavin-dependent oxidase reveals steric control of dioxygen reactivity *FEBS J.*, in press.
39. Winkler, A., Kutchan, T. M., and Macheroux, P. (2007) 6-S-cysteinylation of bi-covalently attached FAD in berberine bridge enzyme tunes the redox potential for optimal activity *J. Biol. Chem.* **282**, 24437-24443
40. Winkler, A., Motz, K., Riedl, S., Puhl, M., Macheroux, P., and Gruber, K. (2009) Structural and mechanistic studies reveal the functional role of bicovalent flavinylation in berberine bridge enzyme *J. Biol. Chem.* **284**, 19993-20001
41. Liu, Y. C., Li, Y. S., Lyu, S. Y., Hsu, L. J., Chen, Y. H., Huang, Y. T., Chan, H. C., Huang, C. J., Chen, G. H., Chou, C. C., Tsai, M. D., and Li, T. L. (2011) Interception of teicoplanin oxidation intermediates yields new antimicrobial scaffolds *Nature Chem. Biol.* **7**, 304-309
42. Huang, C.-H., Lai, W.-L., Lee, M.-H., Chen, C.-J., Vasella, A., Tsai, Y.-C., and Liaw, S.-H. (2005) Crystal structure of glucooligosaccharide oxidase from *Acremonium strictum*. A novel flavinylation of 6-S-cysteinyl, 8 α -N1-histidyl FAD *J. Biol. Chem.* **280**, 38831-38838
43. Noinaj, N., Bosserman, M. A., Schickli, M. A., Piszczek, G., Kharel, M. K., Pahari, P., Buchanan, S. K., and Rohr, J. (2011) The crystal structure and mechanism of an unusual oxidoreductase, GilR, involved in gilvocarcin V biosynthesis *J. Biol. Chem.* **286**, 23533-23543
44. Winkler, A., Puhl, M., Weber, H., Kutchan, T. M., Gruber, K., and Macheroux, P. (2009) Berberine bridge enzyme catalyzes the six electron oxidation of (S)-reticuline to dehydroscoulerine *Phytochemistry* **70**, 1092-1097
45. Morreel, K., Ralph, J., Kim, H., Lu, F., Goeminne, G., Ralph, S., Messens, E., and Boerjan, W. (2004) Profiling of oligolignols reveals monolignol coupling conditions in lignifying poplar xylem *Plant Physiol.* **136**, 3537-3549

46. Jamet, E., Canut, H., Boudart, G., and Pont-Lezica, R. F. (2006) Cell wall proteins: a new insight through proteomics *Trends Plant Sci.* **11**, 33-39
47. Tsuji, Y., Chen, F., Yasuda, S., and Fukushima, K. (2005) Unexpected behavior of coniferin in lignin biosynthesis of *Ginkgo biloba* L *Planta* **222**, 58-69
48. Escamilla-Trevino, L. L., Chen, W., Card, M. L., Shih, M. C., Cheng, C. L., and Poulton, J. E. (2006) *Arabidopsis thaliana* β -Glucosidases BGLU45 and BGLU46 hydrolyse monolignol glucosides *Phytochemistry* **67**, 1651-1660
49. Xu, Z., Escamilla-Trevino, L., Zeng, L., Lalgondar, M., Bevan, D., Winkel, B., Mohamed, A., Cheng, C. L., Shih, M. C., Poulton, J., and Esen, A. (2004) Functional genomic analysis of *Arabidopsis thaliana* glycoside hydrolase family 1 *Plant Mol. Biol.* **55**, 343-367
50. Ober, D., and Kaltenecker, E. (2009) Pyrrolizidine alkaloid biosynthesis, evolution of a pathway in plant secondary metabolism *Phytochemistry* **70**, 1687-1695

Oxidation of monolignols by members of the berberine bridge enzyme family suggests a role in plant cell wall metabolism

2.7. Supplementary Information

Bastian Daniel,¹ Tea Pavkov-Keller,^{2,3} Barbara Steiner,¹ Anđela Dordic,^{2,3} Alexander Gutmann,⁴ Bernd Nidetzky,⁴ Christoph W. Sensen,⁵ Eric van der Graaff,⁶ Silvia Wallner,¹ Karl Gruber² and Peter Macheroux^{1*†}

¹From Graz University of Technology, Institute of Biochemistry, Graz, Austria

²University of Graz, Institute of Molecular Biosciences, Graz, Austria

³ACIB GmbH, Graz, Austria

⁴Graz University of Technology, Institute of Biotechnology and Biochemical Engineering, Graz, Austria

⁵Graz University of Technology, Institute of Molecular Biotechnology, Graz, Austria

⁶Copenhagen University, Copenhagen, Denmark

To whom correspondence should be addressed: Peter Macheroux, Graz University of Technology, Institute of Biochemistry, Petersgasse 12/II, A-8010 Graz, Austria, Tel.: +43-316-873 6450, Fax: +43-316-873 6952; Email: peter.macheroux@tugraz.at

Table S1: Thermofluor measurements with selected compounds.

Substance	CAS-number	T _m [°C]	ΔT _m [°C]
2-Deoxyglucose	154-17-6	78	17
D,L-Proline	609-36-9	77.5	16.5
trans-Cinnamyl alcohol	104-54-1	76.5	15.5
D-Glucose	492-62-6	76	15
3-Aminobenzyl alcohol	1877-77-6	75	14
3,4-Dimethoxybenzyl alcohol	93-03-8	75	14
4-Isopropylbenzyl alcohol	536-60-7	74.5	13.5
(S)-(-)-Limonen	5989-54-8	74	13
Benzylalcohol	100-51-6	73	12
Geraniol	106-24-1	73	12
Lactose monohydrate	64044-51-5	72	11
D-Maltose		72	11
Anthranilic acid	118-92-3	71	10
Cellobiose	528-50-7	71	10
4-Chlorobenzyl alcohol	873-76-7	71	10
D-Galactose	59-23-4	71	10
D-Sorbitol	50-70-4	71	10
Furfuryl alcohol	98-00-0	70.5	9.5
2-Indanol	4254-29-9	70.5	9.5
Polygalacturonic acid	25990-10-7	70	9
(+)-Pulegone	89-82-7	70	9
Eugenol	97-53-0	65.5	4.5
Xylose	58-86-6	66.5	5.5
3-Methoxyphenol	150-19-6	64.5	3.5
D-Lyxose	1114-34-7	64	3
Acetylacetone	123-54-6	63.5	2.5
3-(3,4-Dihydroxyphenyl)-DL-alanine (L-DOPA)	63-84-3	63.5	2.5
3-Aminosalicylic acid	570-23-0	63	2
2-Aminothiophenol	137-07-5	63	2
p-Anisidine	104-94-9	63	2
(S)-(-)-β-Citronellol	7540-51-4	63	2
3,4-Dimethoxybenzotrile	2024-82-1	63	2
Flavone	525-82-6	63	2
Isopropyl salicylate	607-85-2	63	2
Vanillin	121-33-5	63	2
meso-Erythritol	149-32-6	62.5	1.5
2-Acetyl-5-bromothiophene	5370-25-2	62	1
1,1'-Bi-2-naphthol	602-09-5	62	1
3-Chlorocoumarin	92-45-5	62	1
Dihydrocarveol	619-01-2	62	1
3-Aminophenol	591-27-5	61.5	0.5
Coumarin	91-64-5	61.5	0.5
Diacetyldioxim	95-45-4	61.5	0.5

2,6-Lutidin	108-48-5	61.5	0.5
(+/-)-Mandelic acid	611-72-3	61.5	0.5
Acetone cyanohydrin	75-86-5	61	0
Acetonylacetone	110-13-4	61	0
Benzamide	55-21-0	61	0
(R)-(-)-3-Chloromandelic acid	61008-98-8	61	0
trans-Cinnamionitrile	1885-38-7	61	0
o-Cresol	95-48-7	61	0
1,2-Dihydronaphtalen	446-53-0	61	0
4,4'-Dimethoxybenzoin	119-25-8	61	0
2,6-Dimethoxyphenol	91-10-1	61	0
2,6-Dimethylaniline	87-62-7	61	0
2,6-Dimethylanisol	1004-66-6	61	0
8-Hydroxyquinoline	148-24-3	61	0
Maltose	69-79-4	61	0
Mandelonitrile	532-28-5	61	0
D-Mannitol	69-65-8	61	0
exo-Norborneol	497-37-0	61	0
Norcamphor	497-38-1	61	0
Safrole	94-59-7	61	0
Sucrose	57-50-1	61	0
Tannin	1401-55-4	61	0
DL-Tryptophan	54-12-6	61	0
3-Acetylcoumarin	3949-36-8	60.5	-0.5
Adonitol	488-81-3	60.5	-0.5
Amylose	9005-82-7	60.5	-0.5
D-Arabinose	10323-20-3	60.5	-0.5
Benzylamine	100-46-9	60.5	-0.5
p-Bromo-DL-mandelic acid	6940-50-7	60.5	-0.5
rac-Camphor	76-22-2	60.5	-0.5
2-Chlorophenol	95-57-8	60.5	-0.5
Cholin acetate	14586-35-7	60.5	-0.5
4-Chromamone	491-37-2	60.5	-0.5
trans-Cinnamaldehyde	14371-10-9	60.5	-0.5
p-Cresol	106-44-5	60.5	-0.5
L-Frucose	2438-80-4	60.5	-0.5
Galactan	9037-55-2	60.5	-0.5
Hydroxyethylcellulose	9004-62-0	60.5	-0.5
Isobutyl cinnamate predominantly trans	122-67-8	60.5	-0.5
cis-Jasmone	488-10-8	60.5	-0.5
Lactulose	4618-18-2	60.5	-0.5
Methyl-D-mannopyranoside	617-04-9	60.5	-0.5
3-Acetylpyridine	350-03-8	60	-1
Adenine	73-24-5	60	-1
Aniline	62-53-3	60	-1
Anisole	100-66-3	60	-1
Anthranilic acid	118-92-3	60	-1

Arabuigalactan	9036-66-2	60	-1
Butyrophenone	495-40-9	60	-1
Carboxymethylcellulose	9004-32-4	60	-1
Carrageen		60	-1
Carvacrol	499-75-2	60	-1
4-Chloro-3-nitrocoumarin	38464-20-9	60	-1
rac(-)-Citronellic acid	502-47-6	60	-1
Fructose	57-48-7	60	-1
D(+)-Galatosamine hydrochloride	1772-003-8	60	-1
Geranic acid	459-80-3	60	-1
Glucoseamine	3416-24-8	60	-1
Isobutyramide	563-83-7	60	-1
Isophorone	78-59-1	60	-1
4-Isopropyl aniline	99-88-7	60	-1
4-Isopropyl benzoic acid	536-66-3	60	-1
Maltodextrin	9050-36-6	60	-1
Methyl- β -D-glucoside	709-50-2	60	-1
Morpholine	110-91-8	60	-1
2-Naphtol	135-19-3	60	-1
Natriumalginat	9005-38-3	60	-1
D,L-Norvaline	760-78-1	60	-1
8-Quinolinol	148-24-3	60	-1
D-Ribose	50-69-1	60	-1
Trehalose Dihydrat	6138-23-4	60	-1
2,3,3-Trimethylindolenine	1640-39-7	60	-1
Xylitol	87-99-0	60	-1
L-Xylose	609-06-3	60	-1
m-Anisaldehyde	591-31-1	59.5	-1.5
m-Cresol	108-39-4	59.5	-1.5
Indole	120-72-9	59.5	-1.5
Methylnicotinate	93-60-7	59.5	-1.5
Methylvaleraldehyde	123-15-9	59.5	-1.5
L-Arabinose	5328-37-0	59	-2
Cellulose	9004-34-6	59	-2
Chitin	1398-61-4	59	-2
4-Chlorophenol	106-48-9	59	-2
D-Gluconic acid	526-95-4	59	-2
Pyrocatechol	120-80-9	59	-2
Quinoline	91-22-5	59	-2
Xylan	9014-63-5	59	-2
D,L-Phenylalanine	150-30-1	58.5	-2.5
Glucuronolactone	32449-92-6	58	-3
Mannan	9036-88-8	58	-3
D(+)-Glucuronic acid monohydrate	207300-70-7	56.5	-4.5
Valeraldehyde	110-62-3	56	-5
(+/-)-Menthol	89-78-1	55	-6
(-)-Ephedrine	299-42-3	54	-7

Gallic acid	149-91-7	54	-7
Benzoic acid	65-85-0	53.5	-7.5
4-Aminobenzoic acid	150-13-0	50	-11
3-Methylbutylaldehyde (Isovaleraldehyde)	590-86-3	48	-13
3,5-Dihydroxybenzoic acid	99-10-5	40.5	-20.5
D-Mandelic acid	611-71-2	37	-24
4-Acetylbenzoic acid	586-89-0	---	---
2-Acetyl-1-methylpyrrole	932-16-1	---	---
2-Aminophenol	95-55-6	---	---
4-Aminophenol	123-30-8	---	---
5-Aminosalicylic acid	89-57-6	---	---
trans-Anethole	4180-23-8	---	---
p-Anisaldehyde	123-11-5	---	---
p-Anisic acid	100-09-4	---	---
L-Arabinose	5328-37-0	---	---
Benzaldehyde	100-52-7	---	---
Caffeic acid	331-39-5	---	---
3-Chlorobenzylamine	4152-90-3	---	---
3-Chloro-2-norboranone	30860-22-1	---	---
trans-Cinnamic acid	140-10-3	---	---
Curcumin	458-37-7	---	---
2,4-Dihydroxybenzoic acid	89-86-1	---	---
2,5-Dihydroxybenzoic acid	490-79-9	---	---
4-Dimethylaminopyridine, DMAP	1122-58-3	---	---
4-Ethylaniline	589-16-2	---	---
Hydrocinnamaldehyde	104-53-0	---	---
4-Hydroxy-3-nitrocoumarin	20261-31-8	---	---
2-Iodobenzoic acid	88-67-5	---	---
cis/trans Isoeugenol	97-54-1	---	---
Kojic acid	501-30-4	---	---
Lignin		---	---
L-Mandelic acid	17199-29-0	---	---
1-Naphthol	90-15-3	---	---
Pectin	9000-69-5	---	---
Pyrogallol	87-66-1	---	---
Salicylaldehyde	90-02-8	---	---
Valeric acid	109-52-4	---	---

For details of the experimental set-up see “Materials & Methods”;

---, in the presence of these compounds no reproducible signal was obtained;

Table S2: Genes coexpressed with *AtBBE*-like 15 according to ATTET II server.

Rank	Mutual rank	Correlation	Locus	Function
1	2.6	0.72	At1g26820	ribonuclease 3
2	3.5	0.68	At3g10340	phenylalanine ammonia-lyase 4
3	5.3	0.68	At1g62990	KNOTTED-like homeobox of <i>Arabidopsis thaliana</i> 7
4	6.5	0.64	At2g22560	Kinase interacting (KIP1-like) family protein
5	7.3	0.67	At2g14095	-
6	7.5	0.67	At1g28470	NAC domain containing protein 10
7	8.1	0.69	At4g16620	nodulin MtN21 /EamA-like transporter family protein
8	8.7	0.68	At4g18425	Protein of unknown function (DUF679)
9	9.5	0.58	At4g24430	Rhamnogalacturonate lyase family protein
10	9.8	0.65	260208_s_at	At1g70670;At1g70680
11	10.9	0.66	At5g04200	metacaspase 9
12	12.4	0.66	At1g11190	bifunctional nuclease i
13	12.4	0.65	At4g04460	Sapoin-like aspartyl protease family protein
14	13.0	0.62	At2g47670	Plant invertase/pectin methylesterase inhibitor superfamily protein
15	17.9	0.55	At2g18480	Major facilitator superfamily protein
16	22.4	0.66	267343_at	At2g44260
17	27.8	0.56	At1g23560	Domain of unknown function (DUF220)
18	28.0	0.58	At3g21550	DUF679 domain membrane protein 2
19	28.3	0.60	At5g65530	Protein kinase superfamily protein
20	30.5	0.54	At2g22800	Homeobox-leucine zipper protein family
21	32.2	0.59	At5g58730	pfkB-like carbohydrate kinase family protein
22	33.3	0.63	At4g34320	Protein of unknown function (DUF677)
23	33.6	0.58	At5g54570	beta glucosidase 41
24	34.3	0.62	At5g08480	VQ motif-containing protein
25	35.4	0.53	At3g27200	Cupredoxin superfamily protein

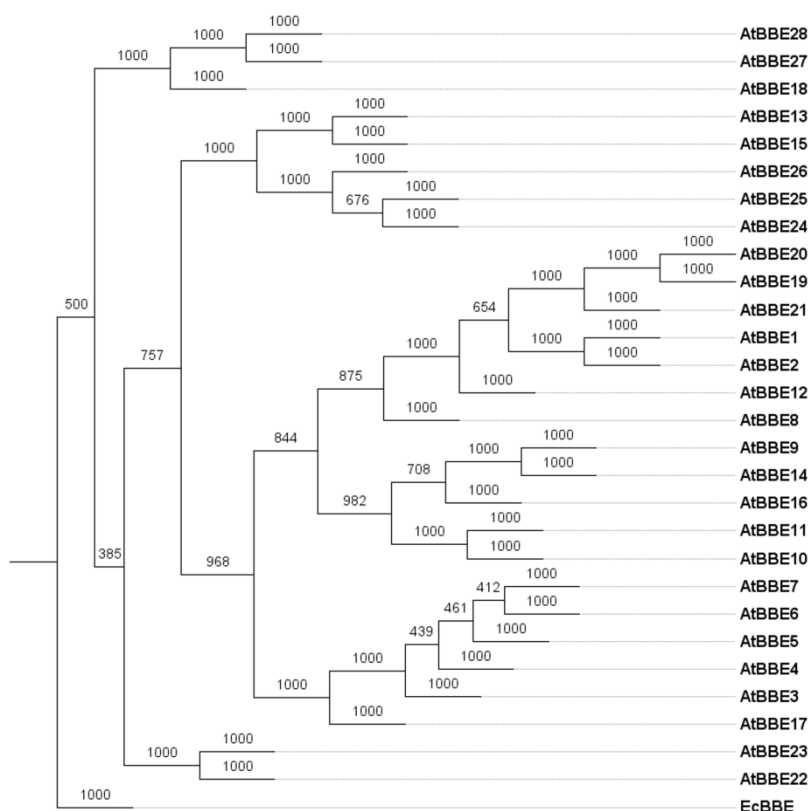


Figure S1: Bootstrapped phylogenetic tree including all *At*BBE-like proteins and *Ec*BBE. The following sequences were used for analysis (locus name/Accession number):

*At*BBE-like 1, AT1G01980.1/Q9LPC3; *At*BBE-like 2, AT1G11770.1/Q9SA99;
*At*BBE-like 3, AT1G26380.1/Q9FZC4; *At*BBE-like 4, AT1G26390.1/Q9FZC5;
*At*BBE-like 5, AT1G26400.1/Q9FZC6; *At*BBE-like 6, AT1G26410.1/Q9FZC7;
*At*BBE-like 7, AT1G26420.1/Q9FZC8; *At*BBE-like 8, AT1G30700.1/Q9SA85;
*At*BBE-like 9, AT1G30710.1/Q9SA86; *At*BBE-like 10, AT1G30720.1/Q9SA87;
*At*BBE-like 11, AT1G30730.1/Q9SA88; *At*BBE-like 12, AT1G30740.1/Q9SA89;
*At*BBE-like 13, AT1G30760.1/Q93ZA3; *At*BBE-like 14, AT1G34575.1/Q9LNL9;
*At*BBE-like 15, AT2G34790.1/O64743; *At*BBE-like 16, AT2G34810.1/O64745;
*At*BBE-like 17, AT4G20800.1/Q9SVG7; *At*BBE-like 18, AT4G20820.1/Q9SVG5;
*At*BBE-like 19, AT4G20830.1/Q9SVG4; *At*BBE-like 20, AT4G20830.2/Q9SVG4;
*At*BBE-like 21, AT4G20840.1/Q9SVG3; *At*BBE-like 22, AT4G20860.1/Q9SUC6;
*At*BBE-like 23, AT5G44360.1/Q9FKV2; *At*BBE-like 24, AT5G44380.1/Q9FKV0;
*At*BBE-like 25, AT5G44390.1/Q9FKU9; *At*BBE-like 26, AT5G44400.1/Q9FKU8;
*At*BBE-like 27, AT5G44410.1/Q9FI25; *At*BBE-like 28, AT5G44440.1/Q9FI21; *Ec*BBE, AAC39358.

CHAPTER 3

Structure of a berberine bridge enzyme-like enzyme with an active site specific to the plant family Brassicaceae

Author contributions

Results and information about *AtBBE*-like protein 28 are summarized in the following chapter. Dr. Bastian Daniel expressed *AtBBE*-like protein 28 heterologously in *Komagataella phaffii* and he elucidated the structure using X-ray crystallography. *AtBBE*-like protein 28 possesses a different active site composition compared to monolignol oxidoreductases and the most distinguishing feature of the active site is a mono-covalent instead of a bi-covalent cofactor tethering. Initial phenotype studies with a T-DNA insertion mutant *Atbbe*-like protein 28 were performed to investigate plant growth and salt tolerance. I contributed to this work by performing salt stress experiments *in vitro*. Moreover, I assisted Dr. Eric van der Graaff to investigate the biomass production of putative *Atbbe*-like protein 28 under standard growth conditions *in vivo*.

Chapter 3

3. Structure of a berberine bridge enzyme-like enzyme with an active site specific to the plant family Brassicaceae

Bastian Daniel¹, Silvia Wallner¹, Barbara Steiner¹, Gustav Oberdorfer², Prashant Kumar², Eric van der Graaff³, Thomas Roitsch^{3,4}, Christoph W. Sensen⁵, Karl Gruber² and Peter Macheroux^{1*}

¹Institute of Biochemistry, Graz University of Technology, Graz, Austria

²Institute of Molecular Biosciences, University of Graz, Graz, Austria

³Department of Plant and Environmental Sciences, University of Copenhagen, Copenhagen, Denmark

⁴Global Change Research Centre, Czech Globe AS CR, v.v.i., Drásov 470, Cz-664 24 Drásov, Czech Republic

⁵Institute of Molecular Biotechnology, Graz University of Technology, Graz, Austria

To whom correspondence should be addressed: Peter Macheroux, Graz University of Technology, Institute of Biochemistry, Petersgasse 12/II, A-8010 Graz, Austria, Tel.: +43-316-873 6450, Fax: +43-316-873 6952; Email: peter.macheroux@tugraz.at

This chapter was published in PLoS One:

Daniel, B. *et al.* (2016) Structure of a berberine bridge enzyme-like enzyme with an active site specific to the plant family Brassicaceae. *PLoS One* 11.

Author contributions

Conceived and designed the experiments: BD SW BS EG KG PM. Performed experiments: BD SW BS GO PK EG. Analyzed the data: BD SW BS EG TR CWS KG PM. Contributed reagents/materials/analysis tools: TR CWS KG. Wrote the paper: BD SW EG TR CWS KG PM.

3.1. Abstract

Berberine bridge enzyme-like (BBE-like) proteins form a multigene family (pfam 08031), which is present in plants, fungi and bacteria. They adopt the vanillyl alcohol-oxidase fold and predominantly show bi-covalent tethering of the FAD cofactor to a cysteine and histidine residue, respectively. The *Arabidopsis thaliana* genome was recently shown to contain genes coding for 28 BBE-like proteins, while featuring four distinct active site compositions. We determined the structure of a member of the *At*BBE-like protein family (termed *At*BBE-like 28), which has an active site composition that has not been structurally and biochemically characterized thus far. The most salient and distinguishing features of the active site found in *At*BBE-like 28 are a mono-covalent linkage of a histidine to the 8 α -position of the flavin-isoalloxazine ring and the lack of a second covalent linkage to the 6-position, owing to the replacement of a cysteine with a histidine. In addition, the structure reveals the interaction of a glutamic acid (Glu426) with an aspartic acid (Asp369) at the active site, which appear to share a proton. This arrangement leads to the delocalization of a negative charge at the active site that may be exploited for catalysis. The structure also indicates a shift of the position of the isoalloxazine ring in comparison to other members of the BBE-like family. The dioxygen surrogate chloride was found near the C(4a) position of the isoalloxazine ring in the oxygen pocket, pointing to a rapid reoxidation of reduced enzyme by dioxygen. A T-DNA insertional mutant line for *At*BBE-like 28 results in a phenotype, that is characterized by reduced biomass and lower salt stress tolerance. Multiple sequence analysis showed that the active site composition found in *At*BBE-like 28 is only present in the Brassicaceae, suggesting that it plays a specific role in the metabolism of this plant family.

3.2. Introduction

Flavoproteins are a large and diverse family that requires either FMN or FAD as cofactor. The majority of flavoproteins (ca. 90%) act as oxidoreductases in a plethora of biochemical redox processes [1]. Among these, the flavin-dependent oxidoreductases berberine bridge enzyme-like enzymes stand out, because of the bi-covalent attachment of the cofactor to the protein via a histidine and a cysteine [2, 3]. The namesake of this protein family is the berberine bridge enzyme from *Eschscholzia californica* (California poppy), which catalyzes the oxidative ring-closure reaction from (*S*)-reticuline to (*S*)-scoulerine. The C-C-bond formed in this reaction is the so called “berberine bridge”. This reaction marks a branch point in the biosynthesis of isoquinoline alkaloids [4]. As the number of sequenced plant genomes increases constantly, more and more genes encoding BBE-like enzymes have been identified in diverse plant families. Interestingly, most of these plant families are not known to synthesize any alkaloids and thus the role of BBE-like enzymes in these plants remains elusive. Despite this lack of knowledge on the biochemical properties of BBE-like enzymes, they have caught the attention of scientists due to their exceptionally high up-regulation observed during the response to pathogens [5, 6, 7] as well as under salt stress conditions [8, 9]. The BBE-like enzymes are predominantly secreted and have been found to contribute a significant part of the plant cell wall proteome (up to 2.5%) [10]. Moreover, BBE-like enzymes contribute to the expressed secretome during infection by various plant pathogens, suggesting a role in plant-pathogen interactions [11, 12, 13].

Recently, we have shown that two BBE-like enzymes from *Arabidopsis thaliana* oxidize monolignols to their corresponding aldehydes, *i.e.* they function as monolignol oxidoreductases [9]. This activity suggests that these enzymes are involved in the manipulation of the extracellular monolignol pool and thereby influence plant cell wall metabolism with as yet unknown implications for lignin formation. A detailed study to reveal the physiological role of the oxidoreductases using knock-out plants is currently under way.

Monolignol oxidoreductase activity appears to be associated with a defined composition of the active site, as shown in Fig 1 (panel A). Characteristic features of this active site, designated type I, are Tyr117 and Gln438, engaging in a hydrogen bond as well as Tyr479, Tyr193 and Lys436, forming the catalytic base motif. In this motif, the hydroxyl groups of Tyr479 and Tyr193 point toward each other (oxygen-oxygen distance = 2.4 Å) and Lys436 apparently engages in a cation- π interaction with Tyr193. The type I composition clearly dominates the BBE-like enzyme family in *A. thaliana* with 18 out of 28 possessing identical or very similar active sites.

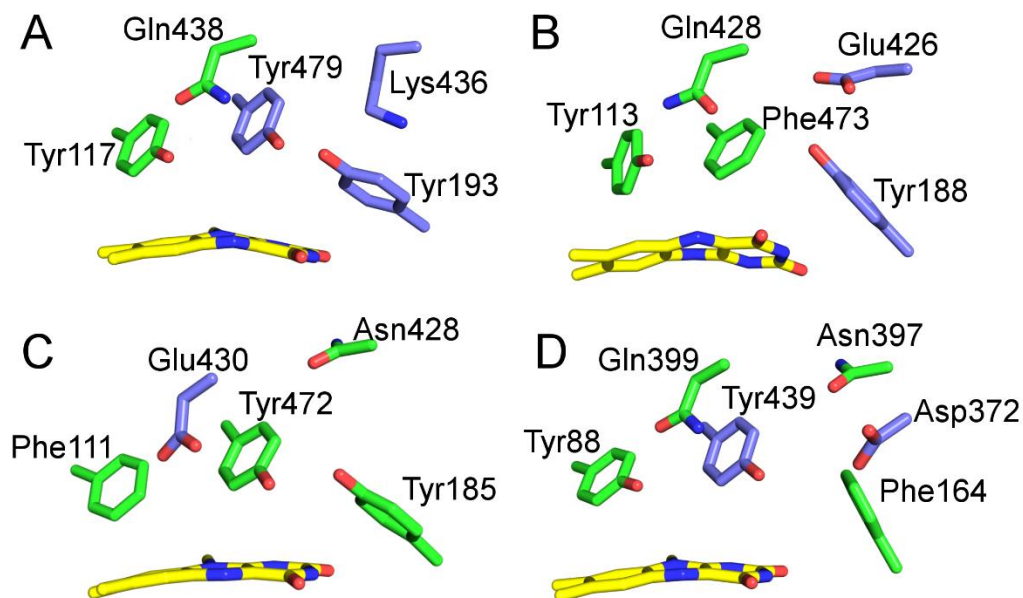


Fig 1. Active site composition of types I-IV (panel A to D) of BBE-like enzymes. The isoalloxazine ring is shown in yellow. Residues forming the active site are shown in green and residues involved in proton abstraction during catalysis are shown in violet. A: Type I: Tyr117 and Gln438 are engaged in a hydrogen bond. Tyr193 acts as catalytic base, it is stabilized in the deprotonated state by Tyr479 and Lys436 (PDB entry 4UD8). B: Type II. Tyr113 and Gln428 are engaged in a hydrogen bond. Tyr188 putatively acts as catalytic base after de-protonation by Glu426 (PDB entry 5D79). C: Type III: Glu430 putatively acts as catalytic base in the active site. The involvement of Tyr472 and Tyr185 is conceivable. A homology model of Q9SA88 based on 4UD8 and prepared with YASARA was used for visualization [14]. D: Type IV: Tyr88 and Gln399 are engaged in a hydrogen bond, Tyr439 acts as catalytic base after de-protonation by Asp372 via a water molecule (PDB entry 4PWC).

Further inspection of multiple sequence alignments and homology models of BBE-like enzymes revealed the presence of three additional and distinct active site compositions in the remainder of BBE-like enzymes, as shown in Fig 1 (panels B-D, designated type II-IV). In the active site of type II, shown in Fig 1B, the hydrogen bond interaction between Tyr113 and Gln428 is retained, however, the catalytic base motif has substantially changed by exchange of a tyrosine to a phenylalanine and a lysine to a glutamic acid (compare panels A and B). Yet other changes are apparent in the composition of the active sites found in type III and IV (Fig 1C and D). The characteristic active site composition described by type II, III and IV are found in 3, 3 and 2 *At*BBE-like enzymes, respectively. Although it appears likely that these BBE-like enzymes also serve as oxidoreductases, neither their substrate spectrum, nor the catalyzed reactions were identified thus far.

Due to the high sequence identity within the BBE-like family, homology models can be valuable tools to support the prediction of the active site composition of structurally uncharacterized members. However, side chain orientations cannot be predicted with the same

confidence and thus homology models are not sufficient to determine how residues are oriented in the active site. Therefore, we set out to crystallize a member of the type II BBE-like enzymes in order to pave the way for further studies into their function. Here we report the crystallographic structure of *AtBBE-like 28*, a member of the type II BBE-like enzyme sub-family. In addition, we have characterized the enzyme with regard to the oxidative half-reaction and its redox potential and performed initial studies with a homozygous T-DNA knock-out strain, revealing effects on plant growth and salt tolerance. By phylogenetic investigations we have elucidated the appearance of BBE-like proteins with a similar active site as *AtBBE-like 28* in the plant kingdom.

3.3. Results

3.3.1. Structural characterization of *AtBBE-like 28*

AtBBE-like 28 was expressed in *Komagataella pastoris* and purified as reported previously [9]. Crystallization was conducted using the sitting-drop method, yielding crystals diffracting to a resolution of 1.8 Å. The structure was solved using molecular replacement employing the structure of BBE from *Eschscholzia californica* (*EcBBE*, PDB code 3D2H) as the search template. Like *EcBBE*, *AtBBE-like 28* adopts the VAO topology, as shown in Fig 2A. The protein consists of two domains: a substrate and a FAD-binding domain, shown in orange and green, respectively (Fig 2). The structural elements directly interacting with the isoalloxazine ring are shown in Fig 2B. Typically, the covalent linkage between the thiol group of a cysteine and the C6-position of the isoalloxazine ring, reported for BBE from *E. californica* and *AtBBE-like 15*, originate from the oxygen binding motif. In the case of *AtBBE-like 28*, the cysteine is replaced by His174, which does not form a covalent bond to the C6-position (Fig 3A and B). However, the covalent linkage established by the conserved GGHD motif was clearly seen in the crystal structure (His111 in Fig 3).

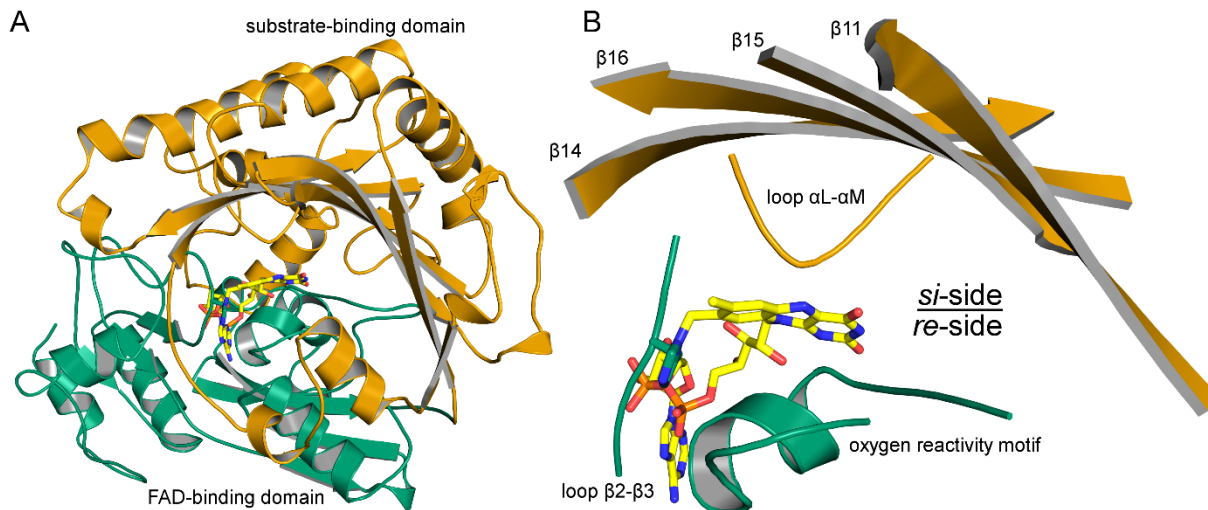


Fig 2. A: Overall topology (A) and active site forming secondary elements (B) of *AtBBE*-like 28. A: Green: FAD-binding domain, orange: substrate-binding domain. The active site is formed between the FAD-binding site and a substrate binding domain B: structural elements interacting directly with the isoalloxazine ring of the FAD-cofactor and structural elements harboring residues involved in the formation of the active site.

As indicated in Fig 2B, the space “above” and “below” the plane of the isoalloxazine ring, *i.e.* the *si*- and *re*-side, play different catalytic roles. A catalytic cycle of a flavoprotein can be split into two half reactions. In the resting state, the flavin is oxidized. In the reductive half reaction a putative substrate is oxidized by the flavin, subsequently dissociates from the active site and leaves the flavin in the reduced state. In BBE-like enzymes, this reaction takes place at the *si*-side. In the oxidative half reaction the reduced flavin reacts with an appropriate electron acceptor, *e.g.* dioxygen. Enzymes that promote the oxidation of the flavin with dioxygen are classified as an oxidase, enzymes that inhibit this reaction are classified as a dehydrogenase. In the BBE-like family, the oxidation of the flavin by dioxygen is catalyzed at the *re*-side.

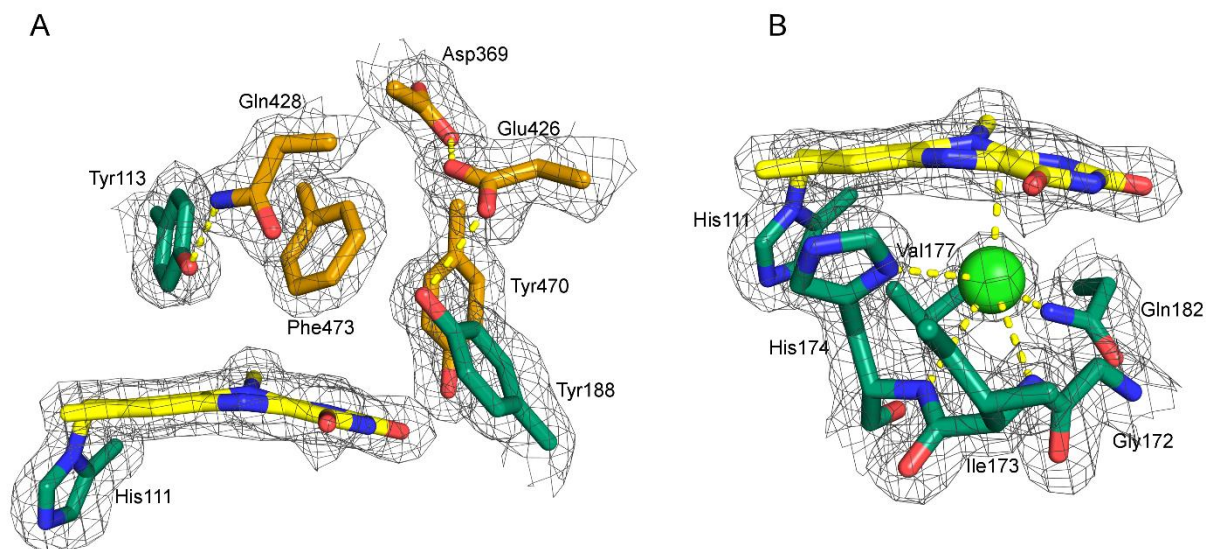


Fig 3. A: Amino acid residues present on the *si*-side (A) and *re*-side (B) of the isoalloxazine ring. A: Residues originating from the FAD- and substrate binding domain are shown in green and orange, respectively. The $2F_o - F_c$ is shown at 1.5σ . The carboxylate groups of Asp369 and Glu426 are found at a distance of 2.4 Å. The proximity of these residues suggests a shared proton and a negative charge delocalized over both carboxylic acids. Glu426 interacts with Tyr188 that putatively acts as catalytic base after de-protonation by Glu426. B: Residues defining the *re*-side of the isoalloxazine ring. An oxygen pocket is formed by the oxygen reactivity motif (compare Fig. 2B). The electron density was interpreted as a chloride ion (light green), which is complexed by the backbone amides of His174 and Ile173, as well as $N\pi$ of His174 and the side chain amide of Gln182.

The residues defining the composition of the protein on the *si*-side of *AtBBE*-like 28 and thereby putatively responsible for the catalysis of the first half reaction are shown in Fig 3A. The flavin adopts a butterfly-bent shape, with an angle at the N5-N10 axis of 6° . A hydrogen bond of 2.6 Å is formed between Tyr113 and Gln428. Tyr470 forms a hydrogen bond to the C(2)=O locus of the isoalloxazine ring. Asp369 and Glu426 are found at a distance of 2.4 Å, indicating that they share a proton. Thus this conformation may stabilize a negative charge, which is delocalized between Asp369 and Glu426 and may be exploited for catalysis.

Direct interactions on the *re*-side of the protein matrix and the isoalloxazine ring are established by the oxygen reactivity motif (Fig 2B). It originates from the FAD binding domain and regulates the reactivity of the enzyme towards dioxygen by sterically controlling access to an oxygen binding pocket near the C(4a)-position of the isoalloxazine ring [15]. Recently, Zafred *et al.* have identified a single residue as the gatekeeper of the oxygen binding pocket: a valine in this position allows the formation of an oxygen-binding pocket, whereas the presence of a leucine occupies the pocket and thus denies access to this site. In *AtBBE*-like 28, this position is occupied by Val177 and thus we assume that the pocket is available for oxygen binding. In agreement with this assumption, an electron density in this pocket was clearly detectable and we propose that a chloride ion, acting as an oxygen surrogate, is bound to the

pocket (Fig 3B, green sphere). It is complexed by N π and the backbone amide nitrogen of His174, with a distance of 3.6 Å and 3.7 Å, respectively. In addition, the chloride ion is complexed by the nitrogen from the backbone amide of Ile173 and side chain amide of Gln182 with a distance of 3.7 Å and 3.3 Å, respectively. The distance between the chloride and the C(4a) of the isoalloxazine ring is 3.1 Å. Dioxygen is thought to attack the reduced flavin to form a C(4a)-peroxy species in the course of the oxidative half reaction.

3.3.2. Biochemical characterization

Recently, we have reported a successful strategy to identify substrates for *At*BBE-like 13 and 15 that involved screening of a chemical compound library based on observed effects on protein thermal stability [9]. In the case of *At*BBE-like 28, this approach was not successful. Similarly, molecular docking of a compound library using our crystallographic structure did not lead to the identification of potential substrates of *At*BBE-like 28. In the absence of a substrate, we thus employed photoreduction according to the method described by Massey *et al.* to gain information on the spectral properties of *At*BBE-28 in its reduced state [16]. Initially, stepwise photoreduction of *At*BBE-like 28 results in an increase of absorption at 370 nm that is characteristic for the anionic (red) flavin semiquinone [17]. Further photoreduction yields the fully reduced dihydroquinone species with a rather featureless absorption spectrum in the visible range. Selected spectra observed during photoreduction are shown in Fig 4A.

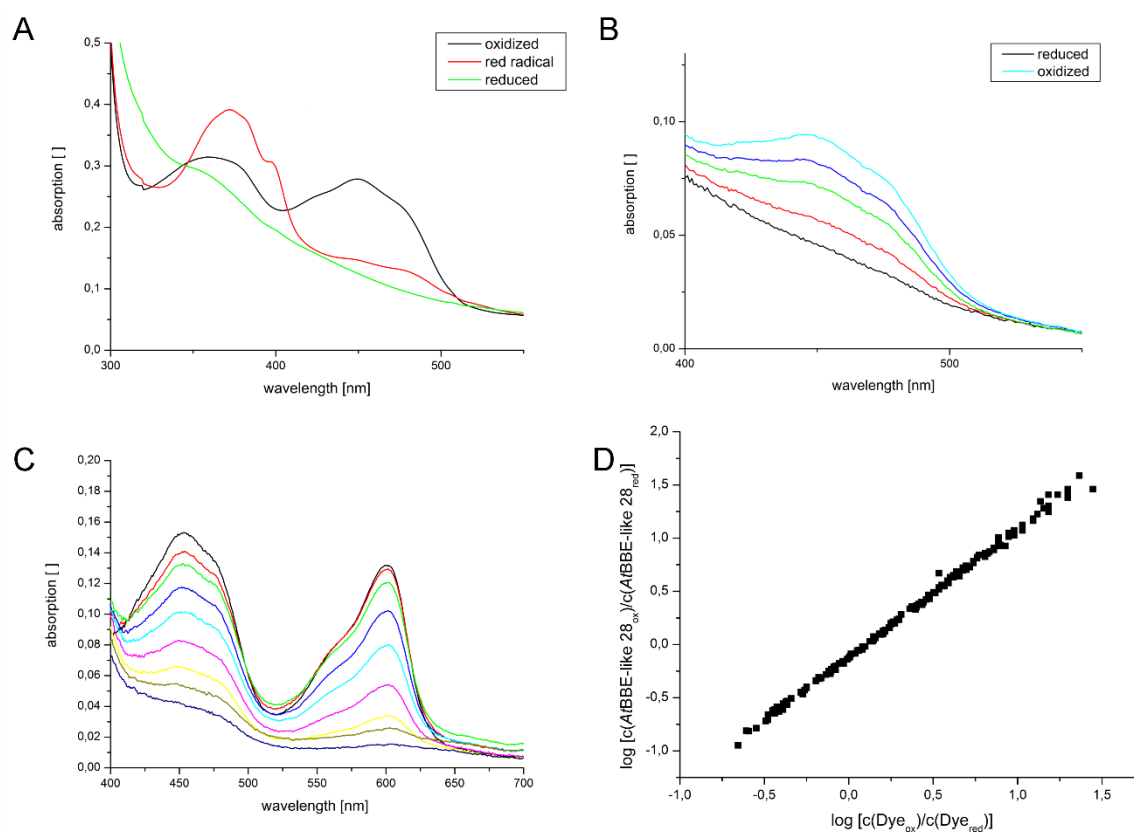


Fig 4. Biochemical characterization of *AtBBE*-like 28. A: Photoreduction of *AtBBE*-like 28: The formation of an anionic radical semiquinone species is indicated by the increase of absorption at 370 nm in the course of the reduction B: Selected spectra recorded during the reoxidation of photoreduced *AtBBE*-like 28 by oxygen to determine the oxidative rate. Inserted in panel B is the time evolution of the absorbance at 450 nm (black) and a monoexponential fit (red) that was used to determine the oxidative rate. C: Selected spectra of the simultaneous reduction of *AtBBE*-like 28 and thionine acetate using the xanthine/xanthine oxidase system as an electron source. D: Double logarithmic plot of the concentration of *AtBBE*-like 28 (ox/red) and thionine acetate (ox/red) used for the determination of the redox potential of *AtBBE*-like 28.

The pronounced spectral difference at 450 nm was exploited in additional experiments to investigate the rate of reoxidation of reduced *AtBBE*-like 28 by molecular oxygen in a stopped-flow device. Photoreduced enzyme was mixed with air-saturated buffer and the course of reoxidation of the flavin was followed at 450 nm. Selected spectra recorded during the experiment are shown in Fig 4B. Kinetic analysis of reoxidation yields a bimolecular rate constant of $3040 \pm 50 \text{ M}^{-1} \text{ s}^{-1}$ and is thus 12 times faster than the reaction of free FAD with molecular oxygen ($250 \text{ M}^{-1} \text{ s}^{-1}$) [18]. Therefore, *AtBBE*-like 28 accelerates the rate of reaction with molecular oxygen and can be classified as an oxidase, in agreement with the presence of an oxygen binding pocket near the C(4a)-atom of the isoalloxazine ring, as described in the previous section.

The redox potential is an important parameter to characterize a redox system. In the case of BBE-like enzymes, the bi-covalent cofactor attachment results in a large shift to ca. +130

mV for BBE or +211 mV for the pollen allergen Phl p 4, to give two examples [19, 15]. For the latter this means that the redox potential is shifted by 411 mV compared to that of free FAD (-210 mV) [17]. The redox potential of *AtBBE*-like 28 was determined with thionine acetate as reference dye, according to Minnaert *et al.* [20]. Using the xanthine/xanthine oxidase electron delivery system, *AtBBE*-like 28 and the dye were simultaneously reduced indicating that the redox systems are in equilibrium during the time course of the experiment. Selected spectra and the double logarithmic plot used for data evaluation are shown in Fig 4 C and D. A redox potential E° of $+61 \pm 1$ mV was determined for *AtBBE*-like 28 at 25 °C and pH 7.0.

AtBBE-like 28 functions in biomass formation and salt stress tolerance. To investigate the *in planta* function for *AtBBE*-like 28, a T-DNA insertional mutant (*bbe28*) was obtained from the SALK collection with a T-DNA insert in the coding region, representing a putative loss-of-function mutant. The presence of the T-DNA insertion and homozygous *bbe28* mutants were identified by kanamycin selection and PCR analysis. No obvious developmental defects were observed for the homozygous *bbe28* mutant. However, more detailed analysis revealed that *bbe28* produced less biomass (on average 10% reduction) compared to Col-0, based on fresh weight (FW) and dry weight (DW) (Fig 5A) in five independent growth experiments. The *bbe28* seeds germinate at the same rate as Col-0, while *bbe28* plants flower two days later than Col-0 (data not shown). After 30 days of growth, *bbe28* plants produced slightly less leaves (14.8), when compared to Col-0 (15.3), a difference that is much smaller than the 10% reduction in both FW and DW. Based on *in-silico* expression analysis, the expression of many *AtBBE*-like family members, is induced under biotic and abiotic stress conditions [21]. Interestingly, the Brassicaceae-specific *AtBBE*-like 28 gene is induced by salt stress, specifically in the root. Therefore, we investigated the growth of *bbe28* under (mild) salt stress conditions (100 mM NaCl). Upon direct germination and growth on salt stress medium, both Col-0 and *bbe28* produced lower number of healthy green seedlings (74.3% and 58.4%, respectively) when compared to plants growing on control medium. This increased salt stress sensitivity of *bbe28* was significantly more pronounced compared to the wild type over three replicate experiments (Fig 5B, $p = 0.024$).

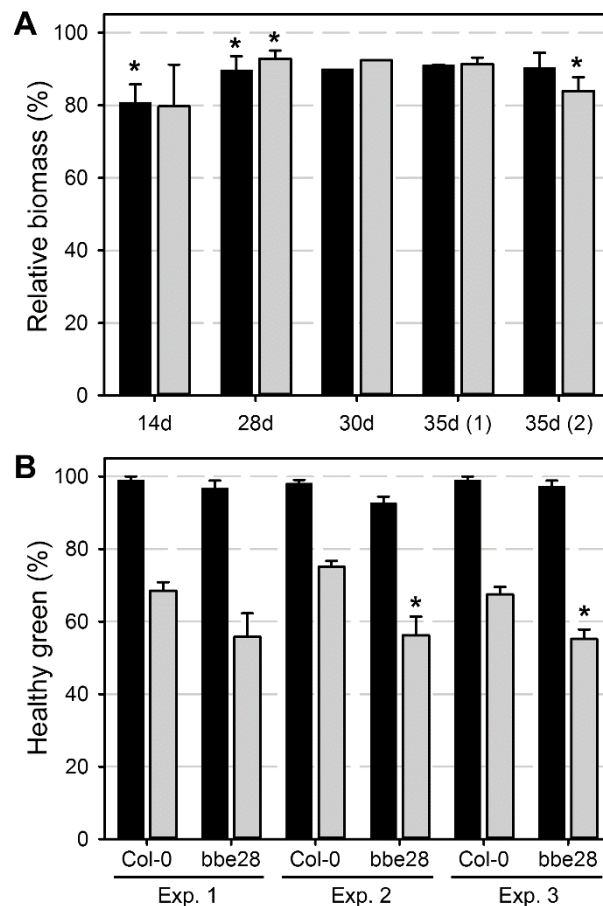


Fig 5. *AtBBE*-like 28 loss-of-function affects biomass formation and salt stress tolerance. A: The *bbE28* mutant forms less biomass compared to Col-0, based on fresh weight (FW, black bars) and dry weight (DW, grey bars). B: The *bbE28* mutant is more sensitive to salt stress compared to Col-0. Black bars control medium, grey bars salt stress medium (100 mM NaCl). Average values \pm SE are shown, with relative biomass (%) compared to Col-0 in A and percentage of green healthy shoots vs. total number seedlings in B. * indicates the statistically significant difference (Student's t-test) when compared to Col-0 at $p < 0.05$.

3.3.3. Sequence comparison and phylogenetic inference

As mentioned in the introduction, *A. thaliana* harbors 3 BBE-like enzymes with the active site composition of type II. To investigate how common this particular active site composition is in other plant families we used the sequence of *AtBBE*-like 28 to search the genomes of a variety of plants for genes coding for BBE-like enzymes. Our analysis revealed that BBE-like enzymes featuring a type II active site composition can be sub-classified according to their mode of covalent attachment into type IIa and IIb showing monocovalent or bicovalent cofactor attachment, respectively.

Surprisingly, type IIa BBE-like enzymes, such as *AtBBE*-like 28, were found exclusively in plant species belonging to the genus Brassicaceae [22]. Therefore, sequences coding for BBE-like enzymes out of the genomes of seven species of this plant family (*i.e.* *Arabidopsis*

lyrata, *Arabidopsis thaliana*, *Boechea stricta*, *Brassica rapa*, *Capsella grandiflora*, *Capsella rubella*, and *Eutrema salsugineum*) were retrieved from the Phytozome website and aligned with Clustal Omega [23][22]. As shown in Fig 6, a phylogenetic tree was generated using the PHYLIP package version 3.69 [24]. In Table 1, the composition of the phylogenetic groups and the assignment of the distinct active site types (compare Fig 1) are summarized. In all Brassicaceae species except *C. grandiflora*, we found at least one enzyme that belongs to type IIa BBE-like enzymes, indicating a widespread occurrence within the Brassicaceae while all other plant families appear to lack BBE-like enzyme with the specific type IIa composition. In our view this may turn out to be an important result in light of the yet unsuccessful search for a cognate substrate of *AtBBE*-like 28. The Brassicaceae family is known to possess several specific metabolites, such as the glucosinolates or camalexin, and thus it appears likely that type IIa BBE-like enzymes are involved in specific metabolic (oxidation) processes, which might be confined to the majority of the members of this plant family [25, 26].

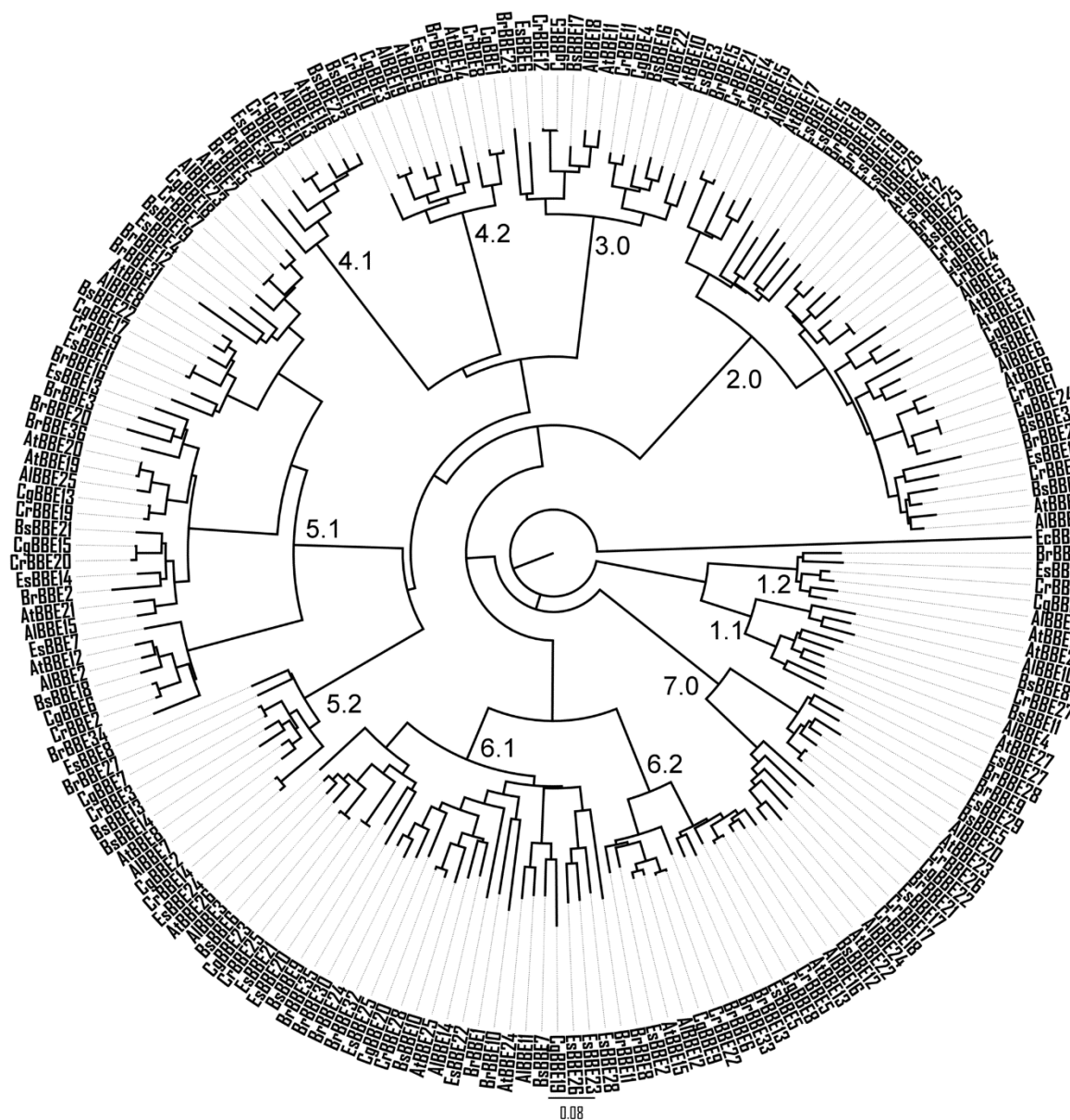


Fig 6. Phylogenetic tree of the BBE-like enzymes within the Brassicaceae family. Sequences from *Arabidopsis lyrata* (Al), *Arabidopsis thaliana* (At), *Boechera stricta* (Bs), *Brassica rapa* (Br), *Capsella grandiflora* (Cg), *Capsella rubella* (Cr), and *Eutrema salsugineum* (Es) were used. The composition of the phylogenetic groups is summarized in Table 1.

Table 1: Composition of the phylogenetic groups of the BBE-like enzymes from *Brassicaceae* as defined in Fig 6 sorted by species and distribution of the active site types.

Group	Active site type	<i>At</i> BBE	<i>A/B</i> BBE	<i>Br</i> BBE	<i>Bs</i> BBE	<i>Cg</i> BBE	<i>Cr</i> BBE	<i>Es</i> BBE
1.1	IIa	27, 28	4, 10	28	8, 11		27	27
1.2	IIb	18	1	17		16	16	18
2.0	I	17, 4, 3, 6, 7, 5	5, 6, 9, 17, 26	18, 19, 25, 26	1, 2, 3, 4	11, 12, 14, 24	1, 4, 6, 13, 15, 21	1, 10, 12, 15, 16, 19
3.0	III	10, 11	18, 22	15, 23	16, 17	4, 5	11, 12	3, 6
4.1	III	16	13	5, 7	23	10	23	30
4.2	I	9, 14	19	29	15	1, 3	8, 10	9
5.1	I	1, 2, 12, 19, 20, 21	2, 8, 15, 23, 25	2, 3, 12, 16, 20, 31, 36, 34	18, 19, 22, 21	6, 13, 15, 17, 18	2, 9, 19, 20,	4, 7, 11, 13, 14
5.2	I	8	7	27	13, 14	7, 2	3, 14	8
6.1	I	24, 25, 26	3, 11, 14	1, 10, 11, 24, 30, 32, 35	6, 7, 9, 10	19, 20, 23	25, 28	20, 21, 22, 23, 24, 25, 26, 28
6.2	I	13, 15	12, 16	6, 8, 13, 33	12	8, 9	5, 22	2, 5
7.0	IV	22, 23	20, 24	9, 21	5	22	17, 18, 26	17, 29

3.3.4. Active site type distribution of BBE-like enzymes

Overall, the same phylogenetic groups as described before in the analysis of the *At*BBE-like enzymes were found in the Brassicaceae [9], if reasonable sub groups of the predefined phylogenetic groups are defined according to sequence distances and active site composition. To visualize and compare the active sites of different groups, we generated sequence logos for the amino acids sequences of the pertinent motifs (Fig 2B) as presented in Fig 7. The sequence logos of the active site-forming residues allow the identification of features that are conserved in the overall family or that are specific for a certain sub group. Amino acids belonging to the β -sheets can be differentiated by the orientation of their side chain. Amino acids with a side chain oriented towards the active site are indicated with a downward arrow, while an upwards arrow indicates the opposite orientation of the side chain. In general, the active site of BBE-like enzymes possess a remarkable plasticity that is mainly achieved by the variation of polar contacts at positions 401, 426, and 428 (black boxes in Fig 7) and aromatic residues 113, 188 and 473 (red boxes Fig 7). The mode of covalent cofactor tethering is indicated by amino acid positions 111 and 174 (labeled with * in Fig 7) whereas the reactivity toward oxygen is revealed by inspection of position 172 or 177 (labeled with ▼ in Fig 7).

The active site composition found in *At*BBE-like enzyme 28 is restricted to group 1 and can be differentiated into type a and b, as noted above. Type IIa is present in group 1.1, with the cofactor being attached strictly mono-covalently via His111 (loop β 2- β 3). In position 174, corresponding to the predominant cysteine responsible for cofactor tethering in other BBE-like enzymes, a histidine or a tyrosine is found (compare Fig 7, group 1.1, Fig 3B). Furthermore, a unique and conserved arrangement is found in type IIa with Asp369 (β 14) replacing a highly conserved serine in the rest of the family. This residue is in close contact to Glu426 (β 16), which is also invariant in group 1.1. In combination, Asp369 and Glu426 presumably facilitate de-protonation of Tyr188 (oxygen reactivity motif, compare also Fig 3A), which presumably acts as active site base. In group 1.2 a similar arrangement of amino acids is found, with the notable exception of Asp369, hence the catalytic triad appears to be replaced by a dyad. On the other hand, the cofactor in group 1.2 is bi-covalently linked to the protein backbone and Gln182 is replaced by histidine, as is typical for BBE-like enzymes with bicovalent cofactor linkage.

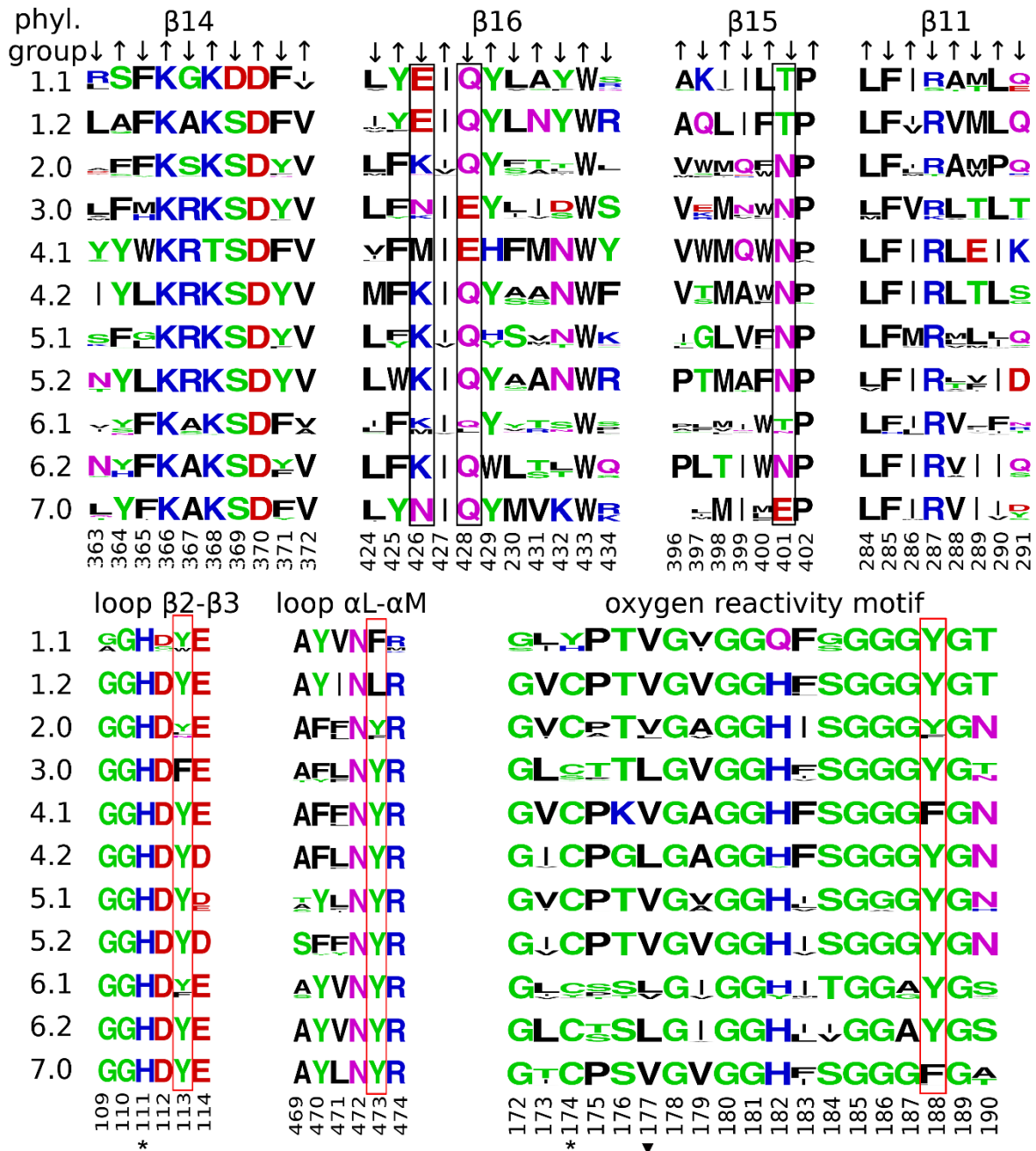


Fig 7. Sequence logos representing the secondary elements directly interacting with the isoalloxazine ring. The numbering is according to the sequence of *AtBBE*-like 28. *: site of covalent cofactor attachment, ▼: Gatekeeper residue controlling access to the oxygen pocket; valine is found in oxidases, leucine in dehydrogenases. Black boxes: Variable polar residues putatively involved in catalysis. Red boxes: Variable aromatic residues putatively involved in catalysis. β14, 16, 15 and 11 cover the *si*-side of the isoalloxazine ring. Arrows indicate the orientation of the residues in the β-strands. An upward arrow indicates the residue points towards the α-helices covering the 7-stranded antiparallel β-sheet (compare Fig 2B). These residues are found to be structurally relevant and are predominantly conserved in the overall family (compare β14 positions 366, 368, 370 and β16 position 433). A downward arrow indicates the residue points towards the active site. Residues contributing to the decoration of the active site are conserved within the phylogenetic groups but are variable within the overall family (compare β16 positions 426, 428 and β15 position 401).

3.4. Discussion

BBE-like enzymes catalyze a broad range of reactions such as two-electron oxidations as reported for *AtBBE*-like 15 or four-electron oxidations as shown for Dbv29 [9, 27]. In the case of BBE from *E. californica*, substrate oxidation is coupled to a ring closure reaction leading to benzoisoquinoline alkaloids [28]. A similar reaction, which couples substrate oxidation with ring formation, was reported for Δ 1-tetrahydrocannabinolic acid synthase [29]. More recently BBE-like enzymes were discovered in the biosynthesis of the ergot alkaloid intermediate chanoclavine I and the indole alkaloid communesin [30, 31]. Although the exact mechanism of the reactions catalyzed by the latter two BBE-like enzymes has not been analyzed in detail yet, the structures of the generated products suggest that a similar coupling of substrate oxidation and ring formation may occur.

3.4.1. The active site type II

Despite the observed structural differences of the cognate substrates, all BBE-like enzymes share the vanillyl oxidase (VAO) fold. The ability to accept different substrates and catalyze regio- and stereospecific cyclization reactions is controlled by the specific composition of amino acid residues in the active sites. *AtBBE*-like 28 has a unique composition of the active site that has not been characterized so far. As the substrate of *AtBBE*-like 28 is still unknown, it is difficult to assign distinct roles to the residues in the active site. Fraaije *et al.* have reported some recurrent features present in flavoenzymes that are carrying out an oxidation reaction [32]. According to their analysis, the position of the oxidized atom relative to the flavin ring is conserved (“site of oxidative attack”, see Fig 8). Furthermore, flavin dependent oxidoreductases have a hydrogen bond donor to N(5), a catalytic base to activate the substrate and possess a redox potential above +25 mV. As shown in Fig 8, *AtBBE*-like 28 features a hydrogen bond donor to N(5) (N π of His174) and a catalytic base to initiate substrate oxidation (Tyr188) and hence shares the hallmarks of a flavoprotein oxidase, as proposed by Fraaije and coworkers [32]. An additional interesting feature of the active site is the proton-relay established between the putative catalytic base, Tyr188, and the neighboring acidic side chains of Glu426 and Asp369, which presumably activate Tyr188 to facilitate proton abstraction. The experimentally determined redox potential of *AtBBE*-like 28 of $+61 \pm 1$ mV is also in accordance with a potential function as an oxidase.

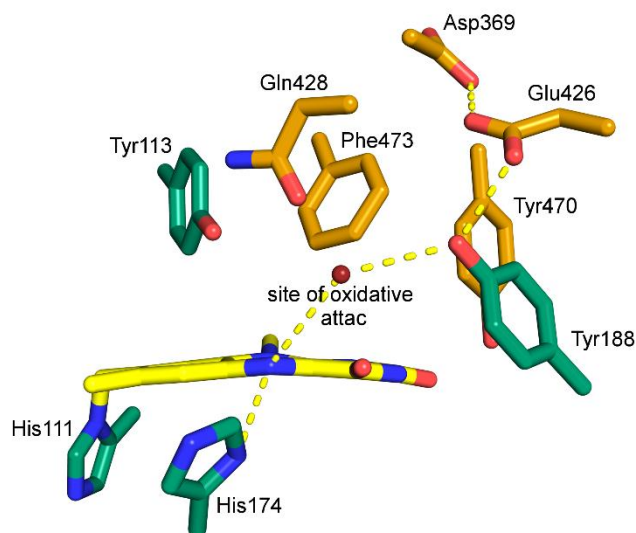


Fig 8. Model of the active site of *AtBBE*-like 28 indicating the putative site of oxidative attack (red sphere). Interactions are represented by dashed yellow lines. One of the unique features of the type IIa active site is the nature and position of the catalytic base, *i.e.* Tyr188 that interacts with Glu426 and a monocovalent attachment of the cofactor. In the active site type IIb, nature and position of the catalytic base are conserved (compare Fig 7 1.1 and 1.2) but a bicovalent attachment of the cofactor is to be expected for this active site type. Interestingly the change from a bicovalent to a monocovalent binding mode goes along with the variation of two amino acids of the oxygen reactivity motif. These are the amino acids at position 174 (*i.e.* cysteine to histidine exchange), responsible for the formation of the covalent bond to C(6) of the isoalloxazine ring and 182 (*i.e.* histidine to glutamine exchange) (Fig 7). This is perfectly in line with findings reported by Kopacz *et al.* [33] on 6-hydroxy-D-nicotine oxidase, a VAO-type flavoprotein with a monocovalent linkage of a histidine to the 8 α -position of the isoalloxazine ring. In this enzyme, bicovalent attachment was achieved by introduction of a cysteine and histidine residue corresponding to position 174 and 182, respectively, indicating that the histidine residue plays a crucial role in the formation of the sulfur-carbon bond [33].

3.4.2. Oxygen reactivity of *AtBBE*-like 28

The oxidative half reaction of BBE-like enzymes was recently analyzed in more detail demonstrating that two amino acids fulfill the function of gatekeeper residues in controlling oxygen reactivity [15, 34]. Specifically, the presence of an “oxygen pocket” on the *re*-side of the isoalloxazine ring in direct vicinity of the reactive C(4a)-atom promotes the reaction between dioxygen and reduced flavin in a similar manner as the “oxyanion hole” stabilizes the transition state in hydrolases [15]. This oxygen pocket is created by the oxygen reactivity motif (see Fig 2B and 3B). The access to the oxygen pocket is controlled by amino acids in position 172 and 177. The amino acid glycine in position 172 will allow oxygen to enter while alanine will deny access. Likewise access to the oxygen pocket can be controlled by the size of the side chain of the amino acid in position 177 [34]. The presence of valine in position 177 creates enough space for oxygen to bind in the oxygen pocket, whereas the presence of leucine occupies the oxygen pocket and hence oxygen cannot react with the C(4a)-atom to oxidize the reduced isoalloxazine ring. Thus oxidases and dehydrogenases typically possess either valine or leucine

in this position. In *AtBBE*-like 28 the gatekeeper positions are occupied by residues typically found in an oxidase, *i.e.* glycine and valine. The apparent oxidative rate of $3040 \pm 50 \text{ M}^{-1} \text{ s}^{-1}$ is surprisingly small for an oxidase although it is still two to three orders of magnitude larger than the rates found for dehydrogenases of the BBE-like enzyme family [9, 15]. In principle, reduced flavoenzymes may be oxidized by formation of a binary complex with dioxygen after the dissociation of the product (as in a “ping-pong”-mechanism) or the formation of a ternary complex involving the oxidized product [35]. In the case of *AtBBE*-like 28 the oxidative and reductive half reaction are spatially separated by the isoalloxazine ring and therefore formation of a ternary complex is conceivable. Thus the rate of reoxidation of reduced *AtBBE*28 by dioxygen may also be affected by the presence of product, *i.e.* differs from the rate of reoxidation in the binary complex.

3.4.3. Comparison of *AtBBE*-like to another BBE-like protein: Phl p 4

Crystallographic studies also demonstrated that dioxygen surrogates, such as halide anions, bind to the oxygen pocket [15]. In the case of *AtBBE*-like enzyme 28 we observed an electron density in the oxygen binding pocket that was interpreted as a bound chloride (Fig 3B). An overlay of the previously reported structure of Phl p 4, a pollen allergen from timothy grass with glucose dehydrogenase activity [36], and the structure of *AtBBE*-like enzyme 28 is shown in Fig 9. The location of the halide binding site relative to the isoalloxazine ring of the flavin is structurally conserved. Previous studies have also shown that a single amino acid replacement at this position reverses reactivity towards oxygen [15, 9]. In this sense, the sequence logos shown in Fig 7 are useful to predict the reactivity towards oxygen in *AtBBE*-like enzymes, *i.e.* enzymes with valine in position 177 will behave more like oxidases while those with leucine in position 177 will act like dehydrogenases.

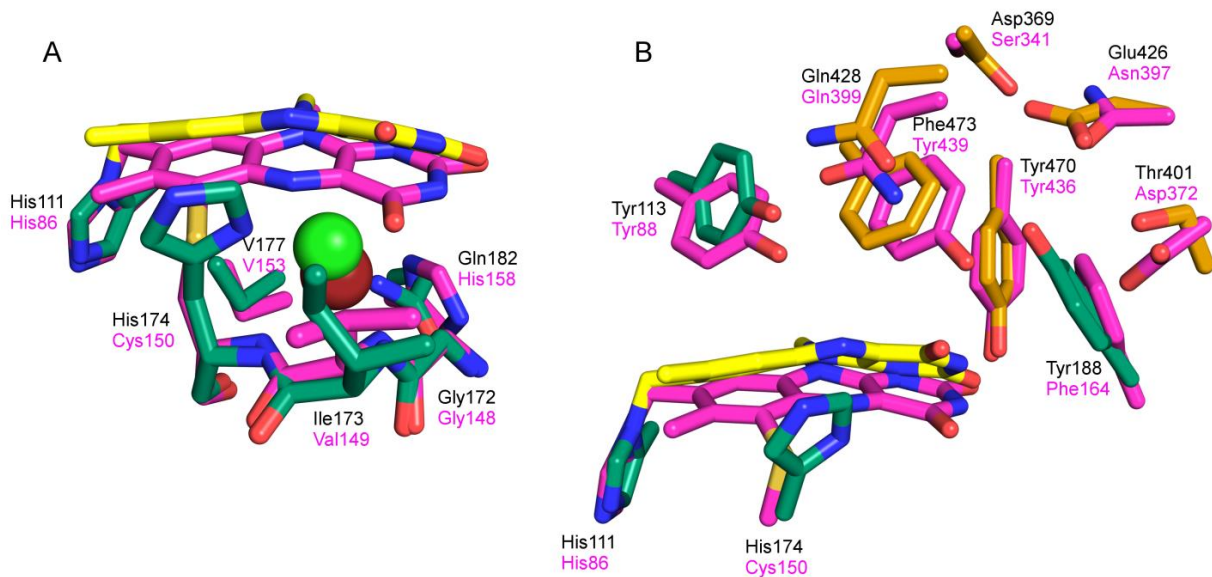


Fig 9. Overlay of *AtBBE*-like 28 and Phl p 4 I153V N158H. A: *re*-side: *AtBBE*-like 28 is shown in green and yellow, Phl p 4 (PDB: 4PWC) is shown in magenta. The chloride ion embedded in *AtBBE*-like 28 is shown in green, bromide from Phl p 4 is shown in red. The oxygen pocket is highly conserved and in both structures occupied by oxygen surrogating halide ions. In Phl p 4 the halide ion is complexed by the nitrogen of the peptide bond between Cys150 and Val149 and the nitrogen of the peptide bond between Val149 and Gly148. In *AtBBE*-like 28 the halide ion is complexed by the corresponding residues, additionally His174 and Gln182 are involved in hydrogen bonds towards the chloride ion. B: *si*-side: The positions of the active site forming residues are conserved. Their nature has been changed, leading to two different active sites embedded in a very similar protein scaffold. Though the position of the isoalloxazine ring is highly conserved in the BBE-like family the C4 C6 axis of the plane N10 C4 C6 has been shifted 32° resulting in a displacement of N5 by 1.6 Å.

3.4.4. Analysis of the phenotype of the *AtBBE*-like 28 loss-of-function mutant

The putative *AtBBE*-like 28 loss-of-function mutant *bbe28* exhibits a reproducible phenotype, both under standard growth and mild salt stress conditions. At a salt concentration of 100 mM, *bbe28* produced significantly less healthy green seedlings when compared to Col-0 indicating that *AtBBE*-like 28 plays a role in salt stress tolerance, which would agree with the specific induction by salt stress in the root [21, 37]. Interestingly, under standard growth conditions *bbe28* produced less biomass, both based on FW and DW, respectively. This 10% reduction cannot be explained by a slower development, since *bbe28* formed only slightly fewer leaves in comparison to Col-0 after 30 days of growth. Equally, the *bbe28* mutant showed only a marginal delay in flowering. More detailed analyses will be required to determine the mechanism by which the Brassicaceae-specific *AtBBE*-like 28 protein functions in plant growth and salt stress tolerance. Based on the *in-silico* expression data, *AtBBE*-like 28 is expressed in the root, specifically in the lateral root cap, endodermis, atrichoblasts and weaker expression in the root xylem. This suggests a function in restricting water transport or minimizing water loss in the root. The weak phenotype associated with the *bbe28* mutant agrees with the fact that

among the *AtBBE*-like family members only for *AtBBE*-like protein 15 a mutant phenotype has been described before [38]. This suggests that detailed phenotyping, combined with biochemical analyses is required to study the *in planta* function for *AtBBE*-like protein family members, preferable under specific growth conditions that cause pronounced changes of their respective expression. Importantly, the putative *AtBBE*-like 28 function in salt stress deduced from *in silico* expression data, was experimentally confirmed under mild salt stress conditions (Fig 5B) [21, 37].

3.5. Experimental Procedures

All chemicals were purchased at Sigma Aldrich (St. Louis, USA) and were of the highest grade commercially available. Restriction enzymes were obtained from Thermo Fisher Scientific (Waltham, Massachusetts, USA). Ni Sepharose 6 Fast Flow column material was purchased from GE Healthcare (Chalfont St Giles, UK). A synthetic gene coding for *AtBBE28* was from VBC Biotech (Vienna, Austria).

3.5.1. Cloning and transformation

The protein was expressed using *Komagataella pastoris* as expression host according the EasySelect™ *Pichia* Expression Kit provided by Invitrogen (Carlsbad, USA). The gene was adapted to *K. pastoris* codon usage and a C-terminal His-tag was added. SignalP was used to identify the native signal sequence of 27 amino acids [39]. The gene lacking the signal sequence was cloned into the pPICZα vector® (Invitrogen), using standard techniques. *K. pastoris* strain KM71H was transformed with pPICK-PDI vector harboring the gene for the protein disulfide isomerase from *Saccharomyces cerevisiae*. The modified KM71H strain was transformed with the linearized pPICZα-*AtBBE*-like 28 construct. All transformations were done by electroporation. Applicable expression strains were identified using the method proposed by Weis *et al.*[40].

3.5.2. Expression and purification

Expression was carried out using a BBI CT-2 fermenter (Sartorius AG, Goettingen, Germany) in basal minimal medium as described by Schrittwieser *et al.* [41]. After 96 h of induction the pH was set to 8.0 and the cells were removed by centrifugation at 3000 g at 4 °C for 30 min. The supernatant was subsequently filtered through membranes with pore diameter of 0.8 μm, 0.45 μm and 0.22 μm. The volume was reduced from 3 to 0.5 L using a cross flow apparatus (Centramate 500S, Pall Corporation, Dreieich, Germany), equipped with a membrane with a cut-off of 22 kDa (Omega Centramate membrane cassettes, Pall Corporation, Dreieich,

Germany). The buffer was changed to 50 mM potassium phosphate pH 7.0 containing 150 mM NaCl and 10 mM imidazole. The supernatant was loaded to a Ni SepharoseTM 6 Fast Flow column. The column was washed with 10 column volumes loading buffer, the protein was eluted using 50 mM phosphate buffer containing 150 mM NaCl and 150 mM imidazole. After elution, the column was stripped using 20 mM potassium phosphate buffer pH 7.4 containing 0.5 M NaCl and 50 mM EDTA. A second yellow flavoprotein containing fraction was collected. The purity of the different fractions was checked by SDS-PAGE. Fractions eluted with 50 mM phosphate buffer containing 150 mM NaCl and 150 mM imidazole were concentrated using Amicon Ultra centrifugal filter units (Merck KGaA, Darmstadt, Germany) and loaded on a Superdex 200 gel filtration column using an Äkta system (GE Healthcare, Little Chalfont, United Kingdom). Separation was achieved using 50 mM TRIS/HCl buffer pH 8 containing 150 mM NaCl. Fractions containing *At*BBE-like 28 were concentrated and the buffer was changed to 20 mM TRIS/HCl (buffer A). The protein was loaded to a MonoQ column and eluted applying a stepwise gradient to 100 % of a 20 mM TRIS/HCl buffer pH 8 containing 1 M NaCl (buffer B). The flow rate was 1 mL/min, buffer A was kept at 100% for 5 min, then a gradient to 20% buffer B in 30 min was set. 20% buffer B was kept for 10 min, and then a gradient to 100% B was set in 20 min.

3.5.3. Crystallization and crystal structure determination

The *At*BBE-like 28 fraction collected during column stripping was used for crystallization without further purification steps. After purification *At*BBE-like 28 was stored over night at 4 °C in 20 mM potassium phosphate buffer pH 7.4 containing 0.5 M NaCl and 50 mM EDTA. The buffer was changed to 20 mM TRIS/HCl pH 9.0 using a PD-10 desalting column (GE Healthcare, Little Chalfont, United Kingdom) and the protein concentration was adjusted to 20 mg/mL. Crystallization in the optimized condition was performed using the microbatch method, mixing 1 µL of protein and 0.5 µL of 0.1 M HEPES buffer pH 7.0 containing 30 % v/v Jeffamine ED 2001 pH 7.0 at 277 K. Tetragonal bipyramidal crystals appeared after streak seeding and grew to a maximum dimension of approximately 300 µm within 14 days. Surplus crystallization buffer was removed by streaking the crystals over the microbatch plate's surface under oil before flash freezing the crystals in liquid nitrogen without any additional cryo protection. A diffraction data set was collected at 100 K at the beam line BM14 (ESRF, Grenoble, France). The diffraction data were processed using XDS [42]. The structure was solved by molecular replacement using the program Phaser with the structure of *Ec*BBE (PDB ID 3D2H) [43] as search template. Structure refinement was done by repetitive runs of the programs COOT [44] and Phenix [45]. A TLS restrained refinement was included using four

TLS groups per chain obtained from the TLSMD webserver [46, 47]. R_{free} values were calculated from 5 % randomly chosen reflections excluded from refinement. A summary of data collection, processing and refinement statistics is given in Table 2. Two protein chains were present in the asymmetric unit. Clear electron density was observed for most residues in both chains with the exception of gaps between Tyr37 and Thr43 in chain A and between Cys34 and Val48 in chain B.

Table 2. Data collection and refinement statistics.

Wavelength (Å)	0.920
Beamline	ESRF BM14
Resolution range (Å)	15.89 - 1.849 (1.915 - 1.849)
Space group	C222 ₁
Unit cell	127.02 133.13 139.00 90 90 90
Total reflections	376130 (35085)
Unique reflections	93337 (9111)
Multiplicity	4.0 (3.9)
Completeness (%)	93.16 (91.72)
Mean I/sigma(I)	7.22 (2.00)
Wilson B-factor	23.30
R-merge	0.1224 (0.5576)
R-meas	0.1406
CC1/2	0.987 (0.767)
CC*	0.997 (0.932)
R-work	0.1781 (0.2913)
R-free	0.2205 (0.3205)
Number of non-hydrogen atoms	9336
Macromolecules	7927
Ligands	118
Water	1291
Protein residues	994
RMS(bonds)	0.007
RMS(angles)	1.10
Ramachandran favored (%)	95
Ramachandran outliers (%)	0.2
Clashscore	9.98
Average B-factor	33.70
Macromolecules	32.80
Ligands	25.70
Solvent	39.70
PDB code	5D79

3.5.4. Redox potential determination

The redox potential was determined using the dye-equilibrium method employing the xanthine/xanthine oxidase system as electron source and thionine acetate as the reporter dye ($E^\circ = 64 \text{ mV}$) as described by Massey *et al.* [48]. Experiments were performed in 50 mM potassium phosphate buffer pH 7.0 at 25 °C. The reaction mixture contained 5 μM methylviologen as mediator, 15 μM enzyme and xanthine oxidase in catalytic amounts (approximately 2 nM). Solutions with methylviologen, *AtBBE*-like 28 and xanthine were mixed under anoxic conditions with solutions of xanthine oxidase and thionine acetate. Reactions were carried out using a stopped flow device SF-61DX2 (TgK Scientific, Bradford-On-Avon, UK) positioned in a glove box (Belle Technology, Weymouth, UK). Spectra were recorded with a KinetaScanT diode array detector MG-6560 (TgK Scientific). One experiment lasted for 50 min, 300 scans were recorded during that time. The potential of *AtBBE*-like 28 was calculated from the plot of $\log([\text{ox}]/[\text{red}])$ of the protein versus $\log([\text{ox}]/[\text{red}])$ of thionine acetate according to Minnaert *et al.* [20].

3.5.5. Photoreduction

Photoreduction was carried out according to Massey *et al.* [16]. Reactions were carried out in 50 mM potassium phosphate buffer pH 7.0 at 25 °C. Solutions were flushed with nitrogen and stored 1 h in an anaerobic glove box to remove all oxygen. Reaction mixtures containing 20 μM *AtBBE*-like 28 and 10 mM EDTA were tightly closed in the glove box and irradiated with a projector (Luminea™ 10 W, Pearl GmbH, Buggingen, Germany). Spectra were recorded with a photometer (Specord 205, Analytik Jena, Jena, Germany).

3.5.6. Determination of the oxidative rate

Photoreduced enzyme was mixed with air saturated buffer in the stopped flow device. Reoxidation of the enzyme was followed at a wavelength of 450 nm. Experiments were performed in 50 mM potassium phosphate buffer pH 7.0 at 25 °C. The oxidative rate was determined using the Kinetic Studio software (TgK Scientific, Bradford-on-Avon, UK). An apparent rate constant was calculated using a monoexponential fitting model.

3.5.7. Plant growth experiments

A. thaliana plants (Col-0 ecotype) were grown on half strength MS medium under short day conditions (8 h light) at 21 °C (light intensity: 180 $\mu\text{mol m}^{-2} \text{ s}^{-1}$) in growth cabinets or in soil under long day conditions (16 h light) in a greenhouse at 20-22 °C and relative humidity 70% as described in [49]. A T2 T-DNA insertion line was obtained for *AtBBE*-like 28

(At5g44440, SALK_007813) from the SALK mutant collection [50]. Homozygous T3 seeds were generated, confirmed by growth of the respective seedlings on kanamycin selection medium and PCR analysis using the primers: *bbe28*-F 5'-CAAATAACCGATGCACA-3', *bbe28*-R 5'-GTCGAGAAAGAAAA-CCCTAA-3' and Salk-LBa1 5'-TGGTTCACGTAGTG-GGCCATCG-3'. The Col-0 and homozygous *bbe28* seeds employed for the growth experiments were obtained from the respective parental plants that were grown in parallel in soil under greenhouse conditions to ensure an equal seed quality. To determine differences in salt stress tolerance, surface sterilized seeds were germinated and grown on plates with half strength MS medium (control) or salt stress (100 mM NaCl) medium for 14 days, three biological replicates, each with three technical replicates and each plate with >30 Col-0 and >30 *bbe28* seeds to minimize variability between plates. For biomass experiments, seeds were germinated and grown on half strength MS medium for 14 days, seedlings were transferred to soil after 14 (28 d) or 16 days (30 d) of growth on half strength MS medium and subsequent growth in soil for 14 days, or seeds were directly germinated on soil and grown for 35 days in two independent experiments. The biomass experiments in plates were performed with four technical replicates and 10 Col-0 or *bbe28* plants were weighed per replicate. The biomass experiments in soil were performed with four technical replicates and 12 Col-0 or *bbe28* plants were weighed per replicate, except for the 30 d biomass experiment where all 48 plants were weighed in one batch.

3.5.8. Phylogenetic analysis

Sequences were retrieved from the Phytosome 10.2 website [22]. Clustal omega was used to create a multiple sequence alignment including all *AtBBE*-like protein family members using the default parameters [23]. The alignment was manually edited by hand using Jalview [51]. The PHYLIP package (PHYLIP 3.69) was used to create a bootstrapped phylogenetic tree using the programs SEQBOOT, PROTDIST, NEIGHBOR and CONSENSE [24]. We created 1000 Jackknife sub-alignments with SEQBOOT, which were subsequently subjected to a bootstrapped protein-distance analysis. We chose *EcBBE* (AC39358) as the outgroup sequence. The tree shown in Fig 5 was visualized using Figtree (Tree Fig Drawing Tool, version 1.4.0 by Andrew Rambaut) [52]. The tree including the bootstrap values is shown in the supplement as S1 Fig. The accession codes for the sequences used for the analysis are given in S1 Table.

3.6. References

1. Macheroux P, Kappes B, Ealick SE. Flavogenomics - A genomic and structural view of flavin-dependent proteins. *FEBS Journal*. 2011. pp. 2625–2634. doi:10.1111/j.1742-4658.2011.08202.x
2. Winkler A, Hartner F, Kutchan TM, Glieder A, Macheroux P. Biochemical evidence that berberine bridge enzyme belongs to a novel family of flavoproteins containing a bi-covalently attached FAD cofactor. *J Biol Chem*. 2006;281: 21276–21285. doi:10.1074/jbc.M603267200
3. Winkler A, Motz K, Riedl S, Puhl M, Macheroux P, Gruber K. Structural and mechanistic studies reveal the functional role of bicovalent flavinylation in berberine bridge enzyme. *J Biol Chem*. 2009;284: 19993–20001. doi:10.1074/jbc.M109.015727
4. Facchini PJ, Penzes C, Johnson AG, Bull D. Molecular characterization of berberine bridge enzyme genes from opium poppy. *Plant Physiol*. 1996;112: 1669–1677. doi:10.1104/pp.112.4.1669
5. Attila C, Ueda A, Cirillo SLG, Cirillo JD, Chen W, Wood TK. *Pseudomonas aeruginosa* PAO1 virulence factors and poplar tree response in the rhizosphere. *Microb Biotechnol*. 2008;1: 17–29. doi:10.1111/j.1751-7915.2007.00002.x
6. González-Candelas L, Alamar S, Sánchez-Torres P, Zacarías L, Marcos JF. A transcriptomic approach highlights induction of secondary metabolism in citrus fruit in response to *Penicillium digitatum* infection. *BMC Plant Biol*. 2010;10: 194. doi:10.1186/1471-2229-10-194
7. Coram T, Huang X, Zhan G, Settles M, Chen X. Meta-analysis of transcripts associated with race-specific resistance to stripe rust in wheat demonstrates common induction of blue copper-binding protein, heat-stress transcription factor, pathogen-induced WIR1A protein, and entkaurene synthase transcri. *Funct Integr Genomics*. Springer-Verlag; 2010;10: 383–392. doi:10.1007/s10142-009-0148-5
8. Zhang J, Feng J, Lu J, Yang Y, Zhang X, Wan D, et al. Transcriptome differences between two sister desert poplar species under salt stress. *BMC Genomics*. 2014;15: 337. doi:10.1186/1471-2164-15-337
9. Daniel B, Pavkov-Keller T, Steiner B, Dordic A, Gutmann A, Nidetzky B, et al. Oxidation of Monolignols by Members of the Berberine Bridge Enzyme Family Suggests a Role in Cell Wall Metabolism. *J Biol Chem*. 2015;290: 18770–18781. doi:10.1074/jbc.M115.659631
10. Jamet E, Canut H, Boudart G, Pont-Lezica RF. Cell wall proteins: A new insight through proteomics. *Trends in Plant Science*. 2006. pp. 33–39. doi:10.1016/j.tplants.2005.11.006
11. Seidl MF, Van den Ackerveken G, Govers F, Snel B. A domain-centric analysis of oomycete plant pathogen genomes reveals unique protein organization. *Plant Physiol*. 2011;155: 628–644. doi:10.1104/pp.110.167841
12. Raffaele S, Win J, Cano LM, Kamoun S. Analyses of genome architecture and gene expression reveal novel candidate virulence factors in the secretome of *Phytophthora infestans*. *BMC Genomics*. 2010;11: 637. doi:10.1186/1471-2164-11-637
13. Morais do Amaral A, Antoniw J, Rudd JJ, Hammond-Kosack KE. Defining the Predicted Protein Secretome of the Fungal Wheat Leaf Pathogen *Mycosphaerella graminicola*. *PLoS One*. 2012;7. doi:10.1371/journal.pone.0049904

14. Krieger E, Koraimann G, Vriend G. Increasing the precision of comparative models with YASARA NOVA - A self-parameterizing force field. *Proteins Struct Funct Genet.* 2002;47: 393–402. doi:10.1002/prot.10104
15. Zafred D, Steiner B, Teufelberger AR, Hromic A, Karplus PA, Schofield CJ, et al. Rationally engineered flavin-dependent oxidase reveals steric control of dioxygen reduction. *FEBS J.* 2015;282: 3060–3074. doi:10.1111/febs.13212
16. Massey V, Hemmerich P. Photoreduction of flavoproteins and other biological compounds catalyzed by deazaflavins. *Biochemistry.* 1978;17: 9–16. doi:10.1021/bi00594a002
17. Mayhew SG. The effects of pH and semiquinone formation on the oxidation-reduction potentials of flavin mononucleotide. A reappraisal. *Eur J Biochem.* 1999;265: 698–702. doi:10.1046/j.1432-1327.1999.00767.x
18. Winkler A, Kutchan TM, Macheroux P. 6-*S*-cysteinylation of bi-covalently attached FAD in berberine bridge enzyme tunes the redox potential for optimal activity. *J Biol Chem.* 2007;282: 24437–24443. doi:10.1074/jbc.M703642200
19. Massey V. Activation of molecular oxygen by flavins and flavoproteins. *Journal of Biological Chemistry.* 1994. pp. 22459–22462.
20. Minnaert K. Measurement of the equilibrium constant of the reaction between cytochrome c and cytochrome a. *Biochim Biophys Acta - Enzymol Biol Oxid.* 1965;110: 42–56. doi:http://dx.doi.org/10.1016/S0926-6593(65)80093-5
21. Winter D, Vinegar B, Nahal H, Ammar R, Wilson G V., Provart NJ. An “electronic fluorescent pictograph” Browser for exploring and analyzing large-scale biological data sets. *PLoS One.* 2007;2. doi:10.1371/journal.pone.0000718
22. Goodstein DM, Shu S, Howson R, Neupane R, Hayes RD, Fazo J, et al. Phytozome: A comparative platform for green plant genomics. *Nucleic Acids Res.* 2012;40. doi:10.1093/nar/gkr944
23. Sievers F, Wilm A, Dineen D, Gibson TJ, Karplus K, Li W, et al. Fast, scalable generation of high-quality protein multiple sequence alignments using Clustal Omega. *Molecular Systems Biology.* 2011. doi:10.1038/msb.2011.75
24. Felsenstein J. Phylip: phylogeny inference package (version 3.2). *Cladistics.* 1989;5: 164–166. doi:10.1111/j.1096-0031.1989.tb00562.x
25. Ishida M, Hara M, Fukino N, Kakizaki T, Morimitsu Y. Glucosinolate metabolism, functionality and breeding for the improvement of Brassicaceae vegetables. *Breed Sci.* 2014;64: 48–59. doi:10.1270/jsbbs.64.48
26. Glawischnig E. Camalexin. *Phytochemistry.* 2007. pp. 401–406. doi:10.1016/j.phytochem.2006.12.005
27. Liu Y-C, Li Y-S, Lyu S-Y, Hsu L-J, Chen Y-H, Huang Y-T, et al. Interception of teicoplanin oxidation intermediates yields new antimicrobial scaffolds. *Nat Chem Biol.* 2011;7: 304–309. doi:10.1038/nchembio.556
28. Winkler A, Lyskowski A, Riedl S, Puhl M, Kutchan TM, Macheroux P, et al. A concerted mechanism for berberine bridge enzyme. *Nat Chem Biol.* 2008;4: 739–741. doi:10.1038/nchembio.123

29. Sirikantaramas S, Morimoto S, Shoyama Y, Ishikawa Y, Wada Y, Shoyama Y, et al. The gene controlling marijuana psychoactivity: molecular cloning and heterologous expression of Δ^1 -tetrahydrocannabinolic acid synthase from *Cannabis sativa* L. *J Biol Chem*. 2004;279: 39767–39774. doi:10.1074/jbc.M403693200
30. Lorenz N, Olšovská J, Šulc M, Tudzynski P. Alkaloid cluster gene *ccsA* of the ergot fungus *Claviceps purpurea* encodes chanoclavine I synthase, a flavin adenine dinucleotide-containing oxidoreductase mediating the transformation of *N*-methyl-dimethylallyltryptophan to chanoclavine I. *Appl Environ Microbiol*. 2010;76: 1822–1830. doi:10.1128/AEM.00737-09
31. Lin H-C, Chiou G, Chooi Y-H, McMahon TC, Xu W, Garg NK, et al. Elucidation of the Concise Biosynthetic Pathway of the Communesin Indole Alkaloids. *Angew Chemie Int Ed*. WILEY-VCH Verlag; 2015;54: 3004–3007. doi:10.1002/anie.201411297
32. Fraaije MW, Mattevi A. Flavoenzymes: Diverse catalysts with recurrent features. *Trends in Biochemical Sciences*. 2000. pp. 126–132. doi:10.1016/S0968-0004(99)01533-9
33. Kopacz MM, Fraaije MW. Turning a monocovalent flavoprotein into a bicovalent flavoprotein by structure-inspired mutagenesis. *Bioorganic Med Chem*. 2014;22: 5621–5627. doi:10.1016/j.bmc.2014.05.051
34. Leferink NGH, Fraaije MW, Joosten HJ, Schaap PJ, Mattevi A, van Berkel WJH. Identification of a gatekeeper residue that prevents dehydrogenases from acting as oxidases. *J Biol Chem*. 2009;284: 4392–4397. doi:10.1074/jbc.M808202200
35. Cleland WW. The kinetics of enzyme-catalyzed reactions with two or more substrates or products. I. Nomenclature and rate equations. 1963. *Biochim Biophys Acta*. 1989;1000: 213–220. doi:10.1016/0926-6569(63)90227-X
36. Zafred D, Nandy A, Pump L, Kahlert H, Keller W. Crystal structure and immunologic characterization of the major grass pollen allergen Phl p 4. *J Allergy Clin Immunol*. 2013;132. doi:10.1016/j.jaci.2013.03.021
37. Dinneny JR, Long T a, Wang JY, Jung JW, Mace D, Pointer S, et al. Cell identity mediates the response of *Arabidopsis* roots to abiotic stress. *Science*. 2008;320: 942–5. doi:10.1126/science.1153795
38. Pagnussat GC, Yu H-J, Ngo Q a, Rajani S, Mayalagu S, Johnson CS, et al. Genetic and molecular identification of genes required for female gametophyte development and function in *Arabidopsis*. *Development*. 2005;132: 603–614. doi:10.1242/dev.01595
39. Petersen TN, Brunak S, von Heijne G, Nielsen H. SignalP 4.0: discriminating signal peptides from transmembrane regions. *Nature Methods*. 2011. pp. 785–786. doi:10.1038/nmeth.1701
40. Weis R, Luiten R, Skranc W, Schwab H, Wubbolts M, Glieder A. Reliable high-throughput screening with *Pichia pastoris* by limiting yeast cell death phenomena. *FEMS Yeast Res*. 2004;5: 179–189. doi:10.1016/j.femsyr.2004.06.016
41. Schrittwieser JH, Resch V, Wallner S, Lienhart W-D, Sattler JH, Resch J, et al. Biocatalytic organic synthesis of optically pure (*s*)-scoulerine and berbine and benzyloquinoline alkaloids. *J Org Chem*. 2011;76: 6703–6714. doi:10.1021/jo201056f
42. Kabsch W. Automatic processing of rotation diffraction data from crystals of initially unknown symmetry and cell constants. *Journal of Applied Crystallography*. 1993. pp. 795–800. doi:10.1107/S0021889893005588

43. McCoy AJ, Grosse-Kunstleve RW, Adams PD, Winn MD, Storoni LC, Read RJ. Phaser crystallographic software. *J Appl Crystallogr*. 2007;40: 658–674. doi:10.1107/S0021889807021206
44. Emsley P, Cowtan K. Coot: model-building tools for molecular graphics. *Acta Crystallogr D Biol Crystallogr*. 2004;60: 2126–2132. doi:10.1107/S0907444904019158
45. Adams PD, Grosse-Kunstleve RW, Hung L-W, Ioerger TR, McCoy AJ, Moriarty NW, et al. PHENIX : building new software for automated crystallographic structure determination. *Acta Crystallogr Sect D Biol Crystallogr*. 2002;58: 1948–1954. doi:10.1107/S0907444902016657
46. Painter J, Merritt EA. Optimal description of a protein structure in terms of multiple groups undergoing TLS motion. *Acta Crystallogr D Biol Crystallogr*. 2006;62: 439–450. doi:10.1107/S0907444906005270
47. Painter J, Merritt EA. web server for the generation of multi-group TLS models. *Journal of Applied Crystallography*. 2006. pp. 109–111. doi:10.1107/S0021889805038987
48. Massey V. Flavins and flavoproteins 1990. B. Curti, S. Ronchi and G. Zanetti (eds). de Gruyter, Berlin and New York. xxiii + 945 pages, DM390 (1991). [Internet]. *Cell Biochemistry and Function*. John Wiley & Sons, Ltd.; 1992. doi:10.1002/cbf.290100117
49. Hyun TK, Van Der Graaff E, Albacete A, Eom SH, Großkinsky DK, Böhm H, et al. The *Arabidopsis* PLAT domain protein1 is critically involved in abiotic stress tolerance. *PLoS One*. 2014;9. doi:10.1371/journal.pone.0112946
50. Alonso JM, Stepanova AN, Leisse TJ, Kim CJ, Chen H, Shinn P, et al. Genome-wide insertional mutagenesis of *Arabidopsis thaliana*. *Science*. 2003;301: 653–7. doi:10.1126/science.1086391
51. Waterhouse AM, Procter JB, Martin DMA, Clamp M, Barton GJ. Jalview Version 2-A multiple sequence alignment editor and analysis workbench. *Bioinformatics*. 2009;25: 1189–1191. doi:10.1093/bioinformatics/btp033
52. Rambaut A. FigTree v1.3.1. 2006-2009. Accessed Novemb 29, 2012. 2009; Program package available at <http://tree.bio.ed.ac>.

Structure of a berberine bridge enzyme-like enzyme with an active site specific to the plant family Brassicaceae

3.7. Supplementary Information

Bastian Daniel¹, Silvia Wallner¹, Barbara Steiner¹, Gustav Oberdorfer², Prashant Kumar², Eric van der Graaff³, Thomas Roitsch^{3,4}, Christoph W. Sensen⁵, Karl Gruber² and Peter Macheroux^{1*}

¹Institute of Biochemistry, Graz University of Technology, Graz, Austria

²Institute of Molecular Biosciences, University of Graz, Graz, Austria

³Department of Plant and Environmental Sciences, University of Copenhagen, Copenhagen, Denmark

⁴Global Change Research Centre, Czech Globe AS CR, v.v.i., Drásov 470, Cz-664 24 Drásov, Czech Republic

⁵Institute of Molecular Biotechnology, Graz University of Technology, Graz, Austria

To whom correspondence should be addressed: Prof. Dr. Peter Macheroux, Graz University of Technology, Institute of Biochemistry, Petersgasse 12/II, A-8010 Graz, Austria, Tel.: +43-316-873 6450; Fax: +43-316-873 6952; Email: peter.macheroux@tugraz.at

S1 Table. Accession numbers. Summarized are the accession numbers of BBE-like coding sequences that were used for the phylogenetic analysis and their abbreviations. Genes of the following species are listed: *Arabidopsis lyrata* (Al), *Arabidopsis thaliana* (At), *Boechera stricta* (Bs), *Brassica rapa* (Br), *Capsella grandiflora* (Cg), *Capsella rubella* (Cr), and *Eutrema salsugineum* (Es).

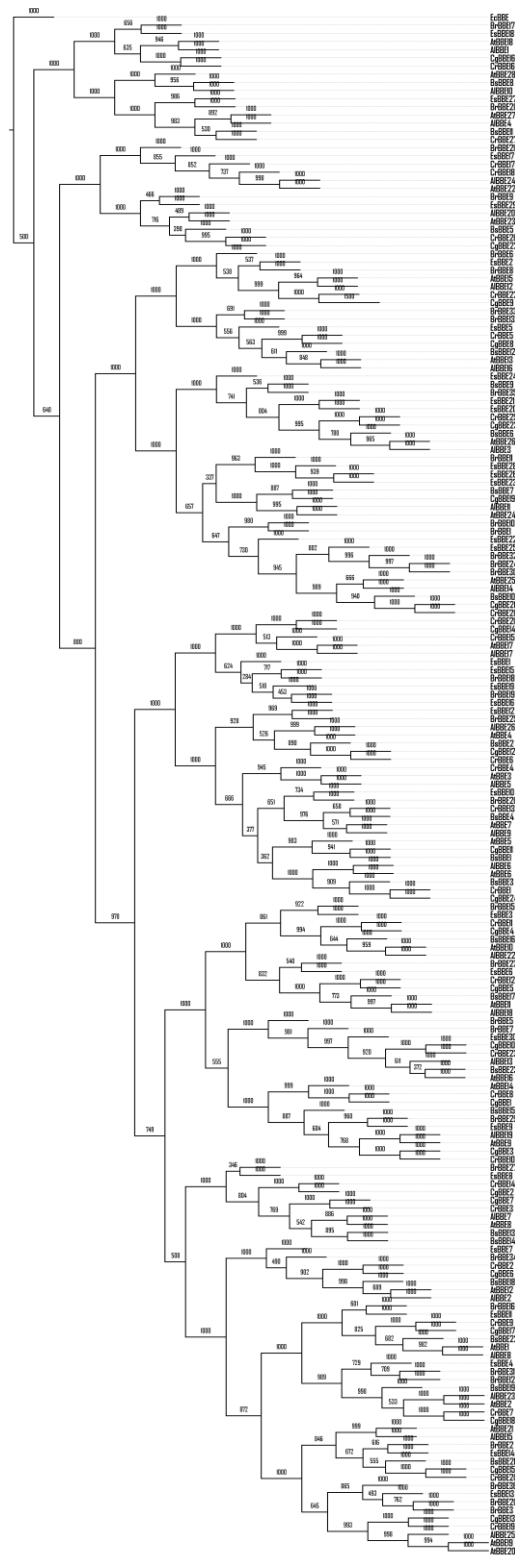
Gene name	Abbreviation
AT1G01980.1	AtBBE1
AT1G11770.1	AtBBE2
AT1G26380.1	AtBBE3
AT1G26390.1	AtBBE4
AT1G26400.1	AtBBE5
AT1G26410.1	AtBBE6
AT1G26420.1	AtBBE7
AT1G30700.1	AtBBE8
AT1G30710.1	AtBBE9
AT1G30720.1	AtBBE10
AT1G30730.1	AtBBE11
AT1G30740.1	AtBBE12
AT1G30760.1	AtBBE13
AT1G34575.1	AtBBE14
AT2G34790.1	AtBBE15
AT2G34810.1	AtBBE16
AT4G20800.1	AtBBE17
AT4G20820.1	AtBBE18
AT4G20830.1	AtBBE19
AT4G20830.2	AtBBE20
AT4G20840.1	AtBBE21
AT4G20860.1	AtBBE22
AT5G44360.1	AtBBE23
AT5G44380.1	AtBBE24
AT5G44390.1	AtBBE25
AT5G44400.1	AtBBE26
AT5G44410.1	AtBBE27
AT5G44440.1	AtBBE28
Alyrata 946113 946113	A/BBE1
Alyrata 922142 922142	A/BBE2
Alyrata 494546 494546	A/BBE3
Alyrata 494545 494545	A/BBE4
Alyrata 472781 472781	A/BBE5
Alyrata 472779 472779	A/BBE6
Alyrata 922138 922138	A/BBE7
Alyrata 470076 470076	A/BBE8
Alyrata 472778 472778	A/BBE9
Alyrata 948675 948675	A/BBE10
Alyrata 948681 948681	A/BBE11
Alyrata 934079 934079	A/BBE12

Alyrata 934080 934080	A/BBE13
Alyrata 330958 330958	A/BBE14
Alyrata 492802 492802	A/BBE15
Alyrata 473307 473307	A/BBE16
Alyrata 492806 492806	A/BBE17
Alyrata 473304 473304	A/BBE18
Alyrata 922139 922139	A/BBE19
Alyrata 494550 494550	A/BBE20
Alyrata 948672 948672	A/BBE21
Alyrata 922140 922140	A/BBE22
Alyrata 471318 471318	A/BBE23
Alyrata 354696 354696	A/BBE24
Alyrata 492803 492803	A/BBE25
Alyrata 472780 472780	A/BBE26
Esalsugineum Thhalv10017619m.g Thhalv10017619m	EsBBE1
Esalsugineum Thhalv10016496m.g Thhalv10016496m	EsBBE2
Esalsugineum Thhalv10009705m.g Thhalv10009705m	EsBBE3
Esalsugineum Thhalv10007344m.g Thhalv10007344m	EsBBE4
Esalsugineum Thhalv10007327m.g Thhalv10007327m	EsBBE5
Esalsugineum Thhalv10007354m.g Thhalv10007354m	EsBBE6
Esalsugineum Thhalv10007308m.g Thhalv10007308m	EsBBE7
Esalsugineum Thhalv10007341m.g Thhalv10007341m	EsBBE8
Esalsugineum Thhalv10007337m.g Thhalv10007337m	EsBBE9
Esalsugineum Thhalv10007352m.g Thhalv10007352m	EsBBE10
Esalsugineum Thhalv10007313m.g Thhalv10007313m	EsBBE11
Esalsugineum Thhalv10007336m.g Thhalv10007336m	EsBBE12
Esalsugineum Thhalv10024789m.g Thhalv10024789m	EsBBE13
Esalsugineum Thhalv10027426m.g Thhalv10027426m	EsBBE14
Esalsugineum Thhalv10027126m.g Thhalv10027126m	EsBBE15
Esalsugineum Thhalv10027093m.g Thhalv10027093m	EsBBE16
Esalsugineum Thhalv10026881m.g Thhalv10026881m	EsBBE17
Esalsugineum Thhalv10024886m.g Thhalv10024886m	EsBBE18
Esalsugineum Thhalv10027353m.g Thhalv10027353m	EsBBE19
Esalsugineum Thhalv10000843m.g Thhalv10000843m	EsBBE20
Esalsugineum Thhalv10000843m.g Thhalv10000842m	EsBBE21
Esalsugineum Thhalv10000840m.g Thhalv10000840m	EsBBE22
Esalsugineum Thhalv10000851m.g Thhalv10000851m	EsBBE23
Esalsugineum Thhalv10000846m.g Thhalv10000846m	EsBBE24
Esalsugineum Thhalv10001137m.g Thhalv10001137m	EsBBE25
Esalsugineum Thhalv10000841m.g Thhalv10000841m	EsBBE26
Esalsugineum Thhalv10000845m.g Thhalv10000845m	EsBBE27
Esalsugineum Thhalv10000844m.g Thhalv10000844m	EsBBE28
Esalsugineum Thhalv10003322m.g Thhalv10003322m	EsBBE29
Esalsugineum Thhalv10016482m.g Thhalv10016482m	EsBBE30
Crubella Carubv10012287m.g Carubv10012287m	CrBBE10
Crubella Carubv10011480m.g Carubv10011480m	CrBBE11

Crubella Carubv10011178m.g Carubv10011178m	CrBBE12
Crubella Carubv10008831m.g Carubv10008831m	CrBBE13
Crubella Carubv10008739m.g Carubv10008739m	CrBBE14
Crubella Carubv10006505m.g Carubv10006505m	CrBBE15
Crubella Carubv10004576m.g Carubv10004576m	CrBBE16
Crubella Carubv10007418m.g Carubv10007418m	CrBBE17
Crubella Carubv10007797m.g Carubv10007797m	CrBBE18
Crubella Carubv10004466m.g Carubv10004466m	CrBBE19
Crubella Carubv10007331m.g Carubv10007331m	CrBBE20
Crubella Carubv10006337m.g Carubv10006337m	CrBBE21
Crubella Carubv10022971m.g Carubv10022971m	CrBBE22
Crubella Carubv10022944m.g Carubv10022944m	CrBBE23
Crubella Carubv10026133m.g Carubv10026133m	CrBBE24
Crubella Carubv10026198m.g Carubv10026198m	CrBBE25
Crubella Carubv10027532m.g Carubv10027532m	CrBBE26
Crubella Carubv10026203m.g Carubv10026203m	CrBBE27
Crubella Carubv10026190m.g Carubv10026190m	CrBBE28
Cgrandiflora Cagra.6571s0003 Cagra.6571s0003.1	CgBBE1
Cgrandiflora Cagra.1508s0130 Cagra.1508s0130.1	CgBBE2
Cgrandiflora Cagra.1508s0129 Cagra.1508s0129.1	CgBBE3
Cgrandiflora Cagra.1508s0128 Cagra.1508s0128.1	CgBBE4
Cgrandiflora Cagra.1508s0127 Cagra.1508s0127.1	CgBBE5
Cgrandiflora Cagra.1508s0126 Cagra.1508s0126.1	CgBBE6
Cgrandiflora Cagra.1508s0131 Cagra.1508s0131.1	CgBBE7
Cgrandiflora Cagra.1508s0123 Cagra.1508s0123.1	CgBBE8
Cgrandiflora Cagra.3346s0030 Cagra.3346s0030.1	CgBBE9
Cgrandiflora Cagra.3346s0031 Cagra.3346s0031.1	CgBBE10
Cgrandiflora Cagra.7100s0001 Cagra.7100s0001.1	CgBBE11
Cgrandiflora Cagra.7100s0002 Cagra.7100s0002.1	CgBBE12
Cgrandiflora Cagra.1062s0054 Cagra.1062s0054.1	CgBBE13
Cgrandiflora Cagra.1062s0058 Cagra.1062s0058.1	CgBBE14
Cgrandiflora Cagra.1062s0053 Cagra.1062s0053.1	CgBBE15
Cgrandiflora Cagra.1062s0055 Cagra.1062s0055.1	CgBBE16
Cgrandiflora Cagra.1968s0134 Cagra.1968s0134.1	CgBBE17
Cgrandiflora Cagra.0568s0086 Cagra.0568s0086.1	CgBBE18
Cgrandiflora Cagra.0629s0019 Cagra.0629s0019.1	CgBBE19
Cgrandiflora Cagra.0629s0018 Cagra.0629s0018.1	CgBBE20
Cgrandiflora Cagra.0629s0016 Cagra.0629s0016.1	CgBBE21
Cgrandiflora Cagra.0629s0021 Cagra.0629s0021.1	CgBBE22
Cgrandiflora Cagra.0629s0017 Cagra.0629s0017.1	CgBBE23
Cgrandiflora Cagra.7100s0003 Cagra.7100s0003.1	CgBBE24
>BrapaFPsc Brara.B02784 Brara.B02784.1	BrBBE1
BrapaFPsc Brara.K01808 Brara.K01808.1	BrBBE2
BrapaFPsc Brara.K01807 Brara.K01807.1	BrBBE3
BrapaFPsc Brara.K00501 Brara.K00501.1	BrBBE4
BrapaFPsc Brara.C01758 Brara.C01758.1	BrBBE5

BrapaFPsc Brara.D02108 Brara.D02108.1	<i>Br</i> BBE6
BrapaFPsc Brara.E00947 Brara.E00947.1	<i>Br</i> BBE7
BrapaFPsc Brara.E00948 Brara.E00948.1	<i>Br</i> BBE8
BrapaFPsc Brara.F03747 Brara.F03747.1	<i>Br</i> BBE9
BrapaFPsc Brara.F03748 Brara.F03748.1	<i>Br</i> BBE10
BrapaFPsc Brara.F03744 Brara.F03744.1	<i>Br</i> BBE11
BrapaFPsc Brara.F00789 Brara.F00789.1	<i>Br</i> BBE12
BrapaFPsc Brara.G00508 Brara.G00508.1	<i>Br</i> BBE13
BrapaFPsc Brara.G00588 Brara.G00588.1	<i>Br</i> BBE14
BrapaFPsc Brara.G00589 Brara.G00589.1	<i>Br</i> BBE15
BrapaFPsc Brara.G01552 Brara.G01552.1	<i>Br</i> BBE16
BrapaFPsc Brara.A01126 Brara.A01126.1	<i>Br</i> BBE17
BrapaFPsc Brara.A01123 Brara.A01123.1	<i>Br</i> BBE18
BrapaFPsc Brara.A01124 Brara.A01124.1	<i>Br</i> BBE19
BrapaFPsc Brara.A01128 Brara.A01128.1	<i>Br</i> BBE20
BrapaFPsc Brara.A01152 Brara.A01152.1	<i>Br</i> BBE21
BrapaFPsc Brara.K01265 Brara.K01265.1	<i>Br</i> BBE22
BrapaFPsc Brara.I02784 Brara.I02784.1	<i>Br</i> BBE23
BrapaFPsc Brara.I01845 Brara.I01845.1	<i>Br</i> BBE24
BrapaFPsc Brara.I03113 Brara.I03113.1	<i>Br</i> BBE25
BrapaFPsc Brara.I03114 Brara.I03114.1	<i>Br</i> BBE26
BrapaFPsc Brara.I02786 Brara.I02786.1	<i>Br</i> BBE27
BrapaFPsc Brara.I01846 Brara.I01846.1	<i>Br</i> BBE28
BrapaFPsc Brara.I02785 Brara.I02785.1	<i>Br</i> BBE29
BrapaFPsc Brara.I01844 Brara.I01844.1	<i>Br</i> BBE30
BrapaFPsc Brara.I05161 Brara.I05161.1	<i>Br</i> BBE31
BrapaFPsc Brara.I01843 Brara.I01843.1	<i>Br</i> BBE32
BrapaFPsc Brara.I02779 Brara.I02779.1	<i>Br</i> BBE33
BrapaFPsc Brara.I02783 Brara.I02783.1	<i>Br</i> BBE34
BrapaFPsc Brara.I03596 Brara.I03596.1	<i>Br</i> BBE35
BrapaFPsc Brara.H01046 Brara.H01046.1	<i>Br</i> BBE36
Bstricta Bostr.12659s0359 Bostr.12659s0359.1	<i>Bs</i> BBE1
Bstricta Bostr.12659s0358 Bostr.12659s0358.1	<i>Bs</i> BBE2
Bstricta Bostr.12659s0356 Bostr.12659s0356.1	<i>Bs</i> BBE3
Bstricta Bostr.12659s0355 Bostr.12659s0355.1	<i>Bs</i> BBE4
Bstricta Bostr.3148s0020 Bostr.3148s0020.1	<i>Bs</i> BBE5
Bstricta Bostr.3148s0015 Bostr.3148s0015.1	<i>Bs</i> BBE6
Bstricta Bostr.3148s0017 Bostr.3148s0017.1	<i>Bs</i> BBE7
Bstricta Bostr.3148s0013 Bostr.3148s0013.1	<i>Bs</i> BBE8
Bstricta Bostr.3148s0018 Bostr.3148s0018.1	<i>Bs</i> BBE9
Bstricta Bostr.3148s0016 Bostr.3148s0016.1	<i>Bs</i> BBE10
Bstricta Bostr.3148s0014 Bostr.3148s0014.1	<i>Bs</i> BBE11
Bstricta Bostr.15697s0380 Bostr.15697s0380.1	<i>Bs</i> BBE12
Bstricta Bostr.15697s0370 Bostr.15697s0370.1	<i>Bs</i> BBE13
Bstricta Bostr.15697s0371 Bostr.15697s0371.1	<i>Bs</i> BBE14
Bstricta Bostr.15697s0372 Bostr.15697s0372.1	<i>Bs</i> BBE15

Bstricta Bostr.15697s0373 Bostr.15697s0373.1	<i>Bs</i> BBE16
Bstricta Bostr.15697s0376 Bostr.15697s0376.1	<i>Bs</i> BBE17
Bstricta Bostr.15697s0377 Bostr.15697s0377.1	<i>Bs</i> BBE18
Bstricta Bostr.13671s0285 Bostr.13671s0285.1	<i>Bs</i> BBE19
Bstricta Bostr.10689s0032 Bostr.10689s0032.1	<i>Bs</i> BBE20
Bstricta Bostr.10689s0037 Bostr.10689s0037.1	<i>Bs</i> BBE21
Bstricta Bostr.5325s0118 Bostr.5325s0118.1	<i>Bs</i> BBE22
Bstricta Bostr.23794s0623 Bostr.23794s0623.1	<i>Bs</i> BBE23



S1 Fig. Phylogenetic tree with bootstrap values. The bootstrap values for the phylogenetic tree of BBE-like enzymes from the following species are depicted: *Arabidopsis lyrata* (Al), *Arabidopsis thaliana* (At), *Boechera stricta* (Bs), *Brassica rapa* (Br), *Capsella grandiflora* (Cg), *Capsella rubella* (Cr), and *Eutrema salsugineum* (Es).

CHAPTER 4

The family of berberine bridge enzyme-like enzymes: A treasure-trove of oxidative reactions

Author contributions

The following chapter is a comprehensive review about the berberine bridge enzyme (BBE)-like family. Structural characteristics of the BBE-like protein family are shown and the occurrence and development of BBE-like enzymes in fungi, plants, bacteria and archaea are depicted. Moreover, a detailed summary of the most important reactions catalyzed by BBE-like enzymes is listed. I contributed to this project by performing comprehensive multiple sequence alignments to find BBE-like homologs within the plant kingdom and additionally, I investigated the distribution of active site types of these BBE-like enzymes. Moreover, I helped to prepare figures and I assisted to write the part “BBE-like proteins in plants” of the manuscript.

Chapter 4

4. The family of berberine bridge enzyme-like enzymes: A treasure-trove of oxidative reactions

Bastian Daniel, Barbara Konrad, Marina Toplak, Majd Lahham, Julia Messenlehner, Andreas Winkler and Peter Macheroux*

Institute of Biochemistry, Graz University of Technology, Petersgasse 12/2, 8010 Graz,
Austria

To whom correspondence should be addressed: Peter Macheroux, Graz University of Technology, Institute of Biochemistry, Petersgasse 12/II, A-8010 Graz, Austria, Tel.: +43-316-873 6450, Fax: +43-316-873 6952; Email: peter.macheroux@tugraz.at

This chapter was published in Archives of Biochemistry and Biophysics:

Daniel, B. *et al.* (2017) The family of berberine bridge enzyme-like enzymes: A treasure-trove of oxidative reactions. *Arch Biochem Biophys* 632, 88-103.

4.1. Abstract

Biological oxidations form the basis of life on earth by utilizing organic compounds as electron donors to drive the generation of metabolic energy carriers, such as ATP. Oxidative reactions are also important for the biosynthesis of complex compounds, *i.e.* natural products such as alkaloids that provide vital benefits for organisms in all kingdoms of life. The vitamin B₂-derived cofactors flavin mononucleotide (FMN) and flavin adenine dinucleotide (FAD) enable an astonishingly diverse array of oxidative reactions that is based on the versatility of the redox-active isoalloxazine ring. The family of FAD-linked oxidases can be divided into subgroups depending on specific sequence features in an otherwise very similar structural context. The sub-family of berberine bridge enzyme (BBE)-like enzymes has recently attracted a lot of attention due to the challenging chemistry catalyzed by its members and the unique and unusual bi-covalent attachment of the FAD cofactor. This family is the focus of the present review highlighting recent advancements into the structural and functional aspects of members from bacteria, fungi and plants. In view of the unprecedented reaction catalyzed by the family's namesake, BBE from the California poppy, recent studies have provided further insights into nature's treasure chest of oxidative reactions.

4.2. Introduction

BBE-like enzymes form a subgroup of the superfamily of FAD-linked oxidases (SCOPe d.58.32) that is structurally characterized by a typical fold observed initially for vanillyl-alcohol oxidase (VAO) [1]. Therefore, the structural architecture has been described initially as the VAO-fold [2] and all members of this superfamily share a common architecture that can be divided into a FAD-binding domain and a substrate binding domain, which is also referred to as the cap domain [1]. A comprehensive review on the first identified members of this family was published by Leferink *et al.* [3]. In recent years, however, the rapidly growing number of member proteins has revealed a relatively low sequence conservation and an astonishing diversity of catalyzed chemical reactions. To account for these observations the superfamily of FAD-linked oxidases can be divided into subfamilies that better reflect structural, functional and evolutionary aspects of individual group members. The family of BBE-like enzymes forms a relatively large subgroup featuring a characteristic C-terminal structural element following the substrate binding region (see below). Considering the differences in chemical reactivities observed for the relatively few enzymes that are characterized in detail, additional sub-classifications are helpful and will be introduced in this review.

The namesake of this family is the (*S*)-reticuline oxidase or berberine bridge enzyme from California poppy (*Eschscholzia californica*) that catalyzes the conversion of (*S*)-reticuline to (*S*)-scoulerine by mediating an oxidative ring closure reaction. The C-C bond that is formed in this reaction is referred to as the berberine bridge and marks a branch point in the biosynthesis of benzyloisoquinoline alkaloids [4] (Figure 1).

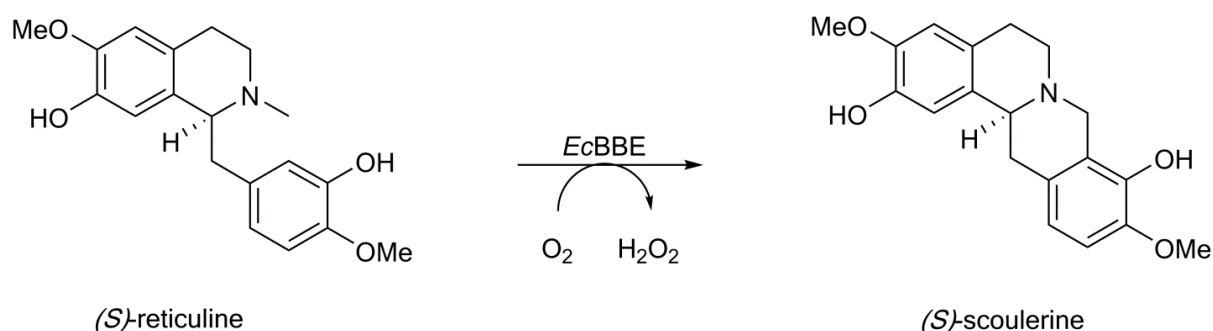


Figure 1: Reaction catalyzed by the berberine bridge enzyme. *EcBBE* catalyzes the oxidative ring closure reaction from (*S*)-reticuline to (*S*)-scoulerine.

Together with glucooligosaccharide oxidase (GOOX) from *Acremonium strictum* [5] [6], the characterization of BBE [7] [8] [9] revealed one interesting hallmark of the family of BBE-like proteins: a bi-covalently attached FAD cofactor. The characteristic 6-*S*-cysteinyl-, 8 α -*N*1-histidyl-FAD linkage is only found in the BBE-subfamily of the FAD-linked oxidases and has been shown to increase the redox potential of the cofactor by more than 300 mV compared to free flavin [10]. How exactly this is linked to the individual reactions catalyzed is still not very well understood, especially since some family members appear to have lost the cysteinyl linkage. Additional highlights of BBE-like family members are the recently identified flavin N5-oxides observed in EncM [11] and challenging carbon-carbon bond formation reactions involving complex biomolecules in natural product biosynthesis [12] [13]. In comparison to the rapidly growing number of group members identified in various sequencing projects, the functional characterization of individual proteins is severely lagging behind also due to the challenge of identifying the true *in vivo* substrates, as exemplified in reference [14]. Considering the stunning reactions catalyzed by members the BBE-like enzyme family that have been analyzed in detail so far, it will be interesting to witness which new surprising functional details of yet uncharacterized family members will be discovered in the future.

4.3. Structural characteristics of BBE-like proteins

4.3.1. Differentiation from other families of FAD-linked oxidases

As mentioned in the introduction, BBE-like enzymes are a sub-family of the large superfamily of FAD-linked oxidases (SCOPE d.58.32). Characteristic structural features of this family are a FAD binding module that is formed by the *N*- and *C*-terminal parts of the protein, and a substrate binding module that, together with the isoalloxazine ring of FAD, provides the environment for efficient substrate binding and oxidation (Figure 2). While the overall fold of BBE-like proteins is similar to that of other prototypic members of this superfamily, a specific structural feature in the vicinity of the FAD-binding site distinguishes the BBE family from other FAD-linked oxidases such as vanillyl alcohol oxidase (VAO)-like enzymes (SCOPE d.58.32.1), the D-lactate dehydrogenase family (SCOPE d.58.32.2), cholesterol oxidase-like enzymes (SCOPE d.58.32.3), cytokinin dehydrogenases (SCOPE d.58.32.4) and alditol oxidase-like enzymes (SCOPE d.58.32.6).

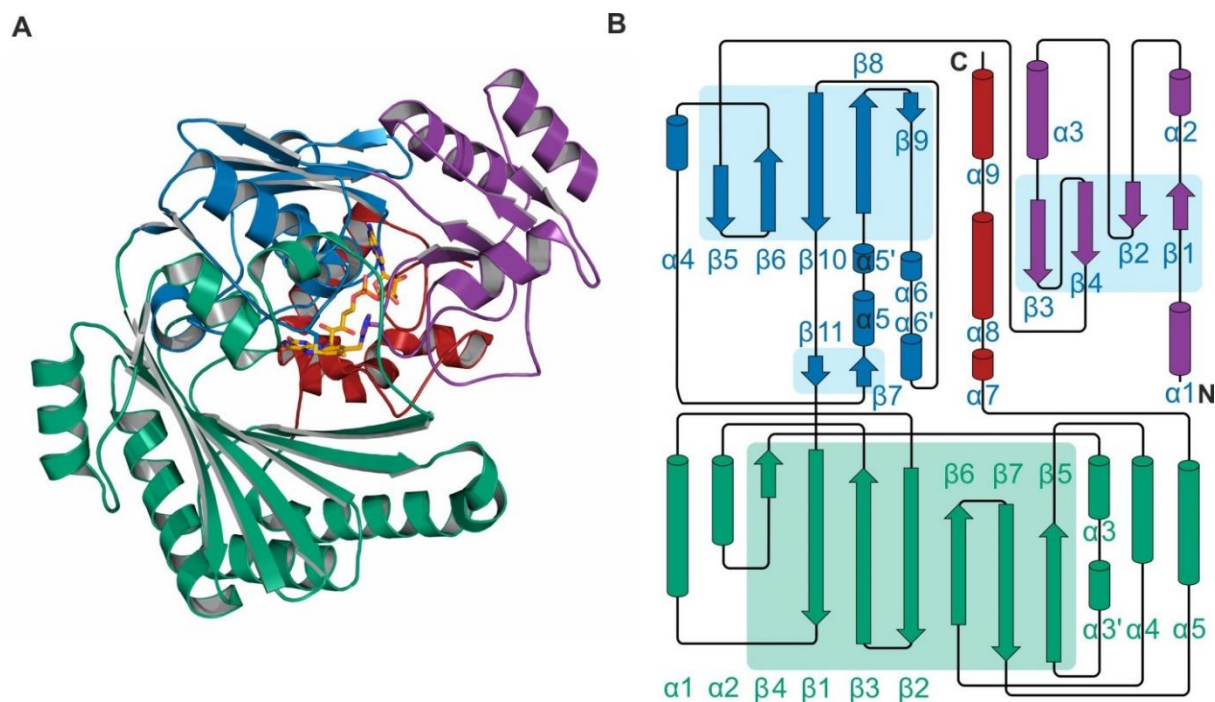


Figure 2: Overview of structural properties of the BBE-like family. A: The overall structure of a representative member (*EcBBE*; pdb 3d2j) is shown in cartoon representation. Individual sub-domains of the upper flavin-binding module are colored in purple, blue and red. The FAD cofactor (shown as orange stick model) is bound in an extended conformation with the ribityl chain and the adenyl moiety sandwiched between all three subdomains. The isoalloxazine ring projects towards the active site that is formed by residues from the substrate binding module (green) and the initial part of the BBE-like specific C-terminus (red, cf. Figure 3). B: Topology plot of the structure shown in panel A. Secondary structure elements are numbered consecutively for α -helices and β -strands in the flavin- and substrate-binding modules and are labeled in green and blue, respectively.

The N-terminal part of the hidden Markov model (HMM) specific for the BBE and BBE-like enzymes (pfam entry: PF08031, [15]) highlights a characteristic Y/FxN motif (Figure 3A). This element contains a highly conserved aromatic residue (Tyr or Phe), which in case of a Tyr interacts with the N1-C2=O locus of the isoalloxazine ring and a strictly conserved Asn residue that hydrogen bonds with the before mentioned Tyr side chain. This arrangement sterically influences the positioning of the ribityl side chain of the cofactor as well as a structural element (residues 169-179 – *EcBBE* numbering) involved in forming part of the oxygen binding pocket on the *re* side of the isoalloxazine ring (Figure 3C) [16]. Additionally, Asn458 is important for the positioning of His174 that stabilizes the negative charge N1-C2=O locus of the reduced flavin and has been shown to be involved in the formation of the C6-cysteinyll linkage [20].

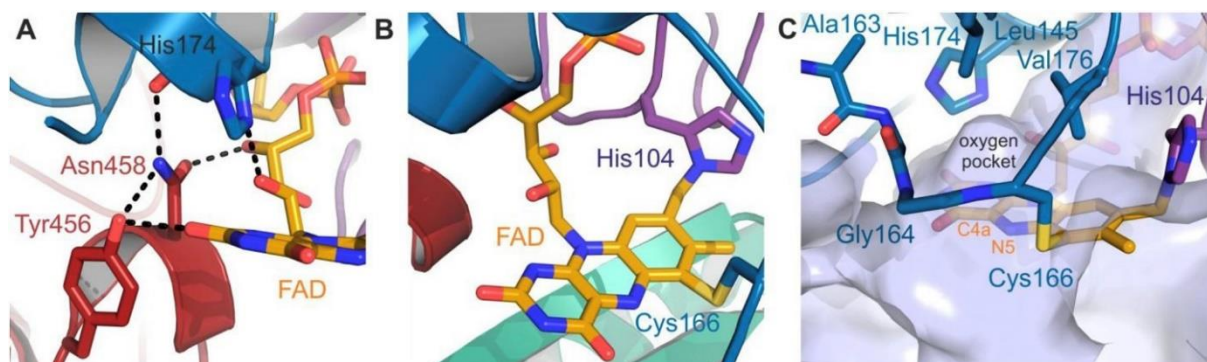


Figure 3: Close-up of the flavin binding site. A: The conserved Y/FxN motif of BBE-like enzymes establishes a defined hydrogen bonding network near the N1-C2=O locus of the isoalloxazine ring. His174, Tyr456, Asn458 and FAD are shown as stick models. B: The bi-covalent 6-*S*-cysteinyl-8 α -N1-histidyl-FAD attachment of the cofactor via residues His104 and Cys166 is shown. The stick models of His174, Tyr456 and Asn458 from panel A are omitted for clarity and the view is modified. Coloration of individual regions corresponds to Figure 2. Numbering reflects residues of *EcBBE* and the structural details correspond to pdb 3d2j. C: Environment of the characteristic oxygen binding pocket in BBE-like enzymes. The active site cavity and the oxygen binding pocket around the flavin cofactor are contoured as transparent surface structures in light blue. Residues surrounding the oxygen binding pocket on the *re*-side of the flavin are shown as stick models (pdb 3d2j).

The remaining conserved features of the HMM logo of the BBE-like protein pfam entry correspond to structurally relevant residues of the C-terminal FAD-binding region and are therefore also present in other groups of the superfamily. However, an additional important structural element that is directly coupled to the Y/FxN motif features another highly conserved element of the BBE-like protein family. In fact, the region closing the active site cavity at its rear part features a conserved salt bridge between Asp192 and Arg409. The structural integrity of this region with its glycine-rich elements (*EcBBE* residues 170-188) is important for accurately positioning both the FAD cofactor (via Tyr456) and the Cys residue involved in the covalent attachment of the cofactor (*EcBBE* Cys166, see below). The characteristic loop region between β 6 and β 7 of the substrate binding module (*EcBBE* residues 390-410) is structurally different to other families in the superfamily and apparently plays an important structural role in establishing the C-terminal connection between the substrate binding region and the FAD-binding module. Interestingly, this region has also been shown to play a role for access to the oxygen binding pocket and tuning of the reactivity of the substrate-reduced FAD cofactor towards molecular oxygen [17]. Additional structural and functional insights into the oxygen reactivity of BBE-like proteins are summarized below.

4.3.2. *Bi-covalent attachment of the flavin cofactor via His and Cys residues*

The linkage of FAD to the protein is maybe the most significant peculiarity of the BBE-like protein family since it features an unusual bi-covalent attachment of FAD that has not been seen in any other family of flavoproteins (Figure 3B).). The formation of this bi-covalent attachment and other covalent modifications of the flavin cofactor has recently been reviewed by Heuts *et al.* [21]. The characteristic dual 6-*S*-cysteinyl-, 8 α -*N1*-histidyl-FAD linkage was observed for the first time in the crystal structure of GOOX [5] [6] and initially characterized biochemically in detail for BBE [7] [8] [9]. Since then it has been observed in many other proteins and can be safely predicted based on two characteristic motifs, *i.e.* the fingerprint motifs R/KxxGH and CxxV/L/IG for covalent attachment of residues His and Cys to the 8 α and 6-position of the isoalloxazine ring, respectively. While most of the members of the BBE-like protein family contain a bi-covalently attached FAD cofactor, there are also members with solved crystal structures that feature only a single 8 α -*N1*-histidyl attachment and at least for one of those it has been proposed that the second covalent linkage can be created by introduction of the Cys residue along with additional substitutions [11] [18] [19] [20]. Mutagenesis studies have shown that both types of covalent attachment can be formed independently, however, so far no naturally occurring single 6-*S*-cysteinyl-FAD linkage within this family of flavoproteins has been described in detail [3] [6] [8] [21]. Based on more extensive sequence alignments, several members of the BBE-like protein family were identified that are missing the residues required for the 6-*S*-cysteinyl-linkage and, in the case of the BBE homolog found in *Chlorella variabilis*, even the 8 α -*N1*-histidyl-FAD attachment appears to be missing. This of course raises the question of the functional and/or structural importance of this unusual type of cofactor attachment. Since bi-covalent attachment is not a prerequisite for proper folding, the divergence of enzymatic reactions and the evolutionary adaptation of BBE-like proteins might be responsible for the absence of a bi-covalent linkage in some family members; nevertheless, there appears to be a general positive effect of this type of attachment as it was observed that the rate of substrate oxidation is generally affected by the redox potential of the attached flavin cofactor, *i.e.* removal of a covalent linkage decreased the redox potential and the rate of flavin reduction in the pertinent protein variants. Equally important appears to be the role of bicovalent flavin attachment for the correct positioning of the substrate in proximity to the isoalloxazine ring [6] [9] [22]. In addition to the functional relevance of boosting the oxidative power by a substantial increase of the redox potential, there is also the structural importance of bi-covalent cofactor attachment for maintaining active site architecture and preventing cofactor dissociation for enzymes accepting bulky substrates [6] [8] [9] [16] [19] [21]. As shown in the detailed

descriptions below, members of the BBE-like family generally accept large substrates and have therefore evolved wide open active sites. In order to facilitate precise orientation of the flavin cofactor in such an open active site environment, the bi-covalent attachment provides a mechanism for appropriately positioning the cofactor relative to bulky substrates [9] [11] [23] [24]. Importantly, comparing different structures of BBE-like proteins it becomes obvious that access to the active site and properties of the active site cavity are modulated extensively by a mobile loop region connecting $\beta 4$ and $\beta 5$ of the β -sheet of the substrate-binding module (Figure 2B). Together with the variation of β -sheet residues projecting into the active site, this structural element enables the evolutionary adaption of family members to a variety of catalytic functions.

4.3.3. The reactivity of BBE-like enzymes with oxygen

Independent of the nature and size of the organic molecules accepted by various BBE-like members, the oxidation of the corresponding substrates results in reduction of the flavin cofactor. In order to regenerate the cofactor for the next round of enzymatic turnover it needs to be reoxidized. Classical oxidases allow a rapid reoxidation of the reduced FAD by molecular oxygen accompanied by the formation and release of hydrogen peroxide. The bimolecular reaction rate constants for the regeneration of the oxidized flavin cofactor in oxidases range from 1×10^4 to $1 \times 10^6 \text{ M}^{-1} \text{ s}^{-1}$. Therefore, the protein environment substantially accelerates the rate of cofactor reoxidation relative to free flavin in solution ($\sim 2.5 \times 10^2 \text{ M}^{-1} \text{ s}^{-1}$) [25] [26]. Subtle changes around the flavin C4a-N5 region, which is involved in the initial one electron reduction of molecular oxygen to form a caged radical pair of the flavin semiquinone and a superoxide anion, can result in pronounced changes in the reactivity towards oxygen. Flavoprotein dehydrogenases typically exhibit bimolecular reaction rate constants for the oxidation of the reduced flavin by oxygen below $1 \times 10^4 \text{ M}^{-1} \text{ s}^{-1}$. It should be pointed out, however, that even the same protein can be converted from its dehydrogenase form to an oxidase by subtle conformational changes, as, for example, induced by thiol oxidation in xanthine dehydrogenase [27] [28].

As far as molecular determinants of oxygen reactivity within the family of BBE-like proteins are concerned, a specific oxygen binding pocket was identified on the *re* side of the flavin cofactor opposite the substrate binding region. This feature is shared by all members of the FAD-linked oxidase superfamily (SCOPE d.58.32) and was initially suggested by chloride binding to this region in VAO [1]. This has later been confirmed by biochemical studies of the closely related L-galactono- γ -lactone dehydrogenase as well as by computational and experimental analysis of alditol oxidase, which is more closely related to BBE-like enzymes than to the members of the VAO family [17] [29]. Even though the position of the oxygen

binding pocket appears to be conserved also in BBE-like enzymes, the bi-covalent attachment of the flavin cofactor and the properties of the Y/FxN element slightly alter the architecture of this region and thereby cause other elements to function as gatekeeper residues for oxygen access and reactivity (Figure 3C). The most comprehensive analysis of how to convert an oxidase of the BBE-like enzyme family to a dehydrogenase and *vice versa* was performed by Zafred *et al.* with *EcBBE* and the plant allergen Phl p 4 [16]. Substitution of a gatekeeper residue (Ile) in the dehydrogenase Phl p 4 with Val results in an increase of oxygen reactivity by almost 5 orders of magnitude whereas the inverse exchange of Val by Ile in *EcBBE* leads to a drop in O₂ reactivity by a factor of 500. Neighboring residues such as the partially conserved His174 in *EcBBE* also influence the rate of cofactor reoxidation and correlate to some extent with the dehydrogenase vs oxidase annotation. While oxidases preferentially have a His at this position, dehydrogenases feature either Asn (Phl p 4) or Gln (*AtBBE*-like 28 with intermediate oxygen reactivity) residues or even hydrophobic side chains (GilR) at this position to further modulate the general dehydrogenase feature of a bulky Leu or Ile gatekeeper residue at the position corresponding to Val176 of *EcBBE* [16] [19] [30] [31]. Therefore, formation of a specific oxygen binding pocket enables flavoproteins to tune the reactivity toward oxygen and to channel the reducing equivalents generated during enzymatic conversion into either the formation of reactive oxygen species or reduction of electron carriers such as for example NAD(P)⁺ or coenzyme Q₀.

4.3.4. Protein-substrate interactions in BBE-like proteins

Since the catalytic turnover of a reduction-oxidation process comprises two half reactions, *i.e.* a reductive and an oxidative, it is important to define on which side of the isoalloxazine system, *i.e.* the *re*- or *si*-side the half reactions occur. In the case of BBE-like enzymes the most prominent interactions of the protein matrix and the isoalloxazine ring are established on the *re*-side and thus activation of oxygen in the course of the oxidative half reaction is orchestrated by these amino acids. On the other hand, the amino acids on the *si*-side of the isoalloxazine ring are involved in substrate binding and thus enable substrate oxidation and concomitant reduction of the isoalloxazine ring. This interaction includes the activation of a putative substrate by base-catalyzed proton abstraction and the stabilization of the transition state. In recent studies, we have shown that by variation of these residues very different active site types can be created in the same overall topology [19] [32]. For example, in the plant family of Brassicaceae, we have recently identified four different frequently occurring active site types that were confirmed by X-ray crystallography [19] [33] [34]. In Figure 4, a representative for the active site type I, II, III and IV is shown. The residues are colored according to the subdomain they belong to.

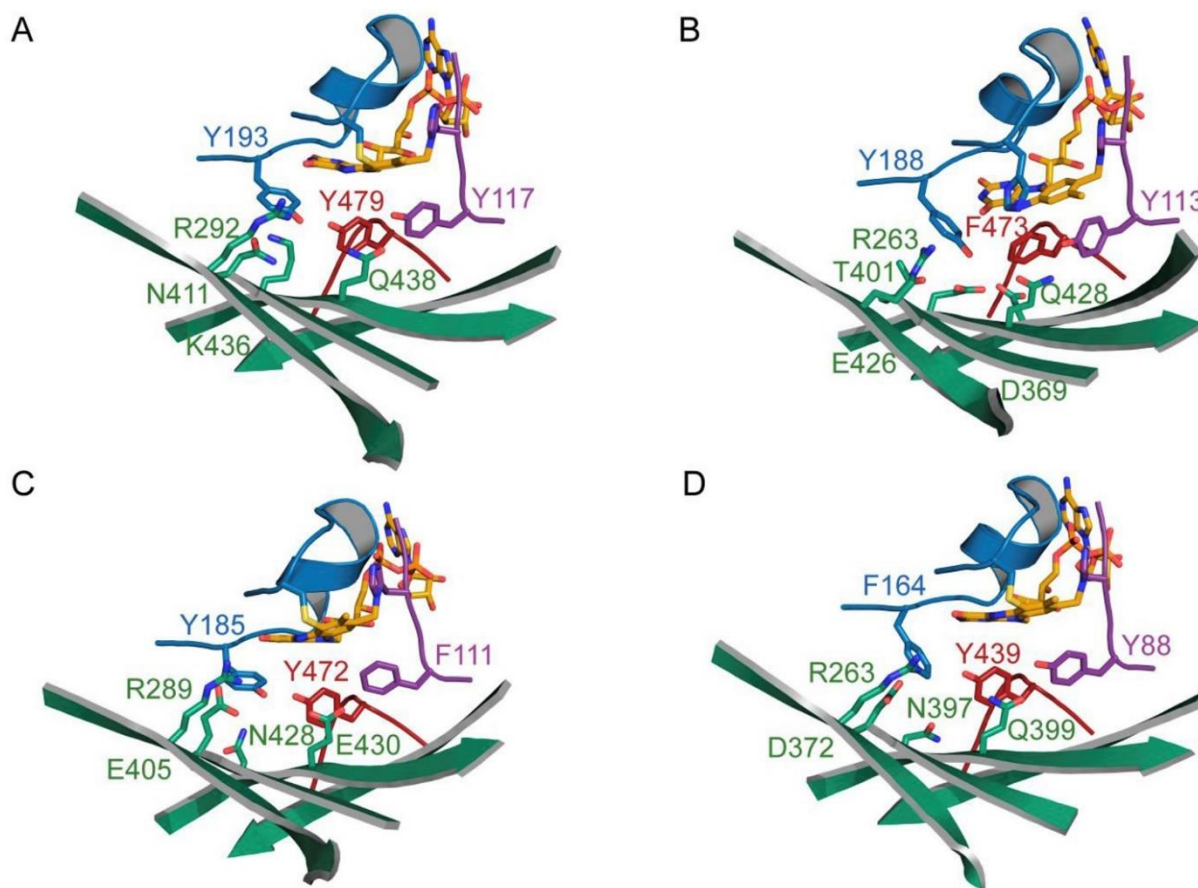


Figure 4: Frequently occurring active site types: A: Type I from *At*BBE-like protein 15 (pdb code 4UD8), B: Type II from *At*BBE-like protein 28 (pdb code 5D79), C: Type III from a homology model of *At*BBE-like 22 (Q9SUC6) based on *At*BBE-like protein 15 (4UD8) D: Type IV from Phl p 4 (pdb code 4PWC).

Active site type I has been described for monoglignol dehydrogenases from *Arabidopsis thaliana* [32] [33]. It is predominantly found in BBE-like enzymes from higher plants, for example 13 out of 27 BBE-like enzymes from *Arabidopsis thaliana*. Other well characterized enzymes harboring the active site type I are carbohydrate oxidases from sunflower and lettuce as well as *At*BBE-like 3 (FOX1) that were reported to oxidize “gluco-oligomers” and 4-hydroxy indole-3-carbonyl nitrile, respectively [14] [35]. Thus, all of these enzymes act on primary or secondary hydroxyl groups with an active site base initiating the reaction by proton abstraction. In the case of *At*BBE-like enzyme 15, Tyr193 was identified as the catalytic base, which is activated by a close contact to Tyr479 and a π -cation-interaction with Lys436. Subsequently, the activated alcoholate substrate transfers a hydride to the N5 position of the flavin. The transition state is proposed to be stabilized by Gln438, which is in close contact to Tyr117 [33].

The active site type II was first described for *At*BBE-like 28 and is associated with mono- or bi-covalent flavin linkage [19]. The nature and position of the residues that stabilize the

transition state is unchanged (compare Figure 4, panel A, amino acids Y117 and N438 to panel B, amino acids Y113 and Q428) with the position of the aromatic amino acids Tyr117, Tyr193 and Tyr479 corresponding to Tyr113, Tyr188 and Phe473 in the active site type I. However, Tyr479 and Lys436 in the active site type I (e.g. *At*BBE-like protein 15) are replaced by Phe473 and Glu426 (e.g. *At*BBE-like 28) enabling a completely new set of interactions, e.g. Glu426 forms a hydrogen bond to the hydroxyl group of Tyr188. The mechanism deduced from this arrangement involves deprotonation of Tyr188 by Glu426 and thus a similar role of Tyr188 as an active site base can be envisaged.

Active site type III is a mixture of type I and II. Similar to active site type I, it features two Tyr residues in the center of the active site but is missing the Lys residue that engages in a π -cation-interaction with one of the Tyr residues. Instead, active site type III possesses a Glu residue (Glu405) that extends into the active site. This active site type is rare and apparently confined to Brassicaceae. The enzymatic activity of BBE-like enzymes with this particular composition is currently unknown.

Active site type IV has been first described for GOOX from *Acremonium strictum* [5]. It was found in BBE-like proteins from fungi and, predominantly, in lower plants (Figure 5). Important examples of this active site type are fungal BBE-like enzymes such as XylO, ChitO and LaO as well as the pollen allergens Phl p 4 and BG60 [34] [36] [37] [38] [39]. Characteristic for this active site type is the deprotonation of Tyr439 by Asp372, which is mediated by a water molecule [5]. The phenolate species of Tyr439 was postulated to act as catalytic base to initiate the hydride transfer by proton abstraction at the anomeric center of the carbohydrate substrate. Similarly, Tyr88 and Gln399 are conserved and play a similar role in the stabilization of the transition state as suggested for the respective residues in active site type I.

4.3.5. Occurrence and development of the BBE-like protein family

Currently, the BBE-like protein family (Pfam 08031) encompasses 6382 sequences found in fungi (3712 sequences in 233 species), plants (1372 sequences in 60 species), bacteria (1156 sequences in 520 species) and archaea (20 sequences in 11 species). A phylogenetic tree of the proteins covered in this article is displayed in Figure 5.

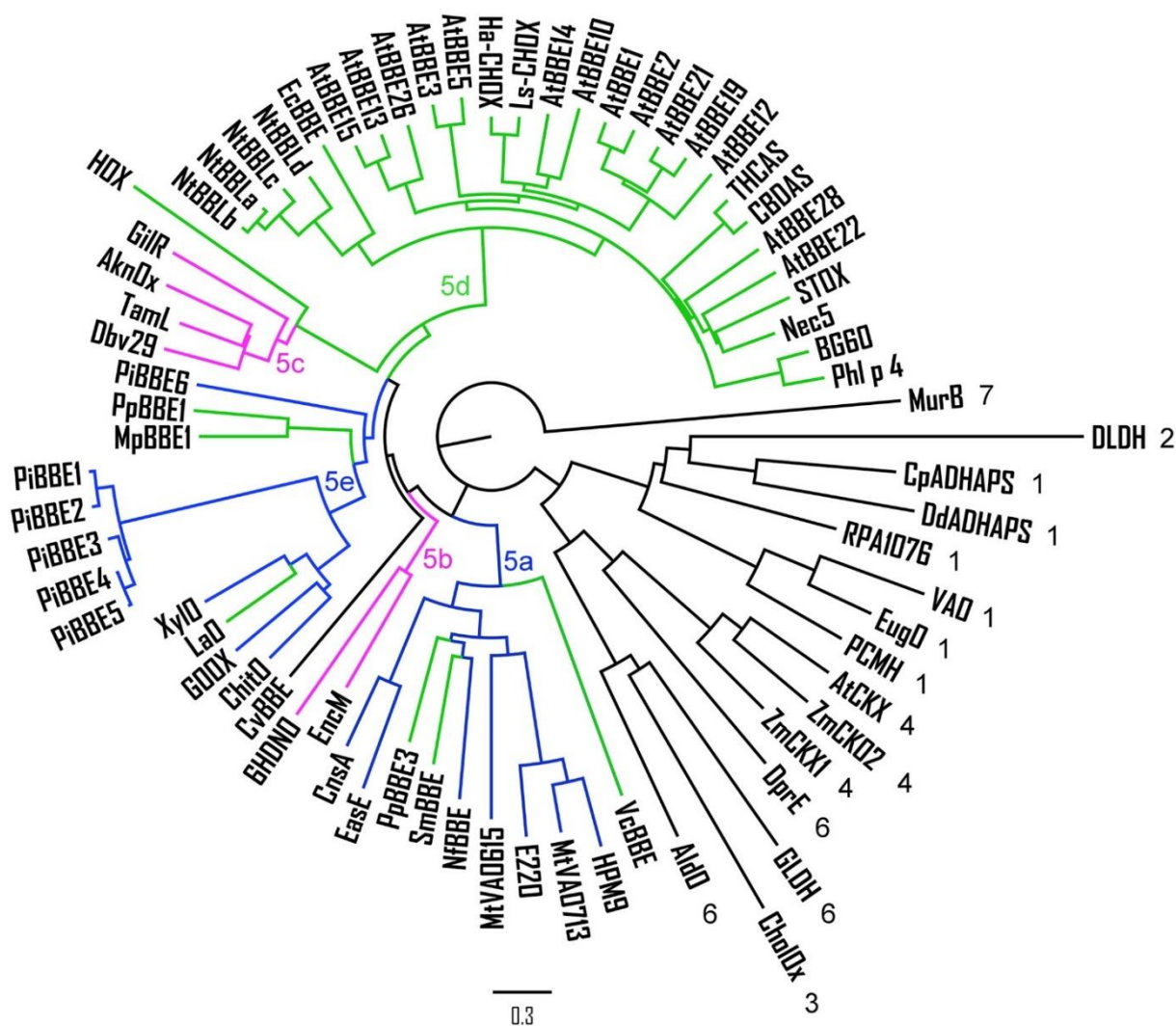


Figure 5: Phylogenetic tree of the superfamily of FAD-like oxidases (SCOPE d.58.32). The numbering of the subfamilies is according to the SCOPE database and indicated at the branch tips except for BBE-like proteins (subfamily 5). The latter are colored according to their origin; BBE-like proteins from fungi, plants and bacteria are depicted in blue, green and violet, respectively. Subfamily 5 has been subdivided into clades 5a-d. The tree was created employing the sequences compiled in Supplemental Table S1 as previously described [19] and visualized using Figtree [40]. A bootstrap analysis was performed and the respective tree is shown in Supplemental Figure S1.

4.3.6. BBE-like proteins in bacteria

The PFAM entry of the BBE-like protein family currently harbors 1156 sequences of BBE-like proteins from bacteria, in average two per species. They do not appear in all species but only in selected strains. The majority of known BBE-like proteins in bacteria can be assigned to the phyla Actinobacteria, Proteobacteria and Firmicutes with 715, 170 and 102 sequences, respectively. A genus that is exceptionally rich in BBE-like proteins is *Streptomyces* with in average of four BBE-like proteins per species. Well known BBE-like proteins from *Streptomyces* are GilR, TamL, Dbv29 and AknOx [23] [31] [41] [42]. All of them are involved in the biosynthesis of antibiotics as described below and their genes are located in the respective gene clusters responsible for the whole biosynthesis of the pertinent antibiotic.

4.3.7. BBE-like proteins in fungi

In fungi, BBE-like proteins are restricted to the subkingdom of the “higher fungi”, Basidiomycota and Ascomycota, which have arisen approx. 600 million years ago [43]. Despite their average occurrence of 16 BBE-homologs per species the vast majority of these proteins are still uncharacterized and possess unknown functions. According to our analysis, BBE-like proteins from fungi can be found in clades 5a and 5e (Figure 5).

4.3.8. BBE-like proteins in plants

In plants, BBE-like proteins represent, like in fungi, a multigene family. Here, we present an analysis of the evolution of the BBE-like protein family in land plants. In Figure 6, a phylogenetic tree of plants, the occurrence of BBE-like proteins and the distribution of the previously categorized active site types is depicted (see Supplementary Table S2).

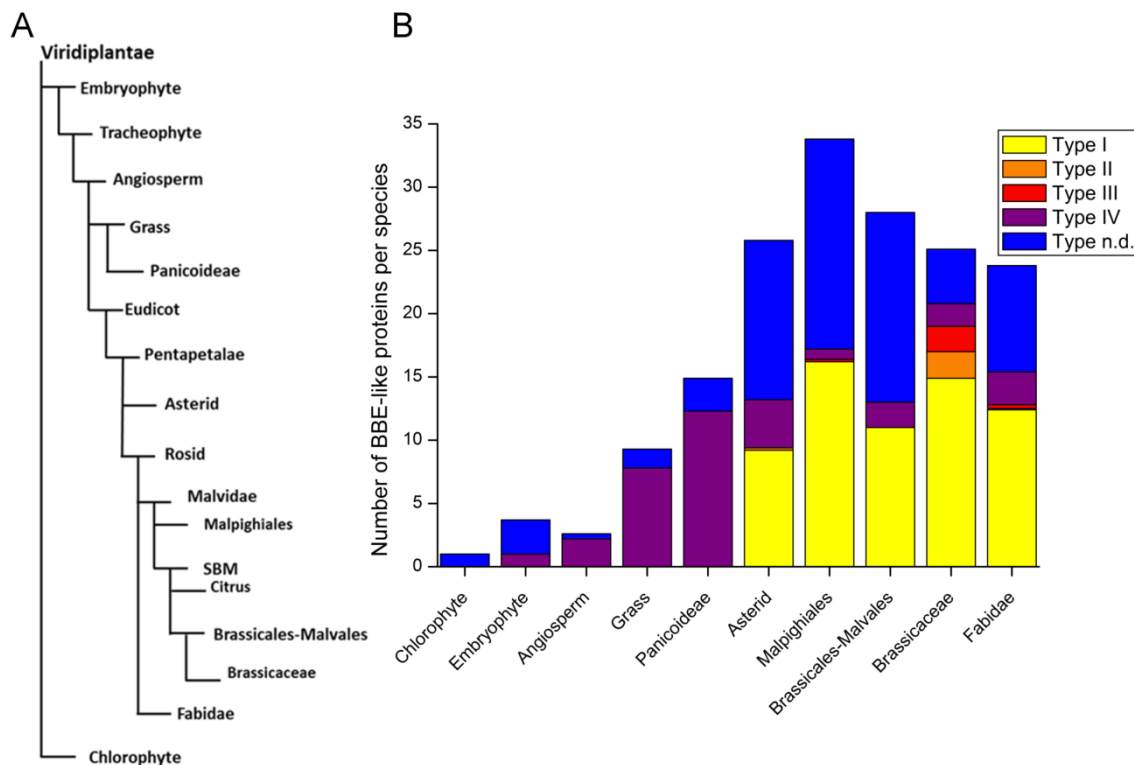


Figure 6: A: Phylogenetic tree of plants (note that the length of the lines does not reflect evolutionary distances) B: Graphical representation of the number of BBE-like proteins per species and the distribution of active site types using the following color code: yellow, type I; orange, type II; red, type III and violet, type IV. In lower plants, active site type IV is predominant, for example Panicoideae have on average twelve BBE-like proteins per species with this active site type. The first appearance of the active site type I occurs in Asterids. In the course of evolution, the abundance of active site type IV is reduced to less than four BBE-like enzymes per species while the abundance of the active site type I increased to up to sixteen on average per species in Malpighiales.

The most basal division in the kingdom of Viridiplantae are the Chlorophytes. These comprise mono-cellular and multicellular organisms including most of the green algae [44]. Not all Chlorophytes harbor genes encoding BBE-like enzymes and the number of genes per species does not exceed two. In Embryophytes, which are formally known as “land plants”, the number of BBE-like proteins has increased to four in *Marchantia polymorpha*, three in *Sphagnum fallax* and two in the moss *Physcomitrella patens*. This is the most basal species currently known to have a BBE-like protein with an active site type IV. During the evolution of monocotyledons, the number of genes encoding BBE-like enzymes has increased from three in angiosperms to eight and fifteen in grasses and Panicoideae, respectively. Predominantly, they contain BBE-like enzymes with the active site type IV. The first appearance of BBE-like enzymes with an active site type I is in eudicots, where the lowest developed species harboring the active site type I is *Aquilegia coerulea* (Colorado blue columbine). In eudicots, active site type I was replaced by the active site type IV as the most prominent active site type. The average

occurrence of BBE-like enzymes in Asterids, Malpighiales, Brassicales-Malvales, Brassicaceae and Fabidae is 26, 34, 28, 25 and 24, respectively. Approximately half of them harbor the active site type I with type IV being present in one quarter of the BBE-homologs. Interestingly, the occurrence of the active site type II and III appears to be restricted to Brassicaceae. While enzymes harboring this active site types have been found in seven Brassicaceae species previously analyzed, they are absent in all other plants [19]. It is noteworthy that in higher plants various BBE-like proteins with yet undefined (n.d.) active site types are present. These are typically not completely new active site types but variations predominantly of type I.

4.4. Reactions catalyzed by BBE-like enzymes

BBE-like enzymes catalyze diverse chemical reactions. In the following section these reactions will be discussed grouped according to their origin (plants, bacteria and fungi) and their appearance in the phylogenetic tree (clades 5a-e in Figure 5).

4.4.1. Reactions catalyzed by BBE-like enzymes from plants: alkaloid and cannabinoid biosynthesis

The majority of BBE-like enzymes from plants are found in clade 5d (Figure 5), with the two BBE-like enzymes from basal plants (*PpBBE1* and *MpBBE*) clustering with fungal carbohydrate oxidases (Figure 5). In the plant kingdom, BBE-like enzymes catalyze a broad variety of reactions. Very prominent is the oxidation of alcohols typically catalyzed by enzymes employing an active site type I or IV. From this pool of alcohol oxidases different BBE-like enzymes have been adapted to catalyze more complex reactions like oxidative ring closure reactions as exemplified by *EcBBE*, Δ^1 -tetrahydrocannabinolic acid (THCA) synthase and cannabidiolic-acid (CBDA) synthase [13] [45] [46]. Figure 7 summarizes the currently known reactions catalyzed by BBE-like enzymes in alkaloid and cannabinoid biosynthesis.

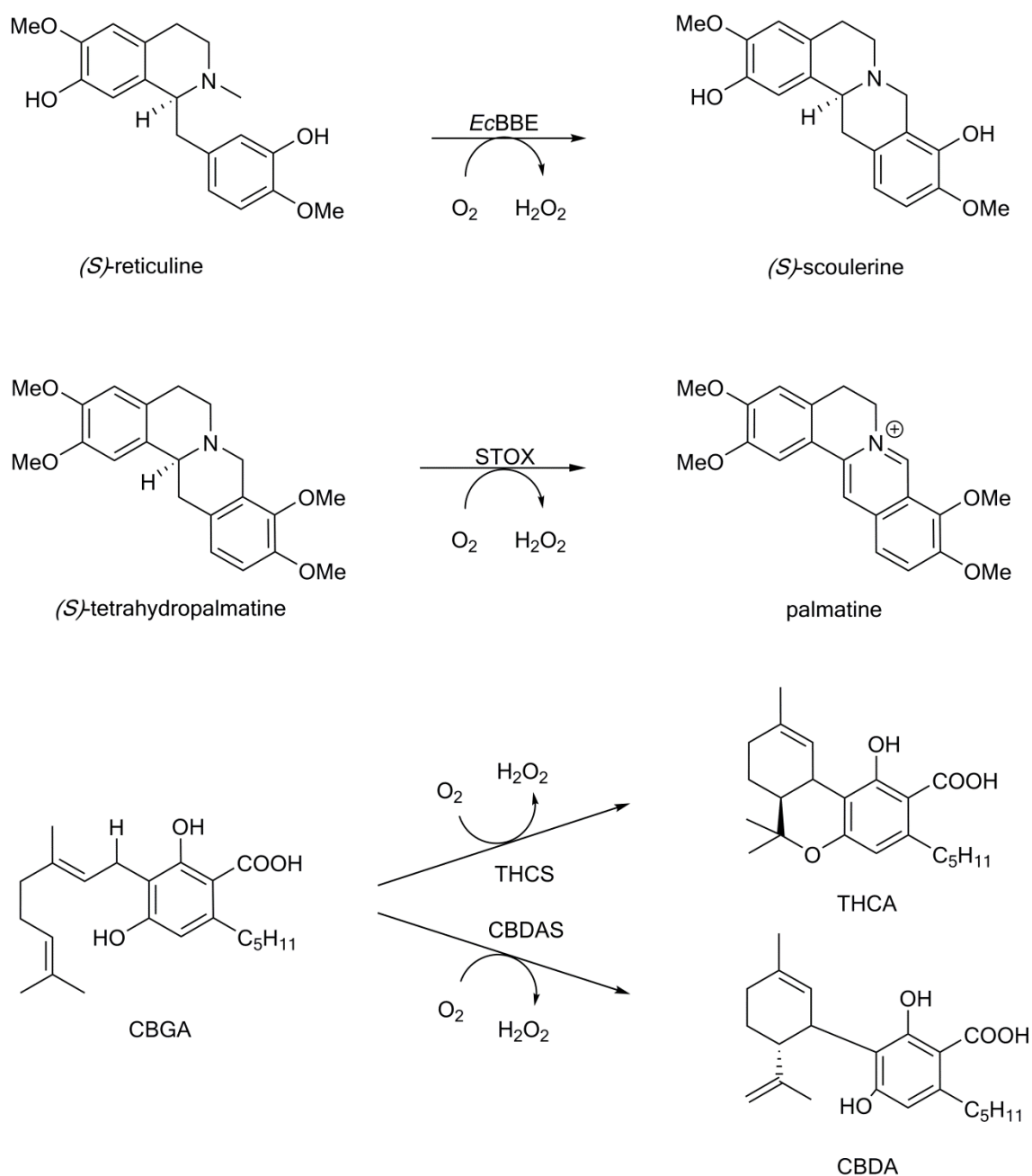


Figure 7: Reactions catalyzed by BBE-like enzymes in alkaloid and cannabinoid biosynthesis from plants. *EcBBE* catalyzes the oxidative ring closure reaction from (*S*)-reticuline to (*S*)-scoulerine [47]. *STOX* catalyzes the oxidation of (*S*)-tetrahydropalmatine to palmatine [48]. Cannabigerolic-acid (CBGA) is converted by tetrahydrocannabinolic-acid (THCA) synthase to THCA and by cannabidiolic-acid (CBDA) synthase to CBDA [46] [49].

BBE is a branch point enzyme in the benzylisoquinoline alkaloid biosynthesis [4]. The enzyme was first isolated in 1975 from *Macleaya microcarpa* cell cultures [50]. Subsequently, BBE activity was found in 66 differentiated plant and cell cultures mainly from *Papaveraceae* and *Fumariaceae* species [47]. Kutchan *et al.* expressed the gene heterologously in insect cells and demonstrated that the FAD cofactor is covalently attached to the produced protein via

a histidine residue at the 8 α -position of the isoalloxazine ring [45] [51]. Larger quantities of the enzyme became available from expression in the methylotrophic yeast *Komagataella phaffii* (previously known as *Pichia pastoris*) by Winkler *et al.* enabling the identification of an additional cysteine residue that covalently binds to the flavin cofactor at the C6 position [7] [8] [9] [12]. In addition, Winkler *et al.* solved the crystal structure and conducted site directed mutagenesis studies to probe the catalytic mechanism of the enzyme [12]. The mutagenesis program was later extended by Wallner *et al.* and Zafred *et al.* to provide a better understanding of key features of the enzyme, such as the stabilization of a negative charge at the N(1)C(2)=O locus that occurs in the course of the reaction and the reactivity of the reduced enzyme towards oxygen [16] [30]. BBE catalyzes the oxidative conversion of (*S*)-reticuline to (*S*)-scoulerine, which is subsequently converted to protoberberine, protobine or benzophenanthridine alkaloids [52]. A concerted mechanism for this enzyme was proposed following the initiation of the reaction by deprotonation of the C3' hydroxyl group of (*S*)-reticuline. The subsequent nucleophilic attack of the C2' atom at the *N*-methyl group of the substrate forms the so called berberine bridge and leads to the (concerted) transfer of a hydride from the *N*-methyl group to the N5-position of the isoalloxazine ring [12]. Later studies, based on the measurement of kinetic isotope effects, have challenged the concerted mechanism and suggested that a previously proposed stepwise mechanism [45] might be more likely [53]. According to this mechanism, the reaction is initiated by hydride transfer from the *N*-methyl group to the flavin to form an iminium intermediate, which is then nucleophilically attacked by the C2' carbon to close the berberine bridge, however, this study could not provide any evidence for the intermediate species required by this mechanism. Similar to BBE, (*S*)-tetrahydroprotoberberine oxidase (STOX) from *Argemone mexicana* and *Berberis wilsoniae* is involved in benzyloquinoline alkaloid biosynthesis [48] [54] [55]. STOX was reported to oxidize tetrahydroprotoberberine to palmatine. Additionally, (*S*)-scoulerine and (*S*)-canadine were accepted as substrates by STOX from *B. wilsoniae*, whereas STOX from *A. mexicana* also oxidizes (*S*)-coreximine [56]. Interestingly, *EcBBE* also features STOX like activity albeit with much lower efficiency [57]. STOX and *EcBBE* share to some extent the same activity and are employed in the same biosynthetic pathway. Still according to our phylogenetic analysis STOX is more closely related to carbohydrate oxidases such as Nec5 or Phl p 4 than to *EcBBE*. Two other BBE-like enzymes employed in the biosynthetic pathway leading to cannabinoids were found in *Cannabis sativa*. Tetrahydrocannabinolic acid (THCA) synthase and cannabidiolic acid (CBDA) synthase convert cannabigerolic acid (CBGA) into THCA and CBDA, respectively [13] [58] [59]. Both enzymes catalyze the stereospecific oxidative cyclization of

the geranyl group of CBGA. For both enzymes the same initial hydride transfer was postulated, followed by the cyclization that is initiated by the deprotonation of a hydroxyl group to form THCA whereas CBGA synthase abstracts a proton from the terminal methyl group of CBGA [49] [53]. Another plant that employs BBE-like enzymes for alkaloid biosynthesis is tobacco (*Nicotiana tabacum*), which features four BBE-like enzymes closely related to *EcBBE* (Figure 5, BBLa-d). They were assigned a role in the final reaction steps of the biosynthesis of pyridine alkaloids and thus affect the levels of nicotine and anabasine [60]. The formal reactions and a hypothetical reaction mechanism for these enzymes are shown in Figure 8.

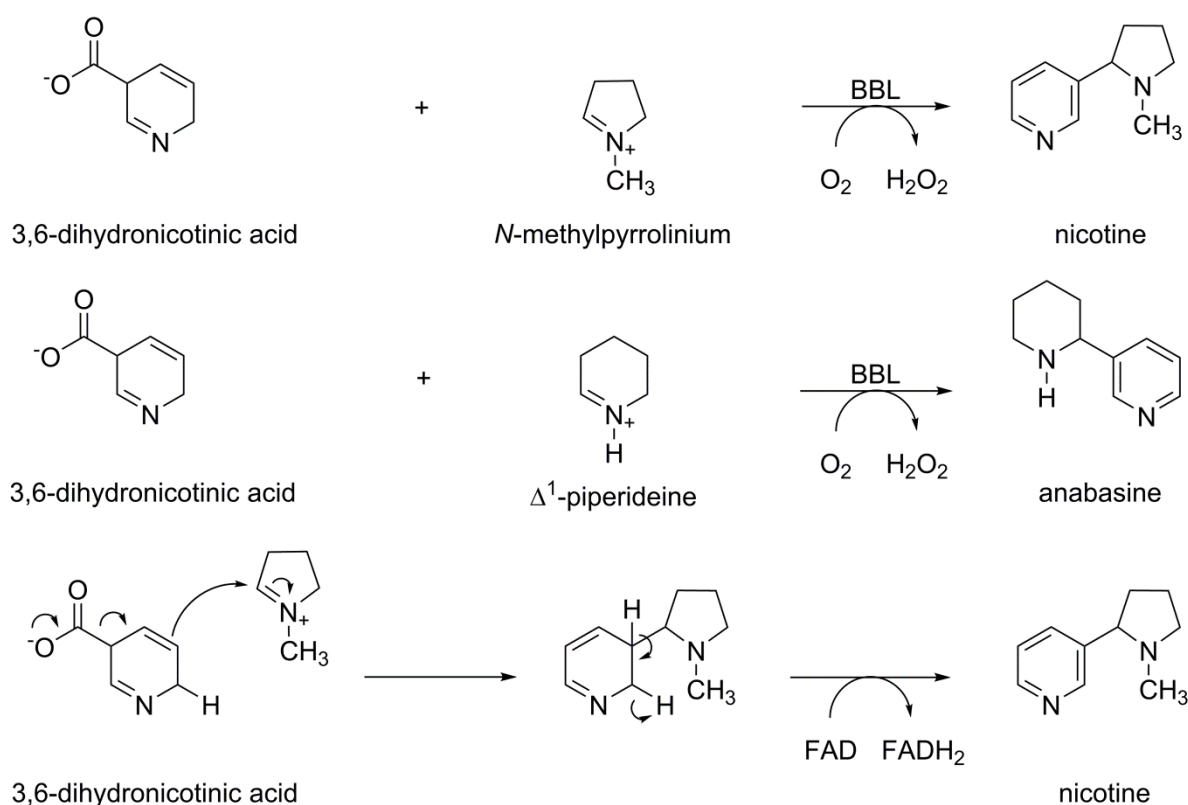


Figure 8: Reactions catalyzed by BBE-like enzymes involved in nicotine and anabasine biosynthesis (top and middle). A hypothetical reaction mechanism for this type of intermolecular C-C bond formation is shown at the bottom for the final biosynthetic step to nicotine. BBLa-d apparently catalyze the decarboxylation to 3,6-dihydronicotinic acid and the subsequent intermolecular C-C-bond to form a non-aromatic intermediate that re-aromatizes via a hydride transfer to the flavin and the concomitant formation of the corresponding alkaloid.

Briefly, they catalyze the C-C bond formation between 3,6-dihydronicotinic acid and *N*-methylpyrrolinium or Δ^1 -piperidine to yield either nicotine or anabasine [61]. In contrast to BBE, which catalyzes an intramolecular C-C bond formation, these BBE-homologs carry out an intermolecular coupling of the two building blocks. These hypothetical reactions receive support from the finding that field grown tobacco plants possess reduced levels of pyridine alkaloids when the expression of BBLa-d is suppressed by RNA interference [61].

4.4.2. Reactions catalyzed by BBE-like enzymes from plants: alcohol oxidation

As the genes of the BBE-like enzymes form a multigene family in all land plants with the majority of them not carrying out alkaloid biosynthesis, it appears that BBE-like enzymes must play a more general role in plant physiology that would explain their ubiquitous presence in plants. In evolutionary terms, enzymes catalyzing reactions in secondary metabolism, *e.g.* alkaloid and terpene biosynthesis, have evolved by duplication of genes encoding enzymes operating in primary metabolism with subsequent neofunctionalization [62]. Thus the question of the general function(s) of the BBE-like enzymes in plant physiology is connected to the search of reactions in primary metabolism that are potentially catalyzed by members of this family. In this contexts, the oxidation of various alcohol groups, as summarized in Figure 9, provides a first lead toward an understanding of the evolutionary origin of the BBE-like enzyme family as some of the reactions (*e.g.* oxidation of mono- and polysaccharides) appear to be present in most, if not all, plants.

A frequently observed reactivity of BBE-like enzymes from plants is the oxidation of carbohydrates at the anomeric center to the corresponding lactone. A representative of these enzymes is hexose oxidase (HOX) from the red algae *Chondrus crispus* that belongs to the division of Rhodophyta [63]. It is more closely related to various bacterial BBE-like enzymes than to members present in plants (compare Figure 5). Initially, a stoichiometric copper ion but no spectroscopic evidence for a FAD cofactor was reported and thus it was postulated that HOX is a copper-dependent enzyme. However, more recently, a bicovalently attached FAD cofactor was confirmed for this enzyme as catalytic active species [64] [65] [66]. HOX has a broad substrate specificity accepting glucose and galactose and a variety of oligomeric sugars derived from these building blocks. Another carbohydrate oxidizing BBE-like enzyme is nectarin V (Nec5) from ornamental tobacco, which converts glucose to gluconolactone [67]. Nec5 was postulated to be part of the pathogen defense system of plants by protecting reproductive organelles [68]. Interestingly, nectarine IV (Nec4) becomes part of the defense strategy by forming an inhibitory protein complex with xylan-specific endoglucanase (XEG), which is released by the pathogen to digest the xyloglucan present in the nectar. This Nec4:XEG-

complex induces the enzymatic activity of Nec5 and thus glucose is oxidized to gluconolactone, followed by rapid hydrolysis to gluconic acid [68]. Additionally, hydrogen peroxide is generated by the reaction of the reduced FAD cofactor with molecular oxygen. Both products, *i.e.* gluconic acid and hydrogen peroxide, are effective antimicrobial agents [69] [70].

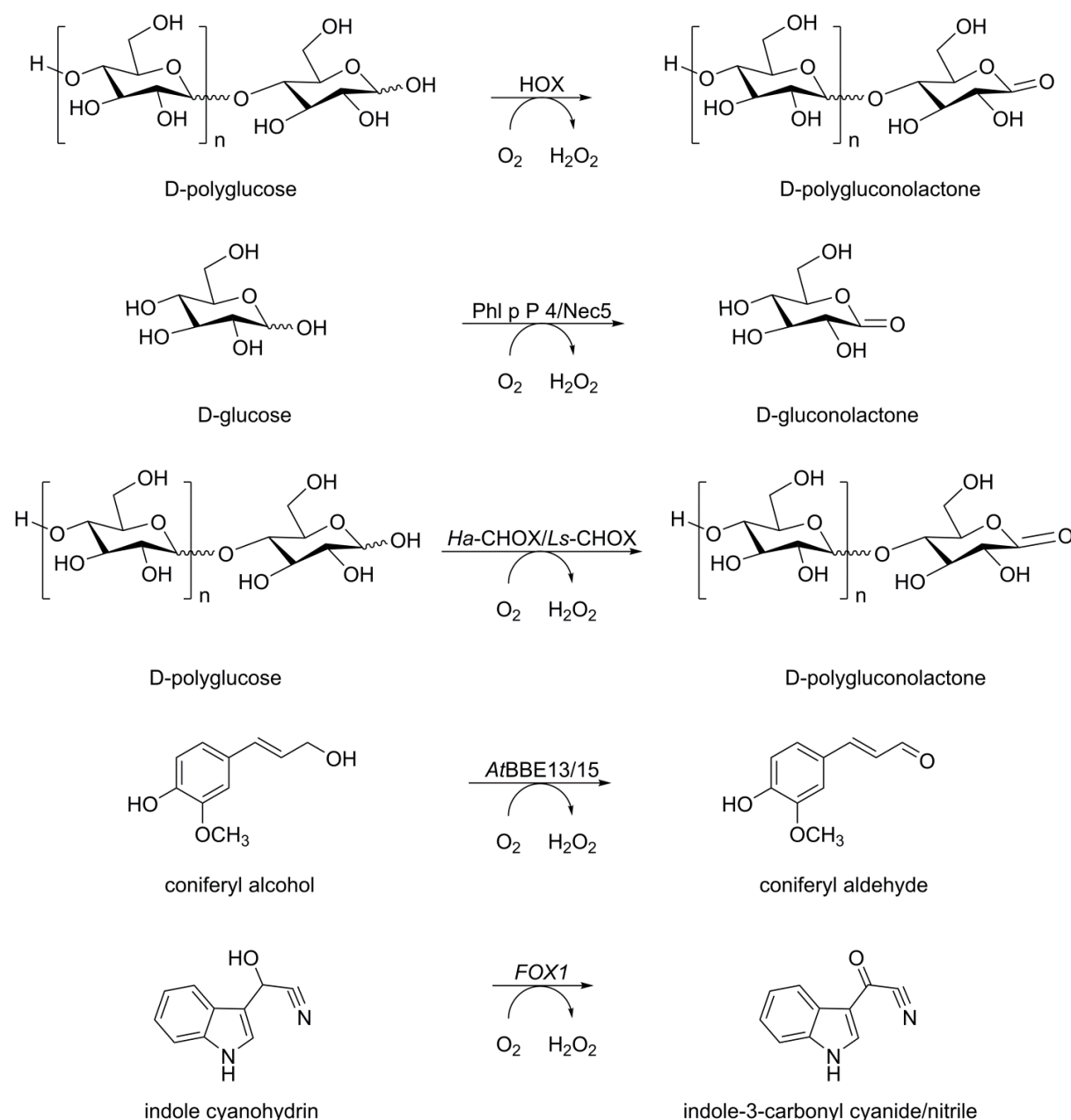


Figure 9: Reactions catalyzed by BBE-like enzymes from plants. HOX oxidizes various carbohydrates and oligomers of glucose to the corresponding lactone [63]. Phl p P 4 and Nec5 oxidize glucose [34] [67]. *Ha*-CHOX and *Ls*-CHOX oxidize carbohydrates and oligomers of glucose to the corresponding lactones [35]. The monolignol oxidoreductases AtBBE-like enzyme 13 and 15 oxidize the monolignols *p*-coumaryl, coniferyl and sinapyl alcohol to the corresponding aldehydes [32]. FOX1 (*At*BBE-like enzyme 3) oxidizes indole cyanohydrin to indole-3-carbonyl cyanide/nitrile.

Similar to Nec5 the pollen allergen Phl p 4 from timothy grass is a BBE-like enzyme that oxidizes glucose and plays a role in plant reproduction [34]. Phl p 4 was identified to be a glucose dehydrogenase and subsequently similar pollen allergens like BG60 from the BBE-like enzyme family were identified [39] [71]. Interestingly, BG60 was isolated in two isoforms that can be distinguished by the presence or absence of a small *N*-terminal domain. According to their spectral properties both isoforms are isolated in the semiquinone state, stabilizing either the neutral or the anionic semiquinone [39].

Two carbohydrate oxidases from the BBE-like enzyme family were identified to play a role in the plant immune response [35]. Custers *et al.* isolated two enzymes, *i.e.* *Ha*-CHOX and *Ls*-CHOX from sunflower (*Helianthus annuus*) and lettuce (*Lactuca sativa*), respectively. Both enzymes were found to be highly upregulated after the treatment of the plants with elicitors or during infection. In other closely related BBE-like enzymes from *A. thaliana* such as *At*BBE-like 10 and 20, a similar expression pattern was observed (see Figure 5) [32]. *Ha*-CHOX was expressed in *E. coli* to further characterize the catalytic properties of the enzyme. It oxidizes glucose to gluconolactone and the subsequent reoxidation of the reduced FAD cofactor produces hydrogen peroxide. In addition, it oxidizes the reducing end of glucose oligomers. In the case of a pathogen attack, oligosaccharides are released due to the degradation of the plant cell wall by the pathogen. These oligosaccharides act as potential elicitors to the plant immune system. The spatial and temporal expression pattern of *Ha*-CHOX near the lesion depends on the nature of the pathogen indicating that this enzyme has a very distinct role in the plant immune response [35]. While hydrogen peroxide has antimicrobial properties the role of the oxidation of oligosaccharides in the plant immune response still requires further investigations. More recently, another BBE-like enzyme involved in the plant immune response was discovered by Rajniak and coworkers [14]. They identified a biosynthetic pathway that leads from tryptophan to 4-hydroxyindole-3-carbonyl nitrile (4-OH-ICN) with one of the steps, *i.e.* the oxidation of indole cyanohydrin to indol-3-carbonyl nitrile, being catalyzed by *At*BBE-like enzyme 3 (also referred to as flavin dependent oxidase 1, FOX1, Figure 9). The gene encoding for *At*BBE-like protein 3 is located in a gene cluster with *At*BBE-like enzymes 4, 5, 6 and 7, and the enzymes share a similar expression pattern indicating a similar role in plant metabolism [14] [72]. They are strongly upregulated under osmotic stress and after the exposure to pathogens [32]. However, no significant change in the levels of ICN metabolites for *At*BBE-like 4, 5, 6 and 7 knock down lines was observed suggesting that they might play a role in the biosynthesis of alternative plant products or the creation of multiple knock out lines might be necessary to observe an effect due to a redundant activity of *At*BBE-like 3, 4, 5, 6 and 7 [14].

Recently, we have discovered yet another oxidation reaction carried out by BBE-like enzymes that suggests an involvement in lignification [32]. *At*BBE-like protein 13 and 15 were identified as monolignol oxidoreductases catalyzing the oxidation of sinapyl-, coniferyl- and *p*-coumaryl alcohol to their corresponding aldehydes. These so-called monolignols as well as their corresponding aldehydes are utilized as building blocks for lignin biosynthesis and thus it is conceivable that *At*BBE13 and 15 (and other monolignol oxidoreductases) shift the extracellular pool of building blocks toward the aldehydes and thus may directly affect the composition of lignin in the plant cell wall.

The natural electron acceptor of the monolignol oxidoreductases is not known yet. For cytokinin dehydrogenases, members of the FAD-linked oxidase superfamily subfamily 4 (SCOPE d.58.32:4), benzoxazinones were identified as electron acceptors that subsequently shuttle the electrons to laccases and peroxidases [73]. As peroxidases and laccases are responsible for the conversion of monolignols to their radical state prior to polymerization via free radical combination a similar mechanism is conceivable for monolignol oxidoreductases [74].

In the case of *At*BBE15, replacement of the gate keeper residue controlling access to the oxygen pocket, *i.e.* leucine to valine significantly accelerated the rate of reaction of the reduced FAD cofactor with molecular oxygen (Figure 3) [33]. This variant was shown to be a useful biocatalyst for the oxidation of a broad spectrum of allylic and benzylic alcohols to the corresponding aldehydes [33].

4.4.3. Reactions of BBE-like proteins from bacteria

Not only plants and fungi possess genes encoding BBE-like proteins but also certain bacteria possess enzymes of that family [23] [31] [41]. According to our analysis, they appear in the clades 5b and 5c (see Figure 5). Studies of gene clusters related to the biosynthesis of antibiotics revealed that in many of these pathways BBE-like enzymes are employed mostly in one of the last steps of these processes [23] [41]. By oxidizing alcohol or aldehyde groups or by desaturating the carbon skeleton these enzymes contribute to the potency of the antibiotics in terms of their defensive function [23] [41].

So far, six bacterial BBE-like enzymes from various species of *Streptomyces* (GilR, TamL and AknOx), *Nonomuraea* (EncM and Dbv29) and *Arthrobacter* (6HDNO) have been studied in detail [11] [18] [23] [24] [31] [41] [42] [75] [76]. The reactions catalyzed by BBE-like enzymes from clade 5c and 5b (see Figure 5) are summarized in Figure 10 and 11, respectively.

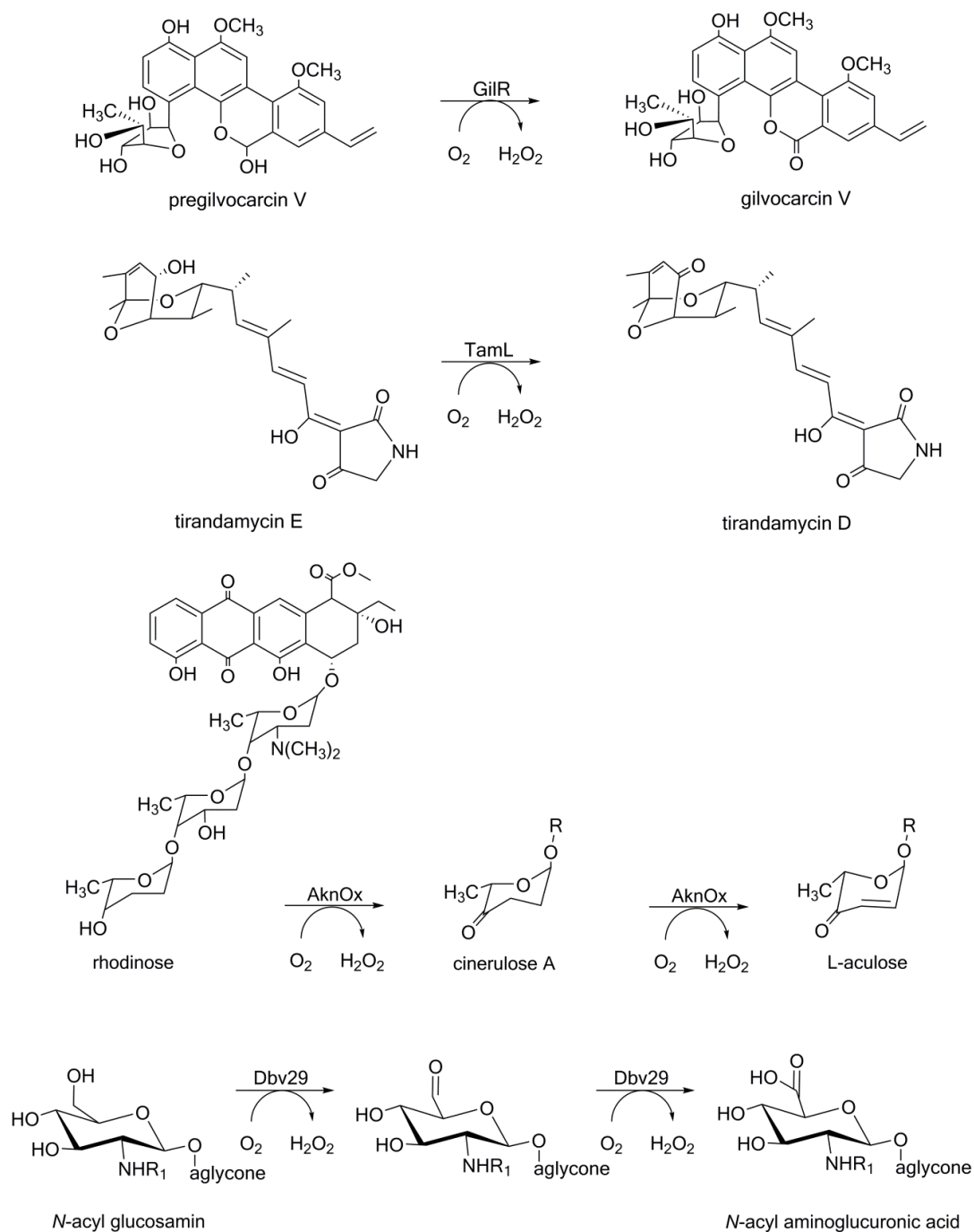


Figure 10: Reactions catalyzed by BBE-like enzymes from clade 5c. GilR catalyzes the conversion of pregilvocarcin V to gilvocarcin V. TamL converts tirandamycin E to tirandamycin D. AknOx catalyzes the four electron oxidation from rhodinoses to cinerulose A to L-aulose. Dbv29 catalyzes a four electron oxidation that are the two last steps in the biosynthesis of A40926 (teicoplanin homolog) [24] [75]. The enzyme converts a *N*-acyl glucosamine to a *N*-acyl aminoglucuronic acid.

Similar to carbohydrate oxidases found in fungi, GilR catalyzes the oxidation of a hemiacetal to its corresponding lactone (Figure 10). This reaction found in gilvocarcin V biosynthesis is of great importance as the resulting lactone moiety carries structural features that are crucial for the stability of the resulting antibiotic. By introducing the lactone function

the naphthyl and benzene ring get “fixed” in the same plane and opening of the pyran ring is inhibited, which increases the stability and hence the potency of the synthesized metabolite [41] [31].

TamL from *Streptomyces* was also shown to be involved in antibiotic metabolism (tirandamycin biosynthesis), where it catalyzes the conversion of tirandamycin E to tirandamycin D. In this two-electron transfer reaction the C10 hydroxyl group is converted to a keto function (Figure 10), which can then be recognized by TamI, a cytochrome P450 monooxygenase that is required in the final step of tirandamycin biosynthesis. Like GilR, TamL is also part of antibiotic metabolism and enhances the potency of the pathway products, which was found to be determined by the number of oxidative modifications [23]. In contrast to the reactions catalyzed by GilR and TamL, the conversion catalyzed by AknOx requires two subsequent oxidation steps. Since four electrons are extracted from the substrate(s) during the reactions, recycling of the flavin cofactor by molecular oxygen in between the two reaction steps is required. Whereas Dbv29 catalyzes the last two steps in A40926 (a teicoplanin homolog) biosynthesis, *i.e.* the conversion of *N*-acyl glucosamine to *N*-acyl aminoglucuronic acid (Figure 10), and thereby oxidizes the same functional group twice, AknOx is involved in the oxidation of two different carbon atoms [41] [31]. In the first reaction, the alcohol group in the C4 position of the rhodnose found in aclacinomycin N is oxidized to a keto function yielding the pathway intermediate aclacinomycin A. The resulting cinerulose A ring system (Figure 10) is then further oxidized by introducing a double bond between C2 and C3 of the ring system to give the final product aclacinomycin Y (Figure 10). The fact that two different loci of the substrate are subject to oxidation by AknOx also rationalizes the finding that two sets of catalytic residues are present in the active site of the enzyme, which is a unique and unprecedented architecture in the BBE-like enzyme family [42].

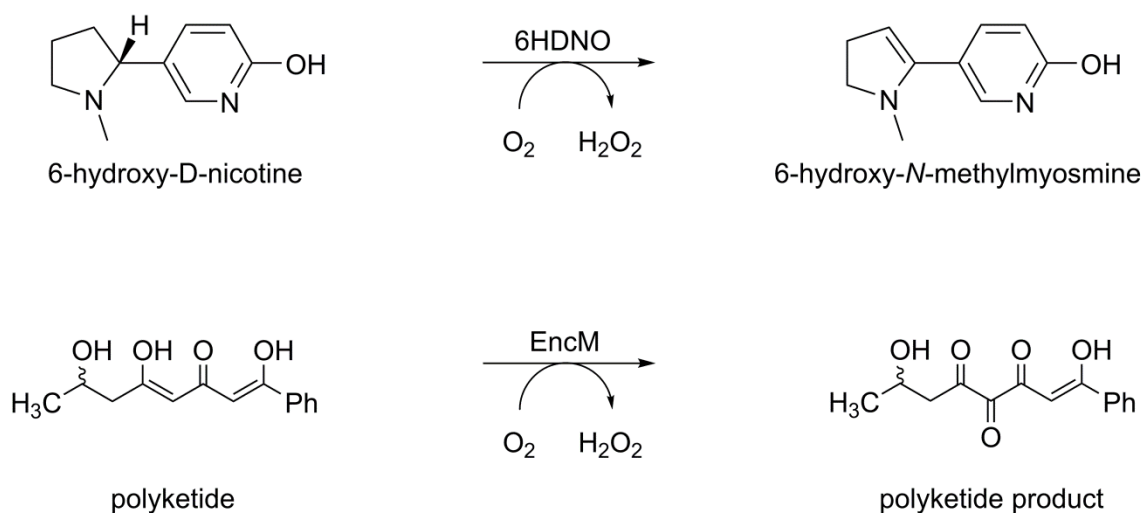


Figure 11: Reactions that are catalyzed by BBE-like enzymes belonging to clade 5b (Figure 5). 6HDNO oxidizes the C2 and C3 position of the pyrrolidine ring of 6-hydroxy-D-nicotine, the reaction product hydrolysis spontaneously [18]. EncM is involved in the generation of enterocin. The enzyme catalyzes a Favorskii-type rearrangement as shown in more mechanistic detail in Figure 12 [11].

While the bacterial BBE-like enzymes from clade 5c (Figure 5) bind the flavin cofactor in a bicovalent manner, 6HDNO and EncM were shown to attach the FAD via a single $\delta\alpha$ -histidyl linkage. This change in cofactor binding does not only affect the oxidative power of these flavoproteins, but also influences the space in the active site and therefore strongly determines the structural features of the accepted substrate(s). In contrast to the bacterial BBE-like enzymes discussed so far, 6HDNO is not involved in an anabolic pathway, but is required for nicotine degradation. By oxidizing the C2 and C3 position of the pyrrolidine ring of 6-hydroxy-D-nicotine (Figure 11) the resulting product becomes destabilized and spontaneously hydrolyses to a ring open product. The resulting pseudooxynicotine is further metabolized yielding the TCA intermediate fumarate as the final product [77] [76].

On the other hand, EncM participates again in antibiotic biosynthesis (enterocin formation), but the catalytic mechanism, shown in Figure 12, radically diverges from the previously discussed oxidation reactions.

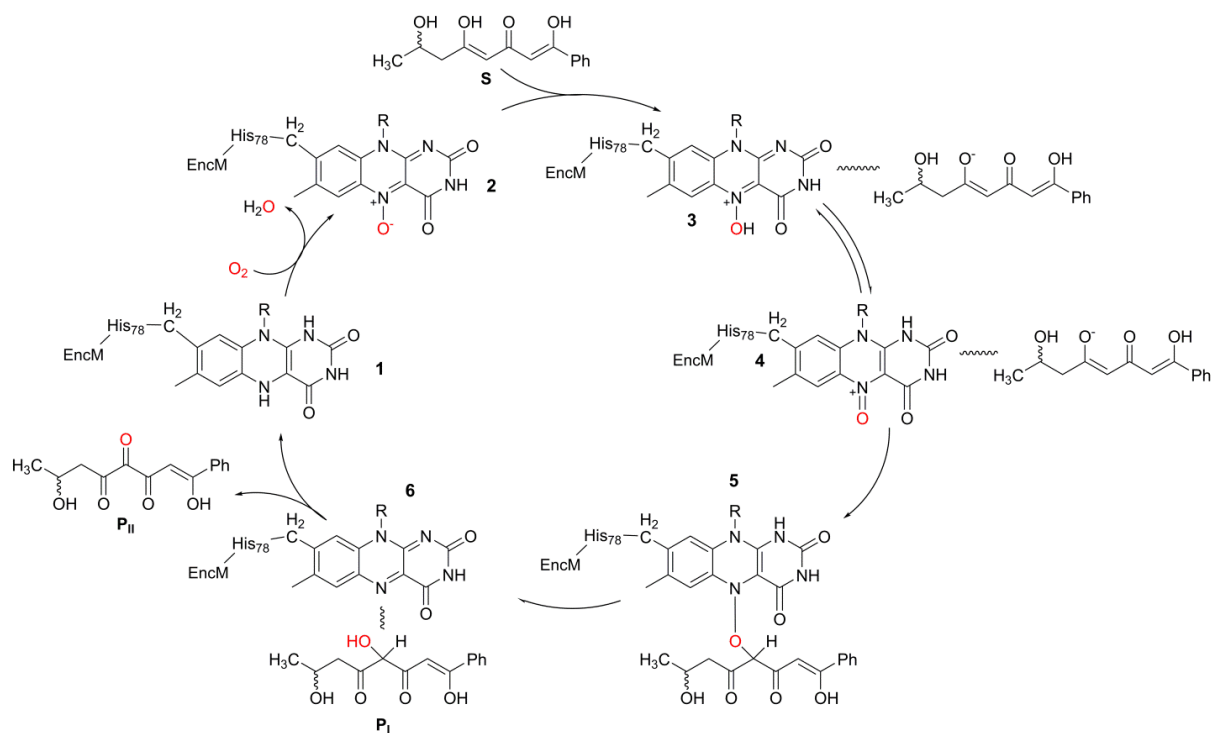


Figure 12: Proposed mechanism of EncM, adapted from Ref. [11]. A detailed description of the reaction is given in the text.

As shown in Figure 12, the reduced flavin cofactor of EncM (**1**) is oxygenated to a rather unusual N-oxide intermediate (**2**) which deprotonates the bound substrate to yield intermediate **3** [11]. Next, tautomer **4**, forms a covalent adduct with the deprotonated substrate **5**, which subsequently decays to the oxidized flavin (**6**) and a hydroxylated substrate-derived intermediate (**P_I**). Finally, the flavin oxidized the newly introduced alcohol group to give the final product (**P_{II}**) Thus the final oxidation of the hydroxyl group regenerates the reduced state of the FAD cofactor priming the enzyme for the turnover of another polyketide substrate [11]. In other words, the enzyme does not require external electron delivery by a reducing agent such as NADH or NADPH, as is typically the case for internal monooxygenases because it has invented an ingenious self-feeding process to maintain the active (reduced) state of its FAD cofactor [78].

Although the diversity of reactions catalyzed by bacterial BBE-like enzymes can already be glimpsed from the few reactions discussed here, it can be expected that the scope of reactions will be further expanded by future studies into the biosynthesis of natural products and in particular into the plethora of antibiotics generated in bacteria.

4.4.4. BBE-like enzymes from fungi

BBE-like enzymes from fungi can be divided into clades 5a and 5e (Figure 5). The latter clade appears to be associated with oligosaccharide oxidation, such as GOOX, XylO, ChitO and LaO (Figure 13). A similar BBE-like enzyme activity was detected in the plant pathogen *Phytophthora infestans*. Apparently, this enzyme belongs to the predicted secretome that is required for the invasion of host plants (*PiBBE1-6*, Figure 5) [5] [36] [37] [38] [79].

In these carbohydrate oxidases the active site type IV is highly conserved. GOOX and LaO are secreted enzymes that oxidize glucose-oligomers (*e.g.* cellotriose) at the reducing end to the corresponding lactone, which subsequently spontaneously hydrolyzes [80] [38]. Also, ChitO and XylO oxidize oligosaccharides that originate from the breakdown of the cell wall components chitin and xylan. Interestingly, GOOX and LaO share the same catalytic activity as *Ha-CHOX*, that has been assigned a role in plant immune response, *i.e.* GOOX, LaO and *PiBBE1-6* might have a similar effect on the plant immune system, *i.e.* the down regulation of the plant immune system through deactivation of the elicitor function of the oligosaccharides.

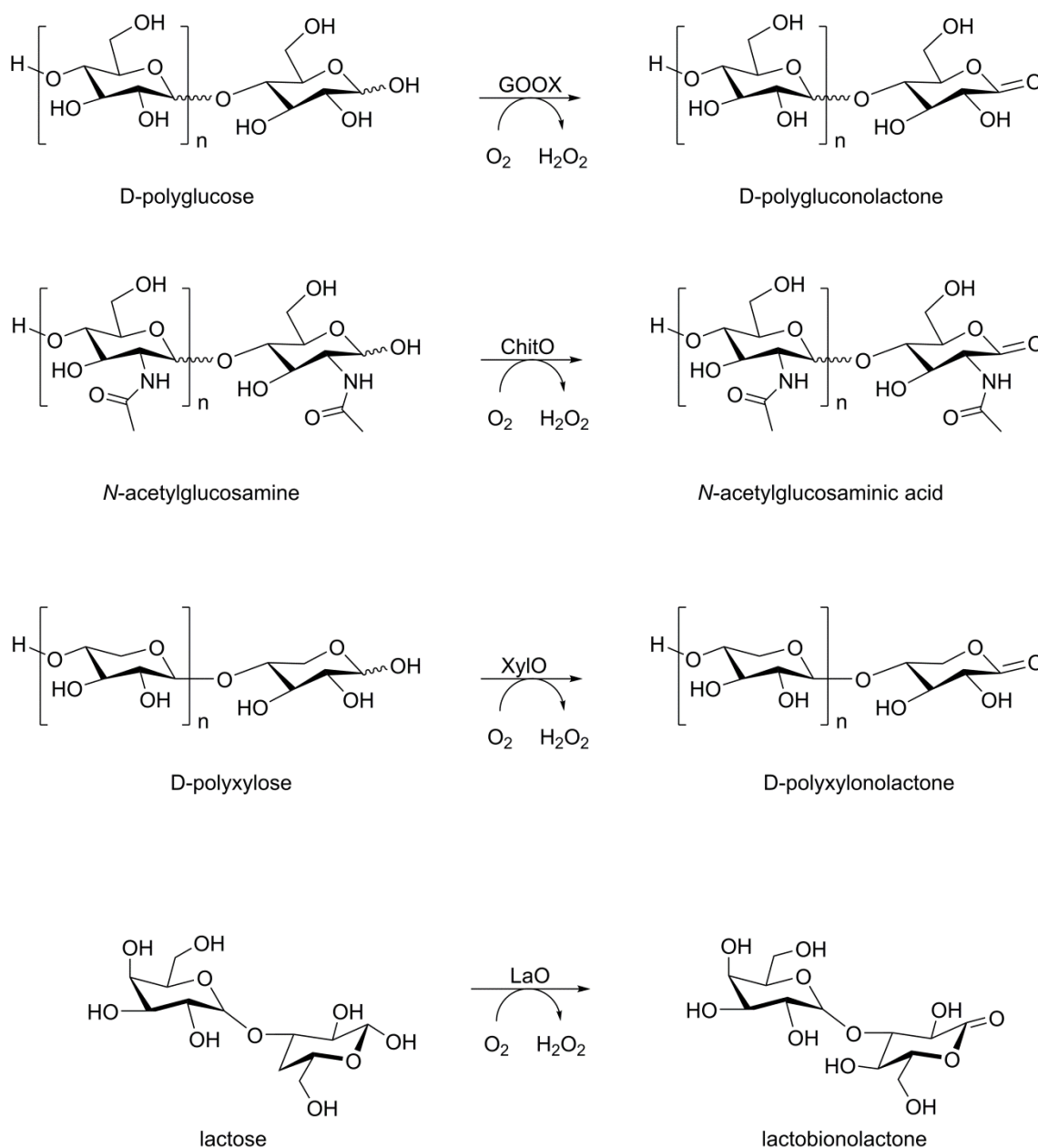


Figure 13: Reactions catalyzed by BBE-like proteins from fungi found in clade 5e (Figure 5). GOOX oxidizes various carbohydrates and oligomers of glucose to the corresponding lactones, which spontaneously hydrolyze [80]. ChitO and XylO oxidize various carbohydrates with the highest specificity for the break down products of the cell wall polymers chitin and xylan, respectively [37] [36]. LaO was found to be a secreted enzyme oxidizing various carbohydrates and oligomers of carbohydrates with the highest specificity for lactose [38].

In the clade 5a (Figure 5), enzymes catalyzing more complex reactions are found. Structural characterization of *MtVAO615* and *MtVAO713* from *Myceliophthora thermophila* was carried out by Ferrari and coworkers [81]. In contrast to the oligosaccharide oxidases discussed in the previous paragraph, enzymes in this clade do not possess the active site type IV, but rather a histidine and glutamic acid in the corresponding positions of the two tyrosines in *AtBBE*-like enzyme 15, *e.g.* Tyr188 and Tyr479, respectively (Figure 4) [32]. As shown in

Figure 14, enzymes from clade 5a can be associated with more complex oxidations (ecdysteroid-22-oxidase, E22O and HPM9 from hypothemycin biosynthesis) and ring closure reactions catalyzed by CnsA and EasE in the biosynthesis of the indole alkaloid communesin and the ergot alkaloids, respectively [82] [83].

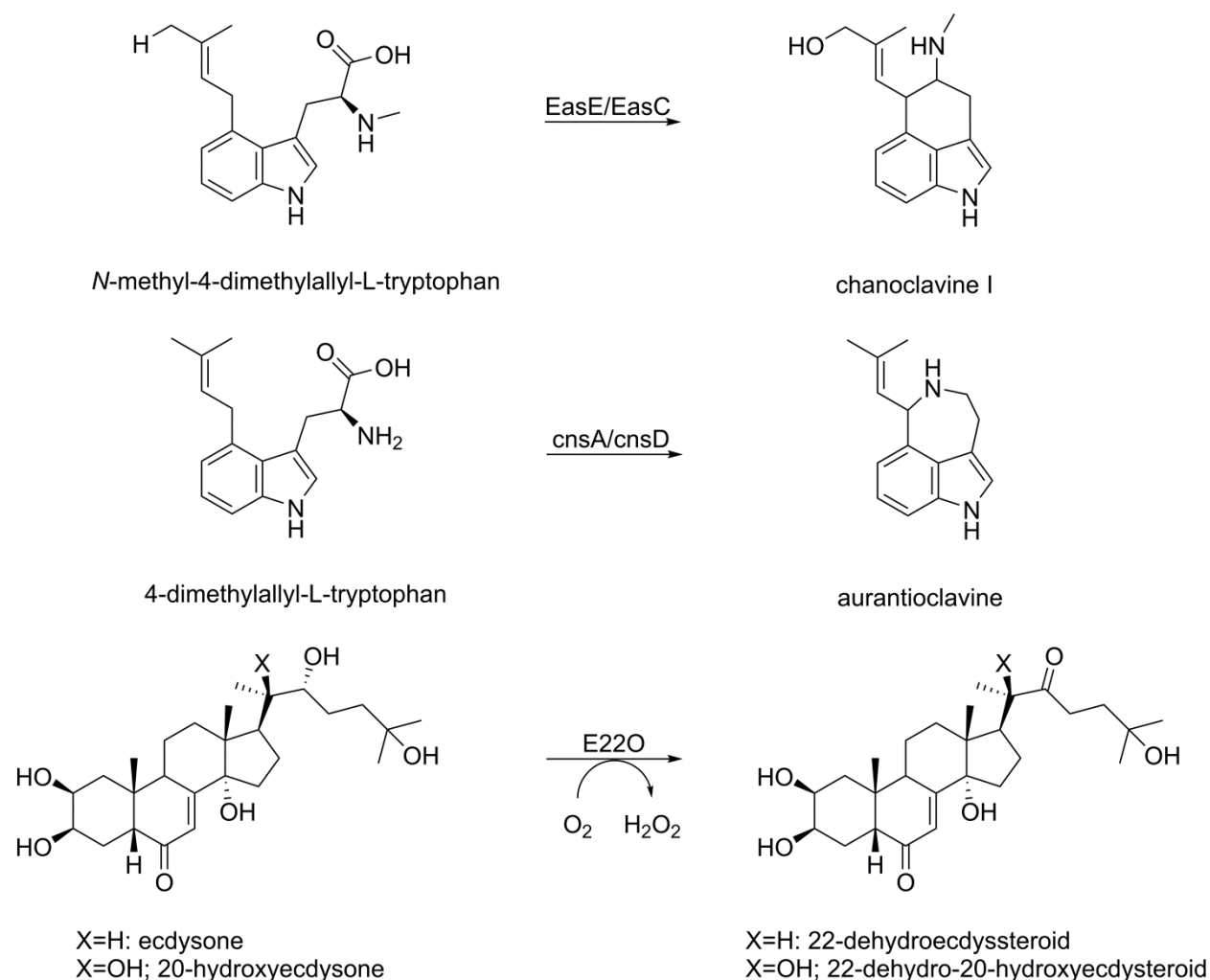


Figure 14: Reactions catalyzed by BBE-like enzymes from fungi belonging to clade 5a (Fig. 4). EasE converts, presumably in cooperation with the catalase homolog EasC the conversion of *N*-methyl-4-dimethylallyl-L-tryptophan to chanoclavine I. The reaction includes hydride transfer, decarboxylation and C-C bond formation [83]. CnsA catalyzes the ring closure reaction from 4-dimethylallyl-L-tryptophan to auroantioclavine. Similar to EasE, CnsA was proposed to catalyze the reaction in cooperation with the catalase homolog cnsD [82]. E22O from *N. rileyi* oxidizes and thereby deactivates the biological function of ecdysteroid from insects during fungal infection.

E22O is an ecdysteroid deactivating enzyme from the entomopathogenic fungus *Nomuraea rileyi* and catalyzes the oxidation of ecdysteroid-22 to the corresponding aldehyde. With this enzyme *N. rileyi* manipulates the insect's hormone system in the course of the infection and

thereby inhibits their molting, presumably to maintain appropriate growth conditions for the fungus [84]. Other members of this clade are involved in alkaloid biosynthesis and, accordingly, the corresponding genes are located in gene clusters responsible for the biosynthesis of the respective alkaloids similar to the BBE-like enzymes from bacteria that are involved in antibiotic metabolism.

CnsA was found to be employed in the biosynthesis of communesins [82]. It catalyzed the ring closure reaction from 4-dimethylallyl-L-tryptophane to aurantioclavine. The reaction involves decarboxylation and a hydride transfer step. Presumably, the reaction requires the action of both CnsA and the catalase homolog CnsD. Similarly, the BBE-like enzyme EasE was proposed to catalyze the ring closure reaction from *N*-methyl-4-dimethylallyl-L-tryptophan to chanoclavine I together with the catalase homolog EasC [85] [86]. Again, this reaction involves a decarboxylation and a hydride transfer step, however the details of this proposed reaction remain to be elucidated. Interestingly, not only oxidoreductases from the BBE-like enzyme family are involved in ring closure reactions. Recently, an enzyme from *Aspergillus fumigatus* (termed fructosyl amine oxidase, FsqB) was shown to catalyze the oxidative ring closure reaction from *N*-methyl DOPA to isoquinoline in a reaction mechanism that was postulated to be analogous to the mechanism proposed for BBE [12] [87]. Similar to many BBE-like proteins involved in alkaloid synthesis, *fsqB* is located in a cluster responsible for the expression of functionalities necessary for the production of fumisoquins [87].

4.5. Outlook

BBE-like enzymes share a common domain organization comprising a typical FAD-binding domain (FAD_binding_domain 4) and a substrate binding domain (“BBE-domain”), which defines the family and sets it apart from other sub-families of the superfamily of FAD-linked oxidases. A remarkable feature of the BBE-like enzymes is the frequently occurring bi-covalent attachment to the protein backbone via a histidine and cysteine residue to positions 8 α and 6 of the isoalloxazine ring, respectively. This has significant electronic (redox potential) and structural implications enabling a plethora of oxidative reactions and accommodating an astonishing diverse range of complex substrates. This versatility results to a large extent from the inherent plasticity of the structural architecture that facilitates the redesign of the active site by adjusting the amino acid residues required for catalysis and/or substrate binding (Figure 4). The proliferation of the enzyme family in bacteria, fungi and particularly in plants clearly testifies to the evolutionary success of this concept. In view of the large number of uncharacterized BBE-like enzymes and the current efforts to understand the biosynthesis of

natural products, it will be exciting to witness the future expansion of reactions and substrates catalyzed by members of the family as well as the physiological functions that BBE-like enzymes are involved in.

4.6. References

- [1] A Mattevi, M.W. Fraaije, A Mozzarelli, L. Olivi, A Coda, W.J. van Berkel, Crystal structures and inhibitor binding in the octameric flavoenzyme vanillyl-alcohol oxidase: the shape of the active-site cavity controls substrate specificity., *Structure*. 5 (1997) 907–20. doi:10.1016/S0969-2126(97)00245-1.
- [2] M.W. Fraaije, W.J.H. van Berkel, J.A.E. Benen, J. Visser, A. Mattevi, A novel oxidoreductase family sharing a conserved FAD-binding domain, *Trends Biochem. Sci.* 23 (1998) 206–207. doi:http://dx.doi.org/10.1016/S0968-0004(98)01210-9.
- [3] N.G.H. Leferink, D.P.H.M. Heuts, M.W. Fraaije, W.J.H. van Berkel, The growing VAO flavoprotein family, *Arch. Biochem. Biophys.* 474 (2008) 292–301. doi:10.1016/j.abb.2008.01.027.
- [4] T.M. Kutchan, Chapter 7 Molecular genetics of plant alkaloid biosynthesis, *Alkaloids Chem. Biol.* 50 (1998) 257–316. doi:10.1016/S1099-4831(08)60045-0.
- [5] C.-H. Huang, W.-L. Lai, M.-H. Lee, C.-J. Chen, A. Vasella, Y.-C. Tsai, S.-H. Liaw, Crystal structure of glucooligosaccharide oxidase from *Acremonium strictum*: a novel flavinylation of 6-S-cysteinyl, 8 α -N1-histidyl FAD., *J. Biol. Chem.* 280 (2005) 38831–38838. doi:10.1074/jbc.M506078200.
- [6] C.H. Huang, A. Winkler, C.L. Chen, W.L. Lai, Y.C. Tsai, P. Macheroux, S.H. Liaw, Functional roles of the 6-S-cysteinyl, 8 α -N1-histidyl FAD in glucooligosaccharide oxidase from *Acremonium strictum*, *J. Biol. Chem.* 283 (2008) 30990–30996. doi:10.1074/jbc.M804331200.
- [7] A. Winkler, F. Hartner, T.M. Kutchan, A. Glieder, P. Macheroux, Biochemical evidence that berberine bridge enzyme belongs to a novel family of flavoproteins containing a bi-covalently attached FAD cofactor., *J. Biol. Chem.* 281 (2006) 21276–21285. doi:10.1074/jbc.M603267200.
- [8] A. Winkler, T.M. Kutchan, P. Macheroux, 6-S-cysteinyl-ation of bi-covalently attached FAD in berberine bridge enzyme tunes the redox potential for optimal activity, *J. Biol. Chem.* 282 (2007) 24437–24443. doi:10.1074/jbc.M703642200.
- [9] A. Winkler, K. Motz, S. Riedl, M. Puhl, P. Macheroux, K. Gruber, Structural and mechanistic studies reveal the functional role of bicovalent flavinylation in berberine bridge enzyme., *J. Biol. Chem.* 284 (2009) 19993–20001. doi:10.1074/jbc.M109.015727.
- [10] V. Massey, Activation of molecular oxygen by flavins and flavoproteins, *J. Biol. Chem.* 269 (1994) 22459–22462.
- [11] R. Teufel, A. Miyanaga, Q. Michaudel, F. Stull, G. Louie, J.P. Noel, P.S. Baran, B. Palfey, B.S. Moore, Flavin-mediated dual oxidation controls an enzymatic Favorskii-type rearrangement., *Nature*. 503 (2013) 552–556. doi:10.1038/nature12643.
- [12] A. Winkler, A. Lyskowski, S. Riedl, M. Puhl, T.M. Kutchan, P. Macheroux, K. Gruber, A concerted mechanism for berberine bridge enzyme., *Nat. Chem. Biol.* 4 (2008) 739–741. doi:10.1038/nchembio.123.
- [13] F. Taura, S. Morimoto, Y. Shoyama, Purification and characterization of cannabidiolic-acid synthase from *Cannabis sativa* L. Biochemical analysis of a novel enzyme that catalyzes the oxidocyclization of cannabigerolic acid to cannabidiolic acid, *J. Biol. Chem.* 271 (1996) 17411–17416. doi:10.1074/jbc.271.29.17411.

- [14] J. Rajniak, B. Barco, N.K. Clay, E.S. Sattely, A new cyanogenic metabolite in *Arabidopsis* required for inducible pathogen defence, *Nature*. 525 (2015) 375–379. doi:10.1038/nature14907.
- [15] R.D. Finn, P. Coghill, R.Y. Eberhardt, S.R. Eddy, J. Mistry, A.L. Mitchell, S.C. Potter, M. Punta, M. Qureshi, A. Sangrador-Vegas, G.A. Salazar, J. Tate, A. Bateman, The Pfam protein families database: Towards a more sustainable future, *Nucleic Acids Res.* 44 (2016) D279–D285. doi:10.1093/nar/gkv1344.
- [16] D. Zafred, B. Steiner, A.R. Teufelberger, A. Hromic, P.A. Karplus, C.J. Schofield, S. Wallner, P. Macheroux, Rationally engineered flavin-dependent oxidase reveals steric control of dioxygen reduction, *FEBS J.* 282 (2015) 3060–3074. doi:10.1111/febs.13212.
- [17] R. Baron, C. Riley, P. Chenprakhon, K. Thotsaporn, R.T. Winter, A. Alfieri, F. Forneris, W.J. van Berkel, P. Chaiyen, M.W. Fraaije, A. Mattevi, J.A. McCammon, Multiple pathways guide oxygen diffusion into flavoenzyme active sites, *Proc Natl Acad Sci U S A.* 106 (2009) 10603–10608. doi:10.1073/pnas.0903809106.
- [18] L. Mauch, V. Bichler, R. Brandsch, Site-directed mutagenesis of the FAD-binding histidine of 6-hydroxy-D-nicotine oxidase. Consequences on flavinylation and enzyme activity, *FEBS Lett.* 257 (1989) 86–88. doi:10.1016/0014-5793(89)81792-2.
- [19] B. Daniel, S. Wallner, B. Steiner, G. Oberdorfer, P. Kumar, E. Van Der Graaff, T. Roitsch, C.W. Sensen, K. Gruber, P. Macheroux, Structure of a berberine bridge enzyme-like enzyme with an active site specific to the plant family Brassicaceae, *PLoS One.* 11 (2016). doi:10.1371/journal.pone.0156892.
- [20] M.M. Kopacz, M.W. Fraaije, Turning a monocovalent flavoprotein into a bicovalent flavoprotein by structure-inspired mutagenesis, *Bioorganic Med. Chem.* 22 (2014) 5621–5627. doi:10.1016/j.bmc.2014.05.051.
- [21] D.P.H.M. Heuts, N.S. Scrutton, W.S. McIntire, M.W. Fraaije, What's in a covalent bond?: On the role and formation of covalently bound flavin cofactors, *FEBS J.* 276 (2009) 3405–3427. doi:10.1111/j.1742-4658.2009.07053.x.
- [22] D.P.H.M. Heuts, R.T. Winter, G.E. Damsma, D.B. Janssen, M.W. Fraaije, The role of double covalent flavin binding in chito-oligosaccharide oxidase from *Fusarium graminearum*, *Biochem. J.* 413 (2008) 175–183. doi:10.1042/BJ20071591.
- [23] J.C. Carlson, S. Li, S.S. Gunatilleke, Y. Anzai, D.A. Burr, L.M. Podust, D.H. Sherman, Tirandamycin biosynthesis is mediated by co-dependent oxidative enzymes., *Nat. Chem.* 3 (2011) 628–633. doi:10.1038/nchem.1087.
- [24] Y.-C. Liu, Y.-S. Li, S.-Y. Lyu, L.-J. Hsu, Y.-H. Chen, Y.-T. Huang, H.-C. Chan, C.-J. Huang, G.-H. Chen, C.-C. Chou, M.-D. Tsai, T.-L. Li, Interception of teicoplanin oxidation intermediates yields new antimicrobial scaffolds., *Nat. Chem. Biol.* 7 (2011) 304–309. doi:10.1038/nchembio.556.
- [25] A. Mattevi, To be or not to be an oxidase: challenging the oxygen reactivity of flavoenzymes, *Trends Biochem. Sci.* 31 (2006) 276–283. doi:10.1016/j.tibs.2006.03.003.
- [26] P. Chaiyen, M.W. Fraaije, A. Mattevi, The enigmatic reaction of flavins with oxygen, *Trends Biochem. Sci.* 37 (2012) 373–380. doi:10.1016/j.tibs.2012.06.005.

- [27] J.L. McManaman, D.L. Bain, Structural and conformational analysis of the oxidase to dehydrogenase conversion of xanthine oxidoreductase, *J. Biol. Chem.* 277 (2002) 21261–21268. doi:10.1074/jbc.M200828200.
- [28] T. Nishino, K. Okamoto, Y. Kawaguchi, H. Hori, T. Matsumura, B.T. Eger, E.F. Pai, T. Nishino, Mechanism of the conversion of xanthine dehydrogenase to xanthine oxidase: Identification of the two cysteine disulfide bonds and crystal structure of a non-convertible rat liver xanthine dehydrogenase mutant, *J. Biol. Chem.* 280 (2005) 24888–24894. doi:10.1074/jbc.M501830200.
- [29] N.G.H. Leferink, M.W. Fraaije, H.J. Joosten, P.J. Schaap, A. Mattevi, W.J.H. van Berkel, Identification of a gatekeeper residue that prevents dehydrogenases from acting as oxidases, *J. Biol. Chem.* 284 (2009) 4392–4397. doi:10.1074/jbc.M808202200.
- [30] S. Wallner, A. Winkler, S. Riedl, C. Dully, S. Horvath, K. Gruber, P. MacHeroux, Catalytic and structural role of a conserved active site histidine in berberine bridge enzyme, *Biochemistry*. 51 (2012) 6139–6147. doi:10.1021/bi300411n.
- [31] N. Noinaj, M. a. Bosserman, M.A. Schickli, G. Piszczek, M.K. Kharel, P. Pahari, S.K. Buchanan, J. Rohr, The crystal structure and mechanism of an unusual oxidoreductase, GilR, involved in gilvocarcin V biosynthesis, *J. Biol. Chem.* 286 (2011) 23533–23543. doi:10.1074/jbc.M111.247833.
- [32] B. Daniel, T. Pavkov-Keller, B. Steiner, A. Dordic, A. Gutmann, B. Nidetzky, C.W. Sensen, E. van der Graaff, S. Wallner, K. Gruber, P. Macheroux, Oxidation of monolignols by members of the berberine bridge enzyme family suggests a role in cell wall metabolism, *J. Biol. Chem.* 290 (2015) 18770–18781. doi:10.1074/jbc.M115.659631.
- [33] S. Pils, K. Schnabl, S. Wallner, M. Kljajic, N. Kupresanin, R. Breinbauer, M. Fuchs, R. Rocha, J.H. Schrittwieser, W. Kroutil, B. Daniel, P. Macheroux, Characterization of the monolignol oxidoreductase AtBBE-like protein 15 L182V for biocatalytic applications, *J. Mol. Catal. B Enzym.* (n.d.). doi:http://doi.org/10.1016/j.molcatb.2016.10.018.
- [34] D. Zafred, A. Nandy, L. Pump, H. Kahlert, W. Keller, Crystal structure and immunologic characterization of the major grass pollen allergen Phl p 4, *J. Allergy Clin. Immunol.* 132 (2013). doi:10.1016/j.jaci.2013.03.021.
- [35] J.H.H. V Custers, S.J. Harrison, M.B. Sela-Buurlage, E. Van Deventer, W. Lageweg, P.W. Howe, P.J. Van Der Meijs, A.S. Ponstein, B.H. Simons, L.S. Melchers, M.H. Stuiver, Isolation and characterisation of a class of carbohydrate oxidases from higher plants, with a role in active defence, *Plant J.* 39 (2004) 147–160. doi:10.1111/j.1365-313X.2004.02117.x.
- [36] A.R. Ferrari, H.J. Rozeboom, J.M. Dobruchowska, S.S. Van Leeuwen, A.S.C. Vugts, M.J. Koetsier, J. Visser, M.W. Fraaije, G. Hart, Discovery of a xylooligosaccharide oxidase from *Myceliophthora thermophila* C1, *J. Biol. Chem.* 291 (2016) 23709–23718. doi:10.1074/jbc.M116.741173.
- [37] D.P.H.M. Heuts, D.B. Janssen, M.W. Fraaije, Changing the substrate specificity of a chitoooligosaccharide oxidase from *Fusarium graminearum* by model-inspired site-directed mutagenesis, *FEBS Lett.* 581 (2007) 4905–4909. doi:10.1016/j.febslet.2007.09.019.
- [38] S.K. Ahmad, D.S. Brinch, E.P. Friis, P.B. Pedersen, Toxicological studies on lactose oxidase from *Microdochium nivale* expressed in *Fusarium venenatum*, *Regul. Toxicol. Pharmacol.* 39 (2004) 256–270. doi:10.1016/j.yrtph.2004.02.003.

- [39] S. Liaw, D.Y. Lee, L.P. Chow, G.X. Lau, S.N. Su, Structural characterization of the 60-kDa bermuda grass pollen isoallergens, a covalent flavoprotein., *Biochem. Biophys. Res. Commun.* 280 (2001) 738–743. doi:10.1006/bbrc.2000.4203.
- [40] I. Letunic, P. Bork, Interactive tree of life (iTOL) v3: an online tool for the display and annotation of phylogenetic and other trees., *Nucleic Acids Res.* (2016) gkw290–. doi:10.1093/nar/gkw290.
- [41] M.K. Kharel, P. Pahari, H. Lian, J. Rohr, GilR, an unusual lactone-forming enzyme involved in gilvocarcin biosynthesis, *ChemBioChem.* 10 (2009) 1305–1308. doi:10.1002/cbic.200900130.
- [42] I. Alexeev, A. Sultana, P. Mäntsälä, J. Niemi, G. Schneider, Aclacinomycin oxidoreductase (AknOx) from the biosynthetic pathway of the antibiotic aclacinomycin is an unusual flavoenzyme with a dual active site., *Proc. Natl. Acad. Sci. U. S. A.* 104 (2007) 6170–6175. doi:10.1073/pnas.0700579104.
- [43] F. Lutzoni, F. Kauff, C.J. Cox, D. McLaughlin, G. Celio, C. Dentinger, M. Padamsee, D. Hibbett, T.Y. James, E. Baloch, M. Grube, V. Reeb, V. Hofstetter, C. Schoch, A.E. Arnold, J. Miadlikowska, J. Spatafora, D. Johnson, S. Hambleton, M. Crockett, R. Shoemaker, G.H. Sung, R. Lücking, T. Lumbsch, K. O'Donnell, M. Binder, P. Diederich, D. Ertz, C. Gueidan, K. Hansen, R.C. Harris, K. Hosaka, Y.W. Lim, B. Matheny, H. Nishida, D. Pfister, J. Rogers, A. Rossman, I. Schmitt, H. Sipman, J. Stone, J. Sugiyama, R. Yahr, R. Vilgalys, Assembling the fungal tree of life: Progress, classification, and evolution of subcellular traits, *Am. J. Bot.* 91 (2004) 1446–1480. doi:10.3732/ajb.91.10.1446.
- [44] S.M. Adl, A.G.B. Simpson, C.E. Lane, J. Luke, D. Bass, S.S. Bowser, M.W. Brown, F. Burki, M. Dunthorn, V. Hampl, A. Heiss, M. Hoppenrath, E. Lara, L. Le Gall, D.H. Lynn, H. McManus, E.A.D. Mitchell, S.E. Mozley-Stanridge, L.W. Parfrey, J. Pawlowski, S. Rueckert, L. Shadwick, C.L. Schoch, A. Smirnov, F.W. Spiegel, The revised classification of eukaryotes, *J. Eukaryot. Microbiol.* 59 (2012) 429–493. doi:10.1111/j.1550-7408.2012.00644.x.
- [45] T.M. Kutchan, H. Dirtrich, Characterization and mechanism of the berberine bridge enzyme, a covalently flavinylated oxidase of benzophenanthridine alkaloid biosynthesis in plants, *J. Biol. Chem.* 270 (1995) 24475–24481. doi:10.1074/jbc.270.41.24475.
- [46] S. Sirikantaramas, S. Morimoto, Y. Shoyama, Y. Ishikawa, Y. Wada, Y. Shoyama, F. Taura, The gene controlling marijuana psychoactivity: molecular cloning and heterologous expression of Δ^1 -tetrahydrocannabinolic acid synthase from *Cannabis sativa* L., *J. Biol. Chem.* 279 (2004) 39767–39774. doi:10.1074/jbc.M403693200.
- [47] P. Steffens, N. Nagakura, M.H. Zenk, Purification and characterization of the berberine bridge enzyme from berberis beaniana cell cultures, *Phytochemistry.* 24 (1985) 2577–2583. doi:10.1016/S0031-9422(00)80672-X.
- [48] M. Amann, M. H. Zenk, Preparation of dehydrobenzylisoquinolines by immobilized (*S*)-tetrahydroprotoberberine oxidase from plant cell cultures, *Phytochemistry.* 26 (1987) 3235–3240. doi:10.1016/S0031-9422(00)82477-2.
- [49] F. Taura, S. Sirikantaramas, Y. Shoyama, K. Yoshikai, Y. Shoyama, S. Morimoto, Cannabidiolic-acid synthase, the chemotype-determining enzyme in the fiber-type *Cannabis sativa*, *FEBS Lett.* 581 (2007) 2929–2934. doi:10.1016/j.febslet.2007.05.043.
- [50] E. Rink, H. Böhm, Conversion of reticuline into scoulerine by a cell free preparation from *Macleaya microcarpa* cell suspension cultures, *FEBS Lett.* 49 (1975) 396–399. doi:10.1016/0014-5793(75)80794-0.

- [51] T.M. Kutchan, A. Bock, H. Dittrich, Heterologous expression of the plant proteins strictosidine synthase and berberine bridge enzyme in insect cell culture, *Phytochemistry*. 35 (1994) 353–360. doi:10.1016/S0031-9422(00)94763-0.
- [52] D.K. Liscombe, P.J. Facchini, Evolutionary and cellular webs in benzyloisoquinoline alkaloid biosynthesis, *Curr. Opin. Biotechnol.* 19 (2008) 173–180. doi:10.1016/j.copbio.2008.02.012.
- [53] H.M. Gaweska, K.M. Roberts, P.F. Fitzpatrick, Isotope effects suggest a stepwise mechanism for berberine bridge enzyme, *Biochemistry*. 51 (2012) 7342–7347. doi:10.1021/bi300887m.
- [54] W.M. Chou, T.M. Kutchan, Enzymatic oxidations in the biosynthesis of complex alkaloids, *Plant J.* 15 (1998) 289–300. doi:10.1046/j.1365-313X.1998.00220.x.
- [55] M. Amann, N. Nagakura, M.H. Zenk, Purification and properties of (*S*)-tetrahydroprotoberberine oxidase from suspension-cultured cells of *Berberis wilsoniae*., *Eur. J. Biochem.* 175 (1988) 17–25. doi:10.1111/j.1432-1033.1988.tb14160.x.
- [56] A. Gesell, M.L.D. Chávez, R. Kramell, M. Piotrowski, P. Macheroux, T.M. Kutchan, Heterologous expression of two FAD-dependent oxidases with (*S*)-tetrahydroprotoberberine oxidase activity from *Argemone mexicana* and *Berberis wilsoniae* in insect cells, *Planta*. 233 (2011) 1185–1197. doi:10.1007/s00425-011-1357-4.
- [57] A. Winkler, M. Puhl, H. Weber, T.M. Kutchan, K. Gruber, P. Macheroux, Berberine bridge enzyme catalyzes the six electron oxidation of (*S*)-reticuline to dehydroscoulerine, *Phytochemistry*. 70 (2009) 1092–1097. doi:http://doi.org/10.1016/j.phytochem.2009.06.005.
- [58] Y. Shoyama, A. Takeuchi, F. Taura, T. Tamada, M. Adachi, R. Kuroki, Y. Shoyama, S. Morimoto, Crystallization of Δ^1 -tetrahydrocannabinolic acid (THCA) synthase from *Cannabis sativa*, *Acta Crystallogr. Sect. F Struct. Biol. Cryst. Commun.* 61 (2005) 799–801. doi:10.1107/S1744309105023365.
- [59] Y. Shoyama, T. Tamada, K. Kurihara, A. Takeuchi, F. Taura, S. Arai, M. Blaber, Y. Shoyama, S. Morimoto, R. Kuroki, Structure and function of Δ^1 -tetrahydrocannabinolic acid (THCA) synthase, the enzyme controlling the psychoactivity of *Cannabis sativa*, *J. Mol. Biol.* 423 (2012) 96–105. doi:10.1016/j.jmb.2012.06.030.
- [60] M. Kajikawa, T. Shoji, A. Kato, T. Hashimoto, Vacuole-localized berberine bridge enzyme-like proteins are required for a late step of nicotine biosynthesis in tobacco, *Plant Physiol.* 155 (2011) 2010–2022. doi:10.1104/pp.110.170878.
- [61] R.S. Lewis, H.O. Lopez, S.W. Bowen, K.R. Andres, W.T. Steede, R.E. Dewey, Transgenic and mutation-based suppression of a berberine bridge enzyme-like (BBL) gene family reduces alkaloid content in field-grown tobacco, *PLoS One*. 10 (2015). doi:10.1371/journal.pone.0117273.
- [62] D. Ober, E. Kaltenecker, Pyrrolizidine alkaloid biosynthesis, evolution of a pathway in plant secondary metabolism, *Phytochemistry*. 70 (2009) 1687–1695. doi:10.1016/j.phytochem.2009.05.017.
- [63] O.C. Hansen, P. Stougaard, Hexose oxidase from the red alga *Chondrus crispus* - Purification, molecular cloning, and expression in *Pichia pastoris*, *J. Biol. Chem.* 272 (1997) 11581–11587.
- [64] J.P. Van der Lugt, Evaluation of methods for chemical and biological carbohydrate oxidation, (1998). uuid:9550f9be-9075-437d-a4a2-27d304c2e67e.

- [65] C. Poulsen, P.B. Hostrup, Purification and characterization of a hexose oxidase with excellent strengthening effects in bread, *Cereal Chem.* 75 (1998) 51–57. doi:10.1094/CCHEM.1998.75.1.51.
- [66] A. M. Wolff, O.C. Hansen, U. Poulsen, S. Madrid, P. Stougaard, Optimization of the production of *Chondrus crispus* hexose oxidase in *Pichia pastoris*, *Protein Expr. Purif.* 22 (2001) 189–199. doi:10.1006/prep.2001.1439.
- [67] C.J. Carter, R.W. Thornburg, Tobacco nectarin V is a flavin-containing berberine bridge enzyme-like protein with glucose oxidase activity, *Plant Physiol.* 134 (2004) 460–469. doi:10.1104/pp.103.027482.
- [68] A.D. Harper, S.H. Stalnaker, L. Wells, A. Darvill, R. Thornburg, W.S. York, Interaction of Nectarin 4 with a fungal protein triggers a microbial surveillance and defense mechanism in nectar, *Phytochemistry.* 71 (2010) 1963–1969. doi:10.1016/j.phytochem.2010.09.009.
- [69] R. Kaur, J. Macleod, W. Foley, M. Nayudu, Gluconic acid: An antifungal agent produced by *Pseudomonas* species in biological control of take-all, *Phytochemistry.* 67 (2006) 595–604. doi:10.1016/j.phytochem.2005.12.011.
- [70] P. Wojtaszek, Oxidative burst: an early plant response to pathogen infection., *Biochem. J.* 322 (Pt 3 (1997) 681–92. doi:10.1042/bj3220681.
- [71] S. Stumvoll, J. Lidholm, R. Thunberg, A.M. DeWitt, P. Eibesteiner, I. Swoboda, A. Bugajska-Schretter, S. Spitzauer, L. Vangelista, L. Kazemi-Shirazi, W.R. Sperr, P. Valent, D. Kraft, R. Valenta, Purification, structural and immunological characterization of a timothy grass (*Phleum pratense*) pollen allergen, Phl p 4, with cross-reactive potential, *Biol. Chem.* 383 (2002) 1383–1396. doi:10.1515/BC.2002.157.
- [72] L. Chae, T. Kim, R. Nilo-Poyanco, S.Y. Rhee, Genomic signatures of specialized metabolism in plants, *Science.* 344 (2014) 510–3. doi:10.1126/science.1252076.
- [73] J. Frébortová, O. Novák, I. Frébort, R. Jorda, Degradation of cytokinins by maize cytokinin dehydrogenase is mediated by free radicals generated by enzymatic oxidation of natural benzoxazinones, *Plant J.* 61 (2010) 467–481. doi:10.1111/j.1365-313X.2009.04071.x.
- [74] R. Vanholme, B. Demedts, K. Morreel, J. Ralph, W. Boerjan, Lignin biosynthesis and structure., *Plant Physiol.* 153 (2010) 895–905. doi:10.1104/pp.110.155119.
- [75] Y.-S. Li, J.-Y. Ho, C.-C. Huang, S.-Y. Lyu, C.-Y. Lee, Y.-T. Huang, C.-J. Wu, H.-C. Chan, C.-J. Huang, N.-S. Hsu, M.-D. Tsai, T.-L. Li, Flavin prim alcohol oxidase [oxidat carboxylate] for glycopeptide A40926 biosyn, *J. Am. Chem. Soc.* 129 (2007) 13384–13385.
- [76] J.W.A. Koetter, G.E. Schulz, Crystal structure of 6-hydroxy-D-nicotine oxidase from *Arthrobacter nicotinovorans*, *J. Mol. Biol.* 352 (2005) 418–428. doi:10.1016/j.jmb.2005.07.041.
- [77] H. Yu, H. Tang, Y. Li, P. Xu, Molybdenum-containing nicotine hydroxylase genes in a nicotine degradation pathway that is a variant of the pyridine and pyrrolidine pathways, *Appl. Environ. Microbiol.* 81 (2015) 8330–8338. doi:10.1128/AEM.02253-15.
- [78] M.M.E. Huijbers, S. Montersino, A.H. Westphal, D. Tischler, W.J.H. Van Berkel, Flavin dependent monooxygenases, *Arch. Biochem. Biophys.* 544 (2014) 2–17. doi:10.1016/j.abb.2013.12.005.
- [79] S. Raffaele, J. Win, L.M. Cano, S. Kamoun, Analyses of genome architecture and gene expression reveal novel candidate virulence factors in the secretome of *Phytophthora infestans*, *BMC Genomics.* 11 (2010) 637. doi:10.1186/1471-2164-11-637.

- [80] S.-F. Lin, T.-Y. Yang, T. Inukai, M. Yamasaki, Y.-C. Tsai, Purification and characterization of a novel glucooligosaccharide oxidase from *Acremonium strictum* T1, *Biochim. Biophys. Acta - Protein Struct. Mol. Enzymol.* 1118 (1991) 41–47. doi:[http://dx.doi.org/10.1016/0167-4838\(91\)90439-7](http://dx.doi.org/10.1016/0167-4838(91)90439-7).
- [81] A.R. Ferrari, *Exploring flavin-containing carbohydrate oxidases*, University of Groningen, 2017.
- [82] H.-C. Lin, G. Chiou, Y.-H. Chooi, T.C. McMahon, W. Xu, N.K. Garg, Y. Tang, Elucidation of the concise biosynthetic pathway of the communesin indole alkaloids, *Angew. Chemie Int. Ed.* 54 (2015) 3004–3007. doi:[10.1002/anie.201411297](https://doi.org/10.1002/anie.201411297).
- [83] C.A.F. Nielsen, C. Folly, A. Hatsch, A. Molt, H. Schröder, S.E. O'Connor, M. Naesby, The important ergot alkaloid intermediate chanoclavine-I produced in the yeast *Saccharomyces cerevisiae* by the combined action of EasC and EasE from *Aspergillus japonicus*, *Microb. Cell Fact.* 13 (2014) 95. doi:[10.1186/s12934-014-0095-2](https://doi.org/10.1186/s12934-014-0095-2).
- [84] M. Kiuchi, H. Yasui, S. Hayasaka, M. Kamimura, Entomogenous fungus *Nomuraea rileyi* inhibits host insect molting by C22-oxidizing inactivation of hemolymph ecdysteroids, *Arch. Insect Biochem. Physiol.* 52 (2003) 35–44. doi:[10.1002/arch.10060](https://doi.org/10.1002/arch.10060).
- [85] C. Nielsen, C. Folly, A. Hatsch, A. Molt, H. Schröder, S.E. O Connor, M. Naesby, The important ergot alkaloid intermediate chanoclavine-I produced in the yeast., *Microb. Cell Fact.* 13 (2014) 95. doi:[10.1186/s12934-014-0095-2](https://doi.org/10.1186/s12934-014-0095-2).
- [86] N. Lorenz, J. Olšovská, M. Šulc, P. Tudzynski, Alkaloid cluster gene *ccsA* of the ergot fungus *Claviceps purpurea* encodes chanoclavine I synthase, a flavin adenine dinucleotide-containing oxidoreductase mediating the transformation of *N*-methyl-dimethylallyltryptophan to chanoclavine I, *Appl. Environ. Microbiol.* 76 (2010) 1822–1830. doi:[10.1128/AEM.00737-09](https://doi.org/10.1128/AEM.00737-09).
- [87] J.A. Baccile, J.E. Spraker, H.H. Le, E. Brandenburger, C. Gomez, J.W. Bok, J. Macheleidt, A.A. Brakhage, D. Hoffmeister, N.P. Keller, F.C. Schroeder, Plant-like biosynthesis of isoquinoline alkaloids in *Aspergillus fumigatus*, *Nat. Chem. Biol.* 12 (2016) 1–9. doi:[10.1038/nchembio.2061](https://doi.org/10.1038/nchembio.2061).

The family of berberine bridge enzyme-like enzymes: A treasure-trove of oxidative reactions

4.7. Supplementary Information

Bastian Daniel, Barbara Konrad, Marina Toplak, Majd Lahham, Julia Messenlehner, Andreas Winkler and Peter Macheroux*

Institute of Biochemistry, Graz University of Technology, Petersgasse 12/2, 8010 Graz,
Austria

To whom correspondence should be addressed: Peter Macheroux, Graz University of Technology, Institute of Biochemistry, Petersgasse 12/II, A-8010 Graz, Austria, Tel.: +43-316-873 6450, Fax: +43-316-873 6952; Email: peter.macheroux@tugraz.at

Table S1: Sequences used for the phylogenetic analysis of the FAD-linked oxidase superfamily.

BBE-like proteins				
Abbreviation	Uniprot	PDB	Organism	Kingdom
HOX	P93762		<i>Chondrus crispus</i>	Algi
GilR	Q7X2G7	3POP	<i>Streptomyces griseoflavus</i>	Bacteria
AknOx	Q0PCD7	2IPI	<i>Streptomyces galilaeus</i>	Bacteria
Dbv29	Q7WZ62	2WDW	<i>Nonomuraea sp. ATCC 39727</i>	Bacteria
TamL	D3Y1I2	2Y08	<i>Streptomyces sp. 307-9</i>	Bacteria
6HDNO	P08159		<i>Arthrobacter oxydans</i>	Bacteria
EncM	Q9KHK2	4XLO	<i>Streptomyces maritimus</i>	Bacteria
EasE	Q4WZ61		<i>Neosartorya fumigata</i>	Fungi
NjBBE	B0XPK7		<i>Neosartorya fumigata</i>	Fungi
MtVAO615	G2QDQ9		<i>Myceliophthora thermophila</i>	Fungi
E22O	I0J0L0		<i>Metarhizium rileyi</i>	Fungi
MtVAO713	G2QMS8		<i>Myceliophthora thermophila</i>	Fungi
HPM9	B3FWS5		<i>Hypomyces subiculosus</i>	Fungi
PiBBE4	D0MXI8		<i>Phytophthora infestans</i>	Fungi
PiBBE5	D0MXJ2		<i>Phytophthora infestans</i>	Fungi
PiBBE3	D0MXI7		<i>Phytophthora infestans</i>	Fungi
PiBBE2	D0N574		<i>Phytophthora infestans</i>	Fungi
PiBBE1	D0N569		<i>Phytophthora infestans</i>	Fungi
LaO	I1SB12	3RJA	<i>Microdochium nivale</i>	Fungi
XylO	G2QG48	5K8E	<i>Myceliophthora thermophila</i>	Fungi
GOOX	Q6PW77	2AXR	<i>Sarocladium strictum</i>	Fungi
ChitO	I1S2K2		<i>Gibberella zeae</i>	Fungi
PiBBE6	D0P2Y8		<i>Phytophthora infestans</i>	Fungi
VcBBE	D8TI34		<i>Volvox carteri f. nagariensis</i>	Viridiplantae
SmBBE	D8SFA1		<i>Selaginella moellendorffii</i>	Viridiplantae
PpBBE3	A9T8D8		<i>Physcomitrella patens subsp. patens</i>	Viridiplantae
Nec5	Q84N20		<i>Nicotiana langsdorffii x Nicotiana glauca</i>	Viridiplantae
AtBBE12	Q9SA89		<i>Arabidopsis thaliana</i>	Viridiplantae
Ls-CHOX	Q8SA60		<i>Lactuca sativa</i>	Viridiplantae
Ha-CHOX	Q8SA59		<i>Helianthus annuus</i>	Viridiplantae
AtBBE14	F4HV09		<i>Arabidopsis thaliana</i>	Viridiplantae
AtBBE10	Q9SA87		<i>Arabidopsis thaliana</i>	Viridiplantae
AtBBE3	Q9FZC4		<i>Arabidopsis thaliana</i>	Viridiplantae
AtBBE5	Q9FZC6		<i>Arabidopsis thaliana</i>	Viridiplantae
AtBBE22	Q9SUC6		<i>Arabidopsis thaliana</i>	Viridiplantae
AtBBE26	Q9FKU8		<i>Arabidopsis thaliana</i>	Viridiplantae
AtBBE15	O64743	4UD8	<i>Arabidopsis thaliana</i>	Viridiplantae
AtBBE13			<i>Arabidopsis thaliana</i>	Viridiplantae
AtBBE28	Q9FI21	5D79	<i>Arabidopsis thaliana</i>	Viridiplantae
THCAS	Q8GTB6	3VTE	<i>Cannabis sativa</i>	Viridiplantae
CBDAS	A0A0E3TJM8		<i>Cannabis sativa</i>	Viridiplantae
Phl p 4	Q2I6V7	3TSH	<i>Phleum pratense</i>	Viridiplantae
BG60	Q5QJ60	4DNS	<i>Cynodon dactylon</i>	Viridiplantae
BBLd	F1T162		<i>Nicotiana Tabacum</i>	Viridiplantae
BBLc	F1T161		<i>Nicotiana Tabacum</i>	Viridiplantae
BBLb	A7WPL6		<i>Nicotiana Tabacum</i>	Viridiplantae
BBLa	F1T160		<i>Nicotiana Tabacum</i>	Viridiplantae
EcBBE	P30986	3D2D	<i>Eschscholzia californica</i>	Viridiplantae
CvBBE	E1ZHF1		<i>Chlorella variabilis</i>	Viridiplantae

<i>Mp</i> BB1	A0A176WJ71		<i>Marchantia polymorpha subsp. polymorpha</i>	Viridiplantae
<i>Pp</i> BBE1	A9SWH5		<i>Physcomitrella patens subsp. patens</i>	Viridiplantae
STOX	F1BVB7		<i>Argemone mexicana</i>	Viridiplantae
<i>At</i> BBE19	Q9SVG4		<i>Arabidopsis thaliana</i>	Viridiplantae
<i>At</i> BBE21	Q9SVG3		<i>Arabidopsis thaliana</i>	Viridiplantae
<i>At</i> BBE2	Q9SA99		<i>Arabidopsis thaliana</i>	Viridiplantae
<i>At</i> BBE1	Q9LPC3		<i>Arabidopsis thaliana</i>	Viridiplantae
CnsA	none		<i>Penicillium expansum</i>	Fungi
FAD-linked oxidases				
<i>Dd</i> ADHAPS	O96759	2UUU	<i>Dictyostelium discoideum</i>	Amoebozoa
AldO	Q9ZBU1	2VFR	<i>Streptomyces coelicolor</i>	Bacteria
RPA1076	Q6NAV4	3PM9	<i>Rhodopseudomonas palustris</i>	Bacteria
EugO	Q0SBK1	5FXD	<i>Rhodococcus jostii</i>	Bacteria
PCMH	P09788	1DII	<i>Pseudomonas putida</i>	Bacteria
MurB	Q9HZM7	4JAY	<i>Pseudomonas aeruginosa</i>	Bacteria
DprE	P9WJF1	4FDN	<i>Mycobacterium tuberculosis</i>	Bacteria
CholOx	Q7SID9	1I19	<i>Brevibacterium sterolicum</i>	Bacteria
VAO	P56216	1VAO	<i>Penicillium simplicissimum</i>	Fungi
<i>Cp</i> ADHAPS	P97275	4BBY	<i>Cavia porcellus</i>	Mammalia
<i>Zm</i> CK02	Q709Q5	4ML8	<i>Zea mays</i>	Viridiplantae
<i>Zm</i> CKX1	Q9T0N8	1W1O	<i>Zea mays</i>	Viridiplantae
<i>At</i> CKX	Q9FUJ1	2EXR	<i>Arabidopsis thaliana</i>	Viridiplantae
GLDH	Q9SU56		<i>Arabidopsis thaliana</i>	Viridiplantae
DLDH	P06149		<i>Escherichia coli</i>	Bacteria

Table S2: Occurrence of BBE-like proteins within the clade Viridiplantae and the assignment of active site types.

Subgroups	Family	Species	BBE-like genes	Active site type					MDH**
				1	2	3	4	n.d.*	
Embryophyte	Marchantiaceae	<i>Marchantia polymorpha</i>	4	-	-	-	-	4	-
	Funariaceae	<i>Physcomitrella patens</i>	2	-	-	-	2	-	-
	Sphagnaceae	<i>Sphagnum fallax</i>	3	-	-	-	-	3	-
Tracheophyte	Selaginellaceae	<i>Selaginella moellendorffii</i>	9	-	-	-	-	9	-
Angiosperm	Bromeliaceae	<i>Ananas comosus</i>	2	-	-	-	2	-	-
	Amborellaceae	<i>Amborella trichopoda</i>	5	-	-	-	5	-	-
	Musaceae	<i>Musa acuminata</i>	4	-	-	-	3	1	-
	Araceae	<i>Spirodela polyrhiza</i>	1	-	-	-	1	-	-
	Zosteraceae	<i>Zostera marina</i>	1	-	-	-	-	1	-
Grass	Poaceae	<i>Brachypodium distachyon</i>	12	-	-	-	10	2	-
	Poaceae	<i>Brachypodium stacei</i>	12	-	-	-	10	2	-
	Poaceae	<i>Oryza sativa v7</i>	11	-	-	-	10	1	-
	Poaceae	<i>Oropetium thomaeum</i>	2	-	-	-	1	1	-
Panicoideae	Poaceae	<i>Panicum hallii</i>	15	-	-	-	13	2	-
	Poaceae	<i>Panicum virgatum</i>	23	-	-	-	16	7	-
	Poaceae	<i>Setaria italica</i>	15	-	-	-	13	1	-
	Poaceae	<i>Setaria viridis</i>	17	-	-	-	15	2	-
	Poaceae	<i>Sorghum bicolor</i>	16	-	-	-	13	3	-
	Poaceae	<i>Zea mays Ensembl</i>	10	-	-	-	9	1	-
	Poaceae	<i>Zea mays PH207</i>	9	-	-	-	7	2	-
Eudicot	Ranunculaceae	<i>Aquilegia coerulea</i>	16	2	-	-	5	9	-
Pentapetalae	Amaranthaceae	<i>Amaranthus hypochondriacus</i>	13	4	-	-	2	7	1
Asterid	Apiaceae	<i>Daucus carota</i>	53	7	-	-	3	43	2
	Phrymaceae	<i>Mimulus guttatus</i>	27	17	1	-	2	7	2
	Solanaceae	<i>Solanum lycopersicum</i>	20	7	-	-	7	6	2
	Solanaceae	<i>Solanum tuberosum</i>	19	7	-	-	6	6	2
	Crassulaceae	<i>Kalanchoe fedtschenkoi</i>	10	8	-	-	1	1	-
	Crassulaceae	<i>Kalanchoe laxiflora</i>	18	12	-	-	5	1	-
Rosid	Myrtaceae	<i>Eucalyptus grandis</i>	27	22	-	-	2	3	3
	Vitaceae	<i>Vitis vinifera</i> <i>Genoscope</i>	3	2	-	-	-	1	-
Malpighiales	Linaceae	<i>Linum usitatissimum</i>	25	10	-	-	-	15	3
	Euphorbiaceae	<i>Manihot esculenta</i>	17	12	-	-	-	5	3
	Salicaceae	<i>Populus trichocarpa</i>	65	24	-	1	2	38	9
	Euphorbiaceae	<i>Ricinus communis</i>	15	12	-	-	2	1	2
	Salicaceae	<i>Salix purpurea</i>	47	23	-	-	-	24	7

Citrus	Rutaceae	<i>Citrus sinensis</i>	23	11	-	-	1	11	3
	Rutaceae	<i>Citrus clementina</i>	41	16	-	-	1	24	4
Brassicales- Malvales	Caricaceae	<i>Carica papaya</i>	12	6	-	-	2	4	1
	Malvaceae	<i>Gossypium raimondii</i>	39	14	-	-	1	24	2
	Malvaceae	<i>Theobroma cacao</i>	33	13	-	-	3	17	3
Brassicaceae	Brassicaceae	<i>Arabidopsis halleri</i>	10	4	1	-	1	4	1
	Brassicaceae	<i>Arabidopsis lyrata</i>	26	15	2	2	2	5	3
	Brassicaceae	<i>Arabidopsis thaliana</i>	28	17	3	2	2	4	3
	Brassicaceae	<i>Boechera stricta</i>	24	14	3	2	1	4	1
	Brassicaceae	<i>Brassica oleracea capitata</i>	19	11	2	2	2	2	2
	Brassicaceae	<i>Brassica rapa FPsc</i>	36	23	2	2	2	7	4
	Brassicaceae	<i>Capsella grandiflora</i>	25	15	2	3	1	4	3
	Brassicaceae	<i>Capsella rubella</i>	28	18	2	3	3	2	3
	Brassicaceae	<i>Eutrema salsugineum</i>	30	17	2	2	2	7	2
	Fabidae	Cucurbitaceae	<i>Cucumis sativus</i>	23	9	-	-	-	14
Rosaceae		<i>Fragaria vesca</i>	17	11	-	-	2	4	2
Fabaceae		<i>Glycine max</i>	43	22	-	1	6	14	5
Rosaceae		<i>Malus domestica</i>	3	1	-	-	1	1	-
Fabaceae		<i>Medicago truncatula</i>	26	12	-	-	4	10	3
Fabaceae		<i>Phaseolus vulgaris</i>	33	17	-	1	4	11	3
Rosaceae		<i>Prunus persica</i>	33	17	-	-	4	12	2
Fabaceae		<i>Trifolium pratense</i>	12	10	1	-	-	1	3
Chlorophyte	Chlamydomonadaceae	<i>Chlamydomonas reinhardtii</i>	2	-	-	-	-	2	-
	Dunaliellaceae	<i>Dunaliella salina</i>	0	-	-	-	-	-	-
	Volvocaceae	<i>Volvox carteri</i>	2	-	-	-	-	2	-
	Coccomyxaceae	<i>Coccomyxa subellipsoidea C-169</i>	1	-	-	-	-	1	-
	Mamiellaceae	<i>Micromonas pusilla CCMP1545</i>	0	-	-	-	-	-	-
	Mamiellaceae	<i>Micromonas sp. RCC299</i>	1	-	-	-	-	1	-
	Bathycoccaceae	<i>Ostreococcus lucimarinus</i>	1	-	-	-	-	1	-

* Active site composition was not defined.

** Monolignol dehydrogenases were identified.

Phylogenetic tree was obtained from <https://phytozome.jgi.doe.gov/pz/portal.html>.

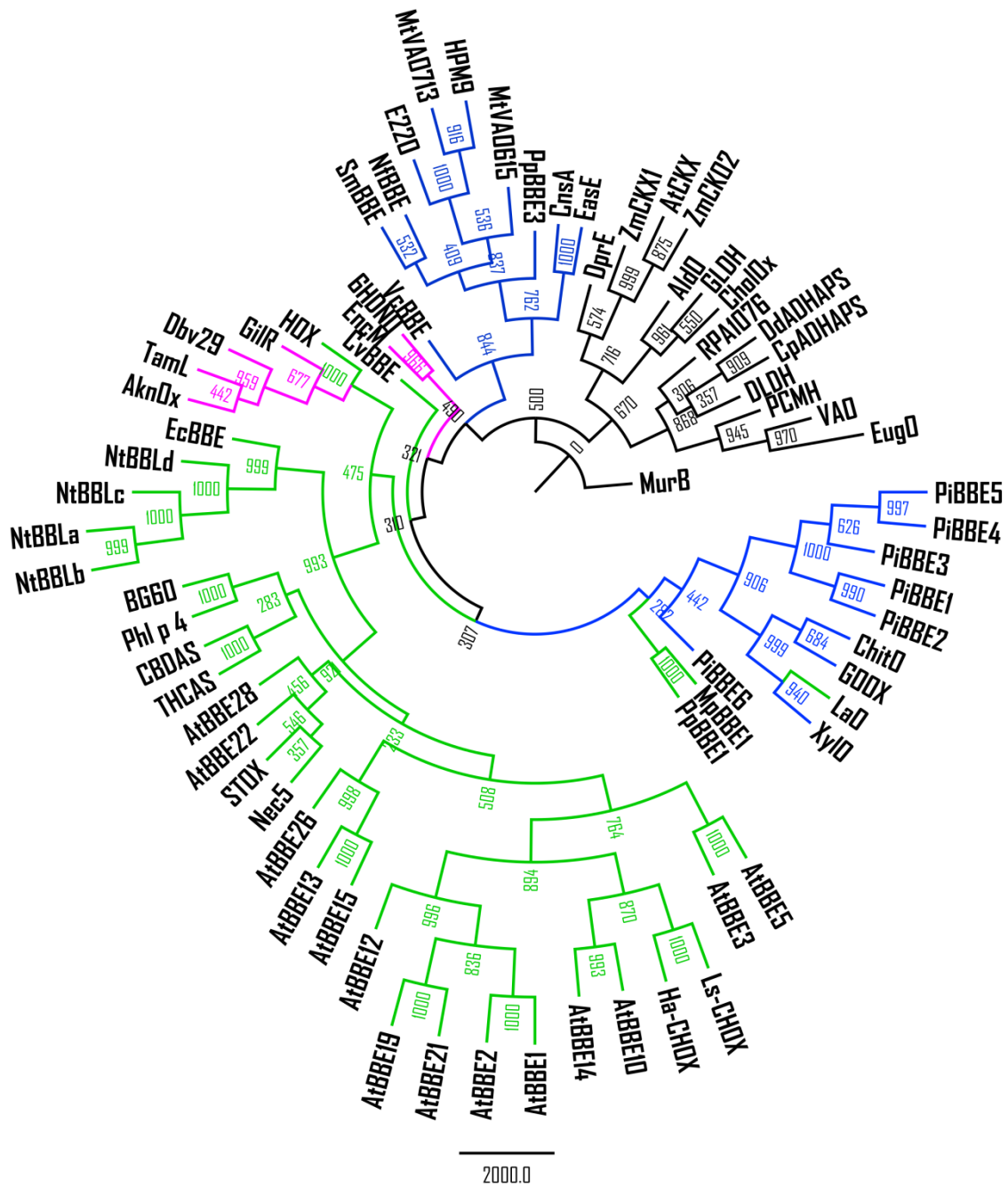


Figure S1: Phylogenetic tree of the FAD linked oxidase superfamily including bootstrap values. For a detailed description see Figure 5.

CHAPTER 5

Berberine bridge enzyme-like proteins in *Arabidopsis thaliana* participate in monolignol metabolism and stress response

Author contributions

The phenotype analysis mainly of the monolignol oxidoreductases, *AtBBE*-like protein 13 and 15, can be regarded as the main objective of this PhD project. Initial phenotyping studies were performed by Dr. Eric van der Graaff at the Institute of Biology, Section Plant Sciences (Karl-Franzens University of Graz) and I continued his work at the Department of Plant and Environment Sciences (University of Copenhagen, Denmark). I performed salt stress experiments with T-DNA insertional mutant lines of all *AtBBE*-like proteins in *A. thaliana* to investigate the salt tolerance. Further, I engineered Promoter GUS-transgenic lines of the most important *AtBBE*-like protein lines. At the Institute of Biology, I performed further abiotic stress experiments *in vitro* and *in vivo* under the supervision of Dr. Alexandra Jammer. Moreover, I performed experiments to analyze the lignin content and composition of putative *Atbbe*-like protein mutants with collaboration partners.

Chapter 5

5. Berberine bridge enzyme-like proteins in *Arabidopsis thaliana* participate in monolignol metabolism and stress response

5.1. Abstract

Berberine bridge enzyme (BBE)-like enzymes form a large family within the plant kingdom and are involved in a variety of biochemical reactions. Today these proteins are found in virtually all plants and this general abundance of BBE-like enzymes attracts the interest in this protein family. Within the clade of Viridiplantae, BBE-like enzymes occur in every subgroup, with increasing numbers in vascular plants. The model plant *Arabidopsis thaliana* belongs to the family of Brassicaceae and possesses 27 genes encoding for BBE-like proteins. This protein family is the focus of the present study highlighting first *in vivo* results under abiotic stress, mainly of the recently biochemically characterized members, termed *AtBBE*-like protein 13 and 15. Both enzymes were identified as monolignol oxidoreductases, suggesting an involvement in lignification. Putative T-DNA insertional mutant lines for *AtBBE*-like protein 13 and 15 were obtained and exhibited a reproducible phenotype with lower salt stress tolerance than the wild type. This phenotype could be confirmed on soil for the putative *Atbbe*-like protein 13 mutant. Furthermore, we generated a putative double *Atbbe*-like protein 13*15 mutant line with the same salt stress sensitivity on soil as the putative single knock-out *Atbbe*-like protein 13. The structure of another member, *AtBBE*-like protein 28, has recently been elucidated, and a T-DNA insertion line also showed a phenotype with higher salt sensitivity in *in vitro* experiments. Additionally, lignin analysis of the putative loss-of-function mutants for *Atbbe*-like protein 13 and 15 revealed a lower aldehyde content and a reduction of the total lignin amount. Initial phenotyping studies under drought stress were performed, and additionally, primary root growth and biomass production were investigated. In the future, the localization of *AtBBE*-like enzymes in plants will be addressed by employing the GUS reporter system. First results showed an involvement of monolignol oxidoreductases in stress response and lignification and suggest further detailed analysis to understand the *in planta* function of *AtBBE*-like family members.

5.2. Introduction

The berberine bridge enzyme (BBE) from California poppy (*Eschscholzia californica*) is the namesake of the ever faster growing BBE-like enzyme family, which forms a subgroup of the FAD-linked oxidases superfamily (SCOPE d.58.32). Characteristic for these enzymes is the structural architecture initially detected for vanillyl-alcohol oxidase, which is referred to as the VAO-fold. All members of the BBE-like enzyme family feature a FAD-binding domain and a substrate binding domain, also termed cap domain [1][2]. The main structural feature of all BBE-like enzymes is the highly conserved C-terminal element, but nevertheless members of this subfamily are very diverse in their functions. *EcBBE* is involved in the biosynthesis of benzyloquinoline alkaloids and catalyzes the formation of (*S*)-reticuline to (*S*)-scoulerine, leading to an oxidative ring closure and to a C-C bond (also termed “berberine bridge”) [3]. *EcBBE* possesses a bicovalently linked FAD cofactor featuring the characteristic 6-*S*-cysteinyl-, 8 α -*N*1-histidyl-FAD linkage, which was only found in the BBE-subfamily of the FAD-linked oxidases [4]. The bicovalent attachment of FAD has not been found in any other family of flavoproteins and was first observed in glucooligosaccharide oxidase (GOOX) from *Acremonium strictum* [5][6]. A bicovalent linked flavin shows a 300 mV higher redox potential compared to free flavin [7], and it seems to play a role in the correct positioning of the substrate to the isoalloxazine ring [6][8][9]. Additionally, a functional role in stabilizing the architecture of the active site and in preventing the cofactor dissociation in enzymes that accept bulky substrates could be observed [6][8][10][11][12][13].

The oxidation of substrates of various BBE-like enzymes results in the reduction of the flavin cofactor, which needs to be reoxidized for the next catalytic turnover. Oxidases need molecular oxygen to reoxidize the reduced FAD, leading to the formation of hydrogen peroxide. In BBE-like enzymes, a specific oxygen binding pocket has been identified on the *re*-side of the flavin cofactor opposite to the substrate binding region, and this feature is typical for all members of the FAD-linked oxidase superfamily [1][14]. The catalytic reaction consists of two half reactions, the reductive and oxidative reaction. The activation of oxygen takes place on the *re*-side of the isoalloxazine ring in most of the BBE-like enzymes, and the amino acids on the *si*-side are involved in substrate binding, leading to substrate oxidation and reduction of the cofactor. The involved amino acid residues of the active site show different types, for example, in the Brassicaceae family we identified four different active site types that frequently appear [12][15]. There are 27 BBE-like enzymes in *A. thaliana*, and 13 members show the active site type I, which has been described for monolignol dehydrogenases [15][16]. Further, BBE-like enzymes with active site type I have been described as carbohydrate oxidases (in sunflower and

lettuce) and e.g. *AtBBE*-like protein 3 (FOX1) is able to oxidize “gluco-oligomers” and 4-hydroxy indole-3-carbonyl nitrile, respectively [17][18]. *AtBBE*-like protein 28 shows the active site type II, featuring a mono-covalent linkage of a histidine to the 8 α -position of the flavin-isoalloxazine ring. Active site type III is a mixture of type I and II [12][14]. The fourth active site type has been found in fungal BBE-like enzymes like XylO (xylooligosaccharide oxidase), ChitO (chitooligosaccharide oxidase) and LaO (carbohydrate oxidase) and was first described for GOOX from *A. strictum* [5]. Additionally, type IV could be found in BBE-like enzymes in the Poaceae family such as Phl p 4 and BG60 [19][20][21][22][23].

5.2.1. Occurrence and function of BBE-like proteins in the plant kingdom

BBE-like proteins are widespread in different organisms, and currently, the superfamily (Pfam 08031) comprises 6382 sequences found in fungi, plants, bacteria and in archaea, as summarized in a comprehensive review by Daniel *et al.* [14]. In plants, 1372 sequences were found in 60 species, and BBE-like enzymes are strongly represented in land plants and form a multigene family. BBE-like enzymes could be found in every subgroup within the clade of Viridiplantae (green plants), in both basal and higher plants (see Chapter 4, Supplementary Table S2; Phylogenetic tree was used from <https://phytozome.jgi.doe.gov/pz/portal.html>). However, the number of BBE-like proteins increased with the order of the plants. The clade of Chlorophyta forms a division of the green algae and is the second basal division of Viridiplantae next to the clade of Streptophyta. Chlorophytes contain both unicellular and multicellular species, and all members of the clade feature flagellated cells [24]. Not all members of the Chlorophytes sequenced to date show genes encoding for BBE-like proteins and the green alga *Volvox carteri* is the only organism harboring two BBE-like genes, but most of them have one or no gene. Furthermore, these BBE-like genes have no known active site type. Embryophyta, informally named as “land plants”, form a clade within the Phragmoplastophyta, a green algae group belonging to the clade Streptophyta [25]. The number of BBE-like genes is higher within the Embryophytes, even lower organisms such as the mosses show more proteins, such as four in *Marchantia polymorpha*, three in *Sphagnum fallax* and two in *Physcomitrella patens*. In addition, *P. patens* is the lowest species with a defined active site type IV. With a higher level of development, the organisms show a higher number of BBE-like proteins. Tracheophytes, also called vascular plants, are known as those land plants with lignified tissues for conducting water and minerals throughout the plant. The model organism *Selaginella moellendorffii* is a representative for a lower Tracheophyte and belongs to the group LycopHYta; its genome includes nine BBE-like genes. The next higher group is formed by the Angiosperms, including monocotyledonous and dicotyledonous plants. The average number of BBE-like

genes has increased during evolution from three in lower Angiosperms to nine and fifteen in grasses and Panicoideae, respectively. *Panicum virgatum*, commonly known as switchgrass, shows the highest number of 23 BBE-like genes within the family of Poaceae. Almost every representative within the family Poaceae contains BBE-like proteins with an active site type IV. Within the eudicots, other active site types start to appear, and within the group of Pentapetalae, Asteridae, Rosidae, Malpighiales, Citrus and Brassicales-Malvales plants harbor BBE-like proteins with an active site type I as well as proteins with active site type IV. The first BBE-like protein with an active site type I was found in *Aquilegia coerulea*, the lowest species of eudicots. Interestingly, active site types II and III seem to be restricted to the family of Brassicaceae. Also the average number of BBE-like genes has generally increased throughout evolution, with fifteen in Pentapetalae, twenty-five in Asterids, thirty-four in Malpighiales, thirty-two in Citrus, twenty-eight in Brassicales-Malvales, twenty-five in Brassicaceae and twenty-four in Fabidae. A considerable number of BBE-like genes can be found in *Populus trichocarpa* and *Daucus carota* with 65 and 53, respectively. Active site type I is the most prominent type within the eudicots, and approximately half of all analyzed species possess active site type I, and a quarter of those also possess active site type IV. All active site types are present in eight Brassicaceae species, containing the model organism *A. thaliana*, and interestingly, they are absent in all other plant species [12][14].

5.2.2. Catalytic and physiological function of BBE-like enzymes in plants

Due to the high number of BBE-like enzymes in plant species, a great interest in their function aroused. *EcBBE* is involved in benzyloquinoline alkaloid biosynthesis [3] leading to the formation of protoberberine, protobine or benzophenanthridine alkaloids [26]. Also Δ^1 -tetrahydrocannabinolic acid (THCA) synthase and cannabidiolic-acid (CBDA) synthase from *Canabis sativa* catalyze complex reactions and convert cannabigerolic-acid to THCA and CBDA, respectively. Those enzymes play an important role in cannabinoid metabolism and leading to the formation of the psychoactive agent tetrahydrocannabinol (THC) and cannabidiol (CBD), respectively [27][28][29]. Another BBE-like enzyme which is involved in benzyloquinoline alkaloid biosynthesis is the (*S*)-tetrahydroprotoberberine oxidase (STOX) from *Argemone mexicana* and *Berberis wilsoniae*. The enzyme is able to oxidize (*S*)-tetrahydropalmatine to palmatine in both species, and further investigations of substrate specificity have shown an additional acceptance of (*S*)-scoulerine and (*S*)-canadine in *B. wilsoniae* and of (*S*)-coreximine in *A. mexicana* [30]. Further, four BBE-like enzymes belonging to the oxidoreductase subfamily were found in a late step of nicotine biosynthesis in tobacco (*Nicotiana tabacum*) by Kajikawa *et al.* [31] and these enzymes (*NtBBLa*, *NtBBLb*,

NtBBLc, *NtBBLd*) have an effect on the nicotine and anabasine level. Nicotine and related pyridine alkaloids, such as anatabine, act as chemical plant defense and are toxic to all herbivores [32]. However, BBE-like proteins do not only play a role in alkaloid biosynthesis, but they are also very well represented in plant physiology in many secondary metabolic pathways [33]. In plants, carbohydrates are often oxidized to the corresponding lactones by BBE-like enzymes, and one representative of these enzymes is hexose oxidase (HOX) from the red alga *Chondrus crispus*. HOX has a broad substrate range and oxidizes a variety of oligomer sugars such as lactose, maltose, cellobiose and maltotriose as well as glucooligosaccharides. Additionally, the enzyme shows a high affinity for glucose and galactose [34][35]. Another BBE-like enzyme with carbohydrate oxidase activity is Nec5 (nectarin 5) from ornamental tobacco (*Nicotiana langsdorffii* X *N. sanderae*), which oxidizes glucose to gluconolactone and hydrogen peroxide [36]. Nec5 seems to play a role in plant defense, and it has been postulated that high levels of hydrogen peroxide contribute to floral defense against microbial growth [37]. Furthermore, the BBE-like enzyme from timothy grass Phl p 4 (major pollen allergen) also shows glucose oxidase activity and is involved in plant reproduction, and shows a high sequence similarity to BG-60 from Bermuda grass (*Cynodon dactylon*) [19]. Further BBE-like enzymes which could be identified as carbohydrate oxidases are *Ha*-CHOX from sunflower (*Helianthus annuus*) and *Ls*-CHOX from lettuce (*Lactuca sativa*). Both enzymes participate in plant immune response due to their antimicrobial effects against pathogens and their substrate acceptance for the majority of mono- and disaccharides. The enzymes convert glucose to gluconolactone and extracellular hydrogen peroxide is produced during substrate conversion. Hydrogen peroxide could be observed as the first antimicrobial response against pathogen attack [18]. Both enzymes showed a high upregulation after pathogenic treatment, and the same immune response could be found in two closely related BBE-like enzymes of *A. thaliana*, in *At*BBE-like enzyme 10 and 20 [14][15].

The model plant *A. thaliana* exhibits 27 BBE-homologs, termed *At*BBE-like protein 1-28 because of two isoforms of one gene (*At*4g20830/*At*BBE-like 19/20) [38][15]. In recent years, the function of some *At*BBE-like proteins could be identified, such as *At*BBE-like protein 3 by Rajniak *et al.* [17]. They investigated metabolites within the biosynthetic pathway from tryptophan to 4-hydroxyindole-3-carbonyl nitrile (4-OH-ICN) in *A. thaliana* under pathogen defense. Within the proposed biosynthetic pathway, a flavin-dependent oxidoreductase, also referred to as FOX1 [39] and *At*BBE-like protein 3, catalyzes the reaction from indole cyanohydrin to indol-3-carbonyl nitrile and is up-regulated under pathogen stress. *At*BBE-like protein 3 is positioned in the same gene cluster as *At*BBE-like enzymes 4, 5, 6 and 7 which

suggests a similar function in plant metabolism, and those enzymes show an up-regulation by osmotic stress and pathogen attack according to Daniel *et al.* [15]. We could identify the function of two further members of the *AtBBE*-like enzyme family, *AtBBE*-like protein 13 and 15, which are presumably involved in lignification. The two proteins were identified as monolignol oxidoreductases, converting the monolignols sinapyl-, coniferyl- and *p*-coumaryl alcohol to their corresponding aldehydes. Daniel *et al.* [15] proposed that monolignol oxidoreductases have an impact on the composition of lignin in the plant cell wall due to a change of the extracellular pool of monolignols to the aldehydes. Furthermore, an extracellular location of *AtBBE*-like protein 15 in the apoplastic fluid of the plant cell wall has been confirmed by mass spectrometric analysis [40][41]. The natural electron acceptor of both *AtBBE*-like protein 13 and 15 is still unknown yet, but a similar mechanism as for cytokinin dehydrogenases is assumed [14]. In cytokinin dehydrogenases, electrons are transferred from the natural electron acceptor benzoxazinones to laccases and peroxidases, which are also responsible for the oxidation of monolignols to their radical forms prior to lignin polymerization [42][43].

More recently, an involvement of *AtBBE*-like protein 13 in the auxin-induced callus formation in *A. thaliana* was discovered by Xu and coworkers [44]. They showed that auxin stabilizes the transcription factor *AtbZIP59* (*Arabidopsis* basic region/leucine zipper motif 59) and enhances the interaction with the transcription factor LBD (Lateral Organ Boundaries Domain), which leads to the auxin-induced callus formation. This complex targets the transcription of FAD-BD (FAD-binding Berberine, also termed as *AtBBE*-like protein 13) with subsequent influence on callus formation. According to microarray data on the Arabidopsis eFP Browser (<http://bar.utoronto.ca/efp/cgi-bin/efpWeb.cgi>), *AtBBE*-like protein 13 is expressed in the lateral root primordia and the xylem pole pericycle. On the one hand, the pericycle strengthens the root and protects the vascular bundles [45], and on the other hand the xylem pole pericycle regulates the formation of the lateral root [46]. Therefore, high expression values could be found during lateral root initiation. Further, *AtBBE*-like protein 13 is involved in the regeneration of root and shoot (Summary of expression values see Supplementary Table S7). *AtBBE*-like protein 15 is highly expressed in the root xylem, and further up-regulation could be seen during seed development, especially in the chalazal endosperm of the mature green stage of the seed. Both *AtBBE*-like protein 13 and 15, and also other *AtBBE*-like enzymes showed an upregulation under osmotic stress and under the treatment with pathogens [47].

Another interesting BBE-like protein in *A. thaliana* with a suspected monolignol oxidoreductase function is *AtBBE*-like protein 26. *AtBBE*-like enzyme 26 shows the same

amino acid residues in the active site and substrate binding pocket as *AtBBE*-like protein 13 and 15, suggesting the same enzymatic function and an involvement in lignin metabolism. *AtBBE*-like protein 26 is located in the root procambium and shows, in comparison to *AtBBE*-like 13 and 15, a higher upregulation under various stress factors, especially under drought and salt stress, and also under the exposure to the fungus *Botrytis cinerea* and the pathogen *Pseudomonas syringae* [47].

Recently, four further BBE-like enzymes from the phylogenetic subgroup 5 in *A. thaliana* with a function in plant immunity were identified by an Italian research group. They identified the function of four *AtBBE*-like proteins termed OG OXIDASE or OGOX1-4 (OGOX1/*AtBBE*-like 20; OGOX2/*AtBBE*-like 21; OGOX3/*AtBBE*-like 2; OGOX4/*AtBBE*-like 1), which are able to oxidize and inactivate oligogalacturonides (OGs). Oxidized OGs show a reduced influence on the plant immune response and are less hydrolysable by fungal polygalacturonases. *AtBBE*-like protein 8 showed no OG-oxidizing activity but could be identified as a carbohydrate oxidase by multiple amino acid alignments with other well-known carbohydrate oxidases such as *Ha*-CHOX and *Ls*-CHOX [48].

The biochemical function of seven BBE-like enzymes (*AtBBE*-like 3/FOX1; *AtBBE*-like 1, 2, 20 and 21/ OGOX1-4; *AtBBE*-like 13 and 15/Monolignol oxidoreductases) in *A. thaliana* could be discovered so far, but the enzymatic function of twenty further proteins is still unknown, which makes them enigmatic for us. The crystallographic structure of the oxidase *AtBBE*-like protein 28, a member of phylogenetic group 1, could be elucidated, but the natural substrate of this flavoprotein is still unknown [12].

In this study, we investigated the phenotype of putative loss-of-function *AtBBE*-like protein mutant plants in *A. thaliana* under standard growth conditions and abiotic stress, such as salt and drought. We chose the monolignol oxidoreductases *AtBBE*-like protein 13, 15 and 26 for a closer analysis. We performed initial studies with putative homozygous T-DNA knock-out lines, and especially salt stress experiments showed reproducible effects on plant growth and development. Furthermore, we examined *Atbbe*-like protein 13 and 15 mutants regarding to their influence on lignin metabolism and we analyzed the lignin composition. In addition, we chose the putative *Atbbe*-like protein 28 mutant line for initial studies of root growth and development.

5.3. Experimental Procedures

All standard chemicals were purchased from Sigma-Aldrich (St. Louis, USA) or Carl Roth (Karlsruhe, Germany) and were of the highest grade commercially available. Restriction enzymes, T4 DNA ligase and FastAP™ were purchased from Thermo Fisher Scientific (Waltham, Massachusetts, USA). Restriction enzymes were obtained either from Thermo Fisher Scientific (Waltham, Massachusetts, USA) or from New England Biolabs (Ipswich, Massachusetts, USA). Q5® High Fidelity Polymerase was received from New England Biolabs (Ipswich, Massachusetts, USA) and the KAPA2G Fast Ready Mix with Dye was obtained from Sigma-Aldrich (St. Louis, USA). The Gene JET Plasmid Miniprep Kit and Gene JET PCR Purification Kit were purchased from Thermo Fisher Scientific (Waltham, Massachusetts, USA). The NucleoSpin® Gel and PCR Clean-up was purchased from Machery-Nagel (Düren, Germany). The used bacterial strains and growth conditions are depicted in Supplementary Table S1 and PCR products and plasmids (for vector maps, see Supplementary Figure S1) were sequenced by LGC genomics (Berlin, Germany) or Microsynth Austria (Vienna, Austria) to ensure correct gene integration. The Murashige & Skoog (MS) medium including vitamins and Micro Agar were purchased from Duchefa Biochemie (Haarlem, The Netherlands).

5.3.1. Plant materials and growth conditions

A. thaliana ecotype Columbia 0 (Col-0) and transgenic plants were grown on soil (Naturahum; Gramoflor, Vechten, Germany) in growth cabinets (KK1200; Pol-Eko Aparatura, Wodisław Śląski, Poland) with a photosynthetically active radiation of $130 \mu\text{mol m}^{-2}\text{s}^{-1}$ or in a greenhouse. For the generation of seeds, Col-0 and transgenic plants were grown in parallel in soil to ensure equal seed quality, under long day conditions (16 h/8 h day/night cycle) at 24 °C/20 °C (day/night) and 50% humidity in growth cabinets or in a greenhouse under long day conditions with 16 h photoperiod at 20–22 °C and a relative humidity of 70% as described by Hyun *et al.* [49]. *A. thaliana* (Col-0 background) T2 T-DNA insertion lines were obtained for the *AtBBE*-like 1 (1) (SALK_097190 (BN)), *AtBBE*-like 2 (2) (SAIL_278_A03), *AtBBE*-like 3 (1) (GK-813E 08), *AtBBE*-like 4 (1) (GK-393H02), *AtBBE*-like 5 (1) (SALK_045724 (AH)), *AtBBE*-like 6 (1) (SALK_054180 (AL)), *AtBBE*-like 7 (1) (SALK_079001), *AtBBE*-like 8 (2) (SALK_117810C), *AtBBE*-like 9 (1) (SALK_150104C), *AtBBE*-like 9 (2) (SALK_112240C), *AtBBE*-like 10 (1) (GK-650C11), *AtBBE*-like 11 (2) (SAIL_197_F12), *AtBBE*-like 12 (1) (SALK_129845C), *AtBBE*-like 13 (1) (SALK_000581(F)), *AtBBE*-like 14 (1) (GK-389A02), *AtBBE*-like 15 (1) (SALK_069340C), *AtBBE*-like 16 (1) (SALK_129633), *AtBBE*-like 17 (1) (GK-338B11), *AtBBE*-like 17 (2) (SALK_143616), *AtBBE*-like 18 (2) (SALK_026974C),

AtBBE-like 19/20 (1) (SALK_089056 (AO) (AS)), *AtBBE*-like 21 (1) (SALK_143967), *AtBBE*-like 22 (1) (SAIL_862_H01), *AtBBE*-like 22 (2) (SALK_131268 (BW)), *AtBBE*-like 23 (1) (WiscDsLox472A5), *AtBBE*-like 24 (1) (GK-212D10), *AtBBE*-like 25 (1) (SALK_083990C), *AtBBE*-like 26 (1) (SALK_069865 (AR)), *AtBBE*-like 26 (2) (SAIL_31_A05), *AtBBE*-like 27 (1) (SALK_022408 (AZ)), *AtBBE*-like 27 (2) (SALK_139244 (BY)) and *AtBBE*-like 28 (1) (SALK_007813) gene from the European Arabidopsis Stock Centre (NASC, University of Nottingham, Loughborough, UK) from the SALK, SAIL, GABI-KAT and WISC mutant collection [50] (for NASC order, see Supplementary Table S2). Homozygous T3 seeds were generated and confirmed by growth of the seedlings on half strength MS medium [51] containing selecting agents (50 mg/L; kanamycin for SALK, BASTA (glufosinate) for SAIL and Wisconsin DsLOX, and sulfadiazine for GABI-KAT). Homozygous individuals of *Atbbe*-like protein 13, 15, 26 and 28 of the T3 progeny were isolated, the DNA was extracted by CTAB method [54] and confirmed by PCR genotyping using the following primers: *Atbbe*-like 13-F 5'-TTAAGAAGCGGTGGTCAT-3', *Atbbe*-like 13-R 5'-CATACTTTTGCG-TAAACCC-3', *Atbbe*-like 15-F 5'-GCCCTATTCGTTACAAC-3', *Atbbe*-like 15-R 5'-TTCCAGGCCAATATCAC-3', *Atbbe*-like 26 (1)-F 5'-TCTCATAG-TCTTCATTACCC-3', *Atbbe*-like 26 (1)-R 5'-GAACGTTTTCTCAAGTGG-3' and Salk-LBa1 5'-TGGTTCACG-TAGTGGGCCATCG-3'. The putative double *Atbbe*-like protein 13*15 mutants were generated by crossing homozygous *Atbbe*-like 13 and 15 plants. Homozygous individuals were isolated in the F2 generation and confirmed by PCR genotyping using the primers mentioned above. For growth and stress experiments on plates, homozygous seeds of transgenic plants (*Atbbe*-like protein 1, 2 (2), 3, 4, 5, 6, 7, 8 (2), 9, 9 (2), 10, 11 (2), 12, 13, 14, 15, 16, 17, 17 (2), 18 (2), 19/20, 21, 22, 22 (2), 23, 24, 25, 26, 26 (2), 27, 27 (2), 28, 13*15) and Col-0 were surface-sterilized in 70% ethanol for 1 min and incubated in 1.2% sodium hypochlorite with 1 drop Tween 20 for 10 min, followed by washing twice with sterile distilled water and suspending in 0.1% (w/v) agarose solution. Afterwards, seeds were plated on half strength MS medium [51] containing 2.2 g/L MS, 0.5 g/L MES and 8 g/L Micro Agar at pH 5.7 supplemented with selection agent or 100 mM NaCl for salt stress. Plates were cold treated in the dark at 4 °C for 2 days for stratification.

5.3.2. Construction of *GUS* reporter transgenic plants

The genomic DNA (gDNA) of *A. thaliana* Col-0 was extracted by using the CTAB method [52]. The promoter regions of *AtBBE*-like protein 13 (1962 bp), *AtBBE*-like protein 15 (1502 bp), *AtBBE*-like protein 24 (936 bp), *AtBBE*-like protein 25 (1175 bp), *AtBBE*-like protein 26 (2074 bp), *AtBBE*-like protein 27 (1037 bp) and *AtBBE*-like protein 28 (1917 bp)

were amplified by PCR according to the protocol of Q5[®] High Fidelity DNA Polymerase from New England Biolabs (Ipswich, Massachusetts, USA) with gene specific primers (oligonucleotides for amplification see Supplementary Table S3). The amplified promoter fragments were cloned by standard techniques into an adapted promoter GUS reporter vector (Figure S1) to generate a construct (*AtBBE-likep:GUS*) harboring the *AtBBE*-like promoters upstream of the *GUS* reporter gene (β -glucuronidase *gusA(uidA)* EC 3.2.1.31). The plasmids containing the constructs were transformed into calcium competent *Escherichia coli* Top10 cells and selected on ampicillin selection medium (100 mg/L). The *AtBBE-likep:GUS* constructs were confirmed by Colony PCR (confirmation primers see Supplementary Table S3) and sequenced prior to cloning into the linearized plant transformation vector pHB325 (Figure S1) harboring a prokaryotic kanamycin resistance marker and a plant hygromycin resistance marker between the T-DNA borders. The pHB325 plasmids containing the *AtBBE-likep:GUS* constructs were transformed into calcium competent *E. coli* Top 10 cells and selected on kanamycin selection plates (50 mg/L). Plasmids confirmed by Colony PCR and sequencing were transferred by electroporation into *Agrobacterium tumefaciens* strain LBA4404 (Thermo Fisher Scientific, Waltham, Massachusetts, USA) containing the Ti plasmid with a streptomycin selection marker (50 mg/L). *AtBBE-likep:GUS* transgenic *Arabidopsis* plants were obtained by the standard floral dip method [53]. The plants were transformed about 5 days after clipping the inflorescence bolts above the first cauline leaf in order to enhance flower development and to increase the yield of transformation. Plants were incubated in closed containers for one night in dark, to increase humidity and to avoid damages from light, and were grown in a climate chamber (KK1200, Pol-Eko Aparatura, Wodisław Śląski, Poland) in long day conditions (16 h/8 h day/night cycle) at 24 °C/20 °C (day/night) and 50% humidity for generation of seed stocks. Seeds were dried at 37 °C for two weeks, and transgenic offspring were selected on half strength MS medium (2.2 g/L MS, 0.5 g/L MES and 8 g/L Micro Agar at pH 5.7) containing 20 mg/L hygromycin at continuous light at 23 °C and 60% humidity. Additionally, the selected individuals containing the *AtBBE-likep:GUS* construct were confirmed by PCR using the following confirmation primers: *AtBBE-like13p:GUS-F* 5'-CAGCAAAAACGATCACCC-3', *AtBBE-like15p:GUS-F* 5'-CTTTTTTTGGTTGGCGA-3', *AtBBE-like24p:GUS-F* 5'-GAGTCTCCTTTGATCACA-3', *AtBBE-like25p:GUS-F* 5'-GGTCACGTTGCTATCATT-3', *AtBBE-like26p:GUS-F* 5'-TGGCACTGAGTTTTTGT-3', *AtBBE-like27p:GUS-F* 5'-GACGTAACCTTATGA-3', *AtBBE-like28p:GUS-F* 5'-CTTGC-GGAGGATTTTTAC-3' and GUS reverse primer R 5'-ACTGATCGTTAAACTGCCTG-3'.

5.3.3. Construction of *AtBBE*-like overexpression transgenic plants

The gDNA of *AtBBE*-like protein 26 (2287 bp) and *AtBBE*-like protein 28 (1756 bp) were amplified by PCR using the gene-specific primers: *AtBBE*-like 26-F 5'-TACTGGATCCAACACCACACTAGTCACACACTTAAATG-3', *AtBBE*-like 26-R 5'-ATCAGCATGCCTTTAAATAGGATTCTCGAGTTGATTGAAG-3', *AtBBE*-like 28-F 5'-TACTGGATCCATCCACCTATCTTAGAAATGGAG-3' and *AtBBE*-like 28-R 5'-ATCAGCATGCAACATGAAAAGTTTATTCAACACAC-3' (Supplementary Table S3). The amplified fragments were cloned into the pEG278 vector (Figure S1) which features the constitutive CaMV 35S promoter to generate overexpression constructs. Plasmids harboring the *35S:AtBBE-like26* and *35S:AtBBE-like28* constructs were transferred into calcium competent *E. coli* Top 10 cells and selected on ampicillin medium (100 mg/L). *35S:AtBBE*-like constructs were confirmed by Colony PCR and sequencing and were cloned into the linearized plant transformation vector pHB325 (confirmation primers see Supplementary Table S3), transferred into calcium competent *E. coli* Top 10 cells and selected on kanamycin selection (50 mg/L) medium. The constructs were transferred to *A. tumefaciens* LBA4404 by electroporation and positive transformants were selected on streptomycin (50 mg/L) and kanamycin (50 mg/L) selection plates. Overexpression constructs confirmed by sequencing were transferred into *Arabidopsis* by the floral dip method as describe above [53] and grew under long day conditions (16 h/8 h day/night cycle) at 24 °C/20 °C (day/night) and 50% humidity in a growth chamber (KK1200, Pol-Eko Aparatura, Wodisław Śląski, Poland). Harvested seeds were dried at 37 °C for two weeks and transformants were selected on half strength MS medium (2.2 g/L MS, 0.5 g/L MES and 8 g/L Micro Agar at pH 5.7) with hygromycin selection (20 mg/L) and confirmed by PCR with following oligonucleotides: *35S* promoter forward primer F 5'-ACAATCCCACTATCCTTC-3', *35S:AtBBE-like26*-R 5'-GCTAAT-GAAGAAGTTGGTG-3' and *35S:AtBBE-like28*-R 5'-GAAAGCAAGAGATTTGGTG-3'.

5.3.4. Salt stress experiments on plates and soil

Surface-sterilized seeds (see *Plant materials and growth conditions*) from homozygous transgenic plants (*Atbbe*-like protein 1, 2 (2), 3, 4, 5, 6, 7, 8 (2), 9, 9 (2), 10, 11 (2), 12, 13, 14, 15, 16, 17, 17 (2), 18 (2), 19/20, 21, 22, 22 (2), 23, 24, 25, 26, 26 (2), 27, 27 (2), 28 and *Atbbe*-like 13*15) were germinated and grown in parallel with Col-0 in petri dishes on half strength MS medium (2.2 g/L MS, 0.5 g/L MES and 8 g/L Micro Agar at pH 5.7) with or without salt (100 mM NaCl) to determine differences in salt stress tolerance. The plates were incubated for 2 days in the dark at 4 °C, for stratification, prior to 14 days of incubation in growth cabinets

under short day conditions (8 h light) at 21 °C (light intensity: 180 $\mu\text{mol m}^{-2} \text{s}^{-1}$). For additional salt stress experiments with *Atbbe*-like protein 15 and 13*15, a climate chamber (Percival SE-41AR3; CLF Plant Climatics GmbH, Wertingen, Germany) with a light intensity of 200 $\mu\text{mol m}^{-2} \text{s}^{-1}$ in short day conditions 8 h/16 h (day/night cycle) at 24 °C/20 °C (day/night) was used. The seedlings were evaluated with an Olympus SZX16 Stereomicroscope, and photographs were taken with an Olympus U-CMAD3 camera (Olympus, Tokyo, Japan) using the CellSens Entry software. Seedlings were categorized according to their direct germination and growth phenotype: large and healthy green, small and healthy green, yellow and too small seedlings. In addition, the seedlings of the single *Atbbe*-like protein 15 and double *Atbbe*-like protein 13*15 mutant were evaluated in detail, with other categories: 0 = healthy with 4 or more green leaves; 1 = healthy with 2 green leaves; 2 = healthy with cotyledons and the first appeared leaves; 3 = healthy, mainly the cotyledons; 4 = very small, cotyledons not open, yellow; 5 = not germinated. Anthocyanin accumulation was also considered and evaluated (categories see Figure 1). The salt stress experiments on plates were performed in three biological replicates, with three technical replicates per transgenic line and 30 seeds of Col-0 and *Atbbe*-likes per plate. For salt stress experiments in soil, seeds were germinated and grown in soil in growth chambers (KK1200, Pol-Eko Aparatura, Wodisław Śląski, Poland) under short day conditions (8 h/16 h day/night cycle) at 24 °C/20 °C (day/night) and 50% humidity with illumination at 130 $\mu\text{mol m}^{-2} \text{s}^{-1}$ for 8 (first experiment) or 10 weeks (second experiment) prior to salt treatment. The soil experiments were performed with 10 pots per line (1 plant per pot) and in two independent biological replicates. To assay salt tolerance, Col-0 and transgenic plants (*Atbbe*-like protein 13, 15, 24, 25, 26) were treated in a first series 8 times (500 mL per tray with 10 pots) with a gradient of salt concentration (50, 100, 150 and 200 mM NaCl) every four days according to methods described previously [54][55]. Control plants were watered every fourth day in parallel. After 31 days of salt stress, plants were allowed to recover for 4 days, and pictures were then taken (Olympus ColorViewIII:Olympus; Olympus, Tokyo, Japan). Based on our first experiment, we used 200 mM NaCl for the second replicate without a gradient. 10-week-old plants were watered with 200 mM NaCl solution every four days for a period of 21 days and evaluated four days after the final treatment.

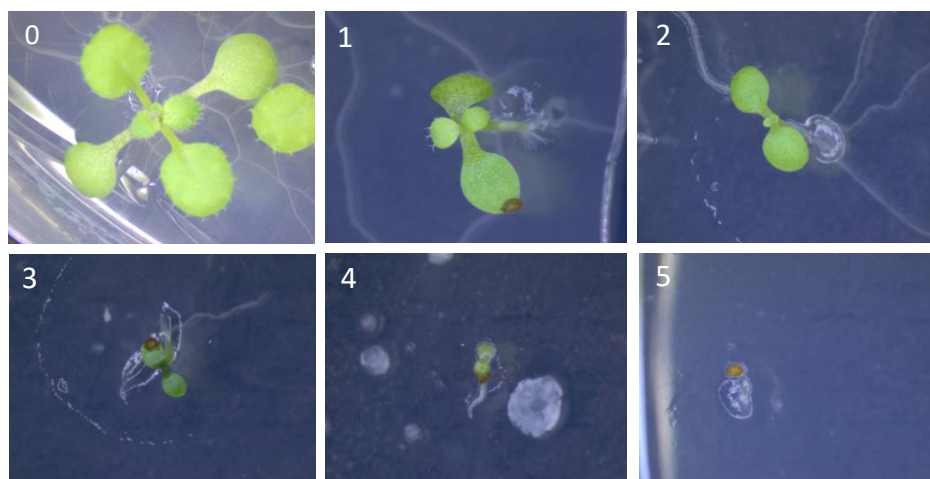


Figure 1. Evaluation of seedlings in categories. 0 = healthy with 4 or more green leaves (without cotyledons); 1 = healthy with 2 green leaves, 2 = healthy with cotyledons and the first appeared leaves; 3 = healthy, mainly the cotyledons; 4 = very small, cotyledons not open, yellow; 5 = not germinated. Plus 0.5 p for anthocyanins and chlorosis.

5.3.5. Drought stress experiments on PEG-infused plates

Surface-sterilized seeds (see *Plant materials and growth conditions*) of *Arabidopsis* plants Col-0 and *Atbbe*-like protein 13, 15, 26, and *Atbbe*-like protein 13*15 were germinated and grown in parallel under control conditions (half strength MS medium) and on half strength MS medium infused with Polyethylene glycol (PEG) [55]. In a previous experiment with *Atbbe*-like protein 15, germination was tested at different concentrations of PEG solution (250 g/L, 400 g/L and 550 g/L) (see Supplementary Figure S2). *Arabidopsis* seedlings were unable to germinate and grow on MS medium with 400 g/L and 550 g/L PEG. Based on our pre-experiments, we decided to use 250 g/L PEG overlay solution for the experiments with *Arabidopsis* seedlings. Half strength MS plates (100 mm diameter), containing 2.2 g/L MS, 0.5 g/L MES and 8 g/L Micro Agar at pH 5.7, were prepared first. An overlay solution containing PEG-8000 (half strength MS medium without agar) was poured on top of solidified MS plates in a ratio of 2:3 (v/v) agar to PEG to achieve a water potential of -0.5 MPa. Plates were incubated overnight for 12-15 h to allow the diffusion of PEG into the agar. After the incubation, the PEG solution was removed and plates were dried before use. Seeds on plates were incubated for 3 days in the dark at 4 °C prior to transfer to a growth chamber (Percival SE-41AR3; CLF Plant Climatics GmbH, Wertingen, Germany) with short day conditions (8 h/16 h day/night cycle) for 14 days with a light intensity of 200 $\mu\text{mol m}^{-2}\text{s}^{-1}$ at 24 °C/20 °C (day/night). The evaluation of the phenotype as affected by drought was carried out in the same manner as for salt stress experiments with detailed categories (Figure 1).

5.3.6. Root length and shoot weight experiments on plates under salt stress

Sterilized seeds (see *Plant materials and growth conditions*) of Col-0, *Atbbe*-like protein 13, 15, 26, 28 and *Atbbe*-like protein 13*15 were incubated for 2 days at 4 °C and germinated and grown on petri dishes with half strength MS medium (2.2 g/L MS, 0.5 g/L MES and 8 g/L Micro Agar at pH 5.7) under short day conditions (8 h/16 h day/night cycle) in a growth chamber (Percival SE-41AR3, CLF Plant Climatics GmbH, Wertingen, Germany) with a light intensity of 200 $\mu\text{mol m}^{-2}\text{s}^{-1}$ at 24 °C/20 °C (day/night) for 1 week. Seedlings were transferred to control and salt (100 mM NaCl) plates, with 7 wild type and mutant individuals per plate, and vertically grown for another week. The root length and biomass experiments were performed in 5 technical replicates, and Col-0 and *Atbbe*-like seedlings were weighed and measured separately for each plate. Pictures were taken with an Olympus ColorViewIII digital camera (Olympus, Tokyo, Japan). Primary root lengths were analyzed using the ImageJ software (Wayne Rasband, National Institute of Health, USA).

5.3.7. Preliminary test of quantitative RT-PCR (qRT-PCR) analysis under salt stress

Arabidopsis seeds of Col-0 were surface-sterilized as described in *Plant materials and growth conditions* and were grown on half strength MS medium (2.2 g/L MS, 0.5 g/L MES and 8 g/L Micro Agar at pH 5.7) in a growth chamber (KK1200, Pol-Eko Aparatura, Wodisław Śląski, Poland) under long-day conditions (16 h/8 h day/night cycle) at 24 °C/20 °C (day/night) and 50% humidity for one week. Seedlings were transferred to control (MS medium without salt) and salt plates (MS medium containing 100 mM NaCl) and incubated under long day conditions for 24 h. Seedlings were harvested and frozen in liquid nitrogen. Total RNA from *Arabidopsis* Col-0 seedlings (one technical replicate) was isolated using the Qiagen RNeasy plant mini kit according to the manufacturer's instructions (Qiagen, Hilden, Germany). Additionally, RNase-Free DNase from Qiagen (Hilden, Germany) was added, and incubated for 1 h at 37 °C, to obtain DNA-free RNA samples. The isolated RNA was reverse transcribed into cDNA using the iScript reverse transcriptase according to the protocol of the iScript™ cDNA Synthesis Kit from BIO-RAD (Vienna, Austria) for two-step RT-PCR. *AtBBE*-like protein 15 expression levels in seedlings were analyzed by qRT-PCR using the protocol of the SsoAdvanced™ SYBR® Green Supermix from BIO-RAD (Vienna, Austria). PCR amplification was performed according to the manual of BIO-RAD (Real-time Applications Guide) with oligonucleotides specific for *AtBBE*-like protein 15 gene: P1-F 5'-TGTACGAGACGCATGTCCAA-3' and P1-R 5'-TTTCGTCCTCGGCAACAAAC-3'; P2-F 5'-ACGTGGCAAGATGGGAAAGT-3' and P2-R 5'-ATACGCCTGTCTCGGGTTCT-3'; P3-F 5'-AGCGAAACGCAACCTTGTTT-3' and P3-R 5'-GGAAGGAGACG-TCGGAGTTG-

3'. Primer efficiency of all 3 primer pairs was tested. Expression levels of *Arabidopsis ACTIN2* (At3g18780) were monitored as an internal control using primers P1-F 5'-TCATGCCATCCTCCGTCTTG and P2-R 5'-GCTCTGCTGTTGTGGTGAAC-3'. C_q (cycle of quantification) values of *AtBBE*-like protein 15 were normalized to the C_q value of the reference gene *ACTIN2*. Melting temperatures and C_q values were determined using the software of Bio-Rad CFX Manager 3.0 (Bio-Rad Laboratories, California, USA).

5.3.8. Histochemical staining to visualize lignin

Arabidopsis Col-0 and *Atbbe*-like protein 13 and 15 individual plants were grown in parallel in pots in a greenhouse under long day conditions (16 h photoperiod) at 20-22 °C and relative humidity of 70 %. Stem material (~ 5 cm) of flowering plants was harvested after around 6 weeks. The lower part of the fresh stem material was embedded in 8 % agarose solution in distilled water (w/v), hardened at 4 °C, and cut into 100 µm sections using a Vibratome (Leica Biosystems, Vienna, Austria). Sections were soaked and stored in 1 x PBS phosphate-buffered saline (1 L of 10 x PBS containing 80 g NaCl, 2 g KCl, 14.4 g Na₂HPO₄ and 2.4 g KH₂PO₄ adjusted to pH 7.5 with KOH). Lignins, coniferyl and sinapyl aldehydes were detected by the Wiesner test by incubating the sections with phloroglucinol solution, composed of saturated, unfiltered phloroglucinol solution in 20 % HCl (v/v) for a few seconds until the purple staining appeared [56][57]. The sections were analyzed under an Olympus BX41 (Olympus, Tokyo, Japan) light microscope equipped with a ColorView I camera and analyzed with "analySIS getIT" (Olympus, Tokyo, Japan). In total, two biological replicates were analyzed, with four technical replicates each.

5.3.9. Lignin quantification with acetyl bromide method

Plants (*Col-0*, *Atbbe*-like protein 13 and 15) were grown in a greenhouse under long day conditions with a 16 h photoperiod at 20-22 °C and a relative humidity of 70 %. Stems of flowering plants were harvested after 6 weeks and cut into 5 cm pieces to divide them into younger and older parts. The fresh material was dried in an oven for 48 h at 60 °C and ground to a fine powder in a ball mill (summary of fresh/dry weights see Supplementary Table S4). The cell wall material was prepared according to the protocol of Carpita *et al.*[58]. The powder (200-500 mg) was washed twice in 96 % ethanol, incubated for 15 min at 70 °C, and homogenized in 50 mM Tris-HCl (pH 7.2) containing 1 % (w/v) SDS detergent for 30 min at 70 °C. This was followed by three washing steps with distilled water, two washing steps with 96 % ethanol and 5 min incubation, one washing step with acetone with 5 min incubation, and another washing step with distilled water. Finally, the material was freeze dried for 48 h at

-45 °C. The quantification of lignin was performed using the acetyl bromide method described by Hatfield *et al.* [59]. Dry cell wall material (46 mg) was incubated with 1 mL of acetyl bromide reagent (25% (v/v) acetyl bromide in glacial acetic acid) for 4 h at 50 °C. After cooling on ice for 5 min, the cell wall material was incubated with 5 mL of glacial acetic acid for 30 min on ice. The mixture was centrifuged for 2 min at 12,000 rpm. 40 µL of 1.5 M NaOH, 30 µL of 0.5 M hydroxylamine and 150 µL of glacial acetic acid were added to 30 µL clear supernatant for each sample in a quartz microplate. The measurements were carried out with a PowerWave HT Microplate Spectrophotometer (BioTek; Bad Friedrichshall, Germany), and the absorbance of the samples was measured at 280 nm. The amount of lignin was calculated using the assumed extinction coefficient of 17,688 L g⁻¹ cm⁻¹. Lignin analysis was performed for one biological replicate with triplicate measurements, for both young and old part of flower stalks of the individual plants.

5.3.10. Root growth phenotyping of transgenic *Atbbe*-like protein 28 seedlings

Seeds from homozygous *Atbbe*-like protein 28 and Col-0 were surface sterilized (see *Plant materials and growth conditions*) and about 15-20 seeds of each line were transferred in single horizontal lines to half strength MS plates (2.2 g/L MS, 0.5 g/L MES and 8 g/L Micro Agar). Plates were incubated vertically for 7 days in growth cabinets (KK1200, Pol-Eko Aparatura, Wodisław Śląski, Poland) under long day conditions (16 h/8 h day/night cycle) at 24 °C/20 °C (day/night), 50 % humidity and a photosynthetically active radiation of 130 µmol m⁻² sec⁻¹. Roots of Col-0 and *Atbbe*-like protein 28, 10 samples each, were incubated for 30 s in Iodine-potassium iodide solution (Lugol solution) from Carl Roth (Karlsruhe, Germany) to visualize the starch granules of the root cap for orientation [60] (see Figure 2A). Afterwards, roots were transferred into a drop of lactic acid on a microscope slide and evaluated with an Axiophot 2 HB0100 microscope equipped with a digital camera (Zeiss AxiocamMRc5, Zeiss, Oberkochen, Germany). Root apical meristem length (RAM) was measured using the Zeiss Axiovision software (version 4.8) by measuring the distance between the quiescent centre cells and the first cortex cell twice as big in size as its distal neighbor [61] (see scheme Figure 2B). Additionally, the diameter of the primary root was determined at the first lateral root primordium and at the first lateral root. Roots of one biological replicate were analyzed, with 10 seedlings per line.

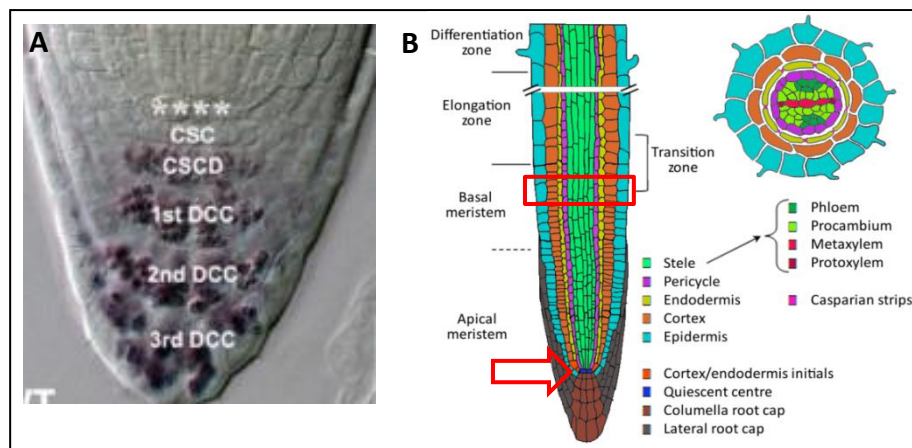


Figure 2. Schematic representations of *A. thaliana* root tips. **A.** Starch granules of different layers of the root cap, stained with Lugol solution, are depicted; **** = quiescent centre cells, CSC = columella stem cells, CSCD = layer of differentiating columella stem cell daughters, 1st DCC = first layer of differentiated columella cells, 2nd DCC = second layer of differentiated columella cells, 3rd DCC = second layer of differentiated columella cells. Scale bar: 20 μ m [60]. **B.** Organization of the *A. thaliana* root. Different cell types are shown in different colors, and distinct developmental zones are formed along the growing root. The framed area indicates the end point for measurement of RAM length from the quiescent centre (red arrow). A cross section of the primary root is depicted on the right with the respective color code [62].

5.3.11. Lignin analysis by thioacidolysis and gas chromatography-mass spectrometry (GC-MS)

Col-0 and *Atbbe*-like protein 13 and 15 mutant seeds were grown in soil in pots (3 plants per pot, 8 pots per tray for each line) and transferred in a greenhouse under long day conditions (16 h light) at 20-22 °C and a relative humidity of 70% as described in [49]. Stem material was harvested after 8-10 weeks when siliques already started to ripen, and 10 cm sections of the lower part of the stems were sampled. The samples were dried at 60 °C for 72 h. In total, 3 biological replicates with 3 technical replicates were generated. The 3 technical replicates within the biological replicates S1 and S2 were pooled to increase sample weight for analysis (harvested material see Supplementary Table S5). Lignin analysis by thioacidolysis [63][64] (principle see Figure 3) was performed by Catherine Lapierre (INRA, Institut Jean-Pierre Bourgin (IJPB), Versailles, France) according to the protocol of Méchin *et al.* [65]. The milled samples were subjected to extraction with water, then with 96% ethanol in an Accelerated Solvent extractor from DionexTM (Thermo Fisher Scientific, Waltham, Massachusetts, USA), and the recovered samples were dried at 60 °C and used for analysis (extracted cell wall (CW) and % of CW see Supplementary Table S5). The thioacidolysis reagent was freshly prepared as described. For each sample, 5 to 10 mg of dry CW material were mixed with 5 mL of thioacidolysis reagent and 100 μ L of internal standard solution (heinecosane C21, 2.516 mg/mL in CH₂Cl₂) and heated at 100 °C for 4 hours. After cooling, 7 mL of 0.2 M NaHCO₃, 0.1 mL of

HCL (6 M) solution to ensure a pH lower than 3, and 7 mL of dichloromethane extraction solvent were added. After mixing, the organic phase was removed and dried over anhydrous sodium sulfate, concentrated to a final volume of about 1 mL, and aliquots (5 μ L) were trimethylsilylated (TMS) with *N,O*-bis(trimethylsilyl) trifluoroacetamide (100 μ L) and ACS-grade pyridine (10 μ L) for 1 h at room temperature (RT). Samples were analyzed on a GC-MS Varian 4000 instrument (Varian, Les Ulis, France) equipped with a VF-1 ms 15 m x 0.25 mm i.d. polydimethylsiloxane capillary column (0.25 μ m film thickness) (Agilent Technologies, Les Ulis, France). The lignin-derived monomers, *p*-hydroxyphenyl (H), guaiacyl (G), and syringyl (S), were determined by GC-MS and reconstructed on ion chromatograms at m/z 239, 269, and 299, respectively and were compared to an internal standard hydrocarbon C21 evaluated on the ion chromatogram reconstructed at m/z (57 + 71 + 85) [66]. The yield in these S and G lignin-derived monomers gives an estimate of the amount only involved in labile beta-*O*-4 bonds. In addition to the lignin-derived monomers originating from arylglycerol lignin units, minor monomers such as the ones derived from coniferaldehyde end-groups (CALD) were evaluated. All samples were analyzed in duplicate.

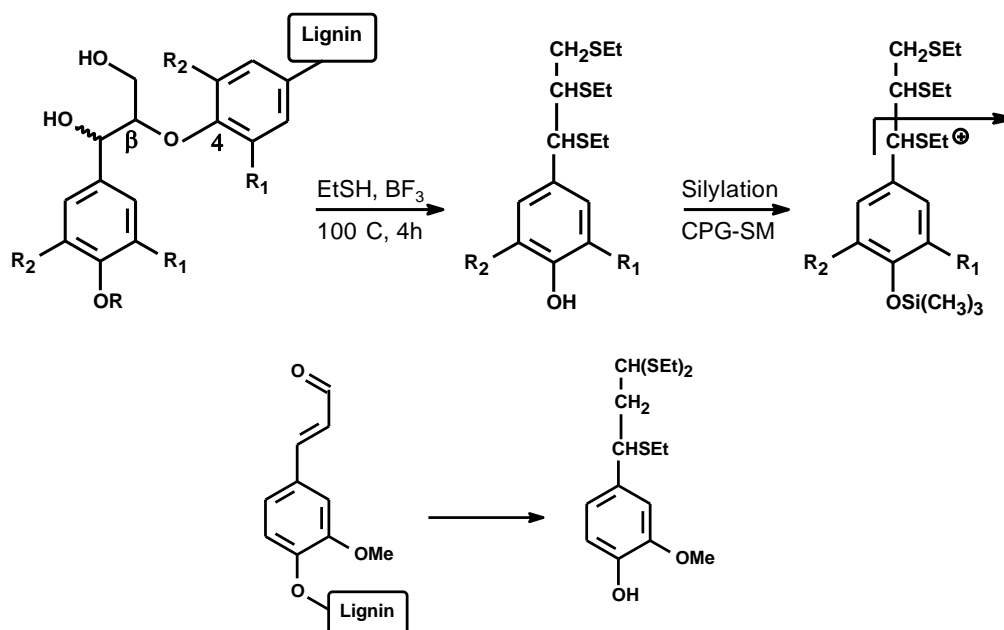


Figure 3. The principle of thioacidolysis. Thioethylated *p*-hydroxyphenyl H ($R_1 = R_2 = H$), guaiacyl G ($R_1 = OMe$, $R_2 = H$) and syringyl ($R_1 = R_2 = OMe$) lignin monomers are released from the typical β -*O*-4 lignin structure. Monomers are obtained as pairs of erythro/threo isomers and analyzed by GC-MS of their trimethylsilylated (TMS) derivatives [63][64].

5.3.12. Statistical analysis

Frequency distribution analyzes and Box Plots were performed with IBM SPSS Statistics version 24.0 and statistical differences were evaluated by the Mann-Whitney-U-Test and pairwise Student's *t*-test. Statistically significant differences were marked with asterisks (* = $P < 0.05$; ** = $P < 0.01$; *** = $P < 0.001$) in the respective figures.

5.4. Results

5.4.1. Tolerance of putative *Atbbe*-like protein mutants to salt and drought stress

AtBBE-like proteins have been reported to play an important role in abiotic stress in plants especially during salt and drought stress [15], and the evaluation of microarray data (<http://bar.utoronto.ca/efp/cgi-bin/efpWeb.cgi>) indicated higher expression levels of these enzymes under osmotic stress [47]. However, the *in planta* function of the *AtBBE*-like protein family in *Arabidopsis* in response to osmotic stress is still not understood. Thus, we explored the possible role of 27 putative *Atbbe*-like proteins in *Arabidopsis*. We obtained homozygous T-DNA insertion lines (background Col-0) of all investigated *AtBBE*-like proteins for the European Arabidopsis Stock Centre (NASC) with a putative T-DNA insertion in the coding region, representing loss-of-function mutants. We confirmed the presence of T-DNA and homozygous individuals by antibiotic selection (performed by Dr. Eric van der Graaff) for *Atbbe*-like protein 1, 2 (2), 3, 4, 5, 6, 7, 8 (2), 9, 9 (2), 10, 11 (2), 12, 13, 14, 15, 16, 17, 17 (2), 18 (2), 19/20, 21, 22, 22 (2), 23, 24, 25, 26, 26 (2), 27, 27 (2), 28, and additionally by PCR for putative *Atbbe*-like protein 13, 15, 13*15, 26 and 28.

For salt stress experiments, we observed the germination of mutants compared to the control Col-0 on half strength MS medium with 100 mM NaCl or without (control) in parallel. The seedlings were evaluated according to their growth and health status after 14 days of growth under short day conditions (8 h light) at 21 °C in three biological replicates, with three technical replicates each. Due to non-ideal growth conditions, some *Atbbe*-like lines were evaluated four times (*Atbbe*-like protein 10, 16, 22, 22 (2), 23, 24 and 25) (see Figure 4-11). Upon direct germination and growth under control conditions, almost all putative *Atbbe*-like protein knock-out/down mutants exhibited highly significant defects in development compared to wild type, except the lines *Atbbe*-like protein 4, 9 (2), 17, 26 and 28, which showed similar numbers of healthy green seedlings compared to Col-0. *Atbbe*-like mutants 6, 9, 15, 16 and 26 (2) showed a highly significant difference in the number of healthy green seedlings ($P < 0,01$), and *Atbbe*-like 1, 2, 3, 5, 7, 8, 10, 11, 12, 13, 14, 17 (2), 18 (2), 19/20, 21, 22, 22 (2), 23, 24, 25, 26 (2), 27 and 27 (2) showed an even higher significance ($P < 0.001$) compared to wild type. The average number of healthy Col-0 seedlings over all experiments was $90.7\% \pm \text{SD } 3.3\%$. The putative knock-out lines showed poor germination and exhibited a more than 10% reduction of healthy green seedlings compared to Col-0. Interestingly, the additional putative knock-out lines for *AtBBE*-like proteins 9, 17 and 26 genes have shown different phenotypes under control conditions compared to the corresponding lines.

Under mild salt stress, Col-0 and almost all *Atbbe*-like protein mutant plants were influenced by salt and showed a significantly decreased amount of healthy green seedlings as expected, except for the *Atbbe*-like protein 3, 4, 9, 14, 16, 17, 18 (2), 26 and 27 (2) mutant lines, which showed the same salt sensitivity as the wild type. Despite the high variability between the three biological replicates of these lines, we observed a tendency towards a decreased amount of healthy seedlings in response to salt compared to wild type. The *Atbbe*-like protein mutant lines 1, 7, 9 (2) and 26 (2) showed less significant differences in healthy seedlings ($P < 0.05$) compared to the mutant plants of *Atbbe*-like proteins 2, 6, 8, 12, 13, 15, 17 (2), 21, 22, 24, 25 and 27 ($P < 0.01$), and *Atbbe*-like proteins 5, 10, 11, 19, 20, 22 (2), 23 and 28 ($P < 0.001$). No obvious connection to the phylogenetic groups was visible for the *Atbbe*-like lines showing the same salt sensitivity as Col-0. They appeared to be scattered in the different subgroups 1, 2, 4 and 6. Also for the other lines, no connection was visible between the significance level and the phylogenetic group. In Table 1, salt sensitivity of all putative *Atbbe*-like knock-outs is depicted compared to wild type.

The most interesting transgenic lines, *Atbbe*-like protein 13, 15, 26 and 26 (2), produced a significantly lower number of relative healthy green seedlings on salt compared to Col-0 (29.4%, 34.9%, 45.7% and 38.2% compared to 55.8%, respectively) (Figure 7, 10 and 11). Additionally, we investigated the germination rate (all germinated seedlings regardless of size and color), and we observed a significant phenotype of seedlings under control conditions for *Atbbe*-like protein 13, 15 and 26 (2) compared to Col-0. The germination of *Atbbe*-like protein 26 was the same as for the wild type on control plates. On salt plates, significantly fewer seedlings survived of *Atbbe*-like protein 13 and 15 compared to Col-0 (relative survival rate on salt 89.8% and 85% compared to 99%, respectively). For both *Atbbe*-like protein 26 and 26 (2), no significant differences in the survival rates on salt could be observed in comparison to wild type (see Figure 12).

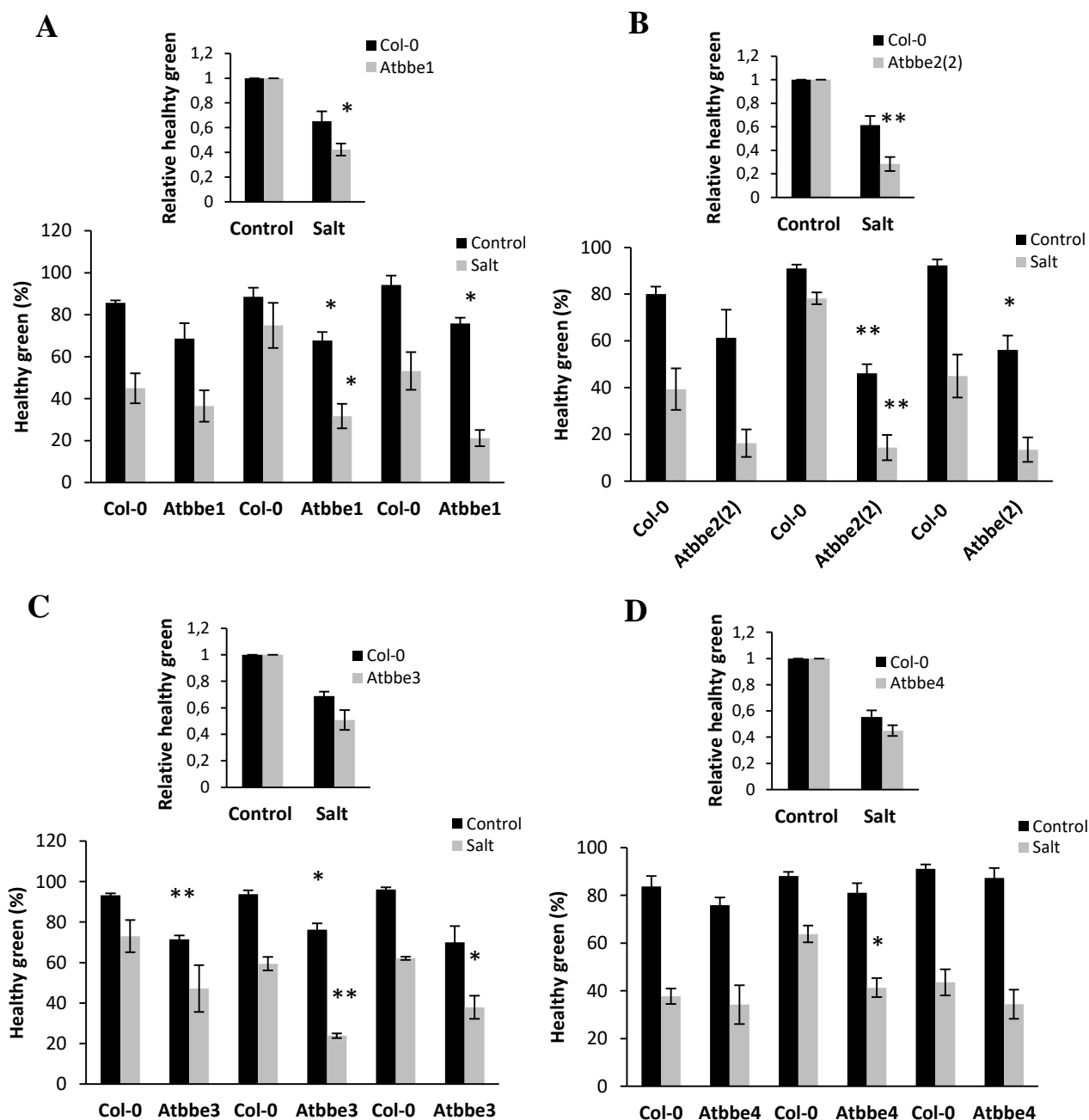


Figure 4. Salt stress tolerance of putative *Atbbe*-like protein 1, 2 (2), 3 and 4 mutants compared to Col-0 A-D. Wild type and transgenic seedlings were grown in parallel on half strength MS medium with salt (100 mM NaCl) or without (control) for 14 days in growth cabinets under short day conditions (8 h light) at 21 °C (light intensity: 180 $\mu\text{mol m}^{-2} \text{s}^{-1}$). Seedlings were evaluated according to their growth stage and health status. Evaluation of healthy seedlings of Col-0 and transgenic lines is depicted in bar charts. Average values (%) \pm SE of three biological replicates (with three technical replicates each) of healthy green seedlings are shown (n = 3). Additionally, the relative number of healthy green seedlings on salt compared to Col-0 (normalized to 1) of all biological replicates is shown (n = 9) above. Asterisks indicate statistically significant differences of putative *Atbbe*-like protein knock-outs or knock-downs compared to wild type, according to Student's *t*-test (* $P < 0.05$, ** $P < 0.01$, *** $P < 0.001$).

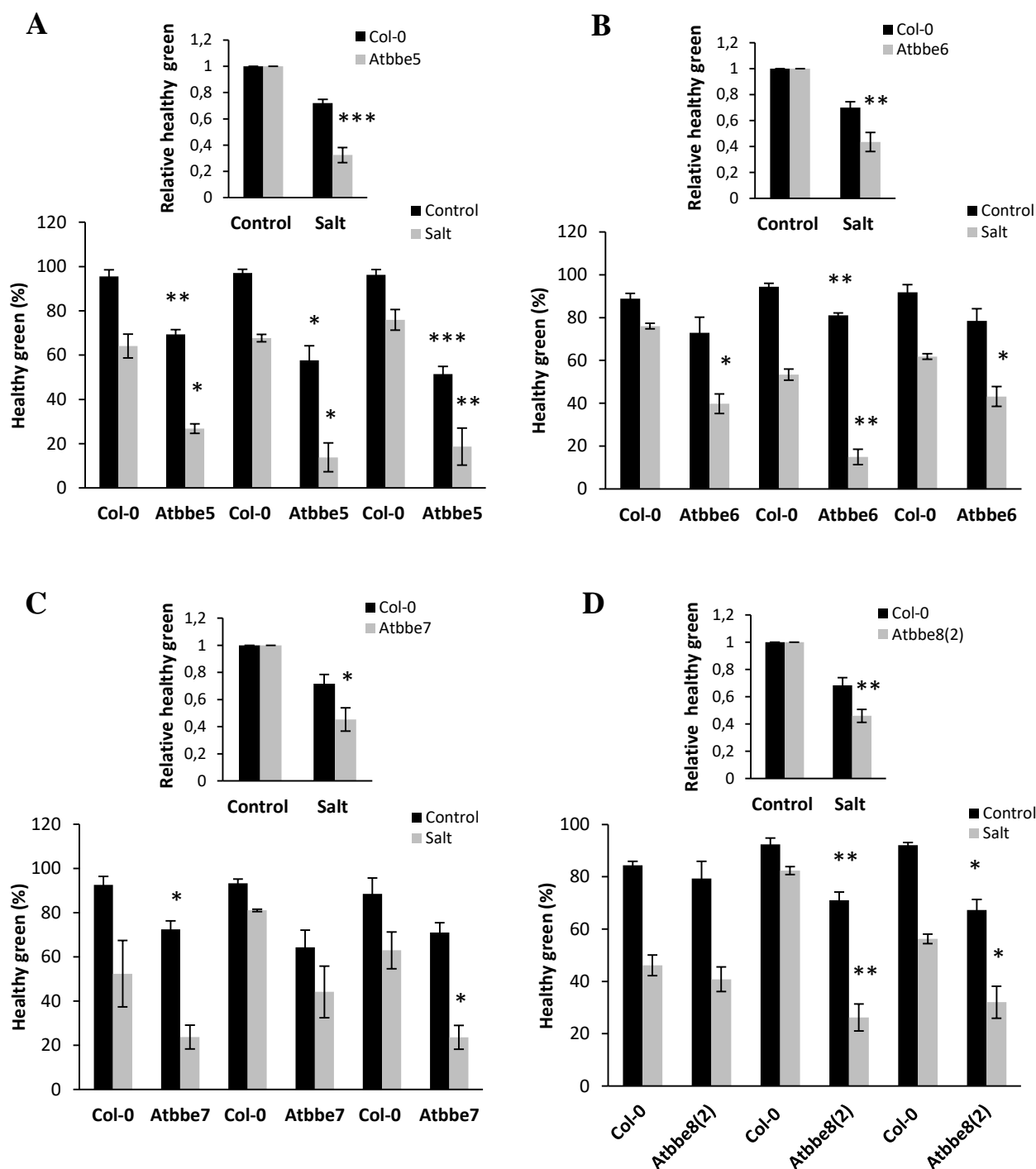


Figure 5. Salt stress tolerance of putative *Atbbe*-like protein 5, 6, 7 and 8 (2) mutants compared to Col-0 A-D. Wild type and transgenic seedlings were grown in parallel on half strength MS medium with salt (100 mM NaCl) or without (control) for 14 days in growth cabinets under short day conditions (8 h light) at 21 °C (light intensity: 180 $\mu\text{mol m}^{-2} \text{s}^{-1}$). Seedlings were evaluated according to their growth stage and health status. Evaluation of healthy seedlings of Col-0 and transgenic lines is depicted in bar charts. Average values (%) \pm SE of three biological replicates (with three technical replicates each) of healthy green seedlings are shown (n = 3). Additionally, the relative number of healthy green seedlings on salt compared to Col-0 (normalized to 1) of all biological replicates is shown (n = 9) above. Asterisks indicate statistically significant differences of putative *Atbbe*-like protein knock-outs or knock-downs compared to wild type, according to Student's *t*-test (* $P < 0.05$, ** $P < 0.01$, *** $P < 0.001$).

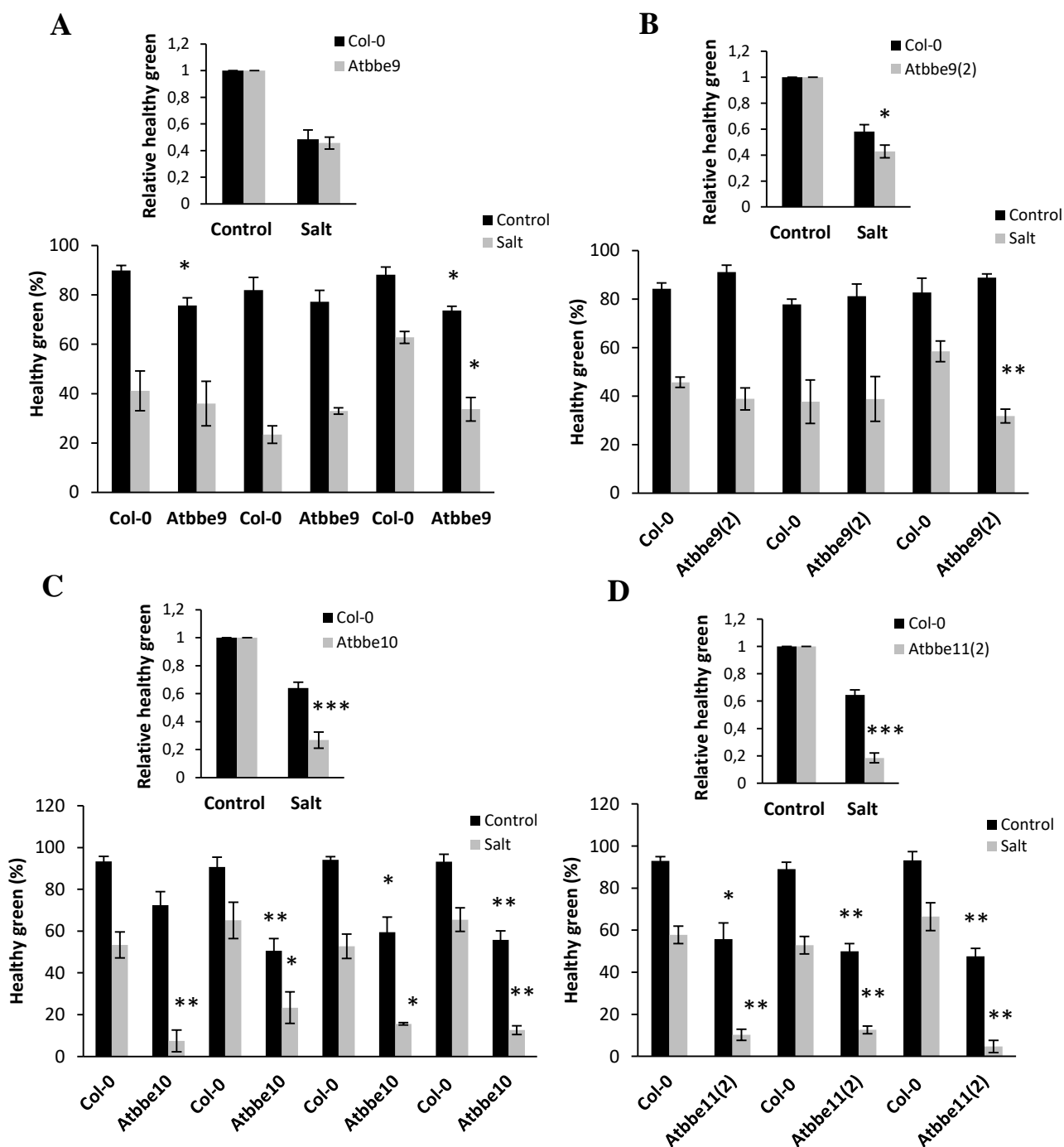


Figure 6. Salt stress tolerance of putative *Atbbe*-like protein 9, 9 (2), 10 and 11 (2) mutants compared to Col-0 A-D. Wild type and transgenic seedlings were grown in parallel on half strength MS medium with salt (100 mM NaCl) or without (control) for 14 days in growth cabinets under short day conditions (8 h light) at 21 °C (light intensity: 180 $\mu\text{mol m}^{-2} \text{s}^{-1}$). Seedlings were evaluated according to their growth stage and health status. Evaluation of healthy seedlings of Col-0 and transgenic lines is depicted in bar charts. Average values (%) \pm SE of three or four biological replicates (with three technical replicates each) of healthy green seedlings are shown (n = 3). Additionally, the relative number of healthy green seedlings on salt compared to Col-0 (normalized to 1) of all biological replicates is shown (n = 9) above. Asterisks indicate statistically significant differences of putative *Atbbe*-like protein knock-outs or knock-downs *t*-test (* $P < 0.05$, ** $P < 0.01$, *** $P < 0.001$).

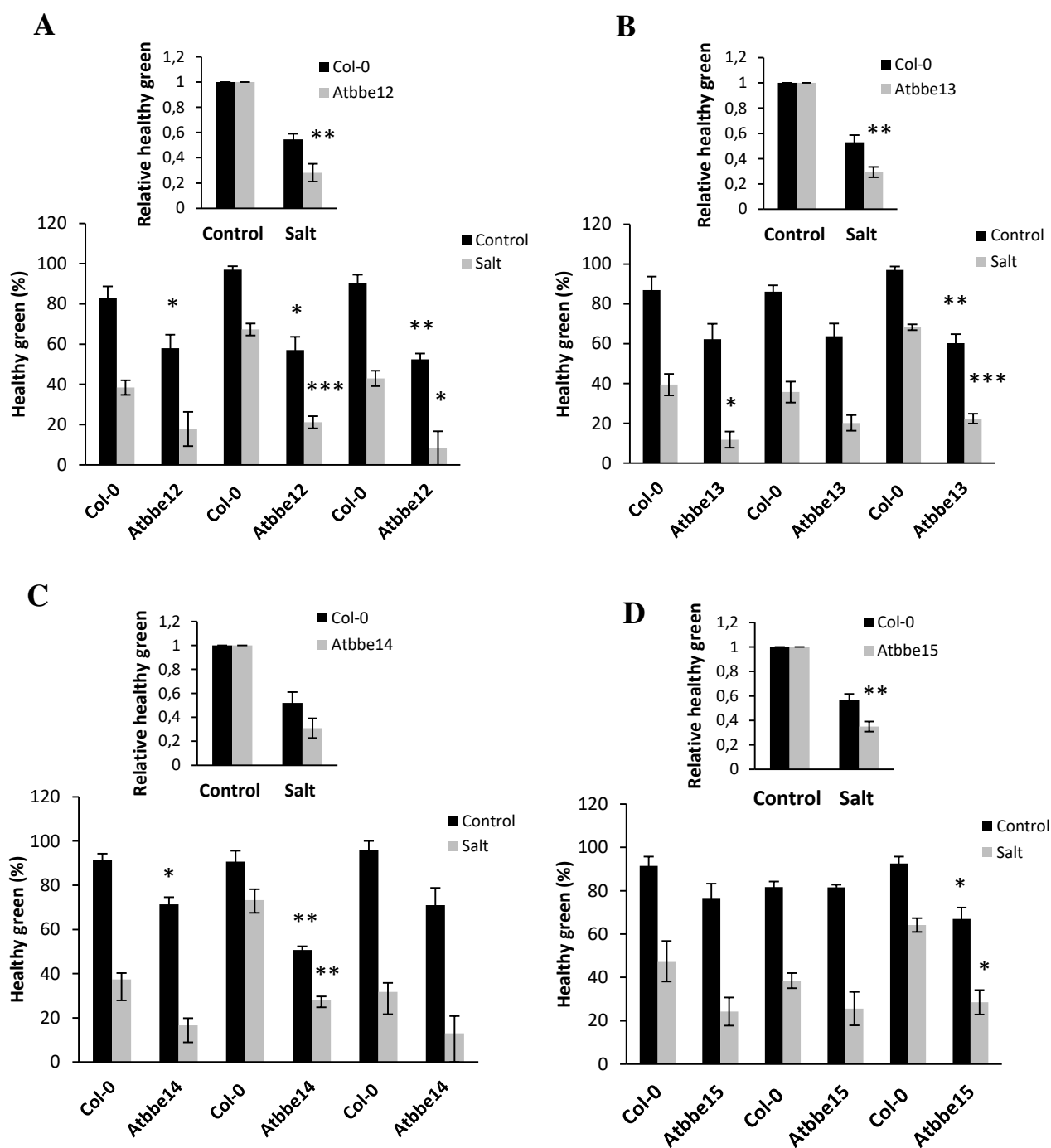


Figure 7. Salt stress tolerance of putative *Atbbe*-like protein 12, 13, 14 and 15 mutants compared to Col-0
A-D. Wild type and transgenic seedlings were grown in parallel on half strength MS medium with salt (100 mM NaCl) or without (control) for 14 days in growth cabinets under short day conditions (8 h light) at 21 °C (light intensity: 180 $\mu\text{mol m}^{-2} \text{s}^{-1}$). Seedlings were evaluated according to their growth stage and health status. Evaluation of healthy seedlings of Col-0 and transgenic lines is depicted in bar charts. Average values (%) \pm SE of three biological replicates (with three technical replicates each) of healthy green seedlings are shown ($n = 3$). Additionally, the relative number of healthy green seedlings on salt compared to Col-0 (normalized to 1) of all biological replicates is shown ($n = 9$) above. Asterisks indicate statistically significant differences of putative *Atbbe*-like protein knock-outs or knock-downs compared to wild type, according to Student's *t*-test (* $P < 0.05$, ** $P < 0.01$, *** $P < 0.001$).

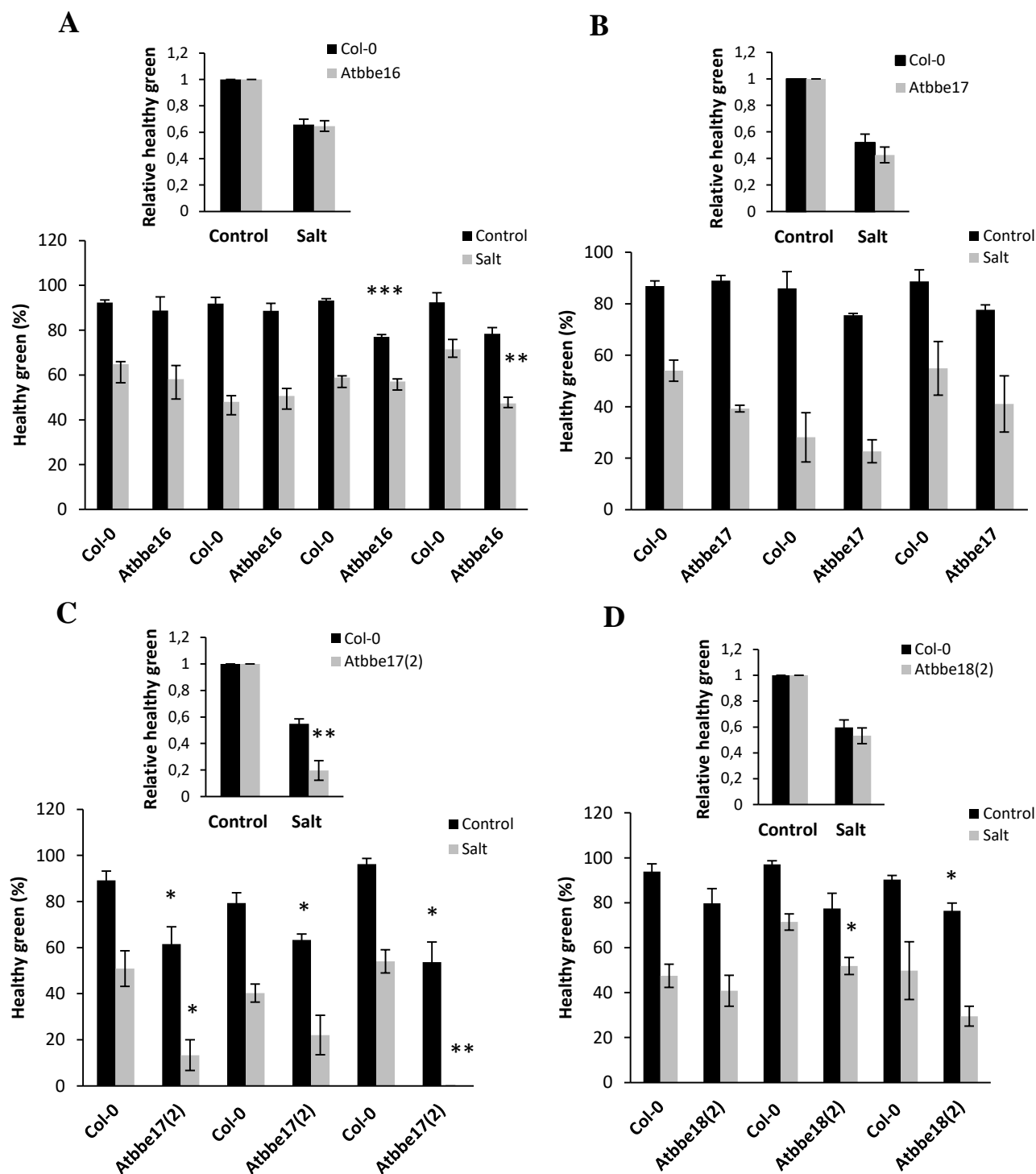


Figure 8. Salt stress tolerance of putative *Atbbe*-like protein 16, 17, 17 (2) and 18 (2) mutants compared to Col-0 A-D. Wild type and transgenic seedlings were grown in parallel on half strength MS medium with salt (100 mM NaCl) or without (control) for 14 days in growth cabinets under short day conditions (8 h light) at 21 °C (light intensity: 180 $\mu\text{mol m}^{-2} \text{s}^{-1}$). Seedlings were evaluated according to their growth stage and health status. Evaluation of healthy seedlings of Col-0 and transgenic lines is depicted in bar charts. Average values (%) \pm SE of three or four biological replicates (with three technical replicates each) of healthy green seedlings are shown (n = 3). Additionally, the relative number of healthy green seedlings on salt compared to Col-0 (normalized to 1) of all biological replicates is shown (n = 9) above. Asterisks indicate statistically significant differences of putative *Atbbe*-like protein knock-outs or knock-downs compared to wild type, according to Student's *t*-test (* $P < 0.05$, ** $P < 0.01$, *** $P < 0.001$).

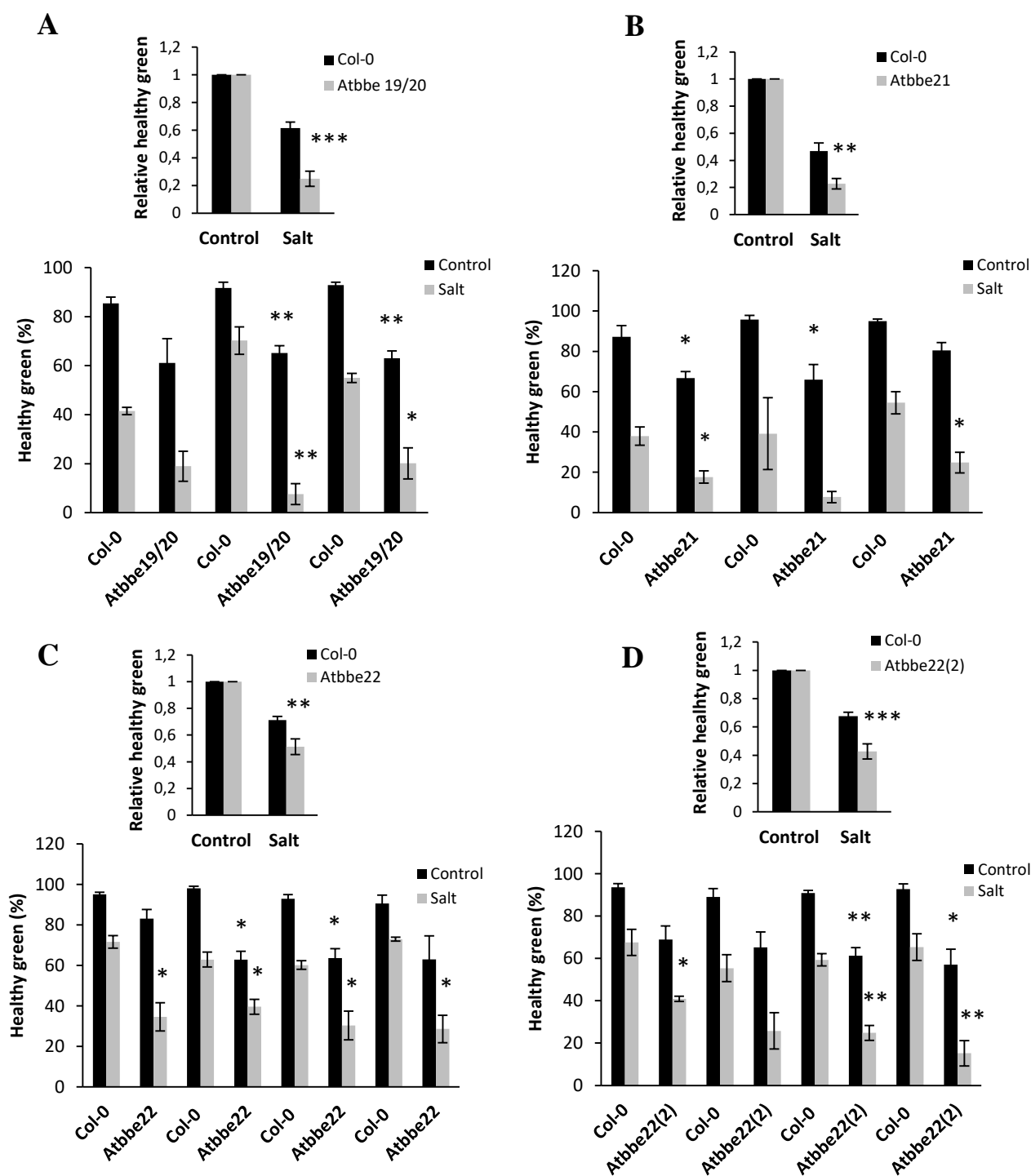


Figure 9. Salt stress tolerance of putative *Atbbe*-like protein 19/20, 21, 22 and 22 (2) mutants compared to Col-0 A-D. Wild type and transgenic seedlings were grown in parallel on half strength MS medium with salt (100 mM NaCl) or without (control) for 14 days in growth cabinets under short day conditions (8 h light) at 21 °C (light intensity: 180 $\mu\text{mol m}^{-2} \text{s}^{-1}$). Seedlings were evaluated according to their growth stage and health status. Evaluation of healthy seedlings of Col-0 and transgenic lines is depicted in bar charts. Average values (%) \pm SE of three or four biological replicates (with three technical replicates each) of healthy green seedlings are shown (n = 3). Additionally, the relative number of healthy green seedlings on salt compared to Col-0 (normalized to 1) of all biological replicates is shown (n = 9) above. Asterisks indicate statistically significant differences of putative *Atbbe*-like protein knock-outs or knock-downs compared to wild type, according to Student's *t*-test (* $P < 0.05$, ** $P < 0.01$, *** $P < 0.001$).

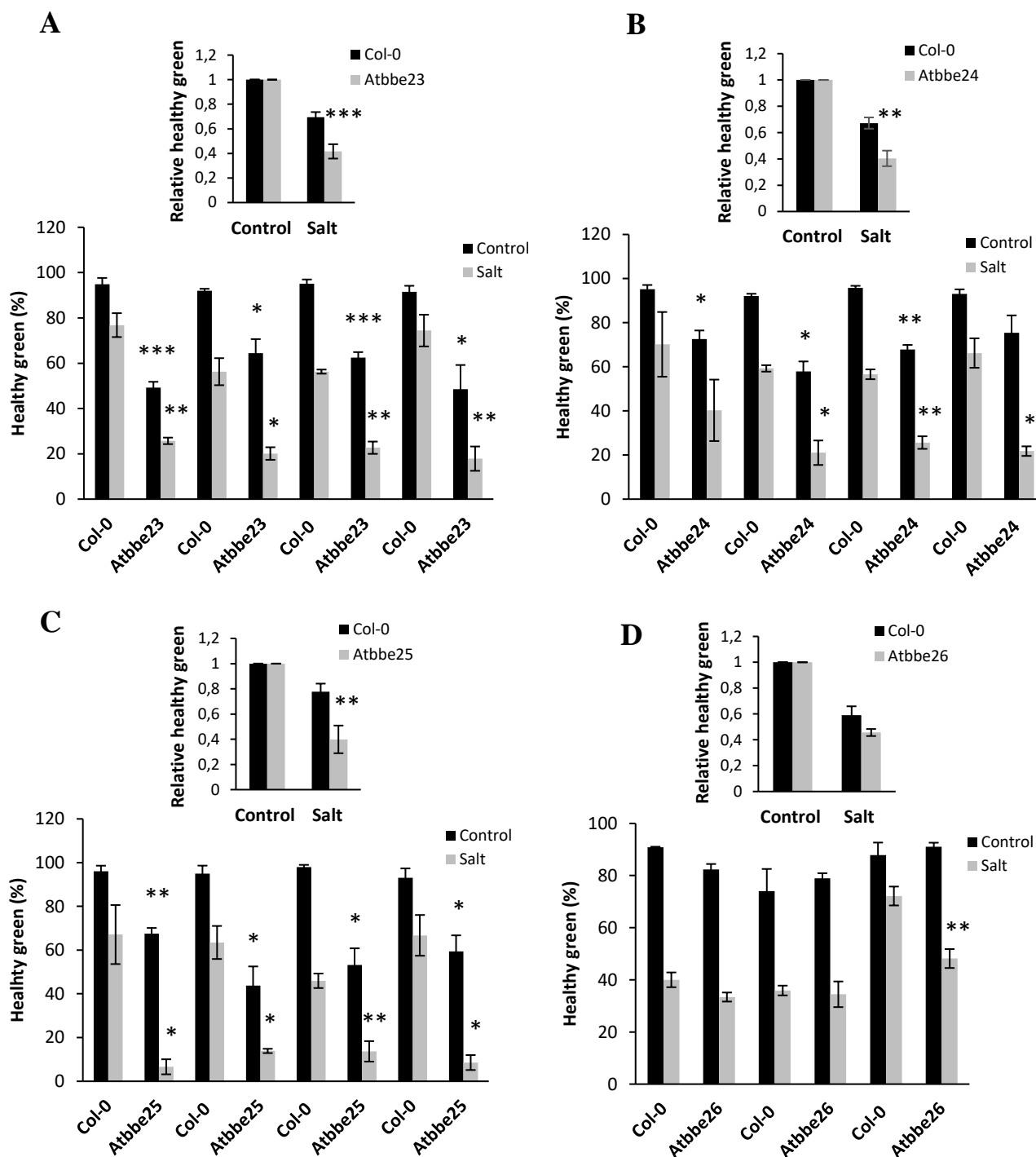


Figure 10. Salt stress tolerance of putative *Atbbe*-like protein 23, 24, 25 and 26 mutants compared to Col-0
A-D. Wild type and transgenic seedlings were grown in parallel on half strength MS medium with salt (100 mM NaCl) or without (control) for 14 days in growth cabinets under short day conditions (8 h light) at 21 °C (light intensity: 180 $\mu\text{mol m}^{-2} \text{s}^{-1}$). Seedlings were evaluated according to their growth stage and health status. Evaluation of healthy seedlings of Col-0 and transgenic lines is depicted in bar charts. Average values (%) \pm SE of three or four biological replicates (with three technical replicates each) of healthy green seedlings are shown (n = 3). Additionally, the relative number of healthy green seedlings on salt compared to Col-0 (normalized to 1) of all biological replicates is shown (n = 9) above. Asterisks indicate statistically significant differences of putative *Atbbe*-like protein knock-outs or knock-downs compared to wild type, according to Student's *t*-test (* $P < 0.05$, ** $P < 0.01$, *** $P < 0.001$).

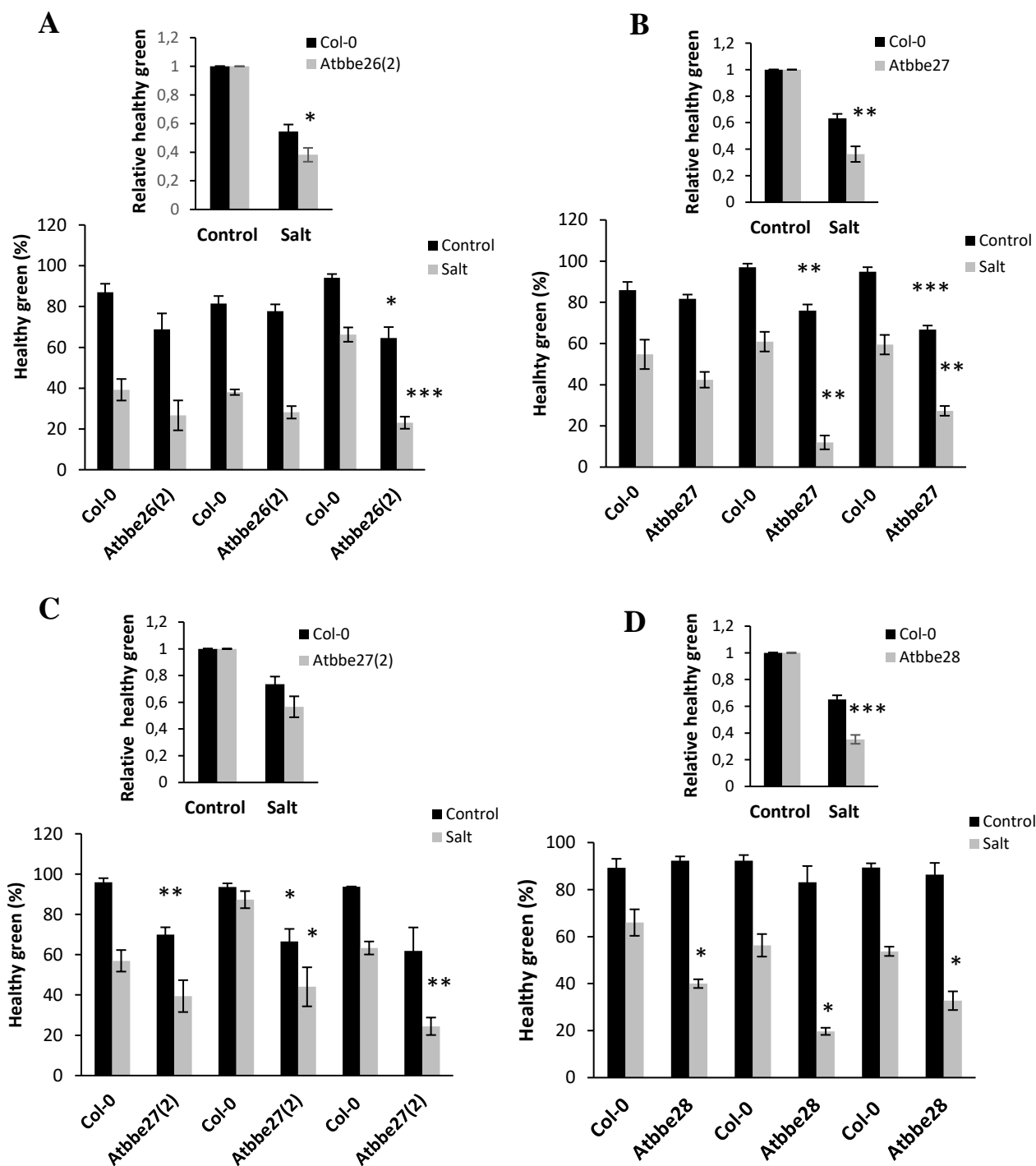


Figure 11. Salt stress tolerance of putative *Atbbe*-like protein 26 (2), 27, 27 (2) and 28 mutants compared to Col-0 A-D. Wild type and transgenic seedlings were grown in parallel on half strength MS medium with salt (100 mM NaCl) or without (control) for 14 days in growth cabinets under short day conditions (8 h light) at 21 °C (light intensity: 180 $\mu\text{mol m}^{-2} \text{s}^{-1}$). Seedlings were evaluated according to their growth stage and health status. Evaluation of healthy seedlings of Col-0 and transgenic lines is depicted in bar charts. Average values (%) \pm SE of three biological replicates (with three technical replicates each) of healthy green seedlings are shown (n = 3). Additionally, the relative number of healthy green seedlings on salt compared to Col-0 (normalized to 1) of all biological replicates is shown (n = 9) above. Asterisks indicate statistically significant differences of putative *Atbbe*-like protein knock-outs compared to wild type, according to Student's *t*-test (* $P < 0.05$, ** $P < 0.01$, *** $P < 0.001$).

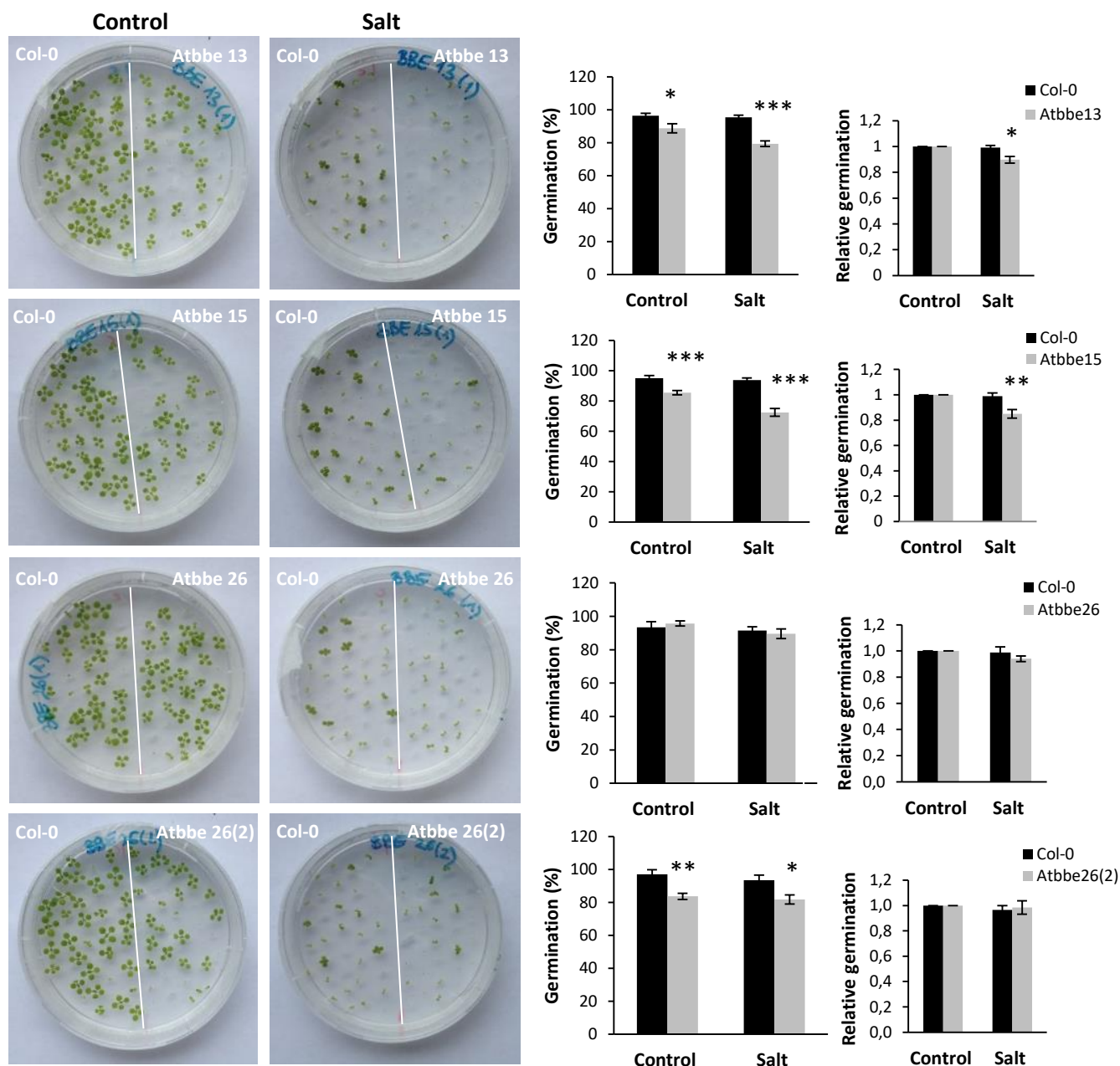


Figure 12. Germination rate of putative *Atbbe*-like protein 13, 15, 26 and 26 (2) mutants compared to wild type. Wild type and transgenic seedlings were grown in parallel on half strength MS medium with salt (100 mM NaCl) or without (control) for 14 days in growth cabinets under short day conditions (8 h light) at 21 °C (light intensity: 180 $\mu\text{mol m}^{-2} \text{s}^{-1}$) for salt stress tolerance experiments. In addition to the health status (see Figure 4-11), the germination rates of *Atbbe*-like protein 13, 15 and 26 and 26 (2) are depicted. Mean values (%) \pm SE of all survived seedlings on control and salt plates are shown (n = 9). Relative germination rate (normalized to Col-0) of the putative knock-outs and the wild type are shown on salt for three biological experiments. In total, three biological replicates were performed, with three technical replicates each. Asterisks indicate statistically significant differences of putative *Atbbe*-like knock-outs compared to wild type, according to Student's *t*-test (* $P < 0.05$, ** $P < 0.01$, *** $P < 0.001$).

Table 1. Summary of salt sensitivity of putative *Atbbe*-like protein knock-outs.

Salt sensitivity of <i>Atbbe</i> -like putative mutants compared to wild type Col-0			
Not significant	* $P < 0.05$	** $P < 0.01$	*** $P < 0.001$
<i>Atbbe</i> 3	<i>Atbbe</i> 1	<i>Atbbe</i> 2	<i>Atbbe</i> 5
<i>Atbbe</i> 4	<i>Atbbe</i> 7	<i>Atbbe</i> 6	<i>Atbbe</i> 10
<i>Atbbe</i> 9	<i>Atbbe</i> 9 (2)	<i>Atbbe</i> 8	<i>Atbbe</i> 11
<i>Atbbe</i> 14	<i>Atbbe</i> 26 (2)	<i>Atbbe</i> 12	<i>Atbbe</i> 19/20
<i>Atbbe</i> 16		<i>Atbbe</i> 13	<i>Atbbe</i> 22 (2)
<i>Atbbe</i> 17		<i>Atbbe</i> 15	<i>Atbbe</i> 23
<i>Atbbe</i> 18 (2)		<i>Atbbe</i> 17 (2)	<i>Atbbe</i> 28
<i>Atbbe</i> 26		<i>Atbbe</i> 21	
<i>Atbbe</i> 27 (2)		<i>Atbbe</i> 22	
		<i>Atbbe</i> 24	
		<i>Atbbe</i> 25	
		<i>Atbbe</i> 27	

To gain a deeper insight into growth and development, the putative *Atbbe*-like protein 15 mutant and the 13*15 double mutant were evaluated in more detail with categories. Seedlings were grown under short day conditions for 14 days in a climate chamber with an 8 h day/16 h night cycle at 24 °C/20 °C (day/night). Seedlings were analyzed according to categories described in *Materials and methods* (Figure 1). Both Col-0 and *Atbbe*-like protein seedlings showed a significantly visible reduction of health status on salt plates (see Figure 13A-E). Evaluation of all categories revealed a tendency towards significant differences between wild type and *Atbbe*-like protein 15 mutants on control and salt plates over all three biological replicates (Figure 13B). *Atbbe*-like protein 15 mutant plants showed a poor germination on control and salt conditions. To include the growth differences on control plates, we statistically evaluated the median shift between Col-0 and *Atbbe*-like protein 15 under control and salt conditions. *Atbbe*-like protein 15 mutants did not exhibit a significantly higher salt sensitivity than the wild type over three biological replicates (Mann-Whitney-U-Test $P = 0.7$). However, the evaluation of healthy seedlings (summarized categories 0-2) yielded a tendency towards a higher salt sensitivity of the mutant lines compared to Col-0 (relative healthy seedlings 57.7% and 66.3%, respectively) (Figure 13C). No differences in germination rates between *Atbbe*-like 15 mutant and Col-0 seedlings under control and salt conditions were visible (Figure 13D) (Col-0 95.4% and *Atbbe*-like 15 97.4%). In Figure 13E, the percentage of affected *Atbbe*-like protein 15 seedlings is depicted which is significantly higher than for Col-0 under control conditions (19.1% and 2.9%, respectively). Under salt stress, the mutant shows a higher level of affected seedlings compared to wild type.

The putative double knock-out line for *Atbbe*-like proteins 13*15 was analyzed with the same categories. The evaluation of the categories showed no differences between wild type and

mutant line, neither under control conditions, nor on salt plates in three independent experiments (Figure 14A-E). There was no visible and also statistical difference upon evaluation of the medians of Col-0 and *Atbbe*-like protein 13*15 plant status on control and salt plates (Figure 14B). In order to possibly find a change in development and health status, the number of healthy, germinated and affected seedlings was identified. The mutant line showed the same number of healthy seedlings as Col-0 in three independent biological experiments under control and salt conditions. By normalizing to Col-0 values, the number of healthy seedlings on salt was still the same over all three experiments (Figure 14C). The germination rate was significantly lower for the double mutant *Atbbe*-like protein 13*15 on control plates compared to Col-0 (94.4% and 98.0%, respectively) (Figure 14D) in three summarized biological experiments but under salt stress there was no difference in salt sensitivity. The overall analysis of seedlings (see Figure 14E) revealed a significantly higher number of healthy plants under control conditions for Col-0 (97.1%) than for the double mutant (88.9%). Therefore, a higher level of affected and un-germinated plants was visible. Nevertheless, no significantly higher salt sensitivity of the double mutant could be shown compared to wild type.

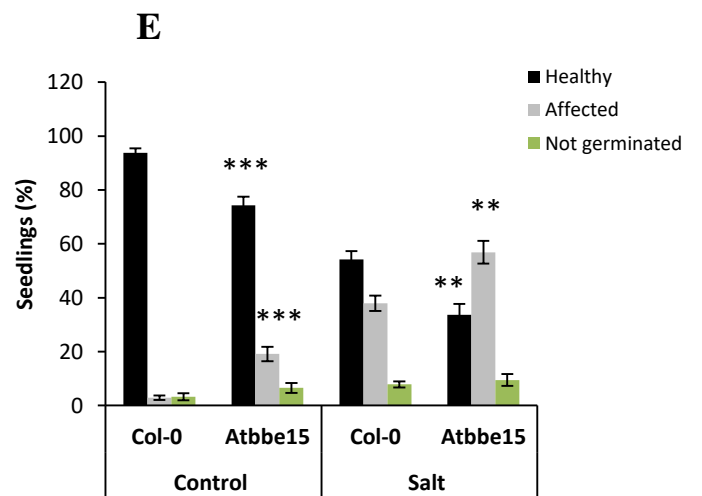
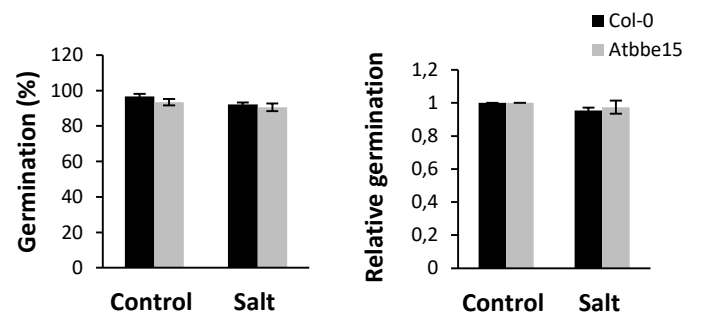
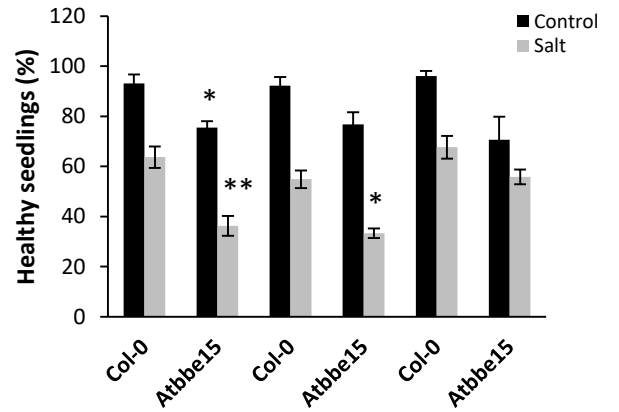
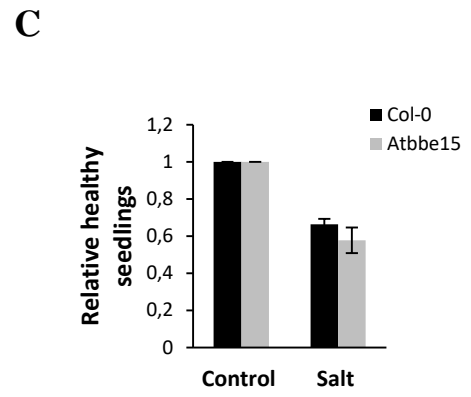
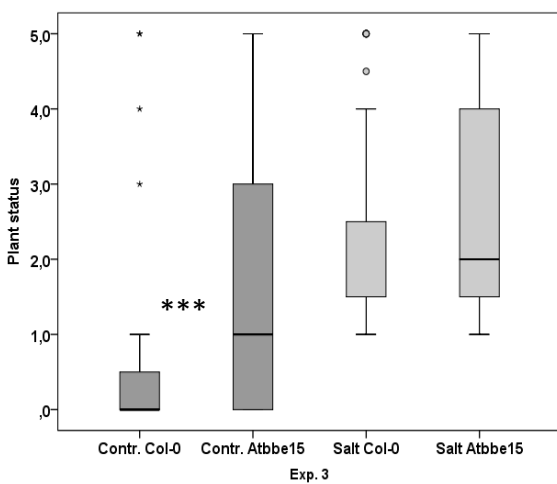
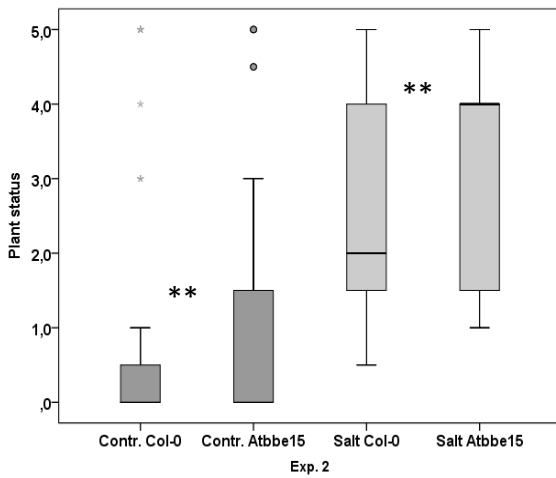
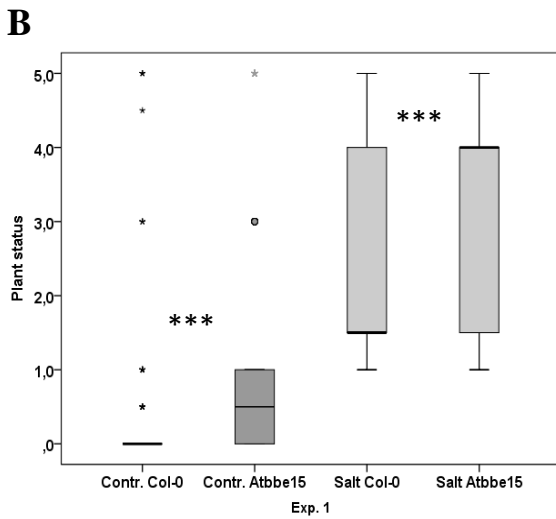
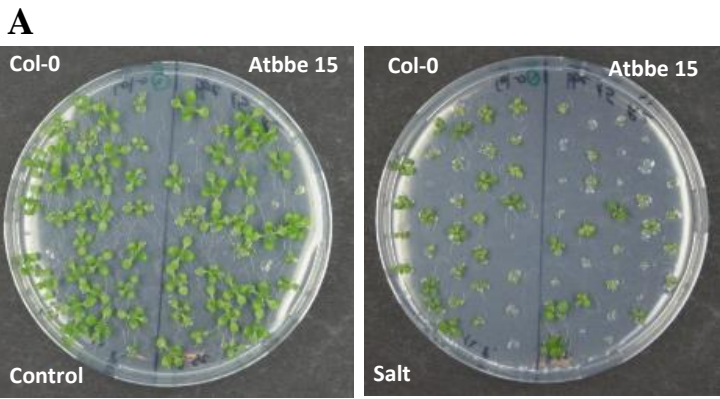
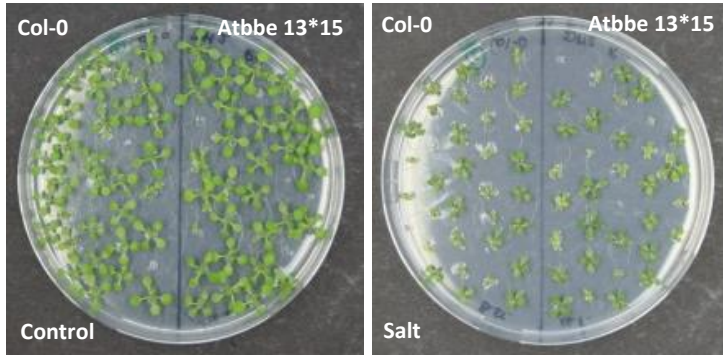
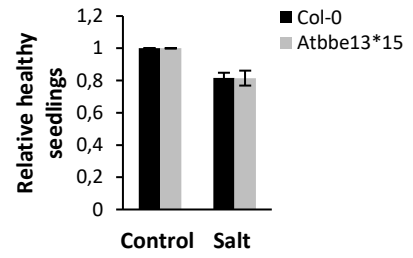


Figure 13. Salt tolerance evaluation of putative *Atbbe*-like protein 15 knock-out and wild type seedlings. A. Wild type Col-0 and mutant seedlings were grown in parallel on half strength MS medium with salt (100 mM NaCl) or without (control) for 14 days in climate chambers under short day conditions (8 h day/16 h night cycle) with $200 \mu\text{mol m}^{-2} \text{s}^{-1}$ light intensity at 24 °C/20 °C (day/night). **B.** Growth and health status of seedlings were evaluated according to different categories: 0 = healthy with 4 or more green leaves (without cotyledons); 1 = healthy with 2 green leaves, 2 = healthy with cotyledons and the first appeared leaves; 3 = healthy, mainly the cotyledons; 4 = very small, cotyledons not open, yellow; 5 = not germinated; plus 0.5 p for anthocyanins and chlorosis. Box plots (n = 102) of three independent biological replicates, with three technical replicates each, are shown \pm SD. Median of Exp. 1: Control Col-0 0.0, *Atbbe*-like 15 0.5, Salt Col-0 1.5, *Atbbe*-like 15 4.0; Exp. 2: Control Col-0 0.0, *Atbbe*-like 15 0.0, Salt Col-0 2.0, *Atbbe*-like 15 4.0; Exp. 3: Control Col-0 0.0, *Atbbe*-like 15 1.0, Salt Col-0 1.5, *Atbbe*-like 15 2.0. Statistical differences were evaluated by Mann-Whitney-U-Test for *Atbbe*-like protein 15 on control and salt plates compared to Col-0. **C.** Average of healthy green seedlings (n = 3; summarized categories 0-2) for three independent biological replicates, and the relative rates of healthy seedlings (Col-0 normalized) on control and salt of summarized three biological replicates (n = 9) are shown **D.** Germination rate and relative germination rate (Col-0 normalized) of all seedlings compared to Col-0 are depicted. **E.** Comparison of healthy (categories 0-2), affected (categories 2.5-4.5) and un-germinated seedlings (category 5) of three biological replicates (n = 9). Bar charts show mean values (%) \pm SE of evaluated seedlings on control and salt plates based on three biological replicates with three technical replicates each. Asterisks indicate statistically significant differences of *Atbbe*-like protein 15 compared to wild type, according to Student's *t*-test (* $P < 0.05$, ** $P < 0.01$, *** $P < 0.001$).

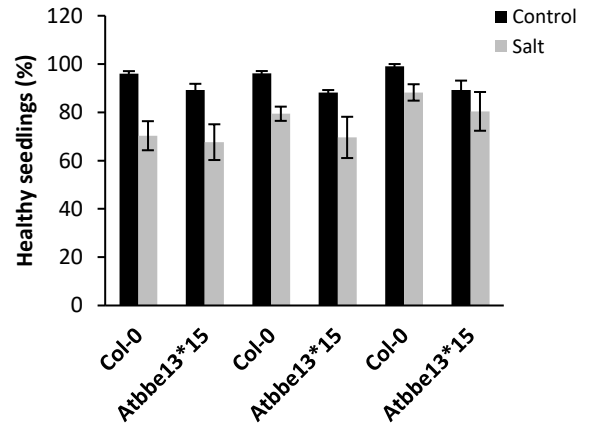
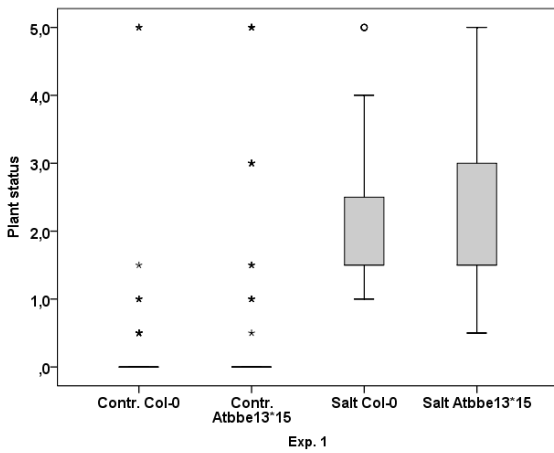
A



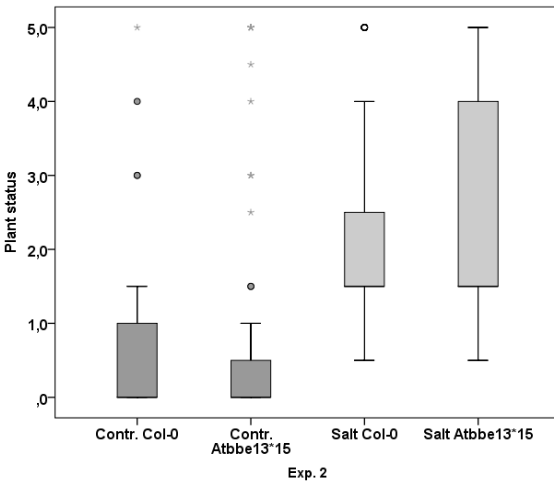
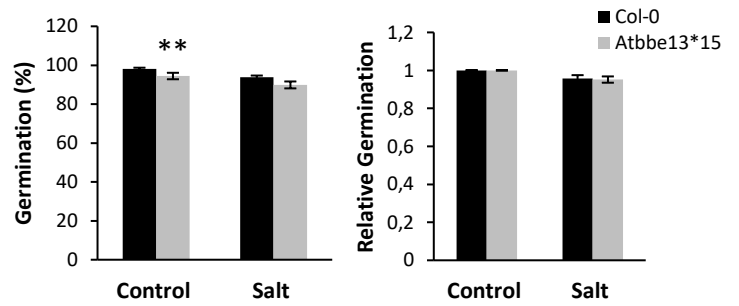
C



B



D



E

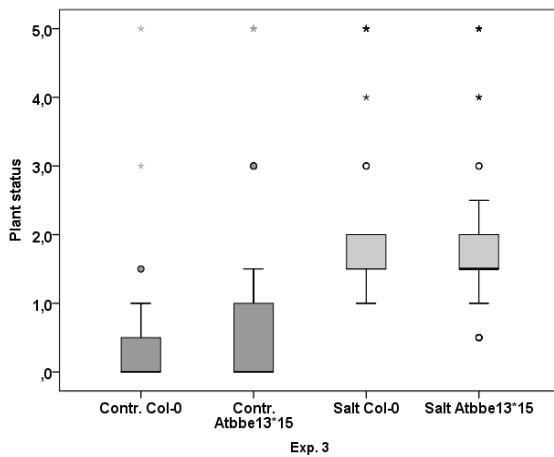
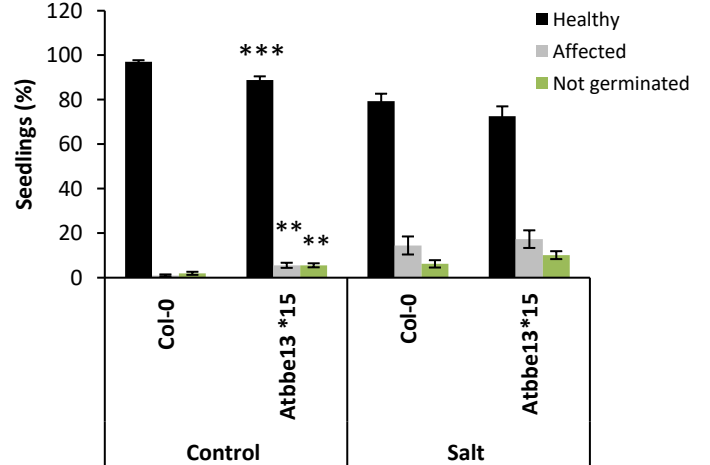


Figure 14. Salt tolerance evaluation of putative *Atbbe*-like protein 13*15 knock-out and wild type seedlings.

A. Wild type Col-0 and mutant seedlings were grown in parallel on half strength MS medium with salt (100 mM NaCl) or without (control) for 14 days in climate chambers under short day conditions (8 h day/16 h night cycle) with 200 $\mu\text{mol m}^{-2} \text{s}^{-1}$ light intensity at 24 °C/20 °C (day/night). **B.** Growth and health status of seedlings were evaluated according to different categories 0 = healthy with 4 or more green leaves (without cotyledons); 1 = healthy with 2 green leaves, 2 = healthy with cotyledons and the first appeared leaves; 3 = healthy, mainly the cotyledons; 4 = very small, cotyledons not open, yellow; 5 = not germinated; plus 0.5 p for anthocyanins and chlorosis. Box plots (n = 102) of three independent biological replicates, with three technical replicates each, are shown \pm SD. Median of Exp. 1: Control Col-0 0.0, *Atbbe*-like 13*15 0.0, Salt Col-0 1.5, *Atbbe*-like 13*15 1.5; Exp. 2: Control Col-0 0.0, *Atbbe*-like 13*15 0.0, Salt Col-0 1.5, *Atbbe*-like 13*15 1.5; Exp. 3: Control Col-0 0.0, *Atbbe*-like 13*15 0.0, Salt Col-0 1.5, *Atbbe*-like 13*15 1.5. Statistical differences were evaluated by Mann-Whitney-U-Test for *Atbbe*-like protein 13*15 on control and salt plates compared to Col-0. **C.** Average of healthy green seedlings (n = 3; summarized categories 0-2) for three independent biological replicates, and the relative rates of healthy seedlings (control normalized to 1) on control and salt of summarized three biological replicates (n = 9) are shown **D.** Germination rate and relative germination rate (Col-0 normalized) of all seedlings compared to Col-0 are depicted. **E.** Comparison of healthy (categories 0-2), affected (categories 2.5-4.5) and un-germinated (category 5) seedlings of three biological replicates (n = 9). Bar charts show mean values (%) \pm SE of evaluated seedlings on control and salt plates based on three biological replicates, with three technical replicates each. Asterisks indicate statistically significant differences of *Atbbe*-like protein 13*15 compared to wild type, according to Student's *t*-test (** $P < 0.01$, *** $P < 0.001$).

To explore and characterize the possible role of *AtBBE*-like proteins during drought, we performed drought stress experiments on plates. The obtained homozygous T-DNA insertion lines for *AtBBE*-like protein 13, 15, 13*15 and 26 were grown for 14 days under short day conditions (8 h light/ 16 h night cycle) at 24 °C/20 °C (day/night). Seedlings were exposed to control (half strength MS medium) and drought conditions (half strength MS medium infused over night with 250 g/L PEG). After cultivation, the seedlings were categorized according to their health and growth status (see categories in *Materials and methods* Figure 1). In addition, healthy and affected seedlings as well as total germination were considered. Under control conditions, no constant growth within the technical replicates of Col-0 and putative *Atbbe*-like knock-outs could be observed. In most cases, the wild type showed even higher growth fluctuations than the mutants. This variation was also visible after the evaluation of the seedlings according to the defined categories. However, under drought conditions, the growth was drastically affected in both Col-0 and *Atbbe*-like mutants. Col-0 showed a significantly poorer plant status than the *Atbbe*-like protein 13 mutant under control conditions in two biological replicates, and this tendency was also visible under drought conditions. The evaluation of the second biological replicate on PEG plates showed a completely different result. Subsequently, no significant difference in medians over all three biological replicates could be determined (median shift $P = 0.7$) (Figure 15B). Due to the influence of the different categories on these results, we evaluated the number of healthy seedlings (summarized categories 0-2), too. Over three independent experiments, the *Atbbe*-like protein 13 mutant showed a significantly higher level of healthy green seedlings (77.3%) compared to Col-0 (56.6%) under control conditions, confirming the results first obtained. However, PEG induced osmotic stress showed similar effects on health and growth status of *Atbbe*-like protein 13 and Col-0 plants (Figure 15C). The relative germination rate of the mutant seems to be more strongly influenced by PEG stress compared to the wild type (Figure 15D). A detailed evaluation of affected and un-germinated seedlings confirmed the results already obtained under control conditions and showed developmental and growth defects of Col-0 (Figure 15E).

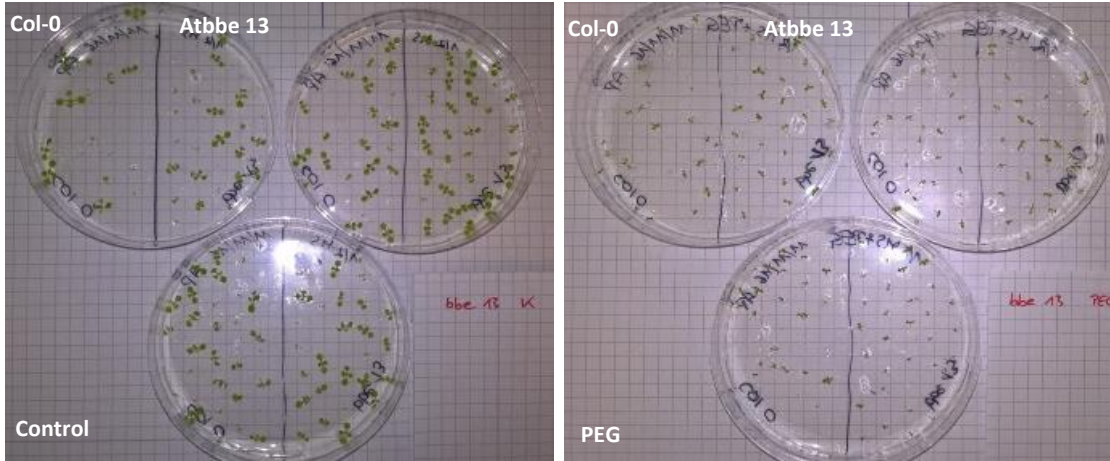
We also screened the *Atbbe*-like protein 15 mutant under control and drought conditions. Interestingly, the mutant showed similar plant growth compared to wild type under control conditions. PEG induced a degradation of plant status of *Atbbe*-like protein 15 mutants only in one biological replicate. This high variability in response to drought within the biological replicates has been observed again, and thereby, no significant changes over all experiments could be determined (median shift $P = 1$) (Figure 16B). Col-0 and the mutant showed the same number of healthy seedlings (categories 0-2), and the examination of the relative germination

yielded a tendency towards poorer development for *Atbbe*-like protein 15 in response to drought (Figure 16C-E). Next, we also examined the number of affected and germinated seedlings, and Col-0 and *Atbbe*-like protein 15 mutant showed similar results over all three experiments on control and PEG plates.

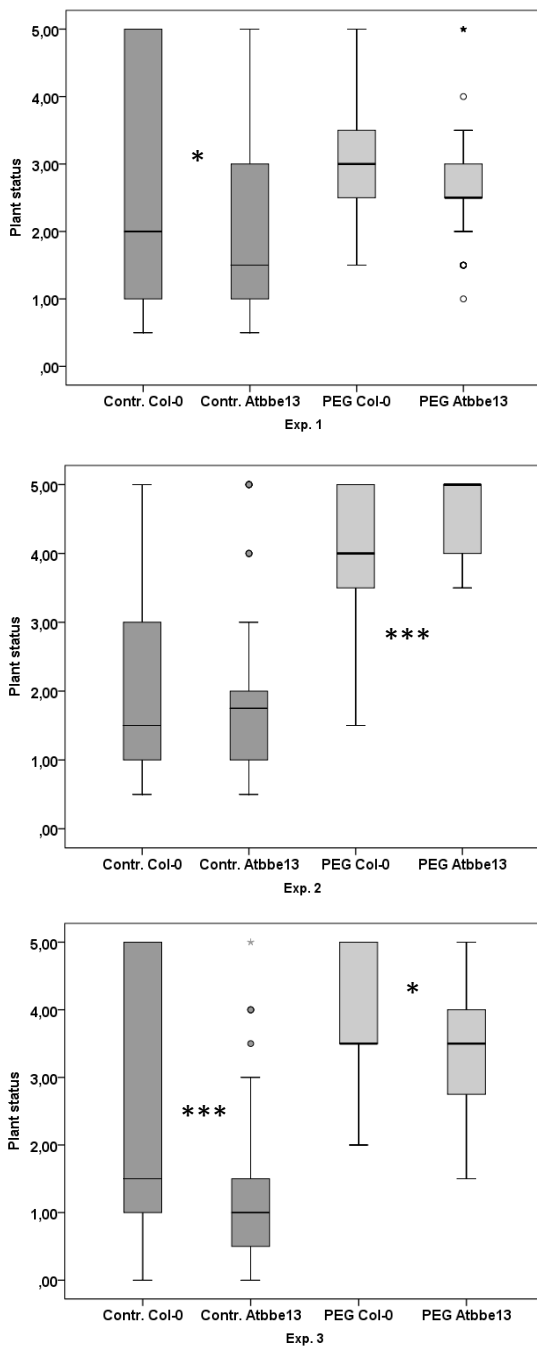
We also observed drought response for the putative double mutant for *Atbbe*-like proteins 13*15. Evaluation of the categories showed rather similar growth of wild type and mutant on half strength MS medium, except for one biological experiment, where Col-0 showed a significantly poorer growth than the mutant. In response to drought, the double mutant showed a distinctly decreased growth phenotype in one biological experiment compared to Col-0. The other two replicates showed a higher drought sensitivity of the wild type (Figure 17B). Over all three replicates, no significant differences of Col-0 and the double mutant were observed (median shift $P = 0.7$). The number of healthy seedlings (categories 0-2) was the same under control and PEG conditions for Col-0 and the double mutant. Analysis of the relative germination showed that there was also no difference in surviving seedlings on control and drought plates in both lines, and the same amount of seedlings was affected by PEG-treated (MS medium) plates (Figure 17C-E).

Phenotyping of *Atbbe*-like protein 26 plants on MS medium again showed a high variation in growth development of both Col-0 and the mutant. In two biological experiments, the plant status was higher for *Atbbe*-like protein 26 than for Col-0. On PEG plates, the mutant showed higher drought sensitivity in one experiment only, with a higher plant status level compared to Col-0. In total, no apparent differences between the two lines could be determined on PEG plates (median shift $P = 1$) (Figure 18B). Further, the effect of drought stress on healthy seedlings of *Atbbe*-like protein 26 and Col-0 was evaluated. In control conditions, no obvious difference could be observed within three biological replicates. However, PEG induced osmotic stress showed a significant decrease of the relative number of healthy *Atbbe*-like protein 26 seedlings compared to Col-0 (Figure 18C). Examination of germination rate showed a slight tendency of a higher drought sensitivity for the mutant. Further, the mutant showed a significant development defect with less germinated seedlings on control conditions (Figure 18D-E).

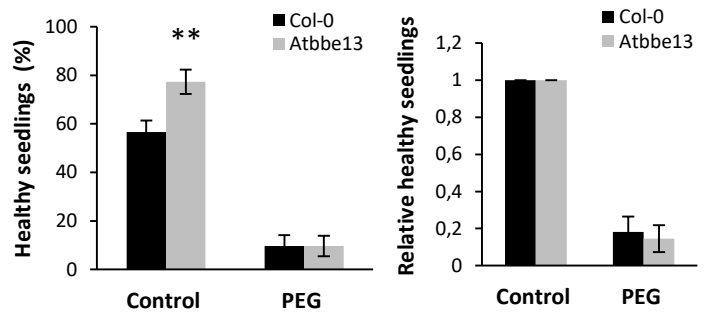
A



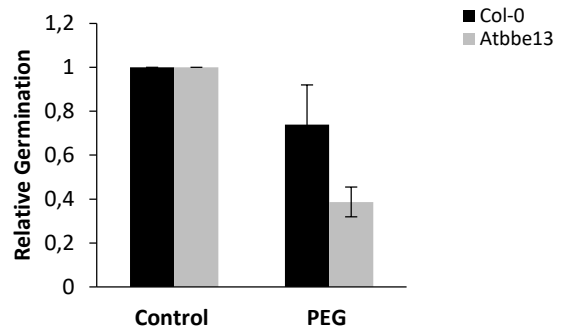
B



C



D



E

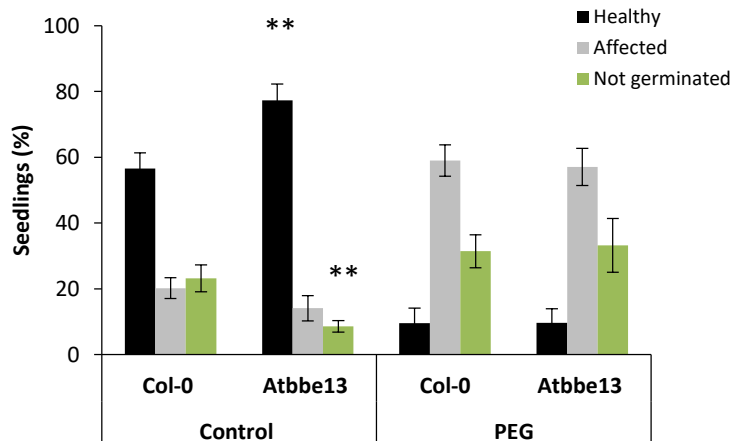


Figure 15. Drought stress (Polyethylene glycol; PEG) tolerance of putative *Atbbe*-like protein 13 mutant and wild type seedlings. **A.** Wild type Col-0 and transgenic seedlings were grown in parallel on half strength MS medium infused with PEG (250 g/L) or without (control) for 14 days in climate chambers under short day conditions (8 h day/16 h night cycle) with 200 $\mu\text{mol m}^{-2} \text{s}^{-1}$ light intensity at 24 °C/20 °C (day/night). **B.** Growth and health status of seedlings were evaluated according to different categories 0 = healthy with 4 or more green leaves (without cotyledons); 1 = healthy with 2 green leaves, 2 = healthy with cotyledons and the first appeared leaves; 3 = healthy, mainly the cotyledons; 4 = very small, cotyledons not open, yellow; 5 = not germinated; plus 0.5 p for anthocyanins and chlorosis. Box plots (n = \pm 90) of three independent biological replicates, with three technical replicates each, are shown \pm SD. Median of Exp. 1: Control Col-0 2.0, *Atbbe*-like 13 1.5, PEG Col-0 3.0, *Atbbe*-like 13 2.5; Exp. 2: Control Col-0 1.5, *Atbbe*-like 13 1.75, PEG Col-0 4.0, *Atbbe*-like 13 5.0, Exp. 3: Control Col-0 1.5, *Atbbe*-like 13 1.0, PEG Col-0 3.5, *Atbbe*-like 13 3.5. Statistical differences were evaluated by Mann-Whitney-U-Test for the *Atbbe*-like protein 13 mutant on control and salt plates compared to Col-0, indicated with * $P < 0.05$ and *** $P < 0.001$. **C.** Average of healthy green seedlings (summarized categories 0-2) and the relative rate of healthy seedlings (control values normalized to 1) on control and salt plates summarized from three biological replicates (n = 9) are shown. **D.** Relative germination rate (control values normalized to 1) of all seedlings compared to Col-0 are depicted. **E.** Comparison of healthy (categories 0-2), affected (categories 2.5-4.5) and un-germinated (category 5) seedlings from three biological replicates (n = 9). Bar charts show mean values (%) \pm SE of evaluated seedlings on control and salt plates based on three biological replicates with three technical replicates each. Asterisks indicate statistically significant differences of *Atbbe*-like protein 13 compared to wild type, according to Student's *t*-test (** $P < 0.01$).

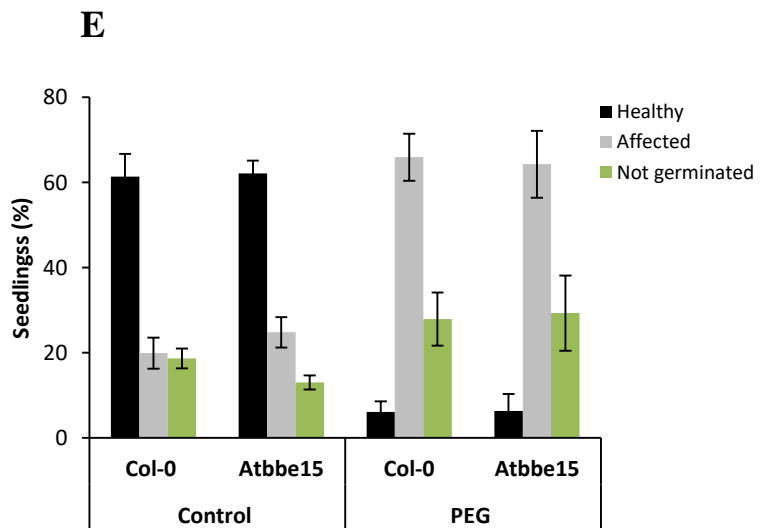
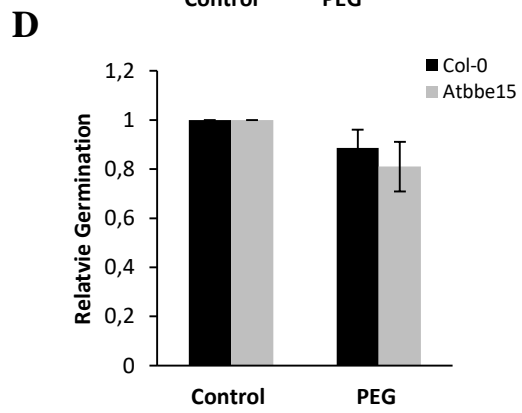
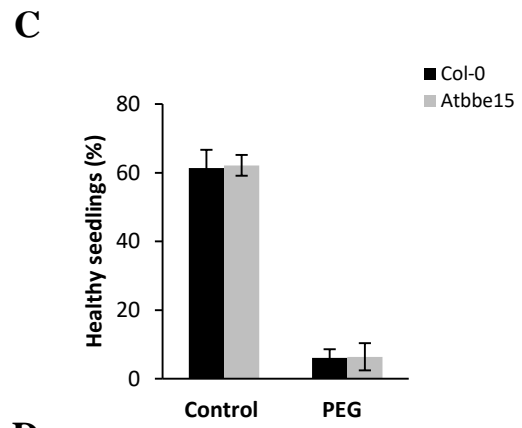
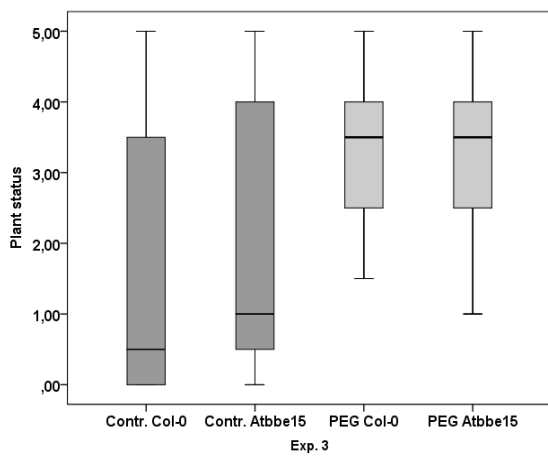
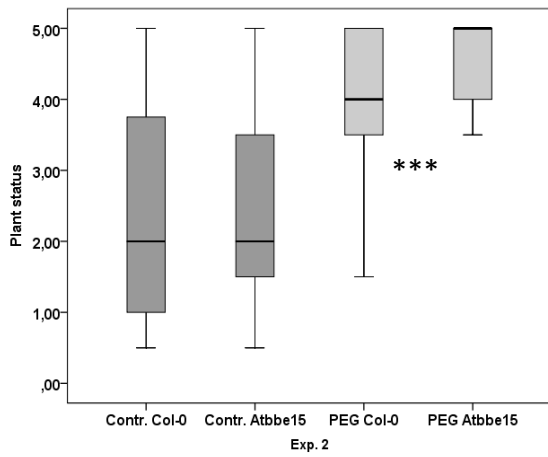
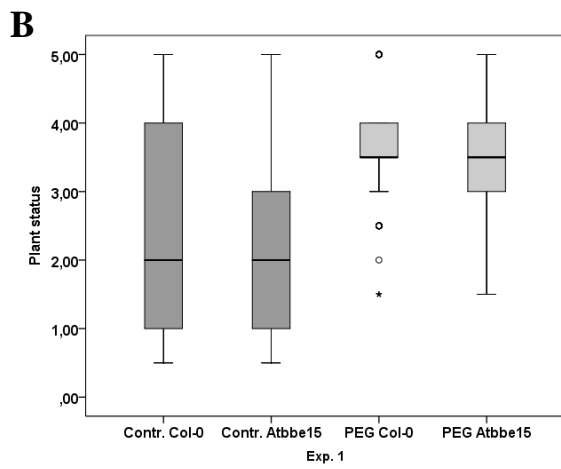
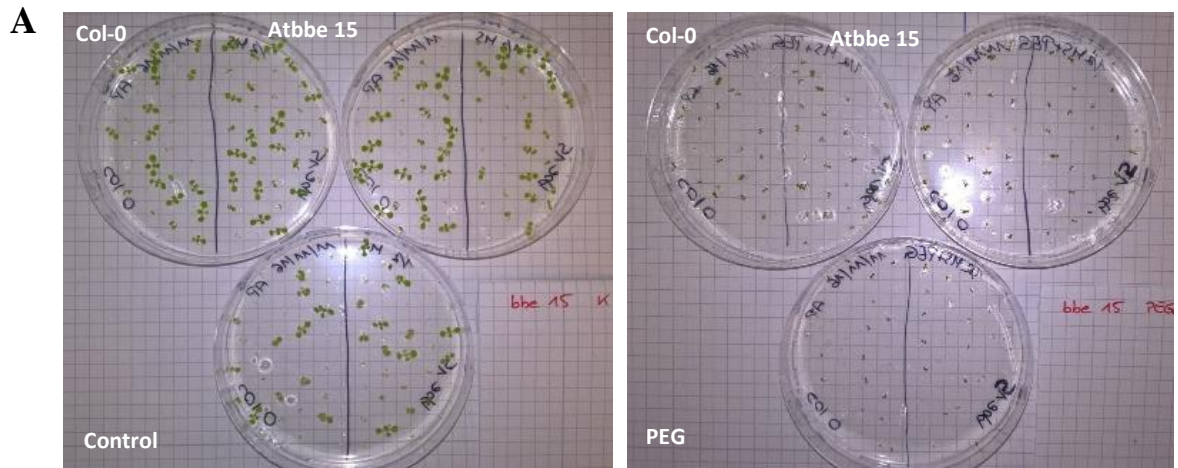


Figure 16. Drought stress (Polyethylene glycol; PEG) tolerance of putative *Atbbe*-like protein 15 mutant and wild type seedlings. **A.** Wild type Col-0 and transgenic seedlings were grown in parallel on half strength MS medium infused with PEG (250 g/L) or without (control) for 14 days in climate chambers under short day conditions (8 h day/16 h night cycle) with 200 $\mu\text{mol m}^{-2} \text{s}^{-1}$ light intensity at 24 °C/20 °C (day/night). **B.** Growth and health status of seedlings were evaluated according to different categories 0 = healthy with 4 or more green leaves (without cotyledons); 1 = healthy with 2 green leaves, 2 = healthy with cotyledons and the first appeared leaves; 3 = healthy, mainly the cotyledons; 4 = very small, cotyledons not open, yellow; 5 = not germinated; plus 0.5 p for anthocyanins and chlorosis. Box plots ($n = \pm 90$) of three independent biological replicates, with three technical replicates each, are shown \pm SD. Median of Exp. 1: Control Col-0 2.0, *Atbbe*-like 15 2.0, PEG Col-0 3.5, *Atbbe*-like 15 3.5; Exp. 2: Control Col-0 2.0, *Atbbe*-like 15 2.0, PEG Col-0 4.0, *Atbbe*-like 15 5.0, Exp. 3: Control Col-0 0.5, *Atbbe*-like 15 1.0, PEG Col-0 3.5, *Atbbe*-like 15 3.5. Statistical differences were evaluated by Mann-Whitney-U-Test for the *Atbbe*-like protein 15 mutant on control and salt plates compared to Col-0, indicated with *** $P < 0.001$. **C.** Average of healthy green seedlings (summarized categories 0-2) on control and salt plates summarized from three biological replicates ($n = 9$) are shown **D.** Comparison of healthy (categories 0-2), affected (categories 2.5-4.5) and un-germinated (category 5) seedlings from three biological replicates ($n = 9$). **E.** Relative germination rate (control values normalized to 1) of all seedlings compared to Col-0 are depicted. Bar charts show mean values (%) \pm SE of evaluated seedlings on control and salt plates based on three biological replicates with three technical replicates each. Statistical analysis was performed according to Student's *t*-test.

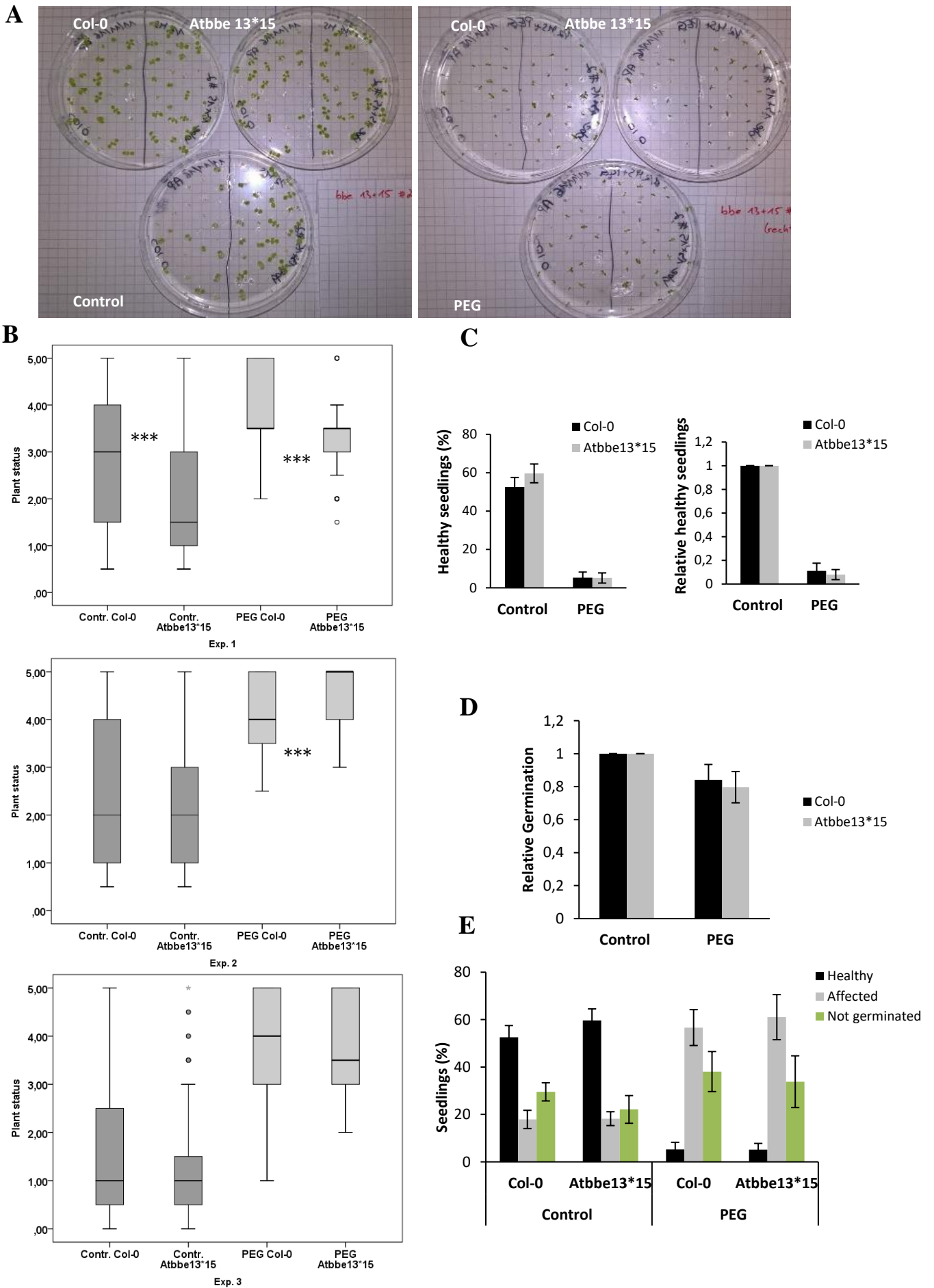
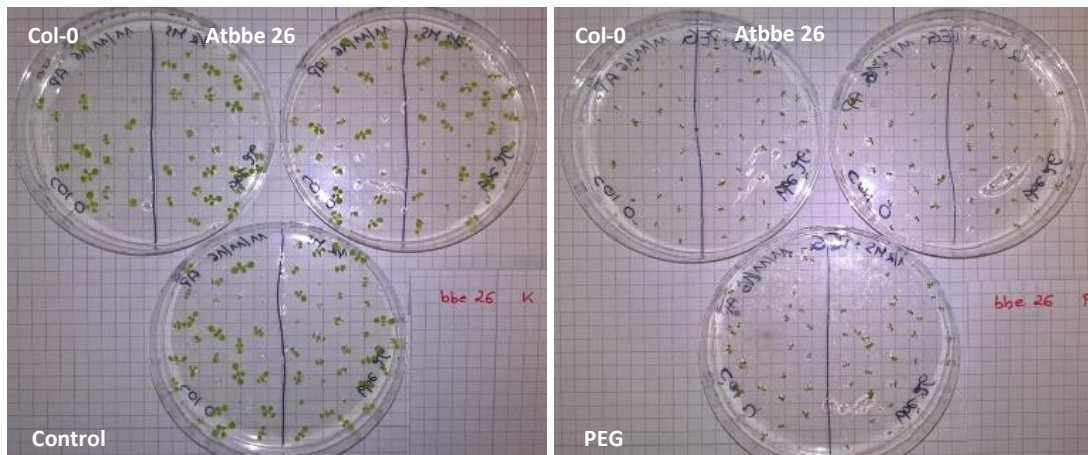
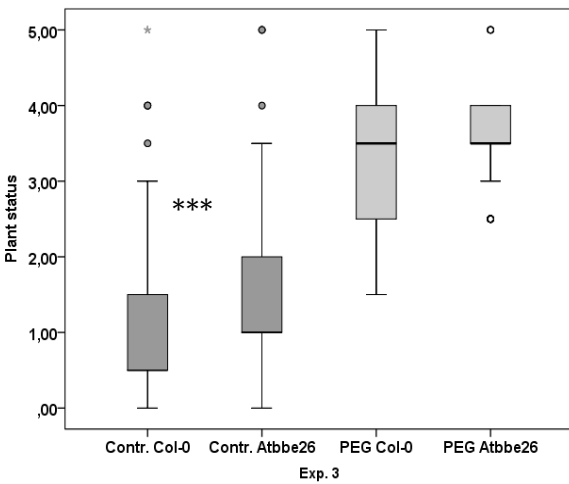
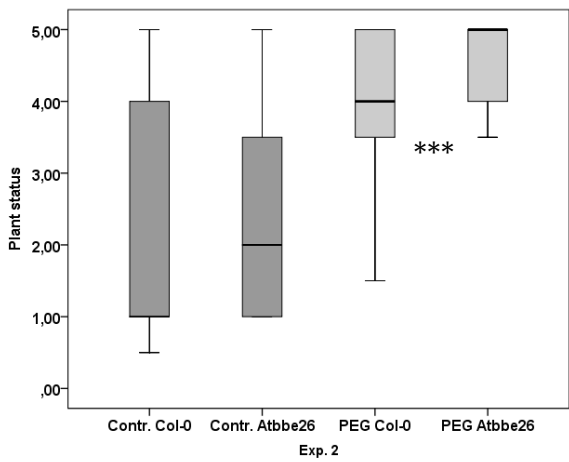
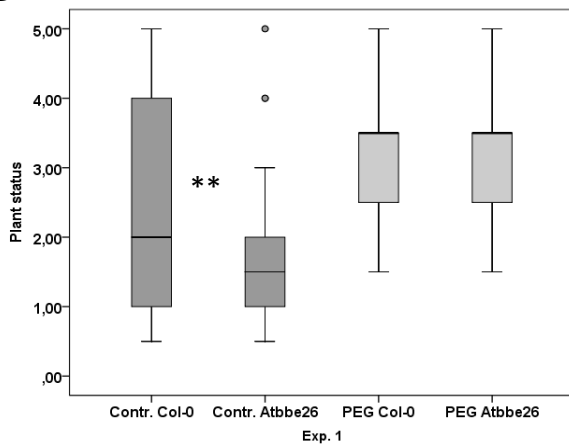


Figure 17. Drought stress (Polyethylene glycol; PEG) tolerance of putative *Atbbe*-like protein 13*15 mutant and wild type seedlings. **A.** Wild type Col-0 and transgenic seedlings were grown in parallel on half strength MS medium infused with PEG (250 g/L) or without (control) for 14 days in climate chambers under short day conditions (8 h day/16 h night cycle) with 200 $\mu\text{mol m}^{-2} \text{s}^{-1}$ light intensity at 24 °C/20 °C (day/night). **B.** Growth and health status of seedlings were evaluated according to different categories 0 = healthy with 4 or more green leaves (without cotyledons); 1 = healthy with 2 green leaves, 2 = healthy with cotyledons and the first appeared leaves; 3 = healthy, mainly the cotyledons; 4 = very small, cotyledons not open, yellow; 5 = not germinated and plus 0.5 p for anthocyanins and chlorosis. Box plots ($n = \pm 90$) of three independent biological replicates, with three technical replicates each, are shown \pm SD. Median of Exp. 1: Control Col-0 3.0, *Atbbe*-like 13*15 1.5, PEG Col-0 3.5, *Atbbe*-like 13*15 3.5; Exp. 2: Control Col-0 2.0, *Atbbe*-like 13*15 2.0, PEG Col-0 4.0, *Atbbe*-like 13*15 5.0, Exp. 3: Control Col-0 1.0, *Atbbe*-like 13*15 1.0, PEG Col-0 4.0, *Atbbe*-like 13*15 3.5. Statistically differences were evaluated by Mann-Whitney-U-Test for the *Atbbe*-like protein 13*15 mutant on control and salt plates compared to Col-0, indicated with *** $P < 0.001$. **C.** Average of healthy green seedlings (summarized categories 0-2) and the relative rate of healthy seedlings (control values normalized to 1) on control and salt plates summarized from three biological replicates ($n = 9$) are shown. **D.** Comparison of healthy (categories 0-2), affected (categories 2.5-4.5) and not germinated (category 5) seedlings for three biological replicates ($n = 9$). **E.** Relative germination rate (control values normalized to 1) of all seedlings compared to Col-0 are depicted. Bar charts show mean values (%) \pm SE of evaluated seedlings on control and salt plates based on three biological replicates with three technical replicates each. Statistical analysis was performed according to Student's *t*-test.

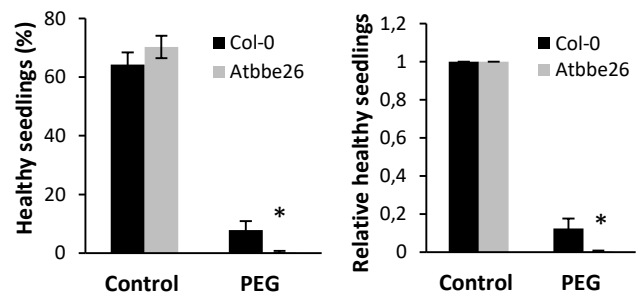
A



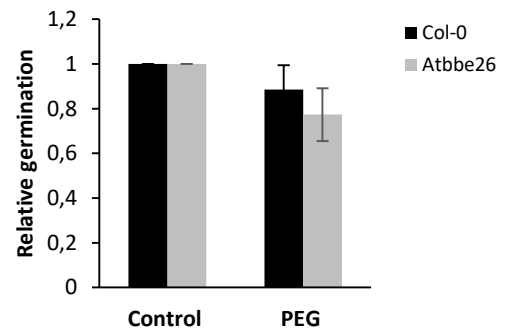
B



C



D



E

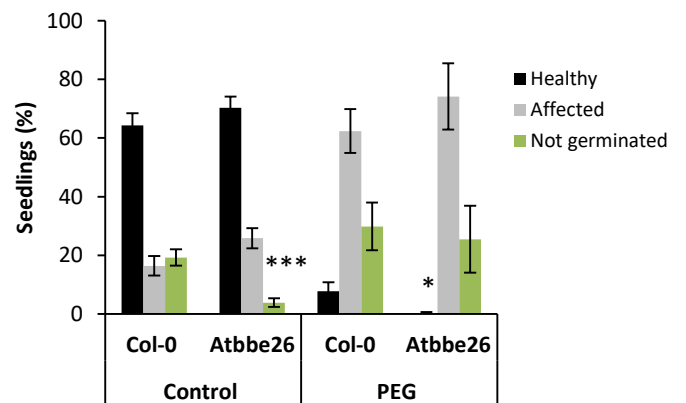
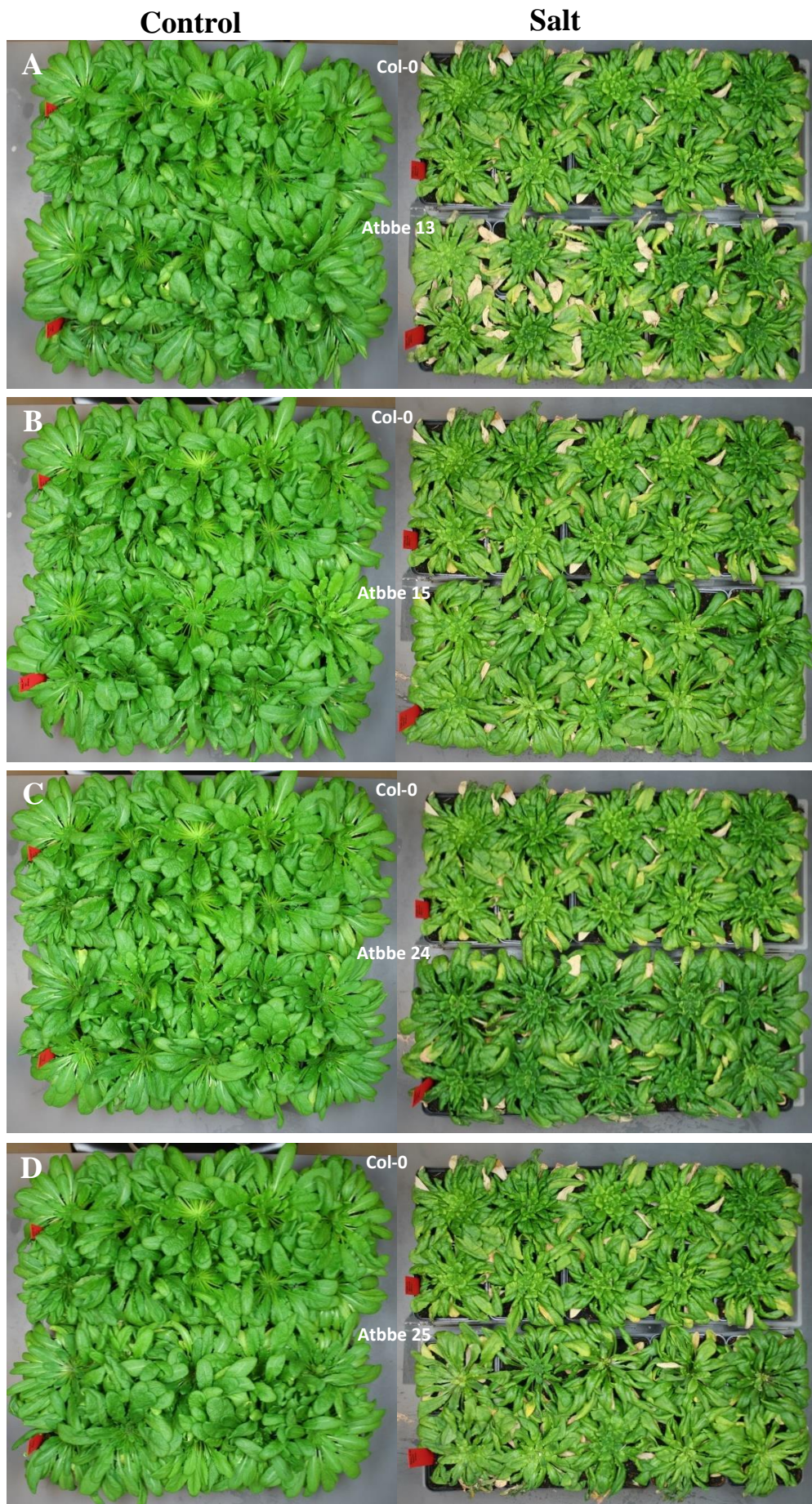


Figure 18. Drought stress (Polyethylene glycol; PEG) tolerance of putative *Atbbe*-like protein 26 mutant and wild type seedlings. **A.** Wild type Col-0 and transgenic seedlings were grown in parallel on half strength MS medium with PEG (250 g/L) or without (control) for 14 days in climate chambers under short day conditions (8 h day/16 h night cycle) with 200 $\mu\text{mol m}^{-2} \text{s}^{-1}$ light intensity at 24 °C/20 °C (day/night). **B.** Growth and health status of seedlings were evaluated according to different categories 0 = healthy with 4 or more green leaves (without cotyledons); 1 = healthy with 2 green leaves, 2 = healthy with cotyledons and the first appeared leaves; 3 = healthy, mainly the cotyledons; 4 = very small, cotyledons not open, yellow; 5 = not germinated; plus 0.5 p for anthocyanins and chlorosis. Box plots ($n = \pm 90$) of three independent biological replicates, with three technical replicates each, are shown \pm SD. Median of Exp. 1: Control Col-0 2.0, *Atbbe*-like 26 1.5, PEG Col-0 3.5, *Atbbe*-like 26 3.5; Exp. 2: Control Col-0 1.0, *Atbbe*-like 26 2.0, PEG Col-0 4.0, *Atbbe*-like 26 5.0, Exp. 3: Control Col-0 0.5, *Atbbe*-like 26 1.0, PEG Col-0 3.5, *Atbbe*-like 26 3.5. Statistical differences were evaluated by Mann-Whitney-U-Test for the *Atbbe*-like protein 26 mutant on control and salt plates compared to Col-0, indicated with ** $P < 0.01$ and *** $P < 0.001$. **C.** Average of healthy green seedlings (summarized categories 0-2) and the relative rate of healthy seedlings (control values normalized to 1) on control and salt plates summarized from three biological replicates ($n = 9$) are shown **D.** Comparison of healthy (categories 0-2), affected (categories 2.5-4.5) and not germinated (category 5) seedlings of three biological replicates ($n = 9$). **E.** Relative germination rate (control values normalized to 1) of all seedlings compared to Col-0 are depicted. Bar charts show mean values (%) \pm SE of evaluated seedlings on control and salt plates based on three biological replicates with three technical replicates each. Statistical analysis was performed according to Student's *t*-test and asterisks indicates * $P < 0.05$ and *** $P < 0.001$.

Due to the *in vitro* salt sensitivity of the *Atbbe*-like protein 13 and 15 mutants, we investigated the salt tolerance of these transgenic lines and of the whole phylogenetic group 6 on soil. We compared the phenotype of 8-week-old Col-0 and homozygous mutants of *Atbbe*-like proteins 13, 15, 24, 25 and 26 plants in a first experiment with a gradient of salt concentrations (50, 100, 150 and 200 mM NaCl). In parallel, control plants of each line and Col-0, were grown to observe the phenotype without salt treatment. We investigated the response to prolonged periods of salt stress with a gradient and found that the *Atbbe*-like protein 13 mutant had a decreased resistance to salt compared to wild type plants (Figure 19A). *Atbbe*-like protein 13 mutant plants showed more yellowed leaves than Col-0. *Atbbe*-like protein 15, 24, 25 and 26 mutant plants did not exhibit any obvious differences in salt tolerance compared to wild type plants. A possible enhanced salt stress tolerance of *Atbbe*-like protein 26 was also observed. Under control conditions, *Atbbe*-like mutant plants showed no clear difference in development compared to Col-0 plants (Figure 19B-E). In a second biological experiment, the tolerance of 10-week-old *Atbbe*-like protein 13, 15, 26 and 13*15 mutant plants was observed under a constant impact of 200 mM NaCl. We again observed a decreased salt resistance of *Atbbe*-like protein 13 mutant plants, and the same result for the double mutant *Atbbe*-like protein 13*15. *Atbbe*-like protein 15 and 26 mutants showed no difference in salt stress response compared to wild type. No obvious developmental defects under control conditions could be observed for homozygous *Atbbe*-like protein 13, 15 and 26 mutant plants, except for the double mutant *Atbbe*-like 13*15, which featured first yellow leaves (Figure 20A-D).



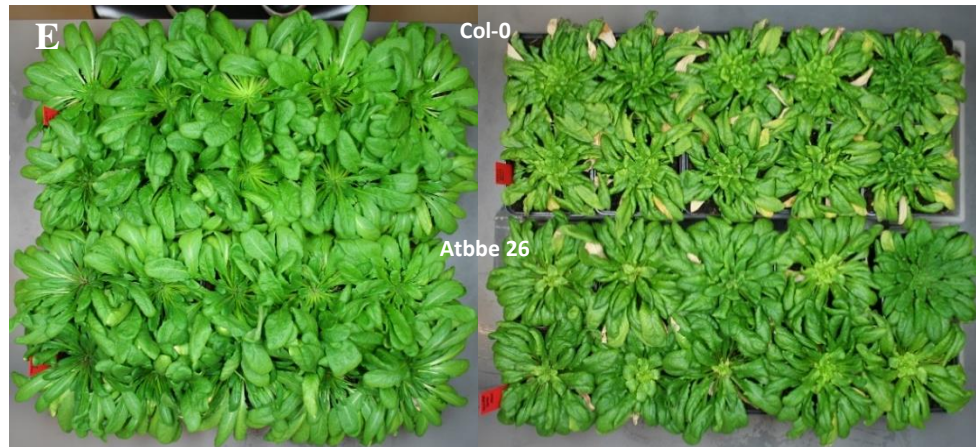


Figure 19. Phenotypes and salt tolerance of putative *Atbbe*-like protein 13, 15, 24, 25 and 26 mutant plants. **A-E.** 8-week-old plants of wild type Col-0 and putative *Atbbe*-like knock-out mutants, growing under short day conditions (8 h light/16 h dark with $130 \mu\text{mol m}^{-2}\text{s}^{-1}$ light intensity at $24^\circ\text{C}/20^\circ\text{C}$), were watered for 31 days (4 days intervals) with increasing NaCl concentrations (50, 100, 150 and 200 mM). Single plants of wild type and *Atbbe*-like mutant lines were grown in pots, and 10 pots per line were used in total. Col-0 and *Atbbe*-like mutant plants were watered in parallel for the same time and at the same intervals. The photographs showing the difference of salt response were taken 4 days after the last treatment. *Atbbe*-like protein 13, 15, 24, 25, 26 mutants and wild type Col-0 plants were grown in parallel and irrigated with water (control, left) or salt solution (right).

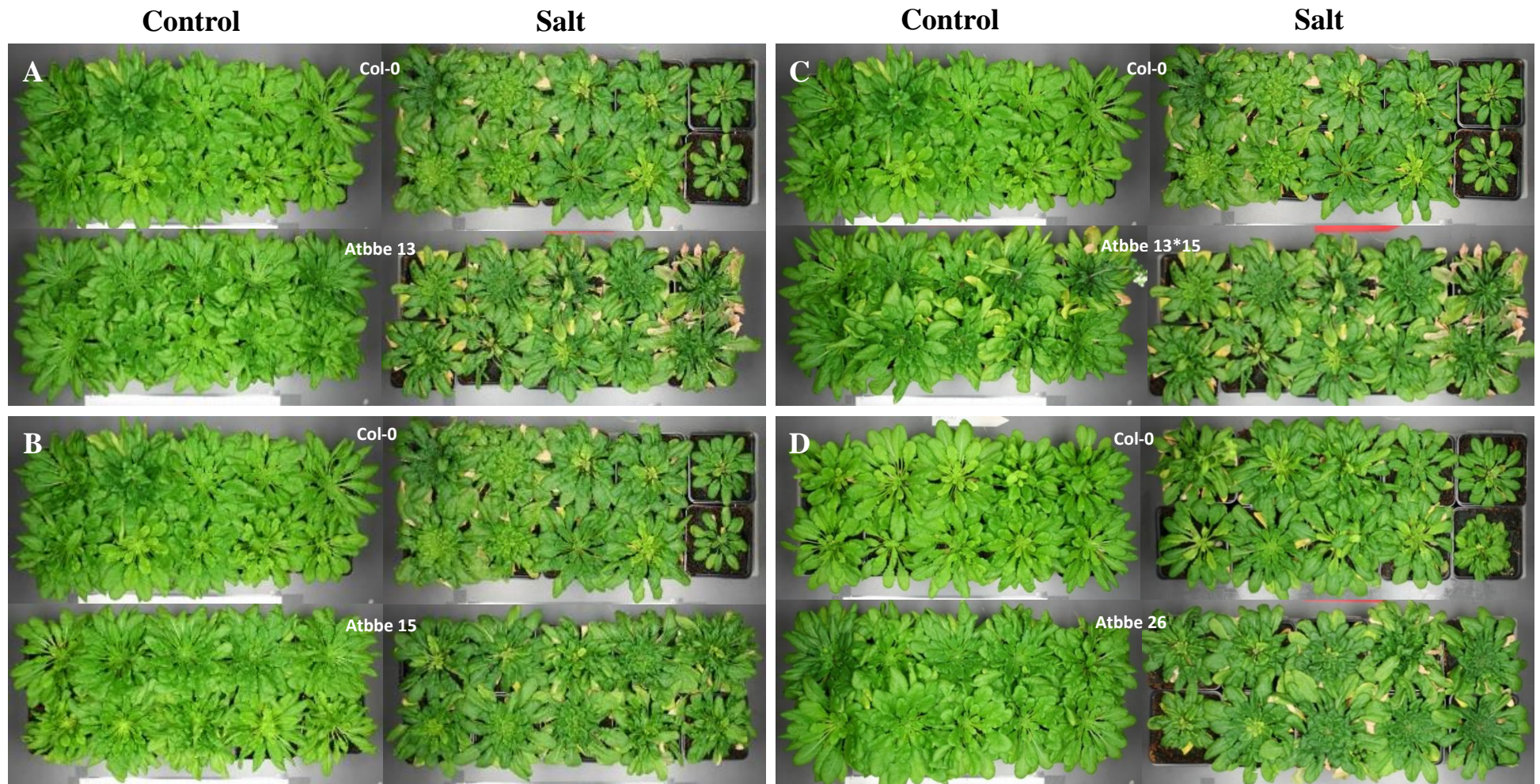


Figure 20. Phenotypes and salt tolerance of putative *Atbbe*-like protein 13, 15, 26 and 13*15 mutant plants. A-D. 10-week-old plants, growing under short day conditions (8 h light/16 h dark with $130 \mu\text{mol m}^{-2}\text{s}^{-1}$ light intensity at $24^\circ\text{C}/20^\circ\text{C}$), of wild type Col-0 and putative *Atbbe*-like knock-out mutants were treated for 21 days at 4-day intervals with 200 mM NaCl. Single plants of wild type and mutants were grown in pots, and 10 pots per line were used in total. Col-0 and *Atbbe*-like mutant plants were watered in parallel for the same time and at the same intervals. The photographs showing the difference of salt response were taken after 4 days after the last treatment. *Atbbe*-like protein 13, 15, 26, 13*15 mutants and wild type Col-0 plants were grown in parallel and irrigated with water (control, left) or salt solution (right).

5.4.2. Root length and shoot weight of putative *Atbbe*-like protein mutants under salt stress

To investigate the influence of salt stress on root development and biomass, seeds of *Atbbe*-like protein 13, 15, 26, 28, 13*15 mutant lines and wild type Col-0 were sown on half strength MS medium without (control) or with 100 mM NaCl. Seedlings were pre-grown under control conditions for 1 week with 8 h light/16 h dark cycle at 24 °C/20 °C and were then transferred to salt and control plates for another week of vertical growth. The primary root length was monitored and evaluated with ImageJ^R. As shown in Figure 21A-C and Figure 22A-B, both wild type and *Atbbe*-like mutant plants showed a significant decrease in primary root length on salt compared to control plates. Seedlings of both wild type and mutant lines showed shorter and thinner primary roots compared to roots on control conditions. Many of the seedlings were influenced in development, with smaller and bleached leaves. When 1-week-old seedlings were transferred to control plates for vertical growth, no significant difference in primary root length was visible between the mutant lines for *Atbbe*-like protein 13 and 13*15 and wild type Col-0. *Atbbe*-like protein 15, 26 and 28 mutant seedlings exhibited shorter root lengths compared to wild type under control conditions. Seedlings were transferred to MS medium supplemented with 100 mM NaCl, and the primary root length of *Atbbe*-like protein mutants 15 and 26 (16% and 15% reduction, respectively) was less influenced by salt compared to a mean of Col-0 (24% reduction). *Atbbe*-like 13*15 double mutant, however, suffered significantly more from salt stress compared to wild type (38% reduction). Control data were normalized to consider root growth variations of Col-0 and *Atbbe*-like mutant seedlings on control medium (Figure 23).

To determine whether salt stress influences the biomass, the same 14-day-old transgenic and wild type seedlings were individually weighed. Wild type Col-0 and *Atbbe*-like protein 13, 15 and 28 mutant plants showed the same fresh weight on control medium, whereas the *Atbbe*-like protein 26 mutant exhibited a significantly lower, and *Atbbe*-like protein 13*15 mutant showed an even higher biomass compared to Col-0. An obvious reduction in biomass could be observed after the transfer of seedlings to salt plates for wild type (18% reduction, Figure 24A-F). However, the mutant seedlings suffered less from salt stress compared to wild type and exhibited the same or an even higher biomass on salt plates than under control conditions. Furthermore, no decrease in relative biomass in response to salt for all mutant lines compared to a mean of Col-0 was observable. *Atbbe*-like protein 13, 26 and 28 mutants showed significantly higher salt resistance than Col-0, and these results suggest an improved salt tolerance of transgenic plants, as they developed higher biomass compared to wild type.

Furthermore, *Atbbe*-like protein 13 and 26 mutants featured even higher biomass on salt plates (4% and 10%, respectively) than under control conditions.

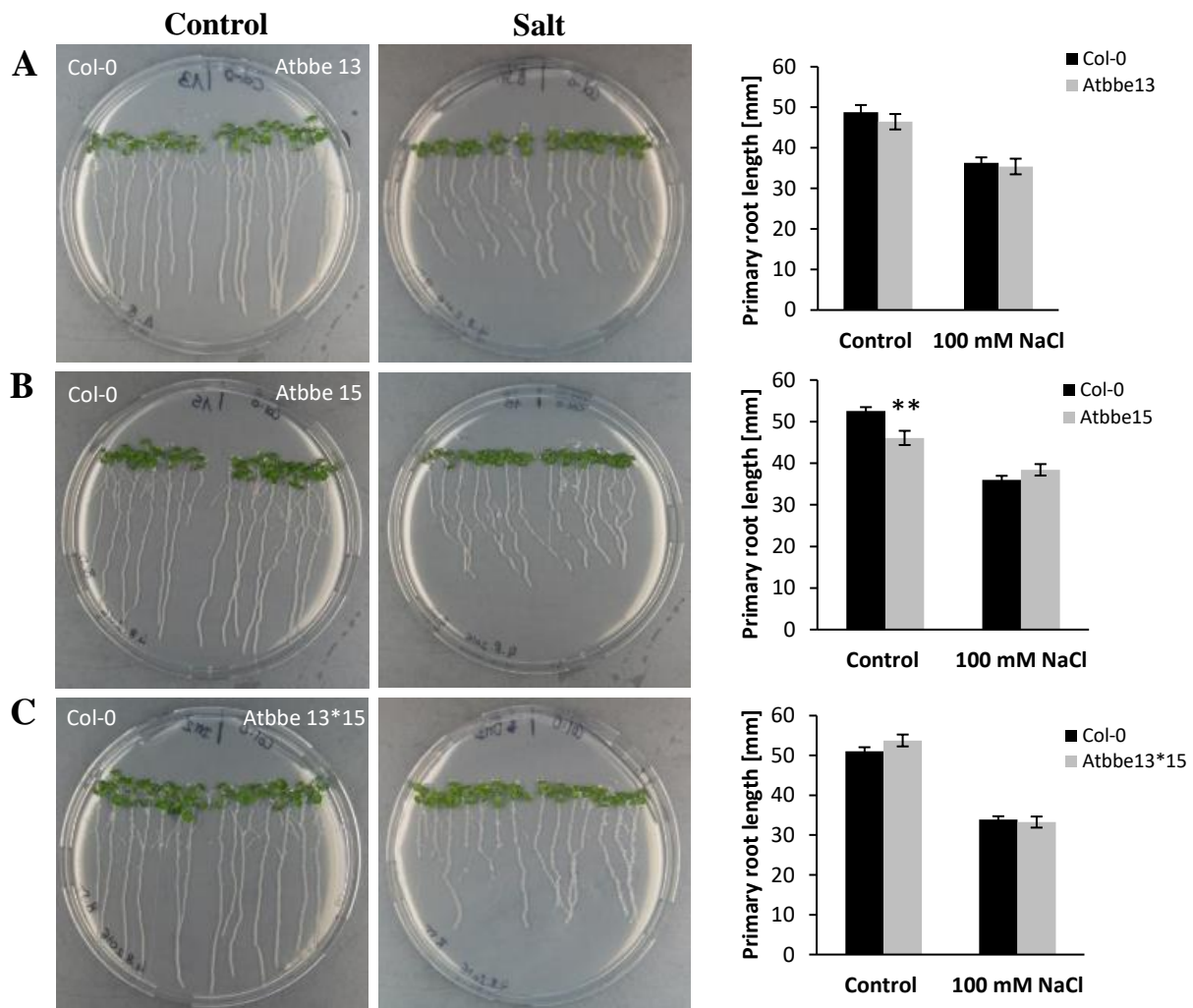


Figure 21. Primary root development of wild type and putative *Atbbe*-like protein 13, 15 and 13*15 mutant plants. A-C. Wild type and *Atbbe*-like protein mutant plants were grown on half strength MS medium (control) for 7 days and were then transferred to control and salt (100 mM NaCl) plates in parallel and grown for another 7 days under short day conditions (8 h light/16 h dark) with $200 \mu\text{mol m}^{-2}\text{s}^{-1}$ light intensity at $24^\circ\text{C}/20^\circ\text{C}$. Primary root length was measured with ImageJ^R, and statistical analysis of primary root lengths of Col-0 and mutant plants is depicted in bar charts. Mean values \pm SE are shown for a summary of five independent experiments ($n = \pm 35$). Asterisks indicate statistically significant differences according to Student's *t*-test (** $P < 0.01$).

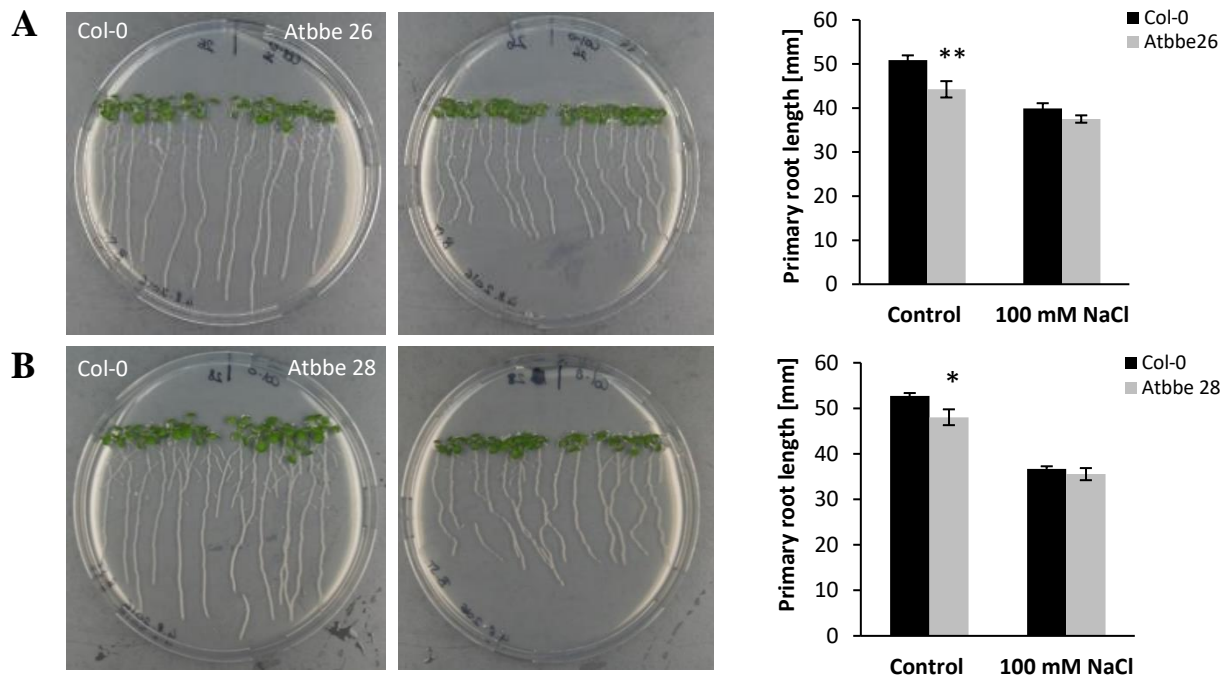


Figure 22. Primary root development of wild type and putative *Atbbe*-like protein 26 and 28 mutant plants. **A-B.** Wild type and *Atbbe*-like protein mutant plants were grown on half strength MS medium (control) for 7 days and were then transferred to control and salt (100 mM NaCl) plates in parallel and grown for another 7 days under short day conditions (8 h light/16 h dark) with $200 \mu\text{mol m}^{-2}\text{s}^{-1}$ light intensity at $24 \text{ }^{\circ}\text{C}/20 \text{ }^{\circ}\text{C}$. Primary root length was measured with ImageJ^R, and statistical analysis of primary root lengths of Col-0 and mutant plants is depicted in bar charts. Mean values \pm SE are shown for a summary of five independent experiments ($n = \pm 35$). Asterisks indicate statistically significant differences according to Student's *t*-test (* $P < 0.05$, ** $P < 0.01$).

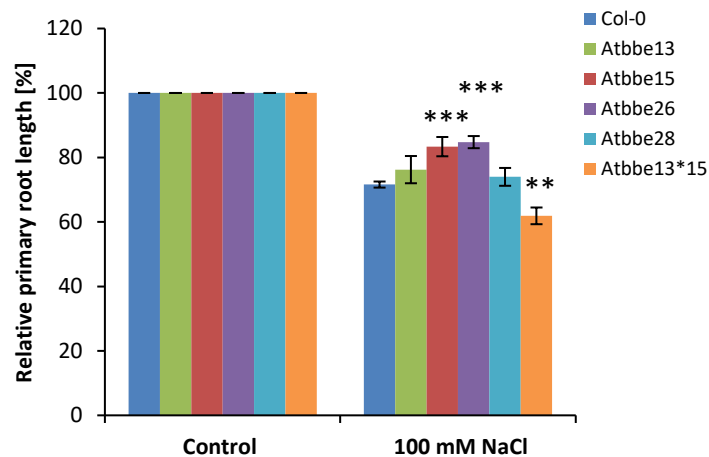


Figure 23. Statistical analysis of the relative primary root length of wild type and putative *Atbbe*-like protein 13, 15, 26, 28 and 13*15 mutants. Root length of 14-day-old seedlings, grown for 7 days on half strength MS medium (control) and another 7 days on half strength MS with salt (100 mM NaCl) under short day conditions (8 h light/16 h dark) with $200 \mu\text{mol m}^{-2}\text{s}^{-1}$ light intensity at $24 \text{ }^{\circ}\text{C}/20 \text{ }^{\circ}\text{C}$. Data is means \pm SE of one biological replicate, with five technical replicates each ($n = \pm 35$) for *Atbbe*-like mutant lines. For Col-0, the mean was calculated from controls from all experiments with the individual transgenic lines ($n = \pm 175$). The primary root length was measured with ImageJ^R, and Student's *t*-test was used to test for statically significant differences (** $P < 0.01$, *** $P < 0.001$) between the *Atbbe*-like protein 13, 15, 26, 28, 13*15 mutant lines and wild type Col-0. Mean values under control conditions were normalized to 100%.

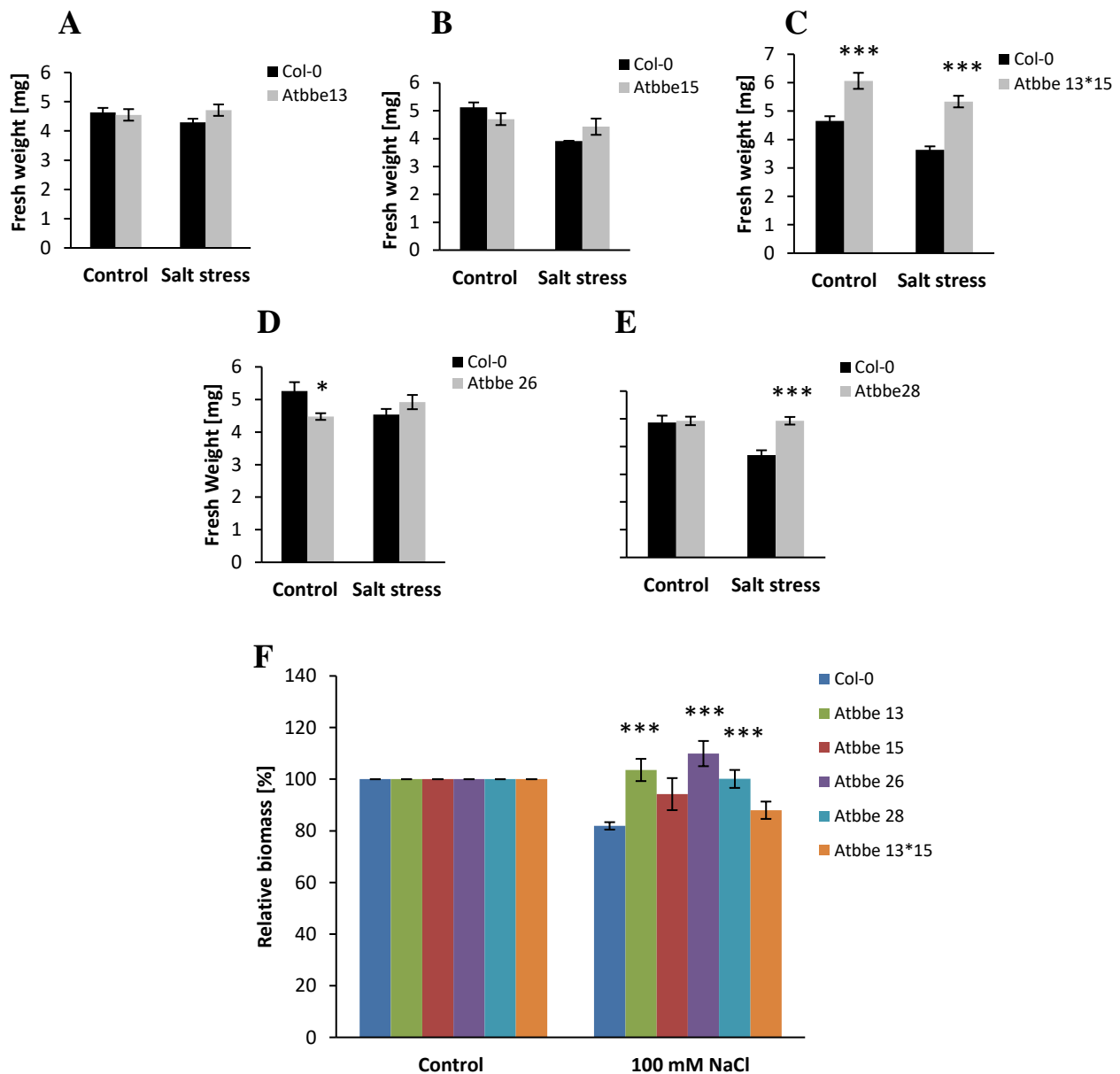


Figure 24. Fresh weight of wild type and *Atbbe*-like protein 13, 15, 26, 28 and 13*15 mutant seedlings on control medium and salt medium A-E. Fresh weight of 14-day-old seedlings, grown for 7 days on half strength MS medium (control) and for another 7 days on half strength MS with salt (100 mM NaCl) under short day conditions (8 h light/16 h dark) with 200 $\mu\text{mol m}^{-2}\text{s}^{-1}$ light intensity at 24 °C/20 °C. Data is means \pm SE for one biological replicate, with five technical replicates each ($n = \pm 35$) for *Atbbe*-like mutant lines. Independent Student's *t*-tests demonstrated that there was a significant (* $P < 0.05$, *** $P < 0.001$) difference between the mutant lines and wild type Col-0 under control and salt conditions. **F.** Relative biomass is indicated after calculation from the same dataset. The mean values under control conditions were normalized to 100%. The mean for Col-0 was calculated from controls from all experiments with the different transgenic lines ($n = \pm 175$).

5.4.3. Lignin content of *Atbbe*-like protein 13 and 15 mutant cell walls determined by the acetyl bromide method

To quantify the lignin content, we analyzed *Arabidopsis Atbbe*-like protein 13 and 15 mutant stems, young and old part, using the acetyl bromide method. The plants were grown in a greenhouse under long-day conditions with a 16 h photoperiod and were harvested after 6 weeks when they were already flowering. Stems were dried for 48 h, and the material was ground, extracted and freeze dried. Dry cell wall (DCW) material (46 mg) was used for calculation of lignin amount by using the absorbance of lignin at 280 nm and an extinction coefficient of $17,688 \text{ L g}^{-1} \text{ cm}^{-1}$ [59]. Evaluated data showed no difference in lignin content per mg dry cell wall material in old stem sections of putative *Atbbe*-like protein 13 and 15 mutants compared to Col-0. Lignin content was 20.3% of total DCW in Col-0 compared to 21% and 20.7% in *Atbbe*-like protein 13 and 15 mutants, respectively. In young stems, *Atbbe*-like protein 13 mutants showed a slightly higher lignin content compared to Col-0. No changes in respect to lignin content in young stems were observed between *Atbbe*-like protein 15 mutants and wild type. The estimated lignin content was 16.7% of total DCW for Col-0, 17.2% for the *Atbbe*-like protein 13 mutant, and 16.7% for the *Atbbe*-like protein 15 mutant. These data generally underline the knowledge about a higher lignification in older parts of plant stems (Figure 25).

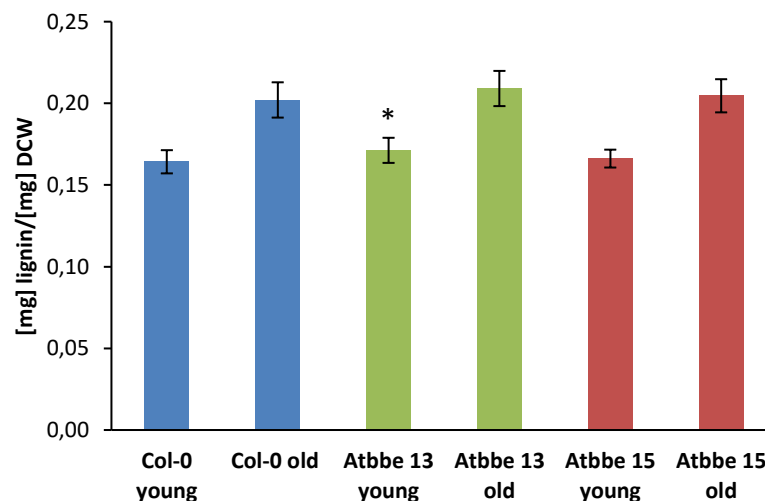


Figure 25. Lignin content of putative *Atbbe*-like protein 13 and 15 mutant stem sections. Lignin was determined using the acetyl bromide method according to Hatfield *et al.* [59]. *Atbbe*-like protein 13 and 15 mutants and wild type Col-0 were grown under long day conditions with a 16 h photoperiod for 6 weeks, and flower stalks (young and old part) were harvested. Mean values \pm SD from one biological replicate, 3 plants per line for young and old flower stalks (4 measured values per sample). Lignin content in dry cell weight is indicated in mg/mg. Asterisk indicates a statistically significant difference of lignin content in young stems of the *Atbbe*-like protein 13 mutant compared to young stems of Col-0 according to Student's *t*-test (* $P < 0.05$).

5.4.4. Lignin composition analysis of *Atbbe*-like protein 13 and 15 mutant cell walls by thioacidolysis and Gas Chromatography-Mass Spectrometry (GC-MS)

Lignin analysis was performed for *Atbbe*-like protein 13 and 15 mutants and wild type Col-0 for three independent biological replicates, with three technical replicates with 24 plants per line each. Plants were grown in a greenhouse under long day conditions (16 h light) for around 7-10 weeks depending on temperature in the greenhouse until the siliques started to ripen and the leaves got yellow. Stem material was harvested and dried at 60 °C for 72 h for lignin analysis (see Supplementary Table S5) and extracted and analyzed with thioacidolysis and GC-MS by Prof. Catherine Lapierre (Institute Jean-Pierre Bourgin, INRA-AgroParisTech, Versailles, France). The lignin units, *p*-hydroxyphenyl (H), guaiacyl (G) and syringyl (S) are involved in the β -O-4 bonding pattern and are indicated as H, G and S thioacidolysis monomers. These monomers, obtained as pairs of erythro/threo isomers (about 50/50 ratio), were analyzed by GC-MS of their trimethylsilylated (TMS) derivatives and quantified from ion chromatograms. The yield of the S and G lignin derived monomers gives an estimate of the amount of units only involved in labile β -O-4 bonds. The yield of lignin-derived H, G and S main monomers and of coniferaldehyde-derived monomers (CALD) were analyzed and expressed in $\mu\text{mol/g}$ CW. Relative frequencies (% molar) are also shown in Supplementary Table S6 for all three biological replicates. The overall lignin content (H, G, S lignin monomers) ($\mu\text{mol/g}$ CW) was estimated for all three biological replicates and compared to the lignin content of Col-0. In the first biological replicate, the lignin content was the same in the *Atbbe*-like protein mutants and in Col-0. The lignin content of all samples, Col-0 and mutant lines, was generally lower compared to the other two biological replicates (Col-0 S1 187 $\mu\text{mol/g}$, *Atbbe*-like 13 S1 186 $\mu\text{mol/g}$, *Atbbe*-like 15 S1 176 $\mu\text{mol/g}$ CW). Reasons for this might be different developmental stages of the individual biological replicates and different greenhouse conditions. In the second replicate, the mutant lines exhibited a reduced lignin content compared to wild type. In replicate 2 the lignin content was reduced by 10% in the *Atbbe*-like protein 13 mutant and by 14% in *Atbbe*-like protein 15 mutant plants. A significant reduced lignin content could be observed again in replicate 3 for both the *Atbbe*-like protein 13 and 15 mutants (9% reduction for both) (Figure 26A).

Furthermore, the total aldehyde percentage of the total lignin content was determined and is depicted in Figure 26B. While replicate 2 and 3 are in good agreement, replicate 1 differs from the other replicates. Since the overall lignin content in the first biological replicate was reduced, a reduction of the overall aldehyde content was to be anticipated. However, *Atbbe*-like protein 15 mutant plants showed a continuous reduction of coniferyl aldehydes throughout all biological replicates compared to wild type. The aldehyde content of *Atbbe*-like protein 13 and

15 mutant plants in replicate 2 was reduced by 22% and 17%, and in replicate 3 significantly by 11% and 27%, respectively, compared to Col-0. To determine if the lignin composition was altered, the percentage of coniferyl aldehyde in total lignin was calculated. A reduction of the aldehyde percentage in putative *Atbbe*-like protein 15 knock out plants by 6% and 11% was observed in replicate 1 and 3, respectively. In contrast to this, in replicate 2 the aldehyde percentage of the putative *Atbbe*-like 13 knock out mutant was reduced by 8% (Figure 26B, C).

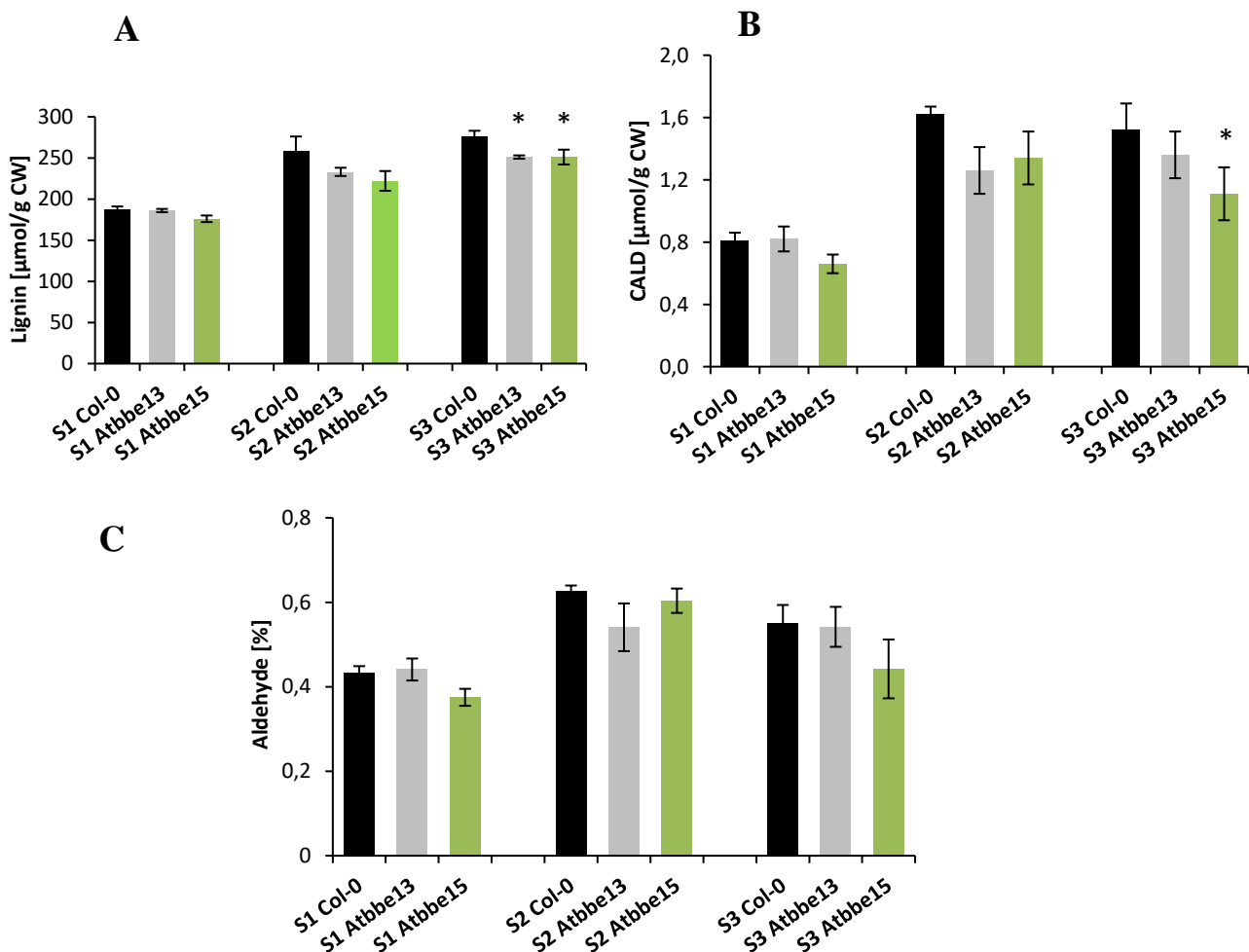


Figure 26. Lignin analysis by thioacidolysis and GC-MS. *Atbbe*-like protein 13 and 15 mutants and wild type Col-0 were grown under long day conditions in a greenhouse with a 16 h photoperiod for 7-10 weeks. In total, three independent biological replicates (S1 = black, S2 = grey, S3 = green), with three technical replicates each (24 plants per line), were generated. Stem material was harvested, dried at 60 °C for 72 h, extracted and analyzed by thioacidolysis and GC-MS. Mean values \pm SD are shown from one biological replicate. Independent Student's *t*-tests demonstrates significant (* $P < 0.05$) differences in lignin or aldehyde content between transgenic lines and controls. **A.** Total lignin content (H, G, and S monomers of lignin) is shown in $\mu\text{mol/g}$ dry cell weight (CW). **B.** Overall coniferylaldehyde (CALD) content in $\mu\text{mol/g}$ CW in total lignin of three biological replicates. **C.** Percentage of CALD in total lignin of three biological replicates.

5.4.5. *Atbbe*-like protein 15 gene expression under salt stress analyzed by qRT-PCR

To investigate the role of *AtBBE*-like protein 15 during stress response, we started to investigate the influence of salt (100 mM NaCl) on the expression level in wild type seedlings. According to the Arabidopsis eFP browser, 18-day-old Col-0 plants showed a higher expression level in roots under salt stress (150 mM NaCl) (absolute expression value 65.8), and also an upregulation in shoots (28.56) compared to control plants (roots 21.7; shoot 10.67) [47]. We analyzed 1-week-old Col-0 seedlings which were grown under long day conditions (16 h/8 h day/night cycle) and transferred in parallel onto MS medium without (control) or with salt for 24 h. The experiment was not repeated. Total RNA was isolated from the whole seedlings, reverse transcribed, and the transcript level of the *AtBBE*-like gene was determined by qRT-PCR using *ACTIN 2* as reference gene. The expression of *AtBBE*-like protein 15 was remarkably up-regulated in seedlings upon salt treatment for 24 h compared to control conditions. We observed a 2.7-fold (relative value) up-regulation of *AtBBE*-like protein 15 expression under salt treatment.

5.4.6. Root apical meristem and root diameter of putative *Atbbe*-like protein 28 mutant seedlings

To study the root development of *Atbbe*-like protein 28 mutant seedlings, we analyzed 7-day-old seedlings under the light microscope, which were grown vertically under long day conditions (16 h/8 h day night cycle). In total, two biological replicates with 10 seedlings of *Atbbe*-like protein 28 mutant and Col-0 each were measured. We evaluated the root apical meristem length (RAM) and the root diameter at two different positions at the first primordium, and the first lateral root of the primary root. We observed for the *Atbbe*-like protein 28 mutant a significantly longer RAM compared to wild type, with a 27% increase in the first experiment. In the second experiment, no obvious differences were found, and a slight elongation of the RAM of 3% in the mutant could be determined (Figure 27E). The root diameters of the first lateral root primordium and at the first visible lateral root were measured and analyzed for the first biological replicate. Statistical evaluation identified a significantly higher diameter at the first lateral root primordium in the mutant compared to wild type. However, at the position of the first lateral root, the primary root diameter of transgenic plants was similar to that of wild type (Figure 27F).

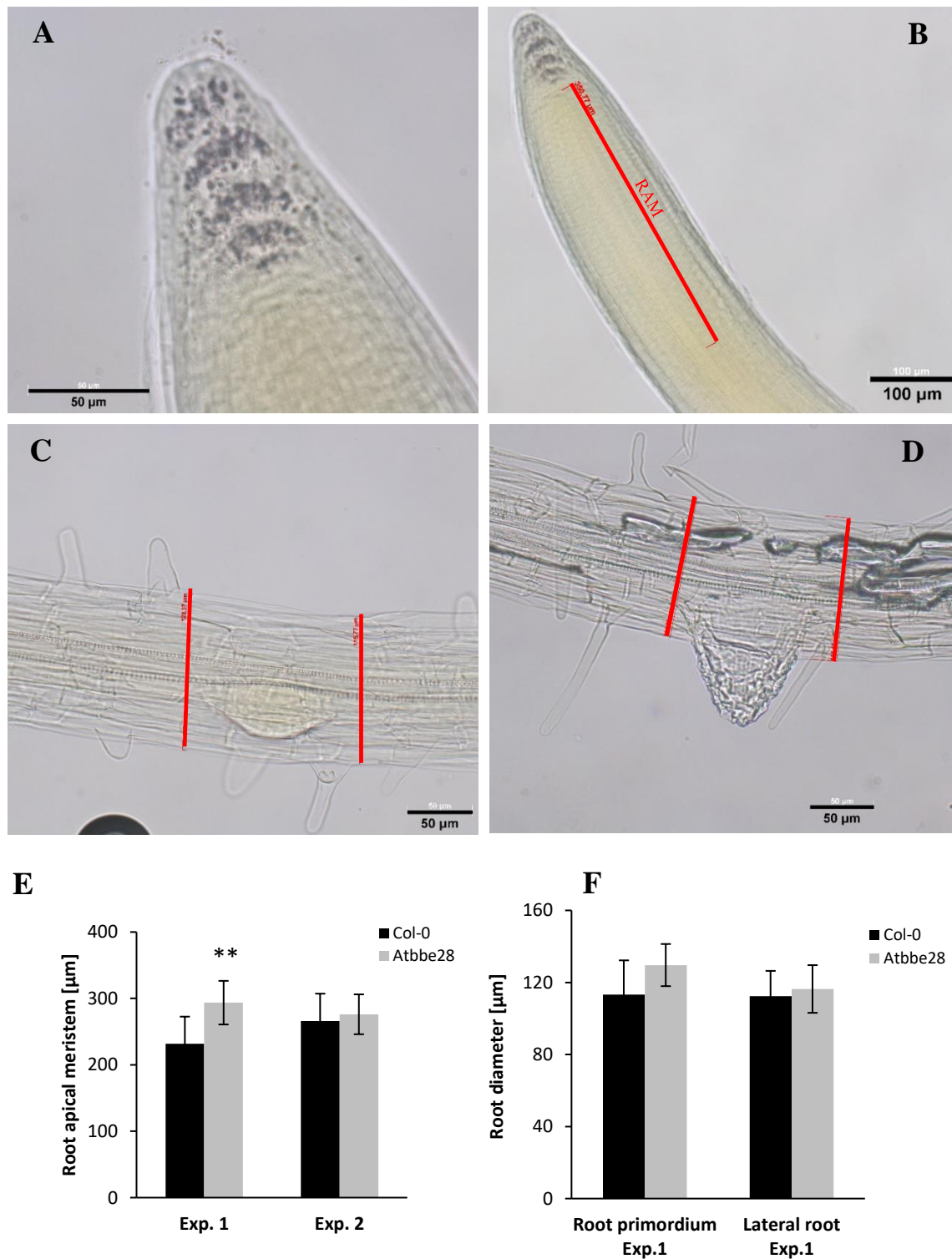


Figure 27. Determination of root apical meristem (RAM) length and diameter of transgenic *Atbbe*-like protein 28 mutant roots. Seedlings were grown vertically for 7 days under long day conditions (16 h/8 h day/night cycle) at 24 °C/20 °C with 130 $\mu\text{mol m}^{-2}\text{sec}^{-1}$ light intensity on half strength MS medium and were evaluated under the light microscope. **A.** Root cap with starch granules in different layers. **B.** The measured root apical meristem is labelled. **C.** Diameter measurements at the first primordium. **D.** Diameter measurements at the first lateral root. **E.** Statistical analysis of root apical meristem length. Mean values and standard deviation (\pm SD) are shown for two independent experiments ($n = 10$). **F.** Root diameter at the first primordium and at the first lateral root was measured and mean values \pm SD are shown for the first experiment ($n = 18$). Independent Student's *t*-tests detects a significant (** $P < 0.01$) difference between mutant line and wild type Col-0.

5.4.7. Status of *GUS*-reporter and 35S transgenic *AtBBE*-like lines

To analyze the promoter activity of *AtBBE*-like genes or the expression of these genes under their native promoters in particular tissues or cells, *GUS*-reporter gene constructs of genes encoding *AtBBE*-like proteins 13, 15, 24, 25, 27 and 28 were established. We generated transgenic *Arabidopsis* plants, expressing an *AtBBE-like promoter:GUS* construct, by using the floral dip method [55] of *A. tumefaciens* - mediated transformation. After plant transformation, T0 seeds of transgenic plants, grown under long day conditions (16 h/8 h day/night cycle), were harvested and the transgenic offspring was selected on half-strength MS medium containing hygromycin. Surviving seedlings were transferred to soil and were grown again in a climate chamber under long day conditions. T1 seeds from individual T0 transgenic plants for *AtBBE*-like protein 13, 15, 24, 25, 26 and 28 constructs were harvested, and homozygous plants of the next generation (T2) containing the *AtBBE-likep:GUS* constructs for *AtBBE*-like protein 13, 15 and 26 were PCR confirmed by Reinmar Eggers, MSc (Institute of Biochemistry, Graz University of Technology). He already performed first histochemical stainings with homozygous T3 reporter plants for *AtBBE*-like proteins 13, 15 and 26 to investigate the tissue-specific expression of *AtBBE*-like genes.

Transgenic plants were generated which express *AtBBE*-like proteins 26 and 28 under the control of a constitutive CaMV 35S promoter. We generated transgenic *Arabidopsis* plants, expressing a 35S:*AtBBE-like* construct, by using the floral dip method [53] of *A. tumefaciens* - mediated transformation, and T0 seeds has already been harvested. Offspring has to be selected on half-strength MS medium with hygromycin to obtain a transgenic T1 generation, and homozygous transgenic plants have to be confirmed by PCR. Phenotyping analyses of the homozygous T3 generation under different stress factors are planned.

5.4.8. Wiesner staining to detect lignin in stem sections of transgenic *Atbbe*-like protein 13 and 15 lines

Plants were cultivated for 6 weeks in a greenhouse under long day conditions with a 16 h photoperiod. The lower part of the stems was harvested, embedded in agarose, and 100 µm sections were generated. Aldehyde groups of lignin were detected by the Wiesner staining by soaking sections in the phloroglucinol reagent. The purple color that appeared was visualized under the light microscope, photographed and the sections were analyzed by ImageJ^R (vascular bundles, xylem, interfascicular fiber region and cell wall). No obvious developmental defects were observed for the homozygous *Atbbe*-like protein 13 and 15 mutants. Both showed the same amount of vascular bundles as Col-0 (8 vascular bundles). Additionally, no differences in diameter and width of the stem sections could be observed. Examinations of the xylem size

revealed a significantly bigger xylem for the *Atbbe*-like protein 13 mutant only in one biological replicate, and for *Atbbe*-like protein 15 mutant no difference in xylem size compared to Col-0 could be observed over two replicates (Figure 28A, B). However, a more detailed analysis of the stem sections showed that *Abbe*-like protein 13 mutants developed significantly thinner cell walls in the interfascicular fibers between the vascular bundles in both dimensions (width and height) compared to Col-0 in two independent biological experiments. *Atbbe*-like protein 15 mutant plants, on the other hand, showed no difference in cell wall thickness compared to wild type in the first experiment, and interestingly, even significantly thicker cell walls in the second replicate (Figure 29A, B). Measurements of the interfascicular ring segment size revealed a significantly lower size in the *Atbbe*-like protein 13 mutant compared to Col-0, and in the second replicate, also the *Atbbe*-like protein 15 mutant showed a decreased size of this specific region (Figure 30A, B). No clear differences in the number of cells of the interfascicular fiber segment were found (data not shown).

A



B

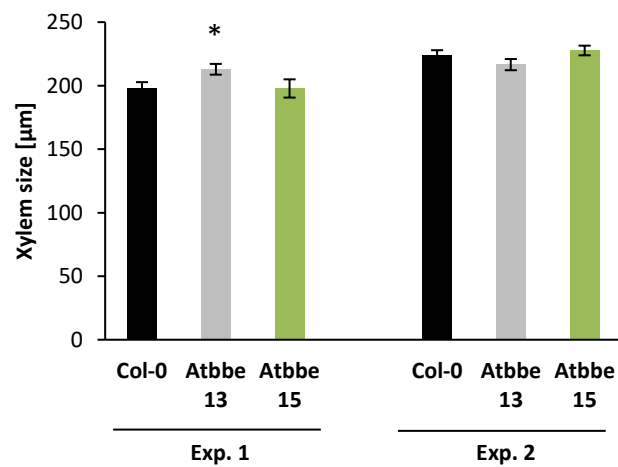
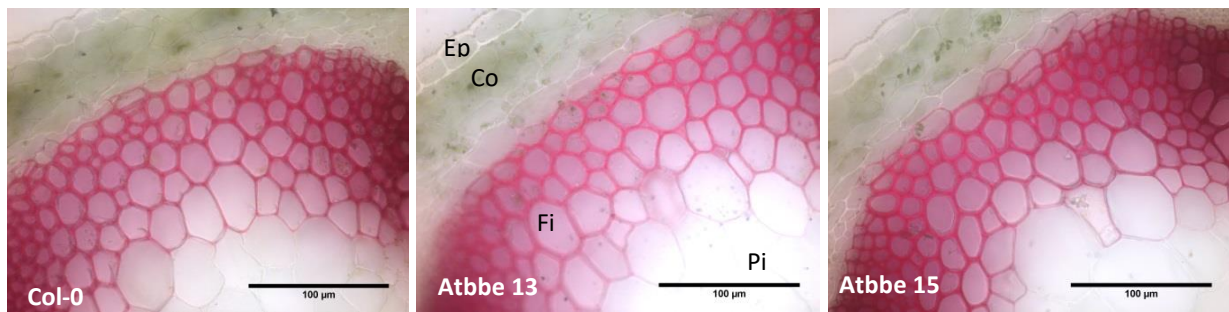


Figure 28. Wiesner staining for lignin detection in putative *Atbbe*-like protein 13 and 15 mutant stem sections. **A.** Transverse stem sections of *Atbbe*-like protein 13 and 15 mutants and wild type Col-0. Fully grown plants were harvested after 6 weeks of cultivation in a greenhouse under long day conditions with a 16 h photoperiod. Lignin was stained using the phloroglucinol staining in 100 μm stem sections and visualized under the light microscope. Sections showed normal lignin deposition in the cell walls of the interfascicular fibers and xylem cells. The vascular bundle (Vb) is labelled with a square in the first picture (10x magnification), and the xylem (Xy) is marked with a green arrow. **B.** Xylem sizes were measured using ImageJ^R, and average values ± SE for two independent biological replicates with 5 and 8 stems, respectively, are shown (R1 n = 36; R2 n = 76). Statistically significant differences (Student's *t*-test) are indicated with * ($P < 0.05$).

A



B

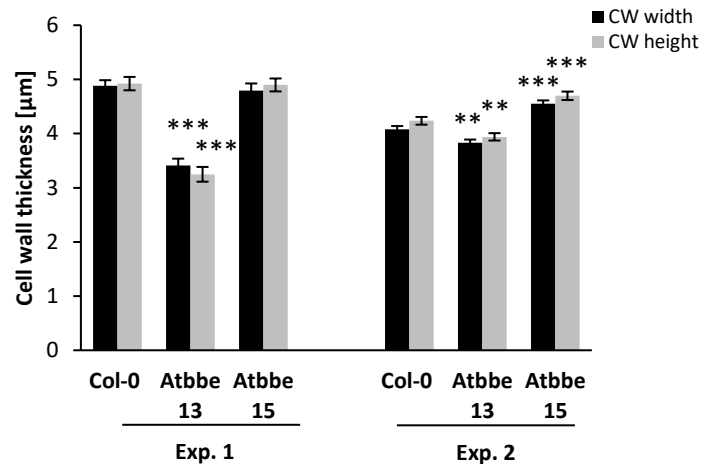


Figure 29. Cell wall thickness determination of putative *Atbbe*-like protein 13 and 15 mutants. **A.** Transverse stem sections of *Atbbe*-like 13 and 15 mutants and wild type. Fully grown plants were harvested after 6 weeks of cultivation in a greenhouse under long day conditions with a 16 h photoperiod. Lignin was stained using the Wiesner staining of 100 μm stem sections and visualized under the light microscope. The positions of the epidermis (Ep) and cortex (Co), interfascicular fibers (Fi) and pith (Pi) are indicated (40x magnification). **B.** Cell wall thickness was measured in both dimensions (width and height) of the interfascicular fibers segments using ImageJ^R at different locations. Average values \pm SE of two independent biological replicates, with 5 and 8 stems respectively, are shown (R1 n = 52; R2 n = 154). Statistically significant differences (Student's *t*-test) are indicated with ** ($P < 0.0$) and *** ($P < 0.001$).

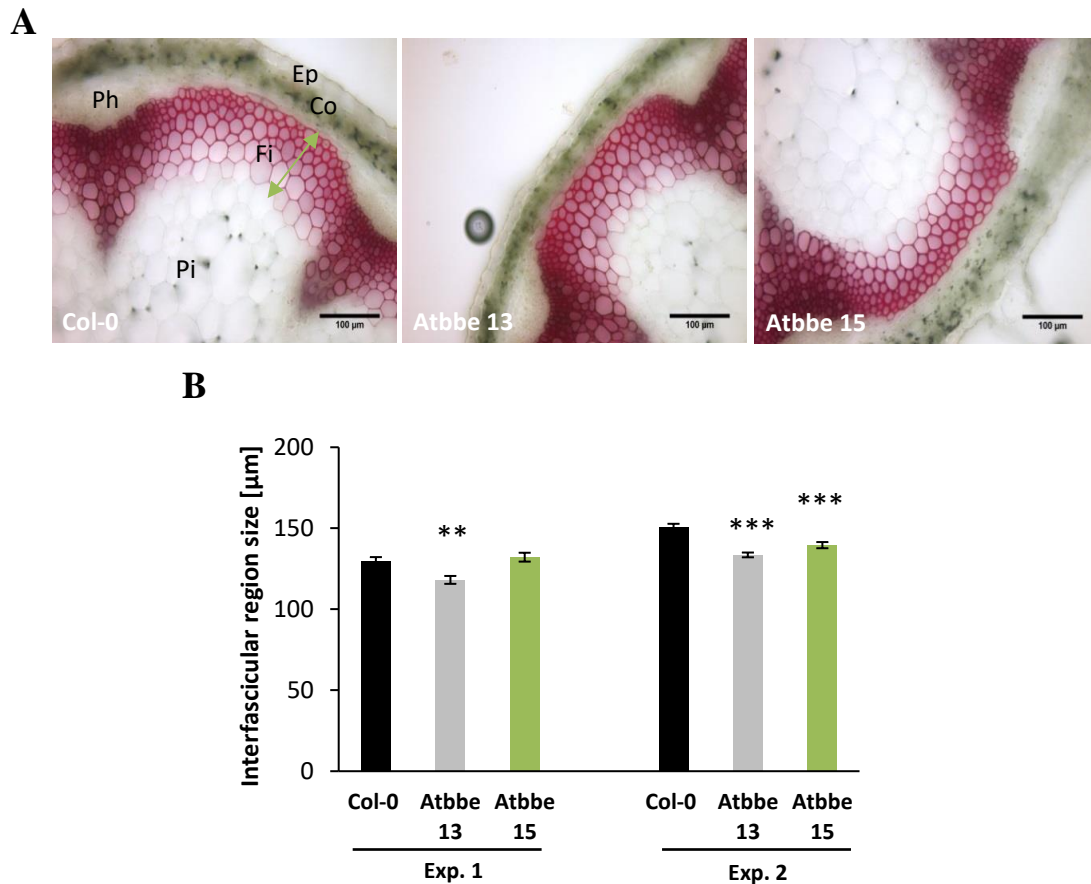


Figure 30. Determination of the size of the interfascicular fiber region of putative *Atbbe*-like protein 13 and 15 mutants. **A.** Transverse stem sections of *Atbbe*-like protein 13 and 15 mutants and wild type. Fully grown plants were harvested 6 weeks after cultivation in a greenhouse under long day conditions with a 16 h photoperiod. Lignin was stained using the Wiesner staining of 100 μm stem sections and visualized under the light microscope. The positions of the epidermis (Ep) and cortex (Co), interfascicular fibers (Fi), pith (Pi), phloem (Ph) and xylem (Xy) are indicated (20x magnification). **B.** The interfascicular region was measured in size (labelled with a green arrow) at three different locations using ImageJ^R. Average values ± SE of two independent biological replicates, with 5 and 8 stems respectively, are shown (R1 n = 150; R2 n = 500). Statistically significant differences (Student's *t*-test) are indicated with ** ($P < 0.01$) and *** ($P < 0.001$).

5.5. Discussion

BBE-like enzymes form a huge protein family (Pfam 08031) within the superfamily of FAD-linked oxidases (SCOPe d.58.32) and the enzymes catalyze a broad spectrum of reactions which are involved in different metabolic pathways [14]. In the model plant *A. thaliana*, 27 BBE-like enzymes were found, and the function of seven BBE-like enzymes has already been discovered. The BBE-like enzymes OGOX1-4 are carbohydrate oxidases and are also referred to as *At*BBE-like proteins 1, 2, 20 and 21. They are able to oxidize and inactivate oligogalacturonides (OGs) and have also been shown to be involved in the immune response of plants [48]. FOX1, also termed as *At*BBE-like protein 3, oxidizes indole cyanohydrin to indole-3-carbonyl cyanide/nitrile and also shows an involvement in pathogen response [17]. Two further enzymes are likely involved in lignin metabolism. *At*BBE-like proteins 13 and 15 are monolignol oxidoreductases, which convert monolignols (sinapyl-, coniferyl- and *p*-coumaryl alcohol) to their corresponding aldehydes [15]. According to multiple sequence alignments and comparisons of the active sites and substrate binding sites, we assume the same catalytic function for *At*BBE-like protein 26. The structure of a further BBE-like enzyme in *Arabidopsis*, *At*BBE-like protein 28, could be elucidated, but the natural substrate is still unknown [12].

5.5.1. Phenotype analysis of putative *At*BBE-like loss-of-function mutants under osmotic stress

We investigated putative *Atbbe*-like protein knock-out lines under standard growth conditions and osmotic stress with a special focus on monolignol oxidoreductases *At*BBE-like protein 13 and 15, and the putative monolignol oxidoreductase 26. Examinations of microarray data on the Arabidopsis eFP Browser [47] revealed that most of the *At*BBE-like proteins showed an up-regulation under osmotic stress [15]. High soil salinity is a major abiotic stress factor in agriculture and can negatively influence crop production and plant growth [67]. The effect of abiotic stress on agriculture was become more and more of interest in recent years, because of climate change with lower rainfalls and temperature extremes [68][69]. Additionally, certain abiotic stresses cause a decrease of the availability of water to plant cells [55]. Soil salinity and drought are the most serious problems, and efforts are made to cope with these problems and enhance salt and drought tolerance of the most important crops [70]. Roots are highly sensitive to environmental changes and plants constantly optimize their root system architecture for an efficient resource uptake [71]. *At*BBE-like proteins 13, 15 and 26 are highly expressed in the root (expression levels [a.u.] according to the Arabidopsis eFP Browser of *At*BBE-like 13: lateral root initiation 1681; *At*BBE-like 15: root xylem 4927, and *At*BBE-like 26: root

procambium 318.96 [47]), suggesting a phenotype of the root system of putative loss-of-function mutants. Furthermore, we suppose a role of the *AtBBE*-like proteins 13, 15 and 26 in root system in response to salt due to the high expression levels of these enzymes in root tissues (summarized expression levels see Supplementary Table S7).

Due to the influence of osmotic stress on plant growth, we started to investigate the phenotype of putative *Atbbe*-like knock-out/-down lines under salt stress. In plate experiments, all 27 *Atbbe*-like putative mutants were investigated according to their germination and health status under control and salt conditions (100 mM NaCl) (see Figure 4-11). Concerning the number of healthy green seedlings, most of the *Atbbe*-like mutant lines showed a reduction of healthy green seedlings under control conditions compared to wild type, except for the lines *Atbbe*-like protein 4, 9 (2), 16, 17, 26 and 28 mutants, which showed similar or even higher numbers of healthy green seedlings in all of the replicates. For some BBE-like genes, two independent putative knock-out lines were investigated, and interestingly, they showed different phenotypes under standard growth conditions, suggesting different sites of insertion of the T-DNA into the genome and, therefore, a different impact on the phenotype of the putative *Atbbe*-like protein knock-out or knock-down lines [72][73]. Looking more closely at the monolignol oxidoreductases, *Atbbe*-like protein 13, 15 and 26 (2) mutant plants also showed significantly reduced germination under control conditions. The second mutant line for *Atbbe*-like protein 26 showed a germination rate comparable to wild type (see Figure 12). On the one hand, the reduced germination rates and the influence on the health status of the putative loss-of-function mutants could be attributed to the gene knock-outs/-downs, or on the other hand, it could be a consequence of poor seed quality [74]. The variability of some lines between the biological replicates could be explained by variations in the experimental set-up or by environmental influences on the seed quality, such as variations in greenhouse conditions [75][76].

At a salt concentration of 100 mM, almost all *Atbbe*-like mutant lines produced significantly reduced numbers of healthy green seedlings when compared to Col-0 except for the *Atbbe*-like protein 3, 4, 9, 14, 16, 17, 18, 26 and 27 (2) mutants, which showed no increased sensitivity, suggesting that these proteins might not play a role in salt stress response. Phenotypes of the other *Atbbe*-like mutant lines suggest an involvement of the respective genes in salt stress tolerance. Looking more closely at the phylogenetic subgroups, the whole groups 3 and 5 show salt sensitivity. *Atbbe*-like protein 28 loss-of-function mutants already showed a reproducible salt stress phenotype in previous studies, with lower numbers of healthy green seedlings [12].

5.5.1.1. Phenotype of a putative *Atbbe*-like protein 13 mutant

The putative *Atbbe*-like protein 13 loss-of-function mutant showed a phenotype under mild salt stress, which would agree with the salt stress microarray data, and suggests a role in regulation of stress response to salinity [47]. Further, the germination rate of the *Atbbe*-like protein 13 mutant was significantly reduced under mild salt stress (Figure 12). The *in vitro* phenotype of *Atbbe*-like protein 13 mutant plants under salt stress could be confirmed by first results on soil, where mutant plants showed higher numbers of senescent leaves than the wild type (see Figure 19 and 20). Phenotyping of primary root growth showed no obvious influence of the *AtBBE*-like protein 13 mutation on root development under standard conditions, which agrees with the localization and supposed function of this protein near the lateral root primordium or in the xylem pole pericycle. This suggests that a detailed phenotyping, including lateral root growth under specific growth conditions, will be required. Under salt treatment, the primary root was clearly influenced in development, featuring thinner and shorter roots, but no obvious difference was visible between *Atbbe*-like protein 13 mutants and wild type. Further, the mutant showed no difference in biomass production under control conditions *in vitro*, but under salt stress, significantly more biomass was produced compared to Col-0 (Figure 21, 23 and 24). The increased biomass production of the mutant under salt stress is unclear and requires further investigation (summarized phenotype of the *Atbbe*-like protein 13 mutant on control and salt conditions, see Table 2).

5.5.1.2. Phenotype of a putative *Atbbe*-like protein 15 mutant

Under mild salt stress, the putative *Atbbe*-like protein 15 loss-of-function mutant showed a clear phenotype with a significantly reduced number of healthy green seedlings compared to Col-0. In addition, the germination rate was clearly influenced by salinity. Further, independent salt plate experiments with *Atbbe*-like protein 15 mutant lines were performed (Figure 13), and an evaluation of the mutant seedlings in categories confirmed the results from the first series of experiments. Influences on growth and development under control conditions could be observed again, and additionally, the number of healthy green seedlings was reduced. However, this kind of evaluation showed no significant difference between wild type and the putative mutant line on salt plates, except for a slight tendency towards higher salt sensitivity, which would agree with the first set of results. The phenotype of the putative *Atbbe*-like protein 15 knock-out under salinity could be confirmed by analyzing the gene expression level, which showed a 2.7-fold up-regulation of *AtBBE*-like protein 15 under salt treatment. On soil, *Atbbe*-like protein 15 mutant plants exhibited the same phenotype as Col-0 under salt treatment, suggesting a role in salt stress response at earlier developmental stages, especially during

germination of the plant (Figure 19 and 20). *Atbbe*-like protein 15 mutant seedlings exhibited significantly shorter primary roots under control conditions than Col-0. Upon salt treatment, seedlings showed shorter and thinner primary roots in general, and compared to Col-0, the mutant exhibited significantly longer primary roots than the wild type in response to salt. A different effect of salt stress on root development could be observed than expected. However, why the mutant developed longer roots needs to be further investigated. The *in vitro* biomass of *Atbbe*-like protein 15 seedlings was similar to wild type under control and salt conditions (Figure 21, 23 and 24) (summary of the phenotype, see Table 2).

5.5.1.3. Phenotype of a putative *Atbbe*-like protein 13*15 double mutant

The putative *Atbbe*-like protein 13*15 double mutant showed no significant differences in healthy green seedling number or in seedling development *in vitro* by evaluation in categories. For the double mutant, we expected a stronger phenotype in response to salt. Possibly, the knock-out of both genes influenced their function, or another *AtBBE*-like protein is able to take over the function. Another explanation would be a wrong experimental setup. Interestingly, the putative double knock-out/-down exhibited a stronger salt response on soil compared to the *in vitro* data (see Figure 14 and 20). However, *Atbbe*-like protein 13*15 mutant plants on soil were already influenced without salt and exhibited a beginning chlorosis. We assume that plant development was influenced by the putative double knock-out of the genes, *AtBBE*-like 13 and 15, and that the salt stress probably did not have more influence as already observed *in vitro*. Investigations of primary root length showed the same phenotype as wild type under control conditions. However, on salt the double mutant featured significantly shorter roots than the wild type. Apparently, salt rather affects the root development of the double mutant than its germination or the health status of the seedlings. We assumed a stronger salt response in roots by knocking out both enzymes which are highly expressed in roots. Further, the double mutant showed a higher production of biomass (fresh weight of seedlings) under control conditions. However, no significant difference on biomass production under salt treatment compared to wild type could be determined (Figure 21, 23 and 24) (summary of the phenotype, see Table 2).

5.5.1.4. Phenotype of a putative *Atbbe*-like protein 26 mutant

Atbbe-like protein 26 mutant seedlings showed no phenotype on control and salt conditions *in vitro* compared to Col-0. The second T-DNA insertion line, *Atbbe*-like protein 26 (2), in contrast, exhibited a different phenotype under control conditions and a significantly

higher salt sensitivity compared to wild type. However, salt showed no influence on the germination of both transgenic lines (

Figure 10, 11 and 12). The different phenotypes of both mutants could be explained by different insertion sites of T-DNA into the gene sequence, which can cause a knock-out/-down or a mutant without a loss-of function. In order to identify the exact integration site, sequencing is required, and RT-PCR is required to quantify gene expression [73][77]. For further experiments, we used the first homozygous T-DNA insertion line of *AtBBE*-like protein 26.

On soil, the *Atbbe*-like protein 26 mutant showed the same or even an enhanced salt tolerance compared to wild type, which is in agreement with the phenotype observed *in vitro* (Figure 19 and Figure 20). The primary root length was clearly influenced by the T-DNA insertion, and the mutant exhibited significantly shorter roots under control conditions compared to wild type. Under mild salt stress, the influence on the primary root length was not as strong as for the wild type, and the mutant produced longer roots. Under standard growth conditions, the *Atbbe*-like protein 26 mutant produced lower biomass (fresh weight of seedlings), and interestingly, under salt higher biomass (Figure 22, 23 and 24). Why the mutant produced more biomass than the wild type under salt stress is unclear and requires further investigation (summary of the phenotype, see Table 2).

5.5.1.5. Drought stress response of the putative Atbbe-like protein 13, 15, 13*15 and 26 mutants

Beside salt stress, drought stress plays a very important role for plant development and productivity. Therefore, we investigated the response to drought stress of putative *Atbbe*-like protein 13, 15, 26 and 13*15 knock-out/-down mutant plants. We evaluated the seedlings according to their health status. The results of the individual biological replicates showed a very large fluctuation, whereby no clear statement about the influence of drought can be made. The wild type and transgenic seeds obviously did not have the same quality, which could explain the poor growth of Col-0 under control conditions and the high variation between the biological replicates. Both Col-0 and transgenic lines, were influenced strongly by water deficit and many seeds did not germinate, but a difference in drought response was not visible. Probably the experimental setup was not optimal, because of the strong influence of PEG on both lines [55], or *AtBBE*-like proteins do not play an important role in drought stress response. This could be confirmed by expression data on the Arabidopsis eFP browser [47]. Total expression values of *AtBBE*-like protein 13 and 15 (expression levels [a.u] 127.68 and 51.02, respectively) are clearly less regulated by abiotic stress than by developmental signals (see Supplementary Table

S7). Only *AtBBE*-like protein 26 seedlings showed a higher expression under salt and drought stress (e-value 370.15) [47].

5.5.1.6. Phenotyping of a putative *Atbbe*-like protein 28 mutant

The structure of *AtBBE*-like protein 28 exhibits a totally different active site composition than the one which is known for monolignol dehydrogenases. Despite the structure of this protein being fully elucidated, its biochemical function is still unknown [12]. Therefore, we started with the phenotyping of a T-DNA insertional mutant line of *AtBBE*-like protein 28 to get an idea of possible functions of this protein in plants. Published phenotyping results showed a reduced biomass formation (fresh and dry weight) under standard growth conditions on soil and a lower salt stress tolerance *in vitro* [12]. The higher salt sensitivity could be confirmed by *in vitro* experiments. Under control conditions, no difference in health status compared to Col-0 was visible. We also determined the biomass of seedlings *in vitro*; however, *Atbbe*-like protein 28 seedlings showed the same fresh weight as Col-0 under control growth conditions. On salt, interestingly, the mutant featured a higher biomass production than the wild type (

Figure 11 and Figure 24). In order to identify the reasons for this higher biomass production in the mutant under salt stress, further investigations and, possibly, a different experimental setup is required. We also started to investigate primary root development due to the high expression of *AtBBE*-like protein 28 in lateral root caps of the meristematic zone according to the Arabidopsis eFP browser [47]. The primary root length of the mutant was significantly lower than for wild type under control growth conditions, and under salt stress, the mutant showed the same phenotype (Figure 22 and 23).

Further, we investigated the primary root in more detail under standard growth conditions and we observed a longer root apical meristem (RAM) for putative *Atbbe*-like protein 28 seedlings in one experiment. However, the first result could not be clearly confirmed in a second biological replicate. The mutant showed a larger diameter at the first primordium and at the first primary root compared to wild type (Figure 27). The obtained results suggest a different root development of putative knock-out/-down *Atbbe*-like plants and an involvement of *AtBBE*-like protein 28 in primary root growth. Further, we assume a role in salt stress tolerance. More biological replicates are needed, and a detailed phenotyping of root growth is required to study the *in planta* function of *AtBBE*-like protein 28 to confirm the first results (summary of the phenotype, see Table 2)

Table 2. Phenotype of putative *Atbbe*-like protein mutants under control and salt conditions compared to wild type.

Phenotype under control conditions					
<i>Atbbe</i> -like	<i>In vitro</i>		<i>In vivo</i>	<i>In vitro</i>	<i>In vitro</i>
	Healthy seedlings	Germination	Adult plants	Primary root length	Biomass seedlings
13	✓	✓	-	-	-
15	✓	✓	-	✓	-
13*15	-	-	✓	-	-
26	-	-	-	✓	✓
26 (2)	✓	✓	n.a.*	n.a.*	n.a.*
28	-	n.a.*	n.a.*	✓	-
Phenotype under salt conditions					
13	✓	✓	✓	-	✓
15	✓	✓	-	✓	-
13*15	-	-	✓	✓	-
26	-	-	-	✓	✓
26 (2)	✓	-	n.a.*	-	-
28	✓	n.a.*	n.a.*	-	✓

✓ Mutants show a different phenotype under control or salt conditions than wild type.

- Phenotype is similar to wild type.

* Parameter was not analyzed.

5.5.2. Role of *AtBBE*-like proteins in monolignol metabolism of *Arabidopsis thaliana*

AtBBE-like proteins 13 and 15 were discovered to be monolignol oxidoreductases, which suggests an involvement in lignification. Furthermore, sequence alignments showed the same catalytic function for *AtBBE*-like protein 26. Monolignols (sinapyl-, coniferyl- and *p*-coumaryl alcohol) are the building blocks of lignin, which is an important component of plant cell wall. Lignin is a complex phenolic polymer, which is, after cellulose, the second most organic compound of plant cell walls and represents about 30% of the organic carbon content in the biosphere [78][79]. Lignin is produced by the phenylalanine/tyrosine biosynthesis pathway and the formation of the monomers occurs in cytoplasm from where they are transported to the apoplast for further polymerization. The three units of lignin (S unit from sinapyl alcohol, G unit from coniferyl alcohol and H-unit from *p*-coumaryl alcohol) are polymerized by peroxidases and laccases in the secondary cell wall. Additionally, other compounds like hydroxycinnamaldehydes, tricin flavones, and hydroxystilbenes can be incorporated into lignin [78][80]. Lignin biosynthesis plays a crucial role in plant growth and development by providing cell wall rigidity and hydrophobic properties to strengthen the xylem elements for water and mineral transport [80][81]. Lignin can protect against pathogen attack and is actively involved in the environmental stress response [80][82].

Monolignol oxidoreductases (*AtBBE*-like protein 13, 15 and putative 26) are localized extracellularly and convert monolignols to their corresponding aldehydes. We suggest a shift of the extracellular pool of lignin monomers towards the aldehydes, which is likely to influence the composition of lignin and makes lignin analysis very interesting for us [15]. Lignin content and composition analysis through thioacidolysis and GC-MS of putative *Atbbe*-like 13 and 15 knock-out/-down lines were performed by Prof. Catherine Lapierre. The results showed that the transgenic lines seem to contain less aldehyde, and also the total lignin amount was reduced. However, between the biological replicates, the results showed high variations and could be only confirmed in two biological replicates. In total, the putative *Atbbe*-like protein 13 and 15 mutants showed around 10% reduction in lignin content in two replicates compared to wild type Col-0. Additionally, a reduction of the aldehyde content was expected and only matched in two biological replicates. *Atbbe*-like protein 13 and 15 mutant plants showed around 20% reduction of coniferyl aldehyde compared to wild type. The *Atbbe*-like protein 15 mutant showed around 10% reduction of coniferyl aldehyde in relation to the total lignin content in two replicates, and *Atbbe*-like 13 only in one replicate. This result suggests a change in the lignin composition in putative *Atbbe*-like protein 13 and 15 mutant plants (Figure 26).

The inconsistency of the biological replicates could be attributed to different ages of the batches of the plant material, which was generated in a greenhouse with variable temperature conditions. However, because of the absence of the monolignol dehydrogenase activity, as expected a tendency of toward lower aldehyde content was visible. Furthermore, a second effect was visible. During the reaction, two “electron equivalents” were set free and the natural acceptor is not known yet [15]. We suggest an involvement of the monolignol oxidoreductases in polymerization of lignin by activation of peroxidases and laccases, which would explain a reduction in total lignin in the knock-out lines. A similar mechanism is known for cytokinin dehydrogenases (subfamily of the FAD-linked oxidase superfamily SCOPe d.58.32:4) [14][42], where benzoxazinones act as electron acceptor and transfer the electrons to laccases and peroxidases.

We also quantified the total lignin content of young and old stems of wild type and *Atbbe*-like mutants with the acetyl bromide method, but the results of the thioacidolysis could be not confirmed (Figure 25). However, more biological replicates are needed to avoid possible experimental errors. Further, the acetyl bromide method is a spectrophotometric method, which is based on the solubilization of lignin. This method also leads to an oxidative degradation of xylans (structural polysaccharides), which leads to an overestimation of lignin by an increased absorbance at 270 - 280 nm [83][59]. The thioacidolysis method is more sensitive and specific

than other spectrophotometric methods and is based on an acid-catalyzed reaction, which leads to the depolymerization of lignin. This method allows the estimation of the amount and also composition of uncondensed alkyl aryl ether structures (except methyl aryl ethers) and especially the detection of C₆C₃ trithioethyl phenylpropane compounds, which are characteristic features of lignin [84].

Additionally, lignin distribution in stem sections of putative *Atbbe*-like protein 13 and 15 mutant plants was detected by Wiesner staining (phloroglucinol staining). Mutant plants showed no difference in the development of inflorescence stems, neither in the amount of the vascular bundles nor in the diameter/width of the stems. *Atbbe*-like protein 13 mutants exhibited thinner cell walls in the interfascicular fiber region compared to wild type in two independent biological replicates. Interestingly, *Atbbe*-like protein 15 mutants featured the same thickness or even thicker cell walls in this region. *Atbbe*-like protein 13 stems also showed a lower size of the interfascicular fiber segments (see Figure 28, 29 and 30). The stronger phenotype of *Atbbe*-like protein 13 mutants could be attributed to a higher expression level of *AtBBE*-like protein 13 in *Arabidopsis* stem sections according to the *Arabidopsis* eFP Browser (*AtBBE*-like 13: stem xylem 617.06, bottom of the whole stem 221.54; *AtBBE*-like 15: stem xylem 89.4, bottom of the whole stem 113.54) [47]. We assume an involvement of BBE-like enzymes in secondary thickening, a typical process for dicotyledonous plants. Secondary thickening leads to the formation of the typical secondary vascular tissues, secondary xylem and phloem, and to the formation of the secondary cell wall [85]. The secondary cell wall is located between the primary cell wall and the plasma membrane and contains, beside cellulose, polysaccharides, and glycoproteins, also lignin, which makes the secondary cell wall thicker and more rigid [86][87][88]. Monolignol dehydrogenases seem to be involved in secondary thickening and may affect the composition of lignin in the secondary cell wall of plants by aldehyde integration. The obtained results in lignin analysis suggest the necessity of further investigations concerning lignin composition and distribution. Additionally, the putative *Atbbe*-like protein 13*15 double knock-out/-down mutant should be analyzed to possibly see a higher impact on lignin structure. Furthermore, lignin analysis of *Atbbe*-like mutants under specific growth condition such as salt stress would be of great interest.

5.6. Conclusion and Outlook

In the presented study, we studied the phenotype of putative *Atbbe*-like loss-of-function mutants (*Atbbe*-like 1-27) and investigated the monolignol oxidoreductases *AtBBE*-like protein 13, 15 and 26, in more detail. In addition, we investigated the phenotype of a putative double mutant line, *Atbbe*-like 13*15. We analyzed the phenotype of all obtained T-DNA insertional mutant lines under standard growth conditions, and we could observe developmental defects *in vitro* in the germination of almost all mutant lines compared to wild type, suggesting loss-of-function mutants and potential knock-outs or knock-downs of the respective *BBE*-like genes. In addition, almost all putative knock-out/-down plants were more sensitive to mild salt stress when compared to wild type in *in vitro* experiments. Putative *Atbbe*-like protein 13 and 15 mutants exhibited a clear phenotype under control conditions and produced significantly less healthy green seedlings under salt conditions, indicating a role in salt stress tolerance. Furthermore, investigation of the primary root system showed developmental defects in *Atbbe*-like protein 15 roots under control conditions, and additionally, developmental defects were caused by salt stress. A higher salt stress sensitivity could be confirmed at least for the *Atbbe*-like protein 13 mutant and also the *Atbbe*-like protein 13*15 double mutant on soil. The stronger phenotype on soil of the *Atbbe*-like protein 13 mutant suggests a more important role in stress response than for *AtBBE*-like protein 15. At least one T-DNA insertion line of *AtBBE*-like protein 26 showed a clear phenotype with a decreased amount of healthy green seedlings under standard and salt conditions suggesting also an involvement in salt stress response. Initial results of lignin analysis of putative *Atbbe*-like protein 13 and 15 knock-out/-down lines revealed a potential influence on lignin biosynthesis where mutant lines showed a reduction in total lignin amount and aldehyde content. Monolignol oxidoreductases seem to be involved in providing extracellular aldehydes for the subsequent polymerization of lignin.

In addition, we initiated the promoter GUS reporter system for *AtBBE*-like enzymes 13, 15, 24, 25 and 26 (phylogenetic group 6) to study the localization of gene expression in different tissues or cells of *Arabidopsis* in more detail. We could establish homozygous plants of the T3 generation for *AtBBE*-like proteins 13, 15 and 26, carrying the *Promotor:GUS* construct, and first GUS-staining experiments were performed by a new PhD student in the project, Reinmar Eggers, MSc. (Institute of Biochemistry, Graz University of Technology). We were able to engineer 35S overexpression transgenic lines for *AtBBE*-like proteins 26 and 28 which we expect to show a more resistant phenotype to salt compared to wild type. Phenotyping experiments under various stress conditions and the generation of further 35S overexpression lines (e.g. for *AtBBE*-like proteins 13 and 15) are planned. Further, we initiated the investigation

of the expression levels of *AtBBE*-like protein 15, and first results revealed an approximately threefold up-regulation under salt stress. Detailed expression analyzes were continued by Alissa Pichler (master student) for *AtBBE*-like protein 13, 15 and 26 during plant development and under abiotic stress. Moreover, we engineered the generation of a putative triple mutant *Atbbe*-like protein 13*15*26 for further phenotyping analysis.

5.7. New Insights

For this work we used homozygous T-DNA insertional mutant lines for *AtBBE*-like proteins 1-27. Homozygous seeds of the T3 generation were generated and confirmed by antibiotic selection by Dr. Eric van der Graff. Additionally, for putative *Atbbe*-like protein 13, 15, 13*15, 26 and 28 mutant lines, homozygosity was also confirmed by PCR. Almost all T-DNA insertional mutants exhibited a phenotype under both control and salt conditions *in vitro*, suggesting a knock-out or down of the BBE-like gene in *Arabidopsis*. Nevertheless, putative knock-out or knock-down transgenic lines have to be checked at the beginning by default on the mRNA level by RT-PCR to check for the presence or absence of the respective transcript. In addition, the expression levels of the BBE-like gene have to be tested by qPCR, particularly if the T-DNA insertion produced a knock-down. According to Wang *et al.* [73], a T-DNA insertion in the protein-coding region of a gene generates a knock-out in 90% of the cases, when it is positioned in an intron or exon, and an insertion before the start codon (5'UTR or promoter) leads to a knock-out in 25% of the cases. An insertion before the start codon can also lead to a knock-down, which has been shown in 67% of the cases. T-DNA insertion can also cause deletion or translocation. In some cases, even if the expression level is almost similar to the wild type, no protein is produced in the mutant. The authors also observed that an insertion upstream of the start codon in some cases increased the transcript level of the downstream gene due to the 35S promoter in the T-DNA vector, and this in turn can influence protein synthesis. In some cases Wang *et al.* [73] observed in mutants with a T-DNA insertion in an intron that the intron was spliced out together with the T-DNA and the mutant produced the wild type transcript at a reduced level. Therefore, it is always advisable to check the gene expression level.

The first control by RT-PCR of the most interesting T-DNA insertional mutant lines for *AtBBE*-like proteins 13, 15 and 26 was performed by Reinmar Eggers, MSc at the Institute of Biology, Section Plant Sciences (Karl-Franzens University of Graz). The following T-DNA insertion lines were obtained from the SALK mutant collection for the *AtBBE*-like 13 (SALK_000581(F), *AtBBE*-like 15 (SALK_069340C) and *AtBBE*-like 26 (1) (SALK_069865

(AR) gene. Further, the rough position of the T-DNA insertion was identified by the SALK Institute Genomic Analysis Laboratory by DNA sequencing (<http://signal.salk.edu/cgi-bin/tdnaexpress>) and is located in introns for SALK_000581(F) and SALK_069340C and in the promoter for SALK_069865(AR) [52]. Due to the fact that the insertion site is given approximately (can be shifted up to ~300 bp from the flanking sequence tag; FST) it is advisable to perform sequencing to identify the exact integration site. The predicted insertion sites could be confirmed by sequencing of a PCR product using following primers: SALK-LBb1.3 5'-ATTTTGCCGATTTTCGGAAC-3' and *AtBBE*-like 13-R 5'-CATACTTTTGCGTAAACCC-3'; *AtBBE*-like 15-R 5'-TTCCAGGCCAATATCAC-3'; *AtBBE*-like 26-R 5'-GAACGTTTTCTCAAGTGG-3' (scheme of T-DNA insertion see Figure 31 and sequencing confirmed T-DNA insertion see Supplementary Figure S3). Further, T-DNA insertion mutants were analyzed by RT-PCR using genomic primers for PCR: *AtBBE*-like 13-F 5'-CTTGCGGTTAAGAAGCGGTG-3'; *AtBBE*-like 13-R 5'-CCAGGCAAGTATTACGCCGA-3' (421 bp); *AtBBE*-like 15-F 5'-CACGACTACGAAGGGCTCTC-3'; *AtBBE*-like 15-R 5'-CTTGCTCAAGCGTCTTCGTG-3' (466 bp); *AtBBE*-like 26-F 5'-TCCGAATGCATCTCCGTGTC-3'; *AtBBE*-like 26-R 5'-CGGTCACGGTCTTAGGAACA-3' (468 bp) (Figure 32 and Supplementary Figure S3). Total mRNA was isolated from 14-day-old seedlings of putative *Atbbe*-like protein 13*15 and 26 mutants and wild type Col-0 seedlings using the Qiagen RNeasy plant mini kit (Qiagen, Hilden, Germany) and was reverse transcribed into cDNA according to the protocol of the iScriptTM cDNA Synthesis Kit from BIO-RAD (Vienna, Austria). T-DNA insertion sites for *Atbbe*-like proteins 13 and 15 are located in the first intron between exon 1 and exon 2, therefore primers were established located in exon 1 and exon 2. For *Atbbe*-like protein 26, the T-DNA insertion is in the promoter, and primers were established in exon 1 and exon 2.

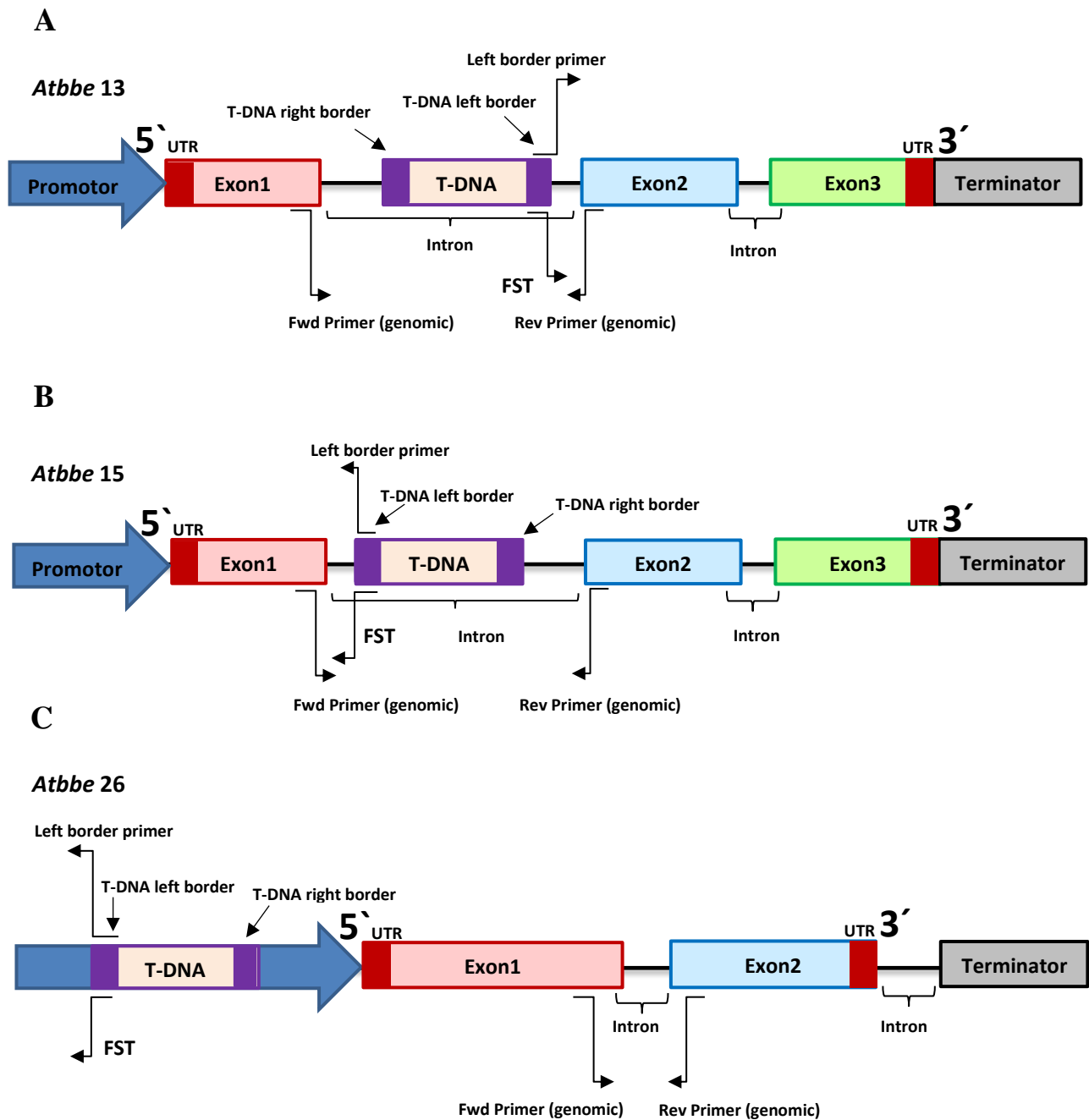


Figure 31. Scheme of T-DNA insertion in the *Atbbe*-like protein 13, 15 and 26 mutants. A. T-DNA was inserted in reverse orientation in the first intron of *AtBBE*-like protein 13. **B.** T-DNA was inserted in the first intron of *AtBBE*-like protein 15. **C.** T-DNA was inserted in the promoter of the *AtBBE*-like protein 26. Flanking sequence tag FST, forward and reverse primers for RT-PCR and left border primer for sequencing are labelled.

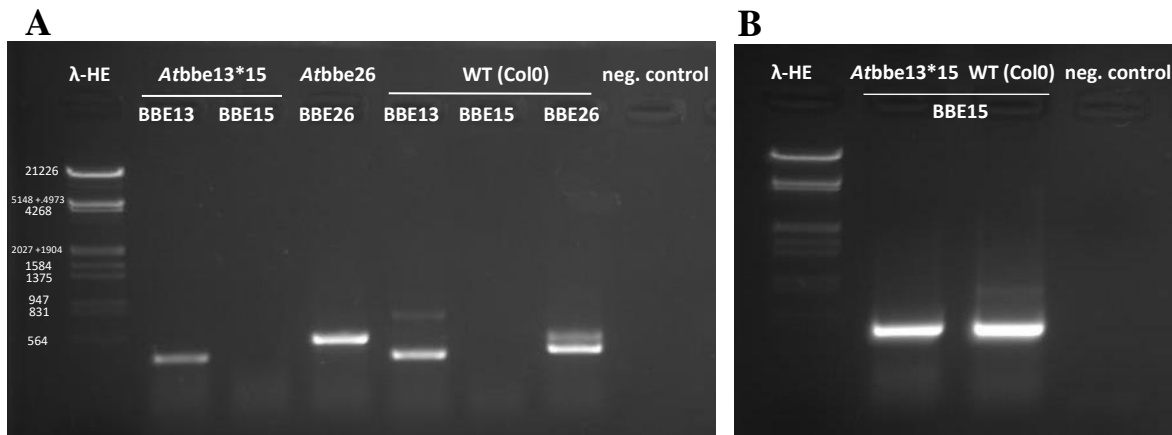


Figure 32. RT-PCR analysis of T-DNA insertion mutants *Atbbe*-like protein 13, 15 and 26. Total mRNA was isolated from 14-day-old seedlings of putative *Atbbe*-like mutants and wild type Col-0 and reverse transcript to cDNA. λ -DNA/EcoRI+HindIII Marker was used as a DNA ladder and nuclease free dH₂O as a negative control. **A.** PCR with cDNA as a template for *AtBBE*-like protein 13 and 26. **B.** PCR for *AtBBE*-like protein 15.

T-DNA insertion mutants for *Atbbe*-like proteins 13, 15 and 26 showed a PCR product on the cDNA level, indicating *AtBBE*-like protein 13, 15 and 26 are not knocked-out (Figure 32). The RT-PCR may be considered as semi-quantitative, due to the same amount of cDNA that was used for the PCR and loaded onto the agarose gel. The intensity of the *Atbbe*-like protein 13 amplification is slightly weaker compared to Col-0, indicating a possible knock-down and explaining the stronger phenotype of *Atbbe*-like protein 13 in response to salt stress *in vitro* and on soil. The putative *Atbbe*-like protein 15 mutant showed the same intensity of the amplification as Col-0 for *Atbbe*-like protein 15, which clearly indicates no knock-out. In case of *Atbbe*-like protein 26, the intensity of the amplification product is higher compared to Col-0 suggesting a higher gene expression of the protein and underlines previous studies mentioned before, that the 35S promoter activity of the T-DNA vector can positively influence gene expression. This could be another reason for the poor phenotype of *Atbbe*-like protein 26 under salt treatment *in vitro* and *in vivo*. However, Col-0 shows for *AtBBE*-like protein 26 an unspecific amplicon with the same intensity but a smaller size. Therefore, it is very speculative to make a statement about *AtBBE*-like protein 26 gene expression on an agarose gel looking at the unspecific bands and pipetting errors, which need to be taken into consideration.

In summary, the T-DNA insertion knock-out lines for *AtBBE*-like 13, 15 and 26 are definitely no knock-outs due the presence of the BBE-like transcript. Nevertheless, previous studies showed that T-DNA insertion could also have an influence on the expression level of the gene even if it was not a knock-out. That would explain why *Atbbe*-like protein 13 and 15 mutants showed a phenotype in salt stress experiments *in vitro* and *AtBBE*-like protein 13 also

on soil. The expression levels have to be analyzed by quantitative RT-PCR for interpreting the data that already exist. Additionally, new T-DNA insertion lines have been ordered from the European Arabidopsis Stock Centre (NASC, University of Nottingham, Loughborough, UK) for *AtBBE*-like proteins 13, 15 and 26, where the putative insertion is denoted on *tair* The Arabidopsis Information Resource (<https://www.arabidopsis.org/>) in the protein coding region (exon), leading to a higher probability of getting a knock-out (ordered T-DNA insertion lines see Table 3).

Table 3. New ordered T-DNA insertion lines for *AtBBE*-like protein 13, 15 and 26.

T-DNA insertion line	<i>AtBBE</i> -like	Putative location
SALK_050796.21.85.x	13	1 st exon
SALK_028487	15	3 rd exon
SALKseq_038142.1	15	2 nd exon
SALKseq_083959.1	15	2 nd exon
GABI_881D12	15	1 st exon
GABI_708E02	26	2 nd exon
SAIL_31_A05	26	1 st exon

5.8. References

1. Mattevi A, Fraaije MW, Mozzarelli A, Olivi L, Coda A, van Berkel WJ. Crystal structures and inhibitor binding in the octameric flavoenzyme vanillyl-alcohol oxidase: the shape of the active-site cavity controls substrate specificity. *Structure*. 1997;5: 907–20. doi:10.1016/S0969-2126(97)00245-1
2. Fraaije MW, van Berkel WJH, Benen JAE, Visser J, Mattevi A. A novel oxidoreductase family sharing a conserved FAD-binding domain. *Trends Biochem Sci*. Elsevier; 1998;23: 206–207. doi:10.1016/S0968-0004(98)01210-9
3. Kutchan TM. Chapter 7 Molecular genetics of plant alkaloid biosynthesis. *Alkaloids Chem Biol*. 1998;50: 257–316. doi:10.1016/S1099-4831(08)60045-0
4. Winkler A, Hartner F, Kutchan TM, Glieder A, Macheroux P. Biochemical evidence that berberine bridge enzyme belongs to a novel family of flavoproteins containing a bi-covalently attached FAD cofactor. *J Biol Chem*. 2006;281: 21276–21285. doi:10.1074/jbc.M603267200
5. Huang CH, Lai WL, Lee MH, Chen CJ, Vasella A, Tsai YC, *et al*. Crystal structure of glucooligosaccharide oxidase from *Acremonium strictum*: a novel flavinylation of 6-S-cysteinyl, 8 α -N1-histidyl FAD. *J Biol Chem*. 2005;280: 38831–38838. doi:10.1074/jbc.M506078200
6. Huang CH, Winkler A, Chen CL, Lai WL, Tsai YC, Macheroux P, *et al*. Functional roles of the 6-S-cysteinyl, 8 α -N1-histidyl FAD in glucooligosaccharide oxidase from *Acremonium strictum*. *J Biol Chem*. 2008;283: 30990–30996. doi:10.1074/jbc.M804331200
7. Massey V. Activation of molecular oxygen by flavins and flavoproteins. *J Biol Chem*. 1994;269: 22459–22462. doi:10.1007/s13398-014-0173-7.2
8. Winkler A, Motz K, Riedl S, Puhl M, Macheroux P, Gruber K. Structural and mechanistic studies reveal the functional role of bicovalent flavinylation in berberine bridge enzyme. *J Biol Chem*. 2009;284: 19993–20001. doi:10.1074/jbc.M109.015727
9. Heuts DPHM, Winter RT, Damsma GE, Janssen DB, Fraaije MW. The role of double covalent flavin binding in chito-oligosaccharide oxidase from *Fusarium graminearum*. *Biochem J*. 2008;413: 175–83. doi:10.1042/BJ20071591
10. Winkler A, Kutchan TM, Macheroux P. 6-S-cysteinyl-ation of bi-covalently attached FAD in berberine bridge enzyme tunes the redox potential for optimal activity. *J Biol Chem*. 2007;282: 24437–24443. doi:10.1074/jbc.M703642200
11. Zafred D, Steiner B, Teufelberger AR, Hromic A, Karplus PA, Schofield CJ, *et al*. Rationally engineered flavin-dependent oxidase reveals steric control of dioxygen reduction. *FEBS J*. 2015;282: 3060–3074. doi:10.1111/febs.13212
12. Daniel B, Wallner S, Steiner B, Oberdorfer G, Kumar P, Van Der Graaff E, *et al*. Structure of a berberine bridge enzyme-like enzyme with an active site specific to the plant family Brassicaceae. *PLoS One*. 2016;11. doi:10.1371/journal.pone.0156892
13. Heuts DPHM, Scrutton NS, McIntire WS, Fraaije MW. What's in a covalent bond?: on the role and formation of covalently bound flavin cofactors. *FEBS Journal*. 2009;276: 3405–3427. doi:10.1111/j.1742-4658.2009.07053.x
14. Daniel B, Konrad B, Toplak M, Lahham M, Messenlehner J, Winkler A, *et al*. The family of berberine bridge enzyme-like enzymes : A treasure-trove of oxidative reactions. *Arch Biochem Biophys*. Elsevier Inc; 2017;632: 88–103. doi:10.1016/j.abb.2017.06.023

15. Daniel B, Pavkov-Keller T, Steiner B, Dordic A, Gutmann A, Nidetzky B, *et al.* Oxidation of monolignols by members of the berberine bridge enzyme family suggests a role in plant cell wall metabolism. *J Biol Chem.* 2015;290: 18770–18781. doi:10.1074/jbc.M115.659631
16. Pils S, Schnabl K, Wallner S, Kljajic M, Kupresanin N, Breinbauer R, *et al.* Characterization of the monolignol oxidoreductase *AtBBE*-like protein 15 L182V for biocatalytic applications. *J Mol Catal B Enzym.* 2016; doi:10.1016/j.molcatb.2016.10.018
17. Rajniak J, Barco B, Clay NK, Sattely ES. A new cyanogenic metabolite in *Arabidopsis* required for inducible pathogen defence. *Nature.* 2015;525: 375–379. <http://dx.doi.org/10.1038/nature14907>
18. Custers JHH V, Harrison SJ, Sela-Buurlage MB, Van Deventer E, Lageweg W, Howe PW, *et al.* Isolation and characterisation of a class of carbohydrate oxidases from higher plants, with a role in active defence. *Plant J.* 2004;39: 147–160. doi:10.1111/j.1365-313X.2004.02117.x
19. Zafred D, Nandy A, Pump L, Kahlert H, Keller W. Crystal structure and immunologic characterization of the major grass pollen allergen Phl p 4. *J Allergy Clin Immunol.* 2013;132. doi:10.1016/j.jaci.2013.03.021
20. Ferrari AR, Rozeboom HJ, Dobruchowska JM, Van Leeuwen SS, Vugts ASC, Koetsier MJ, *et al.* Discovery of a xylooligosaccharide oxidase from *Myceliophthora thermophila* C1. *J Biol Chem.* 2016;291: 23709–23718. doi:10.1074/jbc.M116.741173
21. Heuts DPHM, Janssen DB, Fraaije MW. Changing the substrate specificity of a chitooligosaccharide oxidase from *Fusarium graminearum* by model-inspired site-directed mutagenesis. *FEBS Lett.* 2007;581: 4905–4909. doi:10.1016/j.febslet.2007.09.019
22. Ahmad SK, Brinch DS, Friis EP, Pedersen PB. Toxicological studies on lactose oxidase from microdochium nivale expressed in *Fusarium venenatum*. *Regul Toxicol Pharmacol.* 2004;39: 256–270. doi:10.1016/j.yrtph.2004.02.003
23. Liaw S, Lee DY, Chow LP, Lau GX, Su SN. Structural characterization of the 60-kDa bermuda grass pollen isoallergens, a covalent flavoprotein. *Biochem Biophys Res Commun.* 2001;280: 738–743. doi:10.1006/bbrc.2000.4203
24. Leliaert F, Smith DR, Moreau H, Herron MD, Verbruggen H, Delwiche CF, *et al.* Phylogeny and molecular evolution of the green algae. *CRC Crit Rev Plant Sci.* 2012;31: 1–46. doi:10.1080/07352689.2011.615705
25. Adl SM, Simpson AGB, Lane CE, Luke J, Bass D, Bowser SS, *et al.* The revised classification of eukaryotes. *J Eukaryot Microbiol.* 2012;59: 429–493. doi:10.1111/j.1550-7408.2012.00644.x
26. Liscombe DK, Facchini PJ. Evolutionary and cellular webs in benzyloquinoline alkaloid biosynthesis. *Curr Opin Biotechnol* 2008;19: 173–180. doi:10.1016/j.copbio.2008.02.012
27. Taura F, Morimoto S, Shoyama Y. Purification and characterization of cannabidiolic-acid synthase from *Cannabis sativa* L. Biochemical analysis of a novel enzyme that catalyzes the oxidocyclization of cannabigerolic acid to cannabidiolic acid. *J Biol Chem.* 1996;271: 17411–17416. doi:10.1074/jbc.271.29.17411
28. Sirikantaramas S, Morimoto S, Shoyama Y, Ishikawa Y, Wada Y, Shoyama Y, *et al.* The gene controlling marijuana psychoactivity: molecular cloning and heterologous expression of Δ^1 -tetrahydrocannabinolic acid synthase from *Cannabis sativa* L. *J Biol Chem.* 2004;279: 39767–74. doi:10.1074/jbc.M403693200

29. Taura F, Sirikantaramas S, Shoyama Y, Yoshikai K, Shoyama Y, Morimoto S. Cannabidiolic-acid synthase, the chemotype-determining enzyme in the fiber-type *Cannabis sativa*. *FEBS Lett.* 2007;581: 2929–2934. doi:10.1016/j.febslet.2007.05.043
30. Gesell A, Díaz Chávez ML, Kramell R, Piotrowski M, Macheroux P, Kutchan TM. Heterologous expression of two FAD-dependent oxidases with (*S*)-tetrahydroprotoberberine oxidase activity from *Argemone mexicana* and *Berberis wilsoniae* in insect cells. *Planta.* 2011;233: 1185–1197. doi:10.1007/s00425-011-1357-4
31. Kajikawa M, Shoji T, Kato A, Hashimoto T. Vacuole-localized berberine bridge enzyme-like proteins are required for a late step of nicotine biosynthesis in tobacco. *Plant Physiol.* 2011;155: 2010–2022. doi:10.1104/pp.110.170878
32. Baldwin IT, Jena D, Jagger M. An ecologically motivated analysis of plant-herbivore interactions in native tobacco 1. 2001;127: 1449–1458. doi:10.1104/pp.010762.
33. Ober D, Kaltenecker E. Pyrrolizidine alkaloid biosynthesis, evolution of a pathway in plant secondary metabolism. *Phytochemistry.* 2009;70: 1687–1695. doi:10.1016/j.phytochem.2009.05.017
34. Hansen OC, Stougaard P. Hexose oxidase from the red alga *Chondrus crispus* - purification, molecular cloning, and expression in *Pichia pastoris*. *J Biol Chem.* 1997; 272: 11581–11587.
35. Poulsen C, Hostrup PB. Purification and characterization of a hexose oxidase with excellent strengthening effects in bread. *Cereal Chem.* 1998;75: 51–57. doi:10.1094/CCHEM.1998.75.1.51
36. Carter CJ, Thornburg RW. Tobacco nectarin V is a flavin-containing berberine bridge enzyme-like protein with glucose oxidase activity. *Plant Physiol.* 2004;134: 460–469. doi:10.1104/pp.103.027482
37. Carter C, Thornburg RW. Is the nectar redox cycle a floral defense against microbial attack? *Trends Plant Sci.* 2004;9: 320–324. doi:10.1016/j.tplants.2004.05.008
38. Wallner S, Dully C, Daniel B, Macheroux P. Berberine bridge enzyme and the family of bicovalent flavoenzymes. *Flavoproteins 1.* 2012;1: 1–30. doi:10.1515/9783110268911.1
39. Boudsocq M, Willmann MR, McCormack M, Lee H, Shan L, He P, *et al.* Differential innate immune signalling via Ca²⁺ sensor protein kinases. *Nature.* 2010;464: 418–422. doi:10.1038/nature08794
40. Boudart G, Jamet E, Rossignol M, Lafitte C, Borderies G, Jauneau A, *et al.* Cell wall proteins in apoplastic fluids of *Arabidopsis thaliana* rosettes: identification by mass spectrometry and bioinformatics. *Proteomics.* 2005;5: 212–221. doi:10.1002/pmic.200400882
41. Hooper CM, Tanz SK, Castleden IR, Vacher MA, Small ID, Millar AH. SUBAcon: a consensus algorithm for unifying the subcellular localization data of the *Arabidopsis* proteome. *Bioinformatics.* 2014;30: 3356–3364. doi:10.1093/bioinformatics/btu550
42. Frébortová J, Novák O, Frébort I, Jorda R. Degradation of cytokinins by maize cytokinin dehydrogenase is mediated by free radicals generated by enzymatic oxidation of natural benzoxazinones. *Plant J.* 2010;61: 467–481. doi:10.1111/j.1365-313X.2009.04071.x
43. Vanholme R, Demedts B, Morreel K, Ralph J, Boerjan W. Lignin biosynthesis and structure. *PLANT Physiol.* 2010;153: 895–905. doi:10.1104/pp.110.155119

44. Xu C, Cao H, Zhang Q, Wang H, Xin W, Xu E, *et al.* Control of auxin-induced callus formation by bZIP59-LBD complex in *Arabidopsis* regeneration. *Nat Plants*. 2018;4: 108–115. doi:10.1038/s41477-017-0095-4
45. Beeckman T, De Smet I. Pericycle. *Curr Biol*. 2014;24: 378–379. doi:10.1016/j.cub.2014.03.031
46. Péret B, De Rybel B, Casimiro I, Benková E, Swarup R, Laplaze L, *et al.* *Arabidopsis* lateral root development: an emerging story. *Trends Plant Sci*. 2009;14: 399–408. doi:10.1016/j.tplants.2009.05.002
47. Winter D, Vinegar B, Nahal H, Ammar R, Wilson G V., Provart NJ. An “Electronic Fluorescent Pictograph” browser for exploring and analyzing large-scale biological data sets. *PLoS One*. 2007;2. doi:10.1371/journal.pone.0000718
48. Benedetti M, Verrascina I, Pontiggia D, Locci F, Mattei B, De Lorenzo G, *et al.* Four *Arabidopsis* berberine bridge enzyme-like proteins are specific oxidases that inactivate the elicitor-active oligogalacturonides. *Plant J*. 2018;94: 260–273. doi:10.1111/tpj.13852
49. Hyun TK, Van Der Graaff E, Albacete A, Eom SH, Großkinsky DK, Böhm H, *et al.* The *Arabidopsis* PLAT domain protein1 is critically involved in abiotic stress tolerance. *PLoS One*. 2014;9. doi:10.1371/journal.pone.0112946
50. Alonso JM. Genome-wide insertional mutagenesis of *Arabidopsis thaliana*. *Science*. 2003;301: 653–657. doi:10.1126/science.1086391
51. Murashige T, Skoog F. A revised medium for rapid growth and bio assays with tobacco tissue cultures. *Physiol. Plant*. 1962;15: 473–497. doi:10.1111/j.1399-3054.1962.tb08052.x
52. Murray MG, Thompson WF. Rapid isolation of high molecular weight plant DNA. *Nucleic Acids Res*. 1980;8: 4321–4326. doi:10.1093/nar/8.19.4321
53. Clough SJ, Bent AF. Floral dip: A simplified method for *Agrobacterium*-mediated transformation of *Arabidopsis thaliana*. *Plant J*. 1998;16: 735–743. doi:10.1046/j.1365-313X.1998.00343.x
54. Shi H, Lee B, Wu S-J, Zhu J-K. Overexpression of a plasma membrane Na⁺/H⁺ antiporter gene improves salt tolerance in *Arabidopsis thaliana*. *Nat Biotechnol*. 2002;21: 81–85. doi:10.1038/nbt766
55. Verslues PE, Agarwal M, Katiyar-Agarwal S, Zhu J, Zhu JK. Methods and concepts in quantifying resistance to drought, salt and freezing, abiotic stresses that affect plant water status. *Plant J*. 2006;45: 523–539. doi:10.1111/j.1365-313X.2005.02593.x
56. Pomar F, Merino F, Barceló AR. *O*-4-linked coniferyl and sinapyl aldehydes in lignifying cell walls are the main targets of the Wiesner (phloroglucinol-HCl) reaction. *Protoplasma*. 2002;220: 17–28. doi:10.1007/s00709-002-0030-y
57. Liljegren S. Phloroglucinol stain for lignin. *Cold Spring Harb Protoc*. 2010;5. doi:10.1101/pdb.prot4954
58. Carpita NC, Defernez M, Findlay K, Wells B, Shoue D a, Catchpole G, *et al.* Cell wall architecture of the elongating maize coleoptile. *Plant Physiol*. 2001;127: 551–565. doi:10.1104/pp.010146
59. Hatfield RD, Grabber J, Ralph J, Brei K. Using the acetyl bromide assay to determine lignin concentrations in herbaceous plants: Some cautionary notes. *J Agric Food Chem*. 1999;47: 628–632. doi:10.1021/jf9808776

60. Hong JH, Chu H, Zhang C, Ghosh D, Gong X, Xu J. A quantitative analysis of stem cell homeostasis in the *Arabidopsis* columella root cap. *Front Plant Sci.* 2015;6: 206. doi:10.3389/fpls.2015.00206
61. Casamitjana-Martínez E, Hofhuis HF, Xu J, Liu CM, Heidstra R, Scheres B. Root-specific CLE19 overexpression and the *so11/2* suppressors implicate a CLV-like pathway in the control of *Arabidopsis* root meristem maintenance. *Curr Biol.* 2003;13: 1435–1441. doi:10.1016/S0960-9822(03)00533-5
62. Barrada A, Montané MH, Robaglia C, Menand B. Spatial regulation of root growth: placing the plant TOR pathway in a developmental perspective. *Int J Mol Sci.* 2015;16: 19671–19697. doi:10.3390/ijms160819671
63. Lapierre C, Pollet B, Rolando C. New insights into the molecular architecture of hardwood lignins by chemical degradative methods. *Res Chem Intermed.* 1995;21: 397–412. doi:10.1163/156856795X00323
64. Lapierre C, Pollet B, Petit-Conil M, Toval G, Romero J, Pilate G, *et al.* Structural alterations of lignins in transgenic poplars with depressed cinnamyl alcohol dehydrogenase or caffeic acid *O*-methyltransferase activity have an opposite impact on the efficiency of industrial kraft pulping. *Plant Physiol.* 1999;119: 153–164. doi:10.1104/pp.119.1.153
65. Méchin V, Laluc A, Legée F, Cézard L, Denoue D, Barrière Y, *et al.* Impact of the brown-midrib *bm 5* mutation on maize lignins. *J Agric Food Chem.* 2014;62: 5102–5107. doi:10.1021/jf5019998
66. Bouvier D'Yvoire M, Bouchabke-Coussa O, Voorend W, Antelme S, Cézard L, Legée F, *et al.* Disrupting the cinnamyl alcohol dehydrogenase 1 gene (*BdCAD1*) leads to altered lignification and improved saccharification in *Brachypodium distachyon*. *Plant J.* 2013;73: 496–508. doi:10.1111/tpj.12053
67. Flowers TJ, Garcia A, Koyama M, Yeo AR. Breeding for salt tolerance in crop plants: The role of molecular biology. *Acta Physiol Plant.* 1997;19: 427–433. doi:10.1007/s11738-997-0039-0
68. Boyer JS. Plant productivity and environment. *Science* 1982;218: 443–448. doi:10.1126/science.218.4571.443
69. Araus JL, Slafer GA, Reynolds MP, Royo C. Plant breeding and drought in C3 Cereals: what should we breed for? *Ann Bot.* 2002;89: 925–940. doi:10.1093/aob/mcf049
70. Zhou ML, Ma JT, Pang JF, Zhang ZL, Tang YX, Wu YM. Regulation of plant stress response by dehydration responsive element binding (DREB) transcription factors. *African J Biotechnol.* 2010;9: 9255–9269.
71. Sánchez-Calderón L. Root development and abiotic stress adaptation. In: Ibarra-Cortés ME, editor. *Rijeka: IntechOpen*; 2013. p. Ch. 5. doi:10.5772/55043
72. Radhamony RN, Prasad AM, Srinivasan R. T-DNA insertional mutagenesis in *Arabidopsis*: a tool for functional genomics. *Electron J Biotechnol.* 2005;8: 82–106. doi:10.2225/vol8-issue1-fulltext-4
73. Wang YH. How effective is T-DNA insertional mutagenesis in *Arabidopsis*? *J Biochem Tech.* 2008;1: 11–20.
74. Barnard A, Calitz FJ. The effect of poor quality seed and various levels of grading factors on the germination, emergence and yield of wheat. *South African J Plant Soil.* 2011;28: 23–33. doi:10.1080/02571862.2011.10640009

75. Herrera-C. F, Ocumpaugh WR, Ortega-S. JA, Lloyd-Reilly J, Rasmussen GA, Maher S. Environmental influences on seed quality of windmillgrass ecotypes in South Texas. *Agron J*. 2008;100: 1205–1210. doi:10.2134/agronj2007.0195
76. Penfield S, MacGregor DR. Effects of environmental variation during seed production on seed dormancy and germination. *J Exp Bot*. 2017;68: 819–825. doi:10.1093/jxb/erw436
77. O'Malley RC, Barragan CC, Ecker JR. A user's guide to the *Arabidopsis* T-DNA insertion mutant collections. *Plant Funct Genomics Methods Protoc*. Second Ed. 2015;1284: 323–342. doi:10.1007/978-1-4939-2444-8_16
78. Boerjan W, Ralph J, Baucher M. Lignin biosynthesis. *Annu Rev Plant Biol*. 2003;54: 519–546. doi:10.1146/annurev.arplant.54.031902.134938
79. Ralph J, Lundquist K, Brunow G, Lu F, Kim H, Schatz PF, *et al*. Lignins: natural polymers from oxidative coupling of 4-hydroxyphenyl- propanoids. *Phytochem Rev*. 2004;3: 29–60. doi:10.1023/B:PHYT.0000047809.65444.a4
80. Liu Q, Luo L, Zheng L. Lignins: biosynthesis and biological functions in plants. *Int J Mol Sci*. 2018;19. doi:10.3390/ijms19020335
81. Schuetz M, Benske A, Smith RA, Watanabe Y, Tobimatsu Y, Ralph J, *et al*. Laccases Direct Lignification in the discrete secondary cell wall domains of protoxylem. *PLANT Physiol*. 2014;166: 798–807. doi:10.1104/pp.114.245597
82. Moura JCMS, Bonine CAV, de Oliveira Fernandes Viana J, Dornelas MC, Mazzafera P. Abiotic and biotic stresses and changes in the lignin content and composition in plants. *J Integr Plant Biol*. 2010;52: 360–376. doi:10.1111/j.1744-7909.2010.00892.x
83. Moreira-Vilar FC, Siqueira-Soares RDC, Finger-Teixeira A, De Oliveira DM, Ferro AP, Da Rocha GJ, *et al*. The acetyl bromide method is faster, simpler and presents best recovery of lignin in different herbaceous tissues than klason and thioglycolic acid methods. *PLoS One*. 2014;9. doi:10.1371/journal.pone.0110000
84. Rolando C, Monties B, Lapierre C. Thioacidolysis. *Methods lignin chem*. 1992. 334–349. doi:10.1007/978-3-642-74065-7_23
85. Nieminen K, Blomster T, Helariutta Y, Mähönen AP. Vascular cambium development. *Arab B*. 2015;13: e0177. doi:10.1199/tab.0177
86. Buchanan, BB., Gruissem, W. & Jones RL. *Biochemistry & molecular biology of plants*. 2015. doi:10.1017/CBO9781107415324.004
87. Keegstra K. Plant cell walls. *Plant Physiol*. 2010;154: 483–486. doi: 10.1104/pp.110.161240.
88. Zhao Q, Dixon RA. Transcriptional networks for lignin biosynthesis: more complex than we thought? *Trends Plant Sci*. 2011;16: 227–233. doi:10.1016/j.tplants.2010.12.005

Berberine bridge enzyme-like proteins in *Arabidopsis thaliana* participate in monoglignol metabolism and stress response

5.9. Supplementary Information

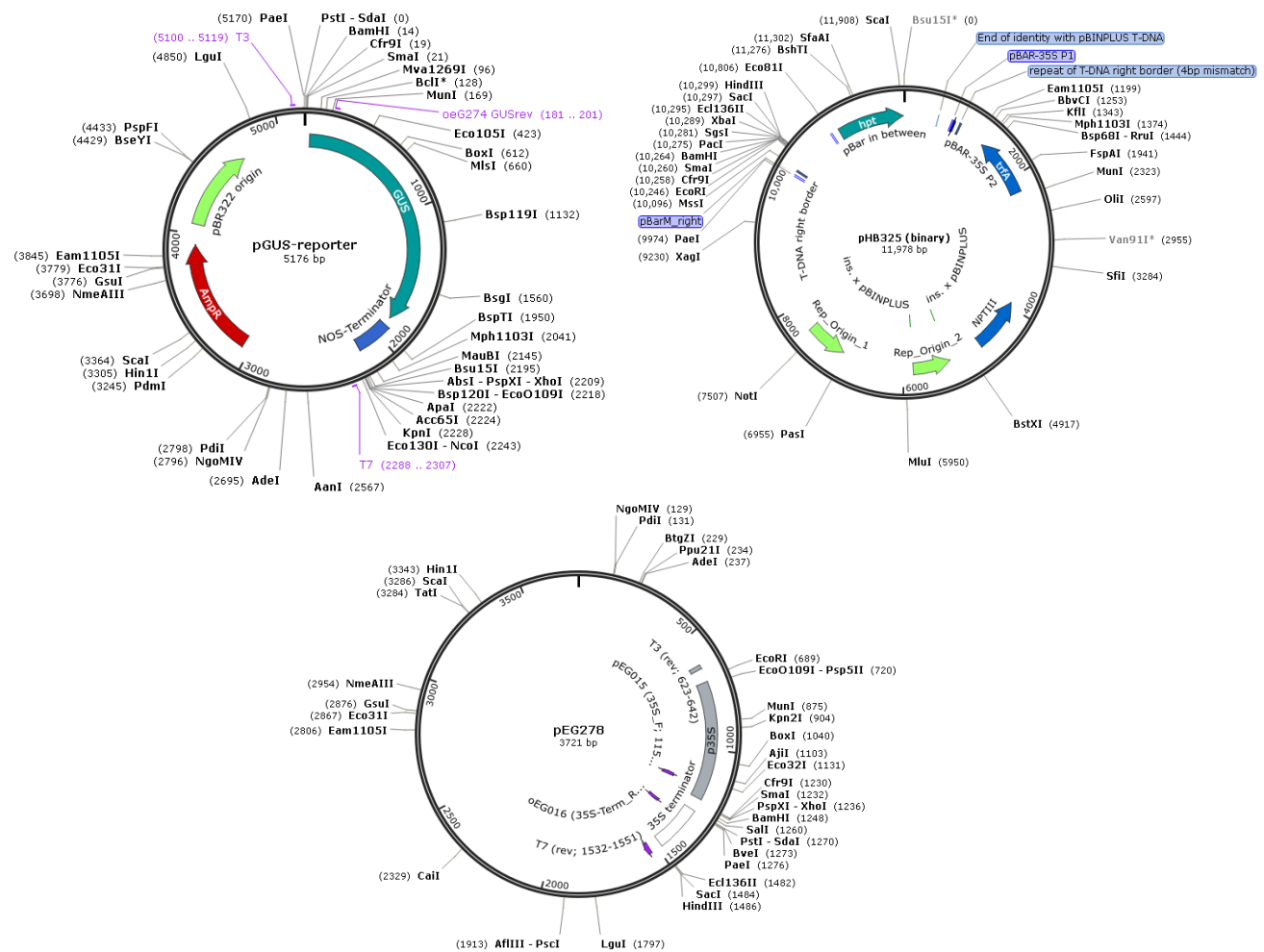


Figure S1. Plasmids used for cloning procedures. **A.** Plasmid pGUS-reporter for *AtBBE-likep-GUS* constructs. Cloning vector features the GUS-reporter gene, NOS-terminator and harbors an ampicillin resistance cassette. **B.** Plasmid pEG278 used for 35S constructs. Cloning vector is equipped with the CaMV 35S promoter, 35S terminator and an ampicillin resistance cassette. **C.** Plant transformation vector pHB325. The plasmid is equipped with a eukaryotic hygromycin marker cassette (hpt) which is shown in cyan, and with a prokaryotic kanamycin cassette (NPTIII) shown in blue. The vector possesses two replication origins, indicated in green, one is for *E. coli* and one for *A. tumefaciens*. Plasmids were kindly provided by Dr. Eric van der Graaff.

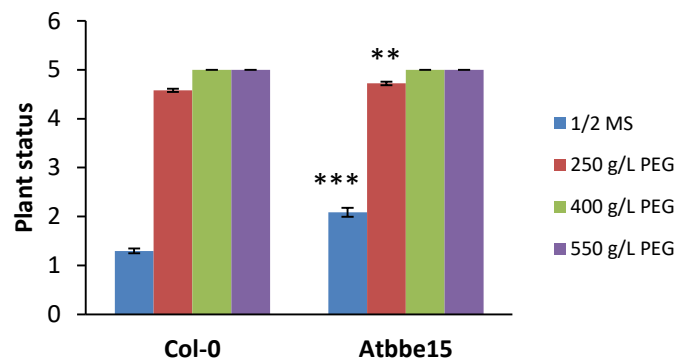


Figure S2. Preliminary test of drought stress response with *Atbbe*-like protein 15 mutant seedlings. Wild type Col-0 and transgenic seedlings were grown in parallel on half strength MS medium with PEG (250 g/L; 400 g/L, 550 g/L) or without (control) for 14 days in climate chambers under short day conditions (8 h day/16 h night cycle) with 200 $\mu\text{mol m}^{-2} \text{s}^{-1}$ light intensity at 24 °C/20 °C (day/night). Growth and health status of seedlings were evaluated in categories: 0 = healthy with 4 or more green leaves (without cotyledons); 1 = healthy with 2 green leaves, 2 = healthy with cotyledons and the first appeared leaves; 3 = healthy, mainly the cotyledons; 4 = very small, cotyledons not open, yellow; 5 = not germinated. Plus 0.5 p for anthocyanins and chlorosis. Bar charts show mean values \pm SE of evaluated seedlings based on one biological replicate with three technical replicates (n = ~200). Statistical analysis was performed according to Student's *t*-test (** P < 0.01, *** P < 0.001).

Table S1. Bacterial strains, antibiotic concentrations and growth conditions

Strain	Plasmid	Antibiotic	Concentration	Conditions
<i>E. coli</i> Top 10	-	-	-	37 °C/LB medium
<i>E. coli</i> Top 10	pEG615*	Ampicillin	100 mg/L	37 °C/LB medium
<i>E. coli</i> Top 10	pEG278*	Ampicillin	100 mg/L	37 °C/LB medium
<i>A. tumefaciens</i> LBA4404	-	Streptomycin	100 mg/L	28 °C/LB medium or YEB medium
<i>A. tumefaciens</i> LBA4404	pHB325*	Kanamycin	50 mg/L	28 °C/LB medium or YEB medium

*kindly provided by E. van der Graaff

Table S2. NASC code of T-DNA insertion lines.

Locus	AtBBE-like	Subgroup	NASC code	T-DNA insertion line	Homozygous*
At1g01980.1	1 (1)	5	N597190	SALK_097190 (BN)	Yes
At1g01980.1	1 (2)	5	N808628	SAIL_178_H03	-
At1g11770.1	2 (1)	5	N603123	SALK_103123 (BO)	-
At1g11770.1	2 (2)	5	N812843	SAIL_278_A03	Yes
At1g26380.1	3 (1)	2	N478008	GK-813E 08	Yes
At1g26390.1	4 (1)	2	N437718	GK-393H02	Yes
At1g26390.1	4 (2)	2	N563965	SALK_063965	-
At1g26400.1	5 (1)	2	N545724	SALK_045724 (AH)	Yes
At1g26400.1	5 (2)	2	N660681	SALK_002408C	Yes
At1g26410.1	6 (1)	2	N554180	SALK_054180 (AL)	Yes
At1g26420.1	7 (1)	2	N579001	SALK_079001	Yes
At1g30700.1	8 (1)	5	N535214	SALK_035214 (E) (AE)	-
At1g30700.1	8 (2)	5	N667127	SALK_117810C	Yes
At1g30710.1	9 (1)	4	N660660	SALK_150104C	Yes
At1g30710.1	9 (2)	4	N667050	SALK_112240C	Yes
At1g30720.1	10 (1)	3	N462339	GK-650C11	Yes
At1g30730.1	11 (1)	3	N536524	SALK_036524 (I) (CJ)	-
At1g30730.1	11 (2)	3	N809266	SAIL_197_F12	Yes
At1g30740.1	12 (1)	5	N684595	SALK_129845C	Yes
At1g30760.1	13 (1)	6	N500581	SALK_000581(F)	Yes, PCR confirmed
At1g34575.1	14 (1)	4	N437250	GK-389A02	Yes
At2g34790.1	15 (1)	6	N662860	SALK_069340C	Yes, PCR confirmed
At2g34810.1	16 (1)	4	N629633	SALK_129633	Yes
At4g20800.1	17 (1)	2	N432375	GK-338B11	Yes
At4g20800.1	17 (2)	2	N643616	SALK_143616	Yes
At4g20820.1	18 (1)	1	N526349	SALK_026349 (BE)	-
At4g20820.1	18 (2)	1	N661935	SALK_026974C	Yes
At4g20830.1	19/20 (1)	5	N589056	SALK_089056 (AO) (AS)	Yes
At4g20840.1	21 (1)	5	N643967	SALK_143967	Yes
At4g20860.1	22 (1)	7	N838709	SAIL_862_H01	Yes
At4g20860.1	22 (2)	7	N631268	SALK_131268 (BW)	Yes
At5g44360.1	23 (1)	7	N857391	WiscDsLox472A5	Yes
At5g44380.1	24 (1)	6	N420302	GK-212D10	Yes
At5g44390.1	25 (1)	6	N663152	SALK_083990C	Yes
At5g44400.1	26 (1)	6	N569865	SALK_069865 (AR)	Yes, PCR confirmed
At5g44400.1	26 (2)	6	N801493	SAIL_31_A05	Yes
At5g44410.1	27 (1)	1	N522408	SALK_022408 (AZ)	Yes
At5g44410.1	27 (2)	1	N639244	SALK_139244 (BY)	Yes
At5g44440.1	28 (1)	1	N507813	SALK_007813	Yes

* Homozygous insertion confirmed by segregation analysis of the T-DNA resistance marker (kanamycin for SALK; BASTA (glufosinat) for SAIL and WiscDsLOX, sulfadiazine for GABI).

Table S3. List of oligonucleotides for amplification of *AtBBE*-like promoters, genes and for confirmation

Promoter	Oligonucleotides	Annealing temp. [°C]
<i>AtBBE</i> -like 13	F 5'-CTTGCATGCGCTTTTGGGTATGAGGTAGA-3'	59
	R 5'-TGTGGATCCGTGGTTGTGAGGTTTTTG-3'	
Confirmation	F 5'-CAGCAAAAACGATCACCC-3'	55
<i>AtBBE</i> -like 15	F 5'-TATCTGCAGGTTGTTTTGATTCTAGCGAGG-3'	60
	R 5'-TATGGATCCGAGGTTTTTGCTTTTGGTTG-3'	
Confirmation	F 5'-CTTTTTTGGTTGGCGA-3'	55
<i>AtBBE</i> -like 24	F 5'-TAAGCATGCGACAACCACACAACCA-3'	60
	R 5'-GCAGGATCCATGCAAGAGAGAAGCCAAA-3'	
Confirmation	F 5'-GAGTCTCCTTTGATCACA-3'	55
<i>AtBBE</i> -like 25	F 5'-GATCTGCAGGTTGTGATGAAACCTTG-3'	55
	R 5'-ATTGGATCCCCTAGCAGCGAATATTA-3'	
Confirmation	F 5'-GGTCACGTTGCTATCATT-3'	55
<i>AtBBE</i> -like 26	F 5'-TACTGCATGCGCTTCCTCTTCTTCATGTCCGATCAC-3'	70
	R 5'-ATCAAGATCTGTTCTTCTGCTCTCGTATTGTTTGTACTC-3'	
Confirmation	F 5'-TGGCACTGAGTTTTTGT-3'	55
<i>AtBBE</i> -like 27	F 5'-AAGGCATGCGAAAACGGAGAAGAAAGAAG-3'	55
	R 5'-ATGGGATCCCGGTGAGAAGACAATAAAG-3'	
Confirmation	F 5'-GACGTAACCTTATGA-3'	55
<i>AtBBE</i> -like 28	F 5'-CGAGCATGCTCTCCTCCATCACCTTAC-3'	55
	R 5'-TCTGGATCCGGTGGATAGTATTGAGAATG-3'	
Confirmation	F 5'-CTTGCGGAGGATTTTTAC-3'	55
GUS reverse	F 5'-ACTGATCGTTAAACTGCCTG-3'	55
Gene	Oligonucleotides	Annealing temp. [°C]
<i>AtBBE</i> -like 26	F 5'-TACTGGATCCAACACCACACTAGTCACACACTTAAATG-3'	64
	R 5'-ATCAGCATGCCTTTAAATAGGATTCTCGAGTTGATTGAAG-3'	
Confirmation	R 5'-GCTAATGAAGAAGTTGGTG-3'	55
<i>AtBBE</i> -like 28	F 5'-TACTGGATCCATCCACCTATCTTAGAAATGGAG-3'	59
	R 5'-ATCAGCATGCAACATGAAAAGTTTATTCAACACAC-3'	
Confirmation	R 5'-GAAAGCAAGAGATTTGGTG-3'	55
p35S Promoter	F 5'-ACAATCCCCTATCCTTC-3'	55

Table S4. Flower stalk material for lignin quantification with acetyl bromide method.

Line	Stem sections	Fresh weight [g]	Dry Weight [g]	Dry Weight [mg]*
Col-0	5 cm young flower stalk	2.1685	1.0176	342
Col-0	5 cm old flower stalk	4.1636	2.2689	1192 (488 used)
<i>Atbbe</i> -like 13	5 cm young flower stalk	2.0006	1.124	379
<i>Atbbe</i> -like 13	5 cm old flower stalk	3.1883	1.3334	511
<i>Atbbe</i> -like 15	5 cm young flower stalk	1.6778	0.7734	157
<i>Atbbe</i> -like 15	5 cm old flower stalk	2.6892	0.9251	348

*Dry weight after grinding

Table S5. Sample list for thioacidolysis (data from Prof. Catherine Lapierre). In total, 3 independent biological replicates with 3 technical (24 plants per line) replicates. The solvent-extracted samples are cell walls CWs %.

Biol. Replicate	Tray	Genotype	Dry weight [g]	Code	Used Dry weight [g]	Extracted Mass [g]	%CW	Simplified Code
S1 (29/10/2015)	1	Col-0	0.2882	B1	0.7351 (B1+B2+B3)	0.44	59.9	A
7-8 weeks old	2	Col-0	0.2133	B2				
Siliques still green	3	Col-0	0.2336	B3				
	1	<i>Atbbe</i> 13	0.2607	B4	0.7491 (B4+B5+B6)	0.48	64.1	B
	2	<i>Atbbe</i> 13	0.2555	B5				
	3	<i>Atbbe</i> 13	0.2329	B6				
	1	<i>Atbbe</i> 15	0.2557	B7	0.7811 (B7+B8+B9)	0.49	62.7	C
	2	<i>Atbbe</i> 15	0.2754	B8				
	3	<i>Atbbe</i> 13	0.25	B9				
S2 (16/11/2015)	1	Col-0	0.1783	B10	0.5353 (B10+B11+B12)	0.36	67.3	D
9-10 weeks old	2	Col-0	0.1722	B11				
Siliques started ripening	3	Col-0	0.1848	B12				
	1	<i>Atbbe</i> 13	0.2183	B13	0.5573 (B13+B14+B15)	0.36	64.6	E
	2	<i>Atbbe</i> 13	0.1612	B14				
	3	<i>Atbbe</i> 13	0.1778	B15				
	1	<i>Atbbe</i> 15	0.1619	B16	0.559 (B16+B17+B18)	0.39	69.8	F
	2	<i>Atbbe</i> 15	0.1859	B17				
	3	<i>Atbbe</i> 15	0.2112	B18				
S3 (16/11/2015)	1	Col-0	0.4891	B19	0.4891	0.29	59.3	G
8-9 weeks old	2	Col-0	0.5112	B20	0.5112	0.28	54.8	H
Siliques not yet ripened	3	Col-0	0.4652	B21	0.4652	0.31	66.6	I
Leaves discoloured	1	<i>Atbbe</i> 13	0.486	B22	0.486	0.32	65.8	J
	2	<i>Atbbe</i> 13	0.4389	B23	0.4389	0.27	61.5	K
	3	<i>Atbbe</i> 13	0.4293	B24	0.4293	0.28	65.2	L
	1	<i>Atbbe</i> 15	0.4269	B25	0.4269	0.3	70.3	M
	2	<i>Atbbe</i> 15	0.3972	B26	0.3972	0.26	65.5	N
	3	<i>Atbbe</i> 15	0.491	B27	0.491	0.33	67.2	O

Table S6. Results of thioacidolysis and GC-MS of three biological replicates. First series with 7-8-week-old plants, second series with 9-10-week-old plants and third series with 8-9-week-old plants.

CODE	sample	(H+G+S) μmol/g CW	CALD μmol/g CW	Relative frequencies (% molar)			S/G
				%H	%G	%S	
A	COL0 B1+2+3	190	0.85	0.6	67.2	32.2	0.48
A	COL0 B1+2+3	185	0.77	0.6	67.3	32.0	0.48
A	mean WT COL0	187	0.81	0.6	67.2	32.1	0.48
	SD	4	0.05	0.0	0.1	0.2	0.00
B	BBE13 B4+B5+B6	184	0.77	0.6	68.6	30.7	0.45
B	BBE13 B4+B5+B6	187	0.88	0.7	67.8	31.6	0.47
B	mean BBE13	186	0.82	0.7	68.2	31.1	0.46
	SD	2	0.08	0.0	0.6	0.6	0.01
C	BBE15 B7+B8+B9	179	0.71	0.6	67.8	31.6	0.47
C	BBE15 B7+B8+B9	174	0.62	0.6	67.6	31.8	0.47
C	mean BBE15	176	0.66	0.6	67.7	31.7	0.47
	SD	4	0.06	0.0	0.2	0.2	0.00
D	COL0 B10+11.12	271	1.65	0.8	68.1	31.1	0.46
D	COL0 B10+11.12	248	1.58	0.8	68.6	30.5	0.44
D	mean WT COL0 B10+11+12	259	1.62	0.8	68.4	30.8	0.45
	SD	17	0.05	0.0	0.4	0.4	0.01
E	BBE13 B13+14+15	237	1.15	0.8	68.0	31.2	0.46
E	BBE13 B13+14+15	229	1.37	0.9	67.6	31.5	0.47
E	mean BBE13 B13+14+15	233	1.26	0.8	67.8	31.3	0.46
	SD	5	0.15	0.1	0.3	0.2	0.00
F	BBE15 B16+17+18	213	1.22	0.8	68.6	30.6	0.45
F	BBE15 B16+17+18	230	1.45	0.8	68.4	30.8	0.45
F	mean BBE15 B16+17+18	222	1.34	0.8	68.5	30.7	0.45
	SD	12	0.17	0.0	0.2	0.2	0.00
G	meanCOL0 B19	283	1.69	0.6	67.1	32.3	0.48
H	mean COL0 B20	271	1.5	0.6	67.5	32.0	0.47
I	COL0 B21	274	1.35	0.6	67.7	31.7	0.47
	mean Col0	276	1.52	0.6	67.4	32.0	0.47
	SD	7	0.17	0.0	0.3	0.3	0.01
J	mean BBE13 B22	251	1.50	0.6	67.7	31.7	0.47
K	BBE13 B23	249	1.20	0.6	67.9	31.5	0.46
L	mean BBE13 B24	254	1.39	0.6	67.6	31.9	0.47
	mean BBE13	251	1.36	0.6	67.7	31.7	0.47
	SD	2	0.15	0.0	0.2	0.2	0.00
M	BBE15 B25	254	1.06	0.6	67.1	32.3	0.48
N	mean BBE15 B26	242	1.30	0.6	67.7	31.7	0.47
O	BBE15 B27	258	0.96	0.5	67.1	32.3	0.48
	mean BBE15	251	1.11	0.6	67.3	32.1	0.48
	SD	9	0.17	0.0	0.4	0.4	0.01

Table S7. Most significant and interesting expression values of *AtBBE*-like protein 13, 15, 26 and 28.

Expression values [a.u.]*	
<i>AtBBE</i>-like	13
Root	
Lateral root primordium	~200
Xylem pole pericycle	478.29
Lateral root initiation	1681
Xylem pole pericycle gene regulation during lateral root initiation induction	
Cytokinin-induced transdifferentiation of lateral root primordia to shoot meristem	1487.52
Root and shoot regeneration from root-explant-derived callus	1373.55
Stem	
Xylem within the cork (hypocotyl)	617.06
Whole stem, bottom of stem	221.54
Abiotic stress	
Osmotic (Mannitol)	43.75
Salt	98.56
Drought	127.68
Light/Dark	
Constant dark	744.87
<i>AtBBE</i>-like	15
Root	
Xylem	4927
Seed	
Seed development (chalazal endosperm mature green stage)	561.67
Seed stage 10	184.36
Flowers	
Flower Stage 10; Stamen	208.44
Stem	
Xylem within the cork (hypocotyl)	89.4
Whole stem, bottom of stem	113.54
Abiotic stress	
Osmotic (Mannitol)	41.53
Salt	65.8
Drought	51.02
<i>AtBBE</i>-like	26
Root	
Root procambium	318.96
Cytokinin-induced transdifferentiation of lateral root primordia to shoot meristem	1132.66
Seedling	
Hypocotyl	565.28
Root	505.11
Flowers	
Flower stage 10/11	252.28
Leaf	
Leaf 7, petiole	305.76
Stem	
Xylem within Cork	615.3
Whole stem, bottom of stem	161.88
Abiotic stress	
Osmotic (Mannitol)	128.21
Salt	604.28
Drought	370.15
Biotic stress	

<i>Botrytis cinerea</i>	259.15
<i>Pseudomonas syringae</i>	250.33
<i>Erysiphe orontii</i>	289.22
Light/dark	
12 h light-dark cycle	1056.98
AtBBE-like	28
Root	
Lateral root cap, Stage I	927.51
Callus formation	
Cotyledon derived callus	477.63
Root derived callus	778.48
Petal derived callus	629.72
Abiotic stress	
Mannitol	12.23
Salt	9.36
Drought	7.4
Light/Dark	
Constant dark	6160.94

* Data were obtained from the Arabidopsis eFP Browser (<http://bar.utoronto.ca/efp/cgi-bin/efpWeb.cgi>)

A

AtBBE-like 13 - At1g30760.1**T-DNA insertion line: SALK_000581.54.75.x**

Chromosome 1: 10918278...10920709 (forward strand) class = mRNA*

aggcttagtactacataggtcagtttgacttctaaagtggcttgcattcacaagtatgaatggcaagcttagcgtttggtggtgcgat
caataaaagattaattatcattagttataatgtattatagatcactatacatctcttattaagtgtatacatcacagatcccacaaaacaatt
tgaactcaatttaaaggtagtaatttttataaagagatttcataaatctaaatgaaaagttaaaggacagaaagtaatacaagttgaacca
acaaccataagaaagaagggaatctgggttataacatagctaaatttgtagttagtattttctagaatccaatatttatatatatata
tatatagctaaataattgatgattttgaaagaaaatttctaaataaaactattactatacctcccacatcaatccgggctaatagttactta
atctcatgcttaattgtgataaaaataatatttgtataagttatacatacgatcaaaactaataatcatataagggttttaatatataacaacg
ccattctaaaaaattgaggcgacaacaatatattctacggactatatagtttgaagggttaaactatataacttctagtagaaaacca
atttataatatttgaatggtgaagttttttccaagtaattaagtaagagttgtaggcttctatttatggatcatccactattttctacttggc
cactcactataaacgtaaaacatattaacgacaaaagtaatttagattctatcttaagagttaagactacactgtacataaaatattttcc
actctaaattttcttttctgtaaaaaattaaagttgacaaaaatctaaaataaaccataataactataccatttagttacagaatattttg
attgagtaggattatgcaacttaagacaactctcaagatttattgtatattttattcaatataaattgaagaaaatataataattttgagcca
caattactggagatggtggtgctcagtatcttgaataatgaagaaattgtcccctctaaagttaaaaccacaaaattgacactcttcaa
acaccatattttccataaaactgggggttcaatcaattaattataaaaacagattgtacattaacattttcctttttcattgacacgaaaattt
tagaaagaggttatccaatgcaataatgtttcattcagattcggctcaaaaatagaaaaatatacaataattgaattaaatataataatg
actttttctcgaactcacagtacataaggcaacaaggtcagatttgatgcatagagataatgacattttctagttttgttaaatataagta
taatacaacattccaaatttctattacagattttaactggatcggataattagatcggcatattttcaagcttcagcaaaaacgatcacct
aaaattattttttgatggaatgattgtttgaggatattgaatatatacactccaattccaaaaaggctataaagtatgaattaaacaatcaag
tagtaatagccattattaatgattcgaatggtaagaataaataacactaaacaagagtcaaaagaacatgacgtaaatattatcatcaa
ctttacgtataaacccttccctctctatttaaaccacaacatacatatgaaactcctcaacaacacaaaaacctcaaacaccactaaa
caacacacaaaa**ATGGCGTTTGTATTAATGAATAACACAAACGCGTTTCTTGTAACG**
CTACTATACTATCCCTTTCTTACATTCCATTGTCTTTTTCCACAATCCAACA
AGACTTCGTGATGTGTCTAGTCGACAACCTCCGACGCTTCCTTTCCAATGGAC
TCATCGTTCTTCACTCACGACCTAAACGCCTCTTCCTTTAAACTCGCCTTAGA
GACGTCAGCTCAAAATCTCCGTTACTTGATGCCTTCAAATCCTAAGCCAGAG
TTCATTTTCGAGCCGCTTTACGAAACGCACGTTTCAGGCCGCCGTTCTTTGCG
CCAAGAAGCTGAAGCTTCACTTGCAGTTAAGAAGCGGTG**GT****CATGACTACGA**
AGGCCTCTCTTACGTCTCGGAGATGGAAACGGCGTTTGTGATCGTCGACTTG
TCCAAGCTTAGACAGATCAGTGTGATATAGAAAGTAACAGCGCGTGGGTTCC
ACGCTGGTGCTTCTATTGGAGAGGTTTATTACAG_{gtaaatcatatgttataatctcttttttaaccac}
gctacaacgatttatattgccaccgagaacgatttaattctaaagctacaccctaaagttttaaataatttgattactt**tatatagtac**
aagatatacttattatgaaagaaaagggaaggttacattcattcatttcaaacatattc_{aaatttacaacaaaatg}**aaatttt**
agtttcttggggacattttccacatttaggcttgggttggttaagctgaacaatttaaatttttaaccgaaccaatttactataaaacaacc
gaatatgatggttaagctgtggttatgaccgggtctcttgggttatatttcatggttttaag**GATCCAAGAGAAAAGCA**
AAATCCACGGTTTTCCGGCGGGTTTATGCACCAGCCTAGGCATCGGCGGTCA
CATAATCGGCGGAGCCTATGGTTCAATGATGCGTAAGTTTGGTCTCGGAGCT
GATAACGTCCTCGATGCTAGGATCGTTGACGCTGACGGCAAAATCTTGAATC
GCGCGGCGATGGGAGAAGACGTTTTCTGGGCGATTTCGAGGAGGTGGAGGAG
GAAGCTTCGGCGTAATACTTGCCTGG**AAAAATAAAGCTCGTTCCGGTGCCAGA**
GATTGTTACGGTGTTTACCGTCACGAGGACGCTTGAGCAAGACGGAACCTAAG
CTTTTGTACAAGTGGCAACAAGTCGCTGATAAGCTCGACGAAGATCTCTTTA
TCCGTGTGATTATTCAGCCGACGAGCAAACTCCGAAGAGCAAAGAAAGAAC
TATCTCGACTTCGTACCAAGGCCAATTTCTCGGCGACGCTAAATCGTTTGTG
CAG_{gtaaaataatggggc}**caaat**_{taatttc}**gtaata**_{ttaggg}**ctgtt**_g**gtaatt**_t**atgaa**_g**gtaatt**_g**gtatgata**_{aa}**taag**_g**aa**
ggaaagttttgattatgacaataaacaccccggttgggtgacag**GTGATGCAAAGGAGTTTCCCACAGCT**

TGGA CTAACGAAGAAAGATTGTTT TAGAGACAAGCTGGATCAAATCGGTGATG
TACATTGCAGGTTTTCCAAGCACTGCCCCATCAGAAGCTTTACTCGATGGGA
AATCGTTGTTCAAGAATTACTTCAAAGCCAAGTCAGACTATGTGGAAGAGCC
AATTCCAGTAGAGGGATTAGAAGGGTTGTGGGAGAAGCTTCTAGAAGAGGA
CTCACCATTGACTATATGGAATCCTTATGGAGGAATGATGGCAAAAATTCCC
GAGACAGAGACACCTTTCCACATAGGAGTGGGACATTGTTCAAGATACAAT
GGCTGACTTTGTGGCAAGATGGGAAAACAAGCGAGGCCGAAGCATATGGGGT
GGATGAGGGAAATGTATAGTTACATGGAGCAGTATGTATCGAAAAGCCCGA
GATCCGCGTACGTGAACTATAGAGATCTTGATTTGGGGATGAATGGTAAAGG
GAGTGATGCAAGAGAATGGGGGAATAGGTATTTCAAGGGTAATTTTGAAAG
GTTGGTGGAGATTAAAGCTAAGTTTGATCCTGAGAATTTCTTTAGACATGAA
CAAAGTATTCTACAGAACTTGAGTGAattggagtagacaagaataagagtggtgtaagatttctctta
ggaaagactgttactgtgttttgtgctttaaacatggccaacacactgtattcaaaattgtatccaatctaacccttatgaggtcttag
aagtaatggcaaatttgctaaaccaaatcaaatcatatttgctataaatgatgatagtttggttaatggcaaactcctattgtccacca
caattcctatttaaacacacactctttaacaatagtgataggatactacctgtagaaaatatgtatctagaaggagatattcatcttccctaa
tttctccaatctttatatttcatcccaagaaagaaaaaatgattgtaataggaatatagaaaccaatttgtac

EXON1 EXON2 EXON3 intron

RT-PCR: **F 5'-CTTGC GGTTAAGAAGCGGTG -3'**

RT-PCR: **R 5'-CCAGGCAAGTATTACGCCGA-3'**

PCR product for sequencing: R 5'-**CATACTTTTGC GTAAACC**-3' with SALK-LBb1.3

tatat = possible T-DNA insertion site based on sequencing emanating from the T-DNA left border primer (**SALK-LBb1.3**); not clear due to the same sequence of this part on T-DNA and *AtBBE*-like 13 DNA

Sequencing result:

ACCAGCGTGGACCGCTTGCTGCAACTCTCTCAGGGCCAGGCGGTGAAGGGCAATCAGCTG
TTGCCCGTCTCACTGGTGAAAAGAAAAACCACCCAGTACATTAAAAACGTCCGCAATGT
GTTATTAAGTTGTCTAAGCGTCAATTTGTTTACACCACAA**TATAT****AGTACAAGATATACTT**
ATTTATGAAAGAAAAGGAAGAAGTTACATTCATTTCAAACATATTCGGGTTTACGC
AAAAGTATGA

identical with T-DNA sequence (sequence of pBin-pROK2-Plasmid)

identical with *AtBBE*-like 13 DNA

unclear area, identical with both sequences

* Gene sequences obtained from aramemnon <http://aramemnon.uni-koeln.de/>.

B***AtBBE-like 15 - At2g34790.1***

Chromosome 2: 14673840-14677398 (reverse strand); class = mRNA*

T-DNA insertion line: SALK_069340.55.50.x

attaaatgaacagtgtacacttttagttttacataagatattatataaagttgaataatattatgcggaatttgaaagaatctgttagtag
 acttttagtttggtcaacttttctttttcgtctatatagtcattagatataatttgattcaattttattatagtggtgatagcgtgtgcatattgaa
 actttgaagcaagtttagcttttagacaatctcactttgttcttttaagctafacatagctcagagctcagaataccatcaatcacaccact
 ttctgaataatcgttaacctaaatcgaacccaaaagtaaaataaagatgggtgttttgattctagcaggatgaaactgagaccaatcac
 attttacatgtattaagaactaaaatatttataggtcatcaatgggtatcgattttaatatagtttaagattataattttggttttgaattttaga
 ttttgggttttagattttccaaaaataaagatataataaaaaaaataggaagaaaaagtcacgttaatattgtaaggaaaagcgaaaaa
 ctcaatttgaaaactcaattttgctatttttactattcataaactcacaatttttaaaaaaatgagtgtgtaaaaaatataagtagaaaaagtc
 aaaacggcattaatctactaaaactcacttttagcatccgtaattttttacgaaaacttaatttagttcagtttttctgctaaagtattcaatta
 attttttgtgattttgtgcataccaatcaagccaaaaacaataaaaaattagtaaatattcaagccgtaattttgaaatagaaatattta
 tattacacttactctttggtcgtcaatattgctgaggtataaaagcgtagggataatgtatgtgtagatttttgattgcttagtcaaaagggt
 aaccggtaacaaggaagattattagttactacaattctaggacaggagagaatgtatttaggcttcacgccacaactactgaagatagtg
 gtgctgctatcttttagatgtgataacataaagtcgtgctcggtatcctgaaaagttgaaattagtcggtattagcattgtttatccctaaagg
 cacatatatattgttcttactttcaaacgacatatatttctcagaacctttgctataatgtctgaataatcattacaatatagtatatacaca
 caaaacttattgatactatgcattctctttggctatgttgaaaactcacttgcactgtataaacttctaagttatgcatgcgttttaataa
 tcaagttactataaattaagatacaggtatgtatagcaattaataaaaactaattaatacagtttagtaatgaataatgatataaacattat
 acagtacagtgtcgtggttcagtaatgatataatcaccatcagattacatgtaaagattcagatcatagcaaatagcaatgaagtaaa
 ggacaatgcaagaattgaccaatfacttgaatattctaataattcatttctttttttggttggcgaacatatatttggttacgtttat
 gcttaaggatatactgctatttttcaagtaatcaaaataaagatagaattatagtaaggagataaaagttgagattttagtaatagaata
 aaaatagtaatgaagtaatatttacaccaactttacgtgtaagccatccccacacacacatcaacctcctataaacctaaacacataact
 caaacaacaaaagcaaaaacctcctcgcacataaaaagaaaa**ATGGCGTTTGCATATCAAAGCGAAA**
CGCAACCTTGTTTCTTGTAACGCTACTACTAATCTCCGTTCCATTGTCTTCTC
CCACGCTACAACAAGATTTTCGTGAAGTGCCTTGTCGACAACTCCGACGTCTC
CTTCCCATAACGGCGTCGTTTTTCTCACCGGACCAAAACGCTACTTTGTTTA
AAGAGGAGCTTGAATCAACGGCACAGAATCTCCGTTACTTGACGCCGTCAA
CCGAAGCCCGTGTTTCATATTCGAGCCTTTGTACGAGACGCATGTCCAAGCA
GCGGTCGTGTGTGCCAAGAAGCTTCAGCTTCACCTCCGGCTACGTAGCGGT
GGTCACGACTACGAAGGGCTCTC**GTTTGTGCGGAGGACGAAACGCCGTTT**
GTGATCGTTGATTGTGCGAAGCTTAGACAGGTTGACGTTGATTGGACAGTA
ACAGTGCGTGGGCTCATGCTGGTGTACCATCGGAGAGGTTTATTACAG_{gtaac}
 gcttacgcatgattatataatatttcttggctcagattttgaaatagtaaaaacaataattgacgcataatttttatggcgagattattcttta
 atttttaagtaggatgataaactgattttggtttagaacttattcgcataattttgactccaatagtaacgggaagtttgacgtcttagg
 ctaagttttctttccattgctattgtctattgccatttggggaacctttttggttctactttattcgtggattccctaaaaacgtcgggt
 aaaggatgacttgccttttctactttcgttactaggcttgggcacgaagcgaatatccggaaaaaattgactattgttattcgttattaa
 tcgaatacttgattttattttgcttgattcgaacttccggatattccggaatttcgaatatccggaattttgtgatatttgcggatattccgc
 ttgatacgtataatattaaaaaatctgtaactatataagcatatcagatattcaaaacttttacttaacatgctttcaaaaataagttataat
 accaaacataaccttgggttattaccggcaacaaaaatgttatcaaaactaattctaaaaactaaaaccgatagtttfaatgcatgattgatc
 aaaacacataaaaaaaaatgatcaaaacaacatcttaacataaaacataaggtagcaacaatacacaactatttatgatattctatat
 atagatataactatattctgatataatcaaaagatacggatcgaagcggatattcattttaaaaaaaacaatattgctatttgattcgggt
 tttagcaatactatattttcatatttcttgggtccaaaactttacggatattcggattttcgaatcaaatcaaatcgaataaccgagtcacaccg
 gatcgaacgaatattttgccaagccctattcgttacaacgcattgtgaattgtagttgtaacatttcttctcattgctttcagttttattatatt
 attatatttttctattttatgacttttaataatattttttccatctatagttattttgtcatctcgaactcaaaactatttaccctaaatgcaaaaacc
 taatagttatttcttggctttaaaggttaataatatttaaaactaacattttttattgggtcaaattagttattatataaaaactttcag**XX**ttat
 tccccctcattagccaaatttataaccattagagtgagtataccaatagatttcattcttactatcttctacaccttaattgaaaaagtttaac
 ataataatcaatggcatatgtagaataatccattcgtcgttcaatcagaaccgggttaaccaaatgccggaaccaacaaaataaaatcaaa

accgatcacatggttgagctttcgttaatgatccgataattaatcggttggtgtctcggttaacag **GATCCAAGAGAAAA**
GCCAAACCCATGGTTTTCCGGCCGGTTTTATGCTCAAGCCTTGGCATCGGTGG
CCACTTAGTCGGTGGAGCGTACGGTTCATGATGAGGAAGTTCGGTCTCGG
CGCTGACAATGTCCTCGACGCCAGAATCGTCGACGCCAACGGCCAAATCCTC
GATCGCGCGGCAATGGGAGAAGACGTCTTCTGGGCGATTTCGCGGCGGCGGC
GGTGGTAGCTTCGGC **CTGATAATGGCTTGA** **AGATTAAGCTCGTCCCCGTT**
CGGCGACCGTTACGGTATTCACAGT **CACGAAGACGCTTGAGCAAG-**
ACGGAACTAAAGTTTTATACAAATGGGAACAAATCGCTGATAAGCTTGACGA
TGATCTCTTCATTCGCGTCATTATTTACCGGCCAGTAAAACCACCAAACCG
GGAAATCGAACCATCTCGATGTCGTACCAAGCTCAGTTTCTCGGAGACTCCA
ATCGGCTCTTGCAAGgtatgatagtggtcaaatccaaacttaagggtctaaattgaactctttatcttttcggtttaacaattc
aagcaataaaacttttaattgtcaattcaacccaacag **GTGATGCAGAAGAGTTTCCCTGAGTTAGG**
ACTGACGAAGAAGGACTGCACAGAAATGAGCTGGATCAAATCAGTGATGTA
CATTGCAGGTTTTCCAAACAGTGCAGCACCGGAAGCTTTACTAGCCGGAAAA
TCATTGTTCAAGAATCACTTCAAAGCCAAGTCAGACTTTGTGAAAGAGCCAA
TTCCAGTAGAAGGTTTAGAAGGATTATGGGAAAGGTTTCTAGAAGAAGATTC
ACCGTTAACGATATGGAACCCTTACGGAGGAATGATGTCGAGGATCTCCGAG
TCAGAGATACTTTCCCTCATAGGAACGGGACATTGTTCAAGATTCAGTGGC
TAAGCACGTGGCAAGATGGGAAAGTGAGCGAGGAAAGGCATATGAAGTGGA
TTAGGGAGATGTATAGTTACATGGAGCAGTATGTGTCGAAGAACCCGAGACA
GGCGTATGTGAATTACAGGGATCTTGATTTGGGGACTAATGAAGGAGAGACT
GATGCTAGAGAGTGGGGTGCTAAGTATTACAAAGGGAATTCGAGAGGTTG
GTGAAGATTAAGGGTGAGTTTGATCCTGATAATTTCTTCAGGCATGAACAGA
GTGTTCCGACAAAGATTGGTTGAtggattggagttcctgttcaatgggttttaattctaataagaaaatata
acacaagatagaataatgtatgtgtttgtcatagggagaattctacattttgtatctatattttgatataacaactttacttatagtgg
tgtcatttgggtttgcttaacattctgaattagacacaaatcgtgtagtggtttatactattgtcaccacaaacacaaagctccaattttaata
atagaaaaaattggaacctcaatgcaatctcattcatatctgcatcctctatgaccaaaggaggcagtcattgaagaatcaaacagtaa
gagactatgtccaaaatttactgcttttgatgacttttgaactgaggaatcatcta

EXON 1 EXON 2 EXON 3 intron

RT-PCR: F 5'-**CACGACTACGAAGGGCTCTC**-3'

RT-PCR: R 5'-**CTTGCTCAAGCGTCTTCGTG**-3'

PCR product for sequencing: R 5'-**TTCCAGGCCAATATCAC**-3' with SALK-LBb1.3

XX = T-DNA insertion site based on sequencing emanating from the T-DNA left border primer (SALK-LBb1.3)

Sequencing result:

Insertion on reverse strand

NNTNGGGGC**AACCAGCGTGGACCGCTTGCTGCAACTCTCTCAGGGCCAGGCGGT**
GAAGGGCAATCAGCTGTTGCCCGTCTCACTGGTGAAAAGAAAAACCACCCAGT
ACATTA AAAACGTCCGCAATGTGTTATTAAGTTGTCTAAGCGTCAATTTGTTTATT
AATTTAGTTTATTCCCCCTCATTAGCCAAATTTTAATACCCATTAGAGTGAGTTA
TACCAATAGATTTCACTTACTATCTTCTACACCTAATTGAAAAGTTAATCATAA
TCAATGGCATATGTAGAAATATTCATTTCGTCGATTCAATCAGAACCGGTTTAAAC
CAAATGCCGGAACCAAACCAAAAATAAAATCAAACCGATCACATGGTTGAGCTTT
CGTTAATGATCCGATAATTAATCGGTTGTTGTGTCTCGGTTAACAGGATCCAAGA
GAAAAGCCAAACCCATGGTTTTCCGGCCGGTTTTATGCTCAAGCCTTGGCATCGGT
GGCCACTTAGTCGGTGGAGCGTACGGTTCATGATGAGGAAGTTCGGTCTCGGCG

CTGACAATGTCCTCGACGCCAGAATCGTCGACGCCAACGGCCAAATCCTCGATCG
CGCGGCAATGGGAGAAGACGTCTTCTGGGCGATTGCGGGCGGGCGGTGGTAG
CTTCGGC**GTGATA**GGGCCTGGAAAA

Very similar to T-DNA sequence of pBin-pROK2, sequence quality is worse

Identical with T-DNA sequence of pBin-pROK2 (reverse complement)

Identical with *Az*BBE-like 15 DNA

Remainder of the primer for the PCR product for sequencing

Similar to *Az*BBE-like 15 DNA, sequence quality is worse due to end of sequence

* Gene sequences obtained from aramemnon <http://aramemnon.uni-koeln.de/>.

C

AtBBE-like 26 – At5g44400.1

Chromosome 5: 17886160-17888530 (reverse strand), class = mRNA*

T-DNA insertion line: SALK_069865.56.00.x

tatgctgacgacaaaaagtaaatgaccacctgaatttcaaagtaattcttcaaataattgacatgtctaattaagaccaaattagttgaa
aacggttgcaatggactgatcgtaatagttagtcacctgtgaacgagttgtatttatccaccaaaaaacaaattgacggatttggtgg
gtttgggcaaaggtatatctgatgaattttctacatctattccaaaaagtcgacctaaccgaaaagtcgacataatagaacaagatag
tgctggtatatgaaaaaagatgaaaacaatagttaaattcacaaggacaggcagcaaatgaatatgttgaattttgtgatattgtgatt
gttttactctagaagtgtttctactaataatattgttcaaatttaactagatatccagtgtcaatccatacatttctgcaaaaataagattttttatt
tattaaagagtacatacatttggtcgttcacccaggtttacagaatcaaagtgaactcataagtattacaccatacatttctagattatga
gctagtataftacattctatctaatgcatggataaagtgaatatttgaaaatttcaagcccaataacttgataggtgaagaagattcgtacca
gaaatatttctgtagtategtgaaaacaaattgatgaacaacctcggatccacgttgatgcattgctgcaaaaacataaaattttaaata
tcatttaaatacaactaaatttcttcttaacttcaaaattttaaacaatattacacaatttaagttacacaataatataatgaatctataataaatac
atataatataatataatctcattttaaatttgaacttttaataatttactgcgttttgaacaaatgttgtttgaagatgacaattacggtgctg
ggaattagcaaatgcatctaaatctaaattttaaataaaaacagctaaaattacggatatataaacacgaatatttctacacct
actaacgtatactccagtttctacaaacacaaactgcaacgtttttaggctacgagaagaaaaaatgtccgtcacgttgcgtcact
gagacaatggctgctgcacattcagccatagaaaatttggccatctaccgtggctgtgacctggaagatataatagctattt
atatacattcacacctatgcaataaaattgactccaaaaacactgaatataataggaattagttacaataagcaattttagttaggta
aagaacaaatagtaatttgacaaatgagaatggagaagattaaggttaaaatataattggaacgactctaaataaagtttgtatttctct
tttcttctctctattactatataatttctcatagcttcattaccctaacaccacactagtcacacactaaatgttcttccgctttgacgcctaa
tctcatctccacaaccttgcaagttggaagtctcttaaaaatgacttctttgtttaaactttaaaggcactgagttttgtggtatca
ctaaaaacaaacgattcatgatgaaaacttgacttgggtccaatatttattataatcaatgactactttatgtaaaagagtttaggccttgagc
aatgattttcaagagagaagaaataaagttggacatttggaaactttagatagaggagaaggttagatttttcttattaataactgga
atttgcatgctgttgggatcaagagtagcaacaatacagagagcagaagaacttactatagaaaaaaATGGGAATTT
CAAACCACTCCCTCTATTTTCGATTTTAGTCCTCTATTTTCACTCTACACC
ATTACACCAACTTCTTCATTAGCCTCCCTCCAAGATCAATTCATCAACTGTGT
CCAAAGAAACACACATGTTTACTTCCCACTGAGAAAACGTTCTTTGCTCCTA
CAAAAAATGTCTCTATGTTTCAGCCAAGTTCTTGAATCGACGGCTCAAAATCT
CCGGTTCCTGAAAAATCCATGCCTAAACCGGGATTCATATTCAGCCCTATT
CACGAGTCTCACGTACAAGCTTCCATCATTGTTCCAAGAAACTCCGAATGC
ATCTCCGTGTCAGAAGCGGCGGTACGACTACGAAGGCTTGTCTTATGTCTC
TCAGATCGATAAACCGTTTATATTGATGGATCTGTCAAAGATGAGACAGGTC
AACATTAATATTCAAGACAACAGTGCTTGGGTTCAATCTGGTGCCACTGTTG
GTGAACTTTATTACAGgtataaataaaagcaacaatgaccaacaaaaacaaaaagattcttatcaaaatttga
tatttgatacaaaatgttgttactgttagGATTGCGGAGAAGAGCAAAGTCCATGGGTTCCCGGC
GGGTTTGTGCTCGAGCTTAGGCATAGGAGGACACATAACAGGCGGTGCGTA
CGGTTCCATGATGCGGAAATATGGTCTAGGTGCAGACAATGTTCTAGACGCA
AAGATTGTTGATGCCAACGGTAAATTACTCGATAGAGCCGCGATGGGTGAG
GATACATTTTGGGCTATTAGAGGAGGCGCTGGAGGGAGTTTTGGGATAATTC
TAGCATGGAAGATCAAGCTTGTTCCTGTTCCTGTTCCCTAAGACCGTGACCGTCTTTAC
CGTCACCAAAACGTTACAACAAGACGTGGGTAACAAGATTATCTCAAAGTGG
CAAAGAGTTGCGGACAAGCTTGTGTAAGAGCTATTCATCAGAGTGCTCTTCA
ACGTAGCTGGAACCGGTGGGAACAAGACTGTGACGACGTCGTACAATGCTC
TGTTTCTTGGCGGAAAGGAACGCTGATGAACGTTATGAAGAAGAGTTTCCC
CGAGCTAGGGCTAACATTTAAAGATTGTATCGAAATGAGCTGGCTTGAATCC
ATTGCTTACATTTCTGGATTCCCGACCCACACGCCTACTAATGTTTTGCTTCA
AGGGAAGTCTCCGTTCCCAAAGGTCAGCTTCAAAGCCAAATCGGATTTCTGTG
AAAACCCCGATTCCCGAATCCGGGCTTCAAAGGATCTTCAAAGAAGCTACTTA
AAGAAGATATTCCATTGATGATATGGAATCCTTACGGAGGAATGATGGCGAA

AATCCCCGAATCCCAAATCCCTTTTCCGCATCGAAAAGGAGTCCTCTTCAAG
 GTTCAGTACGTAACAAGTTGGCTAGACAGTGACAAGAGACCGAGCAGACAC
 ATCAACTGGATCAGAGATCTCTATAGTTACATGACGCCTTATGTCTCAAGTA
 ACCCACGAGAAGCTTACGTGAACTACCGTGATTTAGACCTGGGAAGGAACAC
 GAAAGACGTGAAAACATGCATCAAACAAGCTCAAGTCTGGGGAGCTAACTAC
 TTCAAAAACAATTTCAACAGATTGATGATGATTAAGCAAAGGTTGATCCAG
 AGAACTTCTTTAGACACGAGCAGAGCATTCCACCTATGATGTAACgaggtcaatcaaa
 taagaataaattagaagaaaatcagataatggttcttctgtatttcggaaaaatgtattctagctatgctttagtagtactatgtttcacctaa
 aattcgatatgttcttcttagtacctaattctcaatcaactcgagaatcctattaaagtttgttcttcttcttcttaataaggatcaagtcgt
 taaaaactaaaatcagatgttcttgtaaattaagatcgttatacggtagcctaactctaattaatgatcacaaggtgtgatgaaacctga
 atatttaatacaaaactaacgatataattggatattttggatgtgatctttgttgcata

EXON1 EXON2 intron

RT-PCR: F 5'-TCCGAATGCATCTCCGTGTC-3'

RT-PCR: R 5'-CGGTCACGGTCTTAGGAACA-3'

PCR product for sequencing: R 5'-GAACGTTTTCTCAAGTGG-3' with SALK-LBb1.3

tc =possible area of insertion according to sequencing, sequence assignment to vector or gene not clearly possible; T-DNA insertion in the **promoter region**

Sequencing result:

Insertion on reverse strand

NTGNGGGCAACCAGCGTGGACCGCTTGCTGCAACTCTCTCAGGGCCAGGCGGTG
 AAGGGCAATCAGCTGTTGCCCGTCTCACTGGTGAAAAGAAAAACCACCCAGTA
 CATTAAAAACGTCCGCAATGTGTTATTAAGTTGTCTAAGCGTCAATTTGTCAATAT
 TTATTATAATCAATGACTACTTTATGTAAAAGAGTTTAGGCCTTTGAGCAATGATT
 TTCAAAGAGAAGAAAATAAAGTTGGACATTTGTGGAACTTTAAGATAGAGGAG
 AAGGTTTAGATTTTTTTCCTTATTAATACACTGAATTTTGCAGATGCTGTTGGGATC
 AAAGAGTAGCAAACAATACGAGAGCAGAAGAACTTACTTATAGAAAAAAATGGG
 AATTTCAAACCCTCCCTCTATTTTCGATTTTAGTCTCTATTTTCACTCTACAC
 CATTACACCACTTCTTCATTAGCCTCCCTCCAAGATCAATTCATCAACTGTGTCC
 AAAGAAACACACATGTTTACTTC**CCACTTGAGAAAACGTTCA**

Very similar to T-DNA sequence of pBin-pROK2, sequence quality is worse

Identical with T-DNA sequence of pBin-pROK2 (reverse complement)

Identical with *AtBBE*-like 26 DNA

Identical with both sequences

Primer for the PCR product for sequencing

* Gene sequences obtained from aramemnon <http://aramemnon.uni-koeln.de/>.

Figure S3. T-DNA insertion site based on sequencing of *Atbbe*-like protein 13, 15 and 26 PCR product (A-C). mRNA sequences for *AtBBE*-like proteins are obtained from aramemnon <http://aramemnon.uni-koeln.de/>. Primers for RT-PCR and for PCR-product for sequencing are indicated

List of abbreviations

4-OH-ICN	4-hydroxyindole-3-carbonyl nitrile
6HDNO	6-hydroxy-D-nicotine oxidase
<i>A. thaliana</i> (<i>At</i>)	<i>Arabidopsis thaliana</i>
<i>A. tumefaciens</i>	<i>Agrobacterium tumefaciens</i>
a.u.	arbitrary unit
A40926	teicoplanin homolog
acyl-CoA	acyl coenzyme A
AknOx	aclacinomycin-N/aclacinomycin-A oxidase
<i>Al</i>	<i>Arabidopsis lyrata</i>
AldO	alditol oxidase
<i>At</i> CKX	cytokinin dehydrogenase from <i>Arabidopsis thaliana</i>
ATP	adenosine triphosphate
BBE	berberine bridge enzyme
BF ₃	boron trifluoride
BG60	pollen allergen
BGLU45	β-glucosidase; monolignol glucoside hydrolase
<i>Br</i>	<i>Brassica rapa</i>
<i>Bs</i>	<i>Boechera stricta</i>
BSA	bovine serum albumin
<i>C. crispus</i>	<i>Chondrus crispus</i>
<i>C. grandiflora</i> ,	<i>Capsella grandiflora</i>
CALD	coniferyl aldehyde
CaMV	cauliflower mosaic virus
CAS	chemical abstracts service
CBDAS	cannabidiolic acid synthase
CBGA	cannabigerolic acid
cDNA	complementary deoxyribonucleic acid
<i>Cg</i>	<i>Capsella grandiflora</i>
ChitO	chito oligosaccharide oxidase
CholOx	cholesterol oxidase
cnsA	aurantioclavine synthase
Co	cortex
Col-0	Columbio 0
CpADHAPS	alkyldihydroxyacetonephosphate synthase from <i>Cavia porcellus</i>
C _q	cycle of quantification
<i>Cr</i>	<i>Capsella rubella</i>
CSC	columella stem cells
CSCD	layer of differentiating columella stem cell daughters
CTAB	cetyl trimethylammonium bromide
<i>Cv</i>	<i>Chlorella variabilis</i> ;
CW	cell wall
Dbv29	primary alcohol glycopeptide hexose oxidase

DCC	differentiated columella cells
DCPIP	dichlorophenolindophenol
DCW	dry cell wall
DdADHAPS	alkyldihydroxyacetonephosphate synthase from <i>Dictyostelium discoideum</i>
DLDH	D-lactate dehydrogenase
DMSO	dimethyl sulfoxide
DprE	decaprenylphosphoryl-beta-D-ribose oxidase
DW	dry weight
<i>E. californica</i> (<i>Ec</i>)	<i>Eschscholzia californica</i>
<i>E. coli</i>	<i>Escherichia coli</i>
E_0	redox potential
E22O	Ecdysteroid-22-oxidase
EamA	O-acetyl-serine/cysteine export gene in <i>E. coli</i>
EasE	chanoclavine synthase
EDTA	ethylenediaminetetraacetic acid
Emmdh-flavin	4a,5-epoxyethano-3-methyl-4a,5-dihydrolumiflavin
EncM	FAD-dependent oxygenase
Ep	epidermins
<i>Es</i>	<i>Eutrema salsugineum</i>
EtSH	ethanethiol
EugO	eugenol oxidase
FAD	flavin adenine dinucleotide
Fi	interfascicular fiber
FMN	flavin mononucleotide
FOX	flavin-dependent oxidoreductase
FsqB	fructosyl amino acid oxidase
FST	flanking sequence tag
FW	fresh weight
GABI	Genomanalyse im biologischen System Pflanze
GALDH	L-galactono- γ -lactone dehydrogenase
GC-MS	gas chromatography–mass spectrometry
gDNA	genomic deoxyribonucleic acid
GilR	pregilvocarcin V oxidase
GLDH	L-galactono-1,4-lactone dehydrogenase
GMC	glucose/methanol/choline oxidoreductase
GOOX	glucooligosaccharide oxidase
GUS	β -glucuronidase
H ₂ O ₂	hydrogen peroxide
<i>Ha</i> -CHOX	<i>Helianthus annuus</i> carbohydrate oxidase
HCl	hydrogen chloride
HEPES	4-(2-hydroxyethyl)-1-piperazineethanesulfonic acid
His-tag	histidine tag
HMM	hidden markov model
HOX	hexose oxidase

HPLC	high-pressure liquid chromatography
HPM9	alcohol oxidase from <i>Hypomyces subiculosus</i>
ICN	indole carbonyl nitrile
<i>K. pastoris</i>	<i>Komagataella pastoris</i>
<i>K. phaffii</i>	<i>Komagataella phaffii</i>
k_{cat}	turnover number
KCl	potassium chloride
K_{d}	dissociation constant
KH_2PO_4	potassium dihydrogen phosphate
k_{obs}	observed rate constant
KOH	potassium hydroxide
k_{ox}	oxidation rate constant
k_{red}	reduction rate constant
LaO	carbohydrate oxidase
LBD	lateral organ boundaries domain
<i>Ls-CHOX</i>	<i>Lactuca sativa</i> carbohydrate oxidase
MES	2-(<i>N</i> -morpholino)ethanesulfonic acid
MgCl_2	magnesium chloride
<i>Mp</i>	<i>Marchantia polymorpha</i>
mRNA	messenger ribonucleic acid
MS	Murashige & Skoog medium
MS/MS	tandem mass spectrometry
<i>Mt</i>	<i>Myceliophthora thermophile</i>
MurB	UDP- <i>N</i> -acetylenolpyruvoylglucosamine reductase
<i>N. rileyi</i>	<i>Nomuraea rileyi</i>
Na_2HPO_4	sodium hydrogen phosphate
NAC	nascent polypeptide-associated complex
NaCl	sodium chloride
NaH_2PO_4	sodium dihydrogen phosphate
NaHCO_3	sodium hydrogen carbonate
NaOH	sodium hydroxide
NASC	European Arabidopsis Stock Centre
Nec5	nectarin 5
<i>Nf</i>	<i>Neosartorya fumigate</i>
<i>Nt</i>	<i>Nicotiana tabacum</i>
O_2	oxygen
OGOx	oligogalacturonides oxidase
<i>P. infestans</i>	<i>Phytophthora infestans</i>
<i>P. syringae</i>	<i>Pseudomonas syringae</i>
PAL4	phenylalanine ammonia-lyase 4
PBS	phosphate-buffered saline
PCMH	<i>p</i> -cresol methylhydroxylase
PCR	polymerase chain reaction
PDB ID	protein data bank identification
PDI	protein-disulfide isomerase

PEG 2000 MME	polyethylene glycol methyl ether 2000)
PFAM	protein family
pfkB	phosphofructokinase
Ph	phloem
PHBH	<i>p</i> -hydroxybenzoate hydroxylase
Phl p 4	major pollen allergen (glucose dehydrogenase)
<i>Pi</i>	<i>Phytotropa infestans</i>
Pi	pith
pK _a	negative base-10 logarithm of the acid dissociation constant
<i>Pp</i>	<i>Physcomitrella patens</i>
qRT-PCR	quantitative real-time polymerase chain reaction
RAM	root apical meristem length
RMSD	root-mean-square deviation
RPA1076	oxidoreductase from <i>Rhodopseudomonas palustris</i>
SAIL	Syngenta Arabidopsis Insertion Library
SALK	The Salk Institute
SCOPe	structural classification of proteins – extended
SD	standard deviation
SDS-PAGE	sodium dodecyl sulfate–polyacrylamide gel electrophoresis
SE	standard error
<i>Sm</i>	<i>Selaginella moellendorffii</i>
STOX	(<i>S</i>)-tetrahydroprotoberberine oxidase
TamL	tirandymycin oxidase
T-DNA	transfer desoxyribonucleic acid
TFA	trifluoroacetic acid
THCAS	tetrahydrocannabinolic acid synthase
TMS	trimethylsilyl group
Tris	tris (hydroxymethyl) aminomethane
UDP	uridine diphosphate
UTR	untranslated region
v/v	volume per volume
VAO	vanillyl-alcohol oxidase
Vb	vascular bundle
<i>Vc</i>	<i>Volvox carteri f. nagariensis</i>
VQ motif	valine-glutamine motif
w/v	weight per volume
WiscDsLox	University of Wisconsin collection
XDS	X-ray detector software
XEG	xylanendoglucanase
Xy	xylem
XyIO	xylooligosaccharide oxidase
<i>ZmCKO2</i>	cytokinin oxidase from <i>Zea mays</i>
<i>ZmCKX1</i>	cytokinin oxidase from <i>Zea mays</i>

CURRICULUM VITAE



PERSONAL INFORMATION

Name: Barbara **KONRAD**
Address: Rohrbach 20, 8083 St. Stefan im Rosental
Phone: 0660/5066005
E-mail: babssteiner@hotmail.com
Date/ place of birth: 9th of June 1986, Tamsweg, Austria
Citizenship: Austrian
Marital status: Married, 1 child

EDUCATION

1992 - 1996 Elementary School in Schöder, Austria
1996 - 2000 Grammar School in St. Peter/Kbg., Austria
2000 - 2005 Upper-level secondary college for fashion and clothing techniques, Graz
2006 - 2010 **Studies of Biology** – Specialization in animal behavior at the Karl-Franzens University of Graz
2010 - 2013 **Studies of Biochemistry and molecular Biomedicine** at the Karl-Franzens University of Graz
07/2011 - 08/2011 Project laboratory at the Institute of Pathology at the Medical University of Graz
05/2012 - 11/2012 Diploma thesis project at the Institute of Biochemistry, Graz University of Technology
 Supervisor: Prof. Peter Macheroux
22. 03. 2013 Defense of Diploma thesis, diploma completed
04/2013 - 08/2018 **PhD project** at the Institute of Biochemistry, Graz University of Technology
Doctoral School: Molecular Biosciences and Biotechnology
 Supervisor: Prof. Peter Macheroux

RESEARCH ACTIVITIES

- 07/2010** Project at the Department of Pathophysiology & Immunology at the Medical University of Graz with Prof. Adelheid Kresse: “*Analysis of the NO-synthase by using NADPH diaphorase staining in forebrain of rats*”
- 07/2011 - 08/2011** Project laboratory at the Department of Pathology at the Medical University of Graz offered by Prof. Zatloukal and under the supervision of Mag. Dr. rer.nat. Leopold Fröhlich: “*Analysis of the apoptosis inducing activity of TRAIL and its interplay with the histone deacetylase inhibitor (SAHA) induced cell death in endometrial stromal sarcoma (ESS) cells*”
- 05/2012 - 11/2012** Diploma thesis project entitled: “*Biochemical and structural characterization of the Berberine bridge enzyme variant W165F from Eschscholzia californica*” at the Department of Biochemistry, TU Graz; Supervisor: Prof. Peter Macheroux
- 04/2013 - 08/2018** PhD project entitled: *Biochemical and Physiological Characterization of the Berberine Bridge Enzyme-like family in Arabidopsis thaliana*” at the Department of Biochemistry, TU Graz
Supervisor: Prof. Peter Macheroux
- 05/2015 - 10/2015** Research visit at the Department of Plant and Environmental Sciences, University of Copenhagen, Denmark
Supervisor abroad: Prof. Thomas Roitsch and Dr. Eric van der Graaff

PUBLICATIONS

- Zafred, D. *et al.* (2015) Rationally engineered flavin-dependent oxidase reveals steric control of dioxygen reduction. *FEBS J* 282, 3060–3074.
- Daniel, B. *et al.* (2015) Oxidation of Monolignols by Members of the Berberine Bridge Enzyme Family Suggests a Role in Plant Cell Wall Metabolism. *J Biol Chem* 290 (30), 18770-18781.
- Daniel, B. *et al.* (2016) Structure of a berberine bridge enzyme-like enzyme with an active site specific to the plant family Brassicaceae. *PLoS One* 11.
- Daniel, B. *et al.* (2017) The family of berberine bridge enzyme-like enzymes: A treasure-trove of oxidative reactions. *Arch Biochem Biophys* 632, 88-103.

TEACHING ACTIVITIES

04/2013 – 08/2018

University assistant at the Institute of Biochemistry,
Graz University of Technology, Teaching assistant for
Biochemistry I and II, Molecular biology laboratory
course and Immunological Methods

OTHER QUALIFICATIONS

Language Skills

German as native language,
fluent in English, basics in French

Computer Skills

Microsoft Office, Basics in Bioinformatics (databases,
sequence alignments, Pymol, etc.), OriginPro 7.5 for
graphic modeling

October 21st, 2018